Università degli Studi di Padova

Facoltà di Ingegneria

Scuola di Dottorato in
Scienze dell'Ingegneria Civile e Ambientale

Tesi di Dottorato

Influence of Grout Injection on the Dynamic Behaviour of Stone Masonry Buildings

Dottorando:
Nicola Mazzon

Supervisore:
Maria Rosa Valluzzi

XXII ciclo – 2010

UNIVERSITÀ
DEGLI STUDI
DI PADOVA

Sede Amministrativa: Università degli Studi di Padova

Dipartimento di Costruzioni e Trasporti

SCUOLA DI DOTTORATO DI RICERCA IN:
SCIENZE DELL'INGEGNERIA CIVILE ED AMBIENTALE

CICLO XXII

Influence of Grout Injection on the Dynamic Behaviour of Stone Masonry Buildings

Direttore della Scuola
Prof. Stefano Lanzoni

Supervisore
Dr. Maria Rosa Valluzzi

Dottorando
Ing. Nicola Mazzon

Sommario

Il territorio italiano, così come quello europeo, è caratterizzato da un'ampia diffusione di strutture appartenenti all'edilizia storica minore. Lo stato di degrado, in cui talvolta si trovano tali edifici, rende spesso necessari interventi strutturali volti a garantirne l'integrità. In tale senso, negli ultimi decenni sono state sviluppate nuove metodologie d'intervento, sfruttando sia di materiali tradizionali che innovativi, per preservare tali strutture da ulteriori danni, in particolare quelli indotti da eventi sismici. Tuttavia, nuovi materiali e tecniche d'intervento vengono spesso commercializzati ed applicati senza l'esecuzione di un esaustivo studio preliminare che ne verifichi l'applicabilità e l'efficacia.

La presente ricerca si inserisce in questo contesto prendendo in considerazione le murature multi-strato in pietra, una delle tipologie costruttive maggiormente impiegate nell'edilizia storica minore. Tale muratura è costituita da più paramenti accostati ed è caratterizzata da un'alta percentuale di vuoti interni. Inoltre, si considera l'impiego dell'iniezione di miscela, a base di calce idraulica naturale, come tecnica di consolidamento applicabile a tale tipologia muraria. Lo studio si propone di validare l'impiego di questa metodologia d'intervento, già da tempo ampiamente utilizzata sfruttando materiali di diversa composizione chimica, mediante la realizzazione di un'ampia campagna sperimentale e di una successiva modellazione numerica.

La prima fase sperimentale comprende una serie di prove dinamiche su modelli di edificio, in scala ridotta, realizzati in muratura multi-strato di pietra, successivamente sottoposta ad iniezione di miscela. L'esecuzione di tali prove su tavola vibrante ha permesso di valutare l'influenza della tecnica di consolidamento considerata sul comportamento dinamico globale della struttura su cui si interviene. Inoltre, si è potuto valutare l'incremento di resistenza oltre che la variazione della risposta sismica dei modelli di edificio.

Una complementare fase sperimentale ha coinvolto numerose ed ulteriori prove di laboratorio, realizzate in ambito quasi-statico, su singoli elementi strutturali.
L'esecuzione di prove di compressione ha permesso di verificare sia l'incremento di resistenza di tali elementi strutturali che la variazione delle loro modalità di rottura a seguito dell'iniezione di miscela legante.
Ulteriori prove di taglio e compressione hanno fornito importanti indicazioni riguardo al comportamento meccanico di singoli elementi strutturali soggetti a forze cicliche nel piano.

Infine, si è sviluppata una modellazione numerica del comportamento meccanico di campioni sottoposti a carico di compressione monoassiale. Quest'analisi ha dunque permesso di approfondire lo studio della distribuzione delle tensioni e delle modalità di rottura di singoli elementi strutturali, soggetti ad intervento di consolidamento mediante iniezioni di miscela legante.

Abstract

The Italian and European regions are characterized by a wide diffusion of structures in the minor historical centres. The decay condition, in which part these buildings are, makes often necessary structural interventions to preserve they integrity. This way, during last decades several new intervention methodologies were developed, employing both innovative and traditional materials, with the aim to avoid further damages, particularly those induced by seismic events. However, these new materials and techniques are often commercialized and employed without any preliminary exhaustive study to verify their applicability and their effectiveness.

The present research joins in this contest considering the multi-leaf stone masonries, one of the most diffuse structural systems widely employed on minor historical buildings. This masonry typology is constituted by more approached leaves and it is characterized by a high percentage of internal voids. Furthermore, the employment of hydraulic lime-based grout injection is also considered as strengthening technique suitable for this masonry typology. This study aims to validate the application of this intervention methodology, widely applied since many years employing materials different for chemical composition, trough an extensive experimental campaign and a subsequent numerical modelling.

First experimental phase involves a series of dynamic tests on whole building models, considering a reducing scale factor, realized with multi-leaf stone masonry, subsequently strengthened trough injection of grout. The execution of these shaking table tests allowed to evaluate the influence of the considered strengthening technique on the overall dynamic behaviour of the injected structure. Furthermore, also the increasing of strength and the seismic response of the building models could be evaluated.

A complementary experimental phase involved several further quasi-static laboratory tests tests on single structural elements.
Compression tests allowed to study the strength increasing of this elements as well as their failure mechanisms after the grout injection.
Further shear compression tests provided important informations about the mechanical behaviour of single structural elements subjected to in-plane cyclic forces.

Finally, a numerical modelling of the mechanical behaviour of specimens subjected to compression load was developed. This analysis allowed to deepen the study of the stress distribution and of the failure mechanisms of single structural elements subjected to strengthening trough grout injection.

Acknowledgements

This research work has been developed within the ReLUIS National Project (Progetto esecutivo 2005-2008, Attuazione Accordo di Programma Quadro DPC-Reluis del 15 Marzo 2005).

First of all, I would like to acknowledge Prof. Maria Rosa Valluzzi, who has always supported my activity during these years of doctoral studies, and Prof. Claudio Modena, who has given me the possibility to follow the research project presented in this thesis and to collaborate to several further interesting research activities.
The whole laboratory activity described in the present research was supported by Tassullo S.p.A., which also provided the materials and sustained all the fundamental practical activities to carry out the wide experimental program developed during these three years. A further thanks also to Eng. Victor dal Piaz, who provided his assistance during the realization of the stone masonry building models.
I would like to thank all the people of the ENEA Research Centre, who collaborated within this research. Particular thanks to Engg. Gerardo De Canio, Nicola Ranieri, Ivan Roselli, Maria Luisa Mongelli and all the technicians involved during the tests.
Furthermore, I would like to acknowledge the University of Pavia for the collaboration within the ReLUIS National Project and for the supply of the seismic input employed during the shaking table tests presented in this research.
I am also grateful to Prof. Takayoshi Aoki, Graduate School of Design and Architecture at the Nagoya City University, for its collaboration and support in the analysis of the performed dynamic tests.
I would like to thank Prof. Miha Tomaževič, Slovenian National Building and Civil Engineering Institute, for its precious suggestions and discussions concerning the whole experimental program.
Last, but not least, I would like to express my deep gratitude to all my colleagues, particularly to Engg. Matteo Panizza and Marco Munari, who have shared with me these doctoral years, to Eng. Filippo Casarin, who widely supported me during the execution of the dynamic experiments and the analysis of results, to Eng. Massimo dalla Benetta, whose help during the whole experimental program allowed to carry out both the dynamic and static tests, to Prof. Francesca da Porto and Eng. Flavio Mosele, for the interesting discussions and their help in design part of the experimental program, to Engg. Enrico Garbin and Giovanni Guidi, for the discussions concerning the numerical analyses developed, and to all the people who joined to this experience during these three years, particularly Luca Nicolini, Giulia Bettiol, Bruno Silva, Elena Simonato and Elena Stievanin.
I am also grateful to all the graduate students who gave their important contribution to the laboratory activities and to the analyses of the test results.
A further thanks to all the technicians of the Laboratory of the Department of Structural and Transportation Engineering of the University of Padua, who collaborated to the realization of specimens and allowed the execution of a wide part of the experimental program.

Finally, I would like to express my sincere gratitude to my parents and my brother, who sustained me during these years and particularly during the final period, and also to Francesca, always present by my side.

Contents

List of Tables

List of Figures

List of Symbols

α	Coefficient for the determination of K, depending on boundary conditions
δ_{cr}	Lateral displacement attained at cracking limit
δ_{Hmax}	Lateral displacement attained at maximum lateral resistance
δ_{max}	Maximum attained lateral displacement
γ_i	Shear rotation
ν	Poisson ratio
$\nu_{40\%\sigma_{max}}$	Poisson ratio computed at 40% of compression strength
ω	Angular Frequency
σ'_0	Vertical stress level applied during shear compression tests
σ_{el}	Compressive stress within the elastic range
$\sigma_{I,cr}$	Stress level of first crack appearance
σ_{max}	Compressive strength of the considered element
τ_u	Ultimate shear stress in the wall
τ_ν	Average shear stress in the wall
$\vartheta_{\delta max}$	Angular drift at maximum attained displacement
ϑ_{cr}	Angular drift at cracking limit state
ϑ_{Hmax}	Angular drift at maximum attained lateral resistance
$\varepsilon_{wc,0}$	Strain of an unstrengthened wall
$\varepsilon_{wc,s}$	Strain of a strengthened wall
φ	Friction angle
ξ	Equivalent viscous damping
A	Horizontal cross sectional area
$a_{floorlevel}$	Actual acceleration at each floor level
A_{hys}	Quantity of energy dissipated in a single hysteretic loop

$a_{i,max}$	Maximum absolute acceleration at i-th storey
AF	Amplification Factor of acceleration
b	Shape factor defined as ratio between h and l
BS	Base Shear
BSC	Base Shear Coefficient
c	Cohesion value
d_+	Maximum attained lateral displacement in the positive direction of displacements
d_-	Maximum attained lateral displacement in the negative direction of displacements
dE_{hys}	Quantity of energy dissipated in a single hysteretic loop
dE_{inp}	Quantity of energy input in a single hysteretic loop
du	Infinitesimal displacement
E	Elastic modulus
E_A	Energy dissipated per unit of mass by a simple oscillator with ω as fundamental frequency and ν as damping factor
E_p	Potential Energy referred to a single hysteretic loop
$E_{1/3}$	Secant elastic modulus computed as 1/3 of σ_{max}
E_{hys}	Overall quantity of dissipated energy
E_{inp}	Overall quantity of input energy
$E_{wc,0}$	Elastic modulus of an unstrengthened wall
$E_{wc,s}$	Elastic modulus of a strengthened wall
f_t	Tensile strength of the considered element
f_{gr}	Compressive strength of grout
$f_{inf,s}$	Compressive strength of the internal core of a multi-leaf masonry element
$f_{t,0}$	Tensile strength of an unreinforced wall
$f_{t,i}$	Indirect tensile strength
$f_{t,s}$	Tensile strength of a strengthened wall
$f_{wc,0}$	Compressive strength of the unstrengthened wall
$f_{wc,s}$	Compressive strength of the injected wall
$f_{wt,0}$	Tensile strength of unstrengthened wall

G_k	Shear modulus computed from stiffness at cracking limit
$G_{1/3}$	Shear modulus compute at 1/3 of the τ_{max}
G_{30-60}	Average of shear modulus values, computed between 30% and 60% of τ_{max}
G_{exp}	Shear modulus computed from experimental data
h	Height of the considered element
H_i	Lateral acting force due to seismic loads
H_+	Maximum attained lateral resistance in the positive direction of displacements
H_-	Maximum attained lateral resistance in the negative direction of displacements
$H_{\delta max}$	Lateral resistance attained at maximum lateral displacement
H_{cr}	Lateral resistance attained at cracking limit
H_{max}	Absolute value of the maximum attained lateral resistance
I_A	Arias Intensity
K	Secant stiffness, computed as ratio between the actual lateral lateral load and displacement
K_n	Normal stiffness of interface element
K_{cr}	Secant stiffness at cracking Limit State
K_{tg}	Tangential stiffness of interface element
l	Width of the considered element
m_i	Mass of Building Model concentrated at i-th storey
m_{inj}	Quantity of injected grout [kg]
m_{RM}	Mass of RM model
m_{URM}	Mass of URM model
PGA	Peak Ground Acceleration
Q	Weight of the building model
$S.F.$	Scale Factor
V	Volume of the whole panel
V_{ex}	Volume of the external layer of a multi-leaf masonry element
V_{inf}	Volume of the internal core of a multi-leaf masonry element

Introduction

Masonry is a widespread structural system in Italy and in Europe, as well as in many other non-European Countries. Several masonry typologies have been developed and evolved over the centuries. These structural systems can widely differ due to of many aspects such as materials, brick and stone, and types of masonry, monolithic or multi-leaf elements.

Nowadays, many of these historical and more recent masonry structures need strengthening interventions because of different causes such as age and/or natural occurrences. Furthermore, preserving these buildings from earthquake damage has an important role, since this constitutes one of the most destructive events. Most recent Italian earthquakes (Lunigiana and Garfagnana, 1995; Reggio Emilia, 1996; Umbria and Marche, 1997; Piedmont, 2000; Molise, 2002; Piedmont, 2003; Salò, 2004; Abruzzo, 2009) confirmed the limits and consequences of some intervention techniques developed over the years [Binda and Saisi, 2005; Binda *et al.*, 2000b,c,d; Borri *et al.*, 1999, 2004; Corradi *et al.*, 2002; Modena, 1997; Modena *et al.*, 2000]. Moreover, the damage occurred due to conceptually wrong strengthening interventions, indicate that these operations should be deeply studied before their application.

The Italian Government and the National Department of Civil Protection financed the institution of the ReLUIS national consortium (University Network of Seismic Engineering Laboratories) with the aim to deepen the knowledge of the evaluation and reduction of vulnerability and seismic risk, on the basis of effects caused by seismic events.

One of the main aims of the ReLUIS consortium is to improve existing guidelines and codes for cultural heritage. In this respect, many efforts were made to study the effects of innovative and traditional strengthening techniques, by both theoretical and applicative point of view, and the present work is included in these research activities.

First formal instructions concerning anti-seismic constructions and interventions have been introduced, only relatively recently in Italy, in 1974 [Legge 2/2, 1974]. The first official documents, regarding instructions for intervening on historical structures, were introduced by Circolare 30/7/1981 [1981] and updated on 1986 through D. M. 24/01/1986 [1986], where the concept of "seismic improvement" was introduced in Italy. Reasserted in the D. M. 16/1/1996 [1996], this concept was then applied to the assessment of cultural heritage buildings. In these norms a number of possible strengthening interventions for improvement and upgrading is listed. These indications were provided on the basis of the knowledge and of the state of art when they were issued. Subsequently, research and investigations led, via the OPCM 3274 [2003] and OPCM 3431 [2005], to the D. M. 14/01/2008 [2008], currently in force.
Furthermore, specific guidelines were devised for cultural heritage buildings [D. M. 12/10/2007, 2007], issued by the Ministry of Cultural Heritage. These guidelines propose a multidisciplinary approach for the assessment and reduction of seismic

risk for cultural heritage buildings in which the design is a compromise between the protection from seismic risk and the respect of cultural and artistic values, according to the preservation criteria asserted in the various issued charters for the restoration of historic monuments [The Athens Charter, 1931; The Venice Charter, 1964].
This development process led also to a contextual revaluation of investigations as preliminary study of the structure as well as verification methodology of performed interventions. Actually, the code provides for the better the structural assessment, the higher the confidence factor, allowing to verify the same structure for a lower seismic solicitation. In this sense, the geometrical survey and the mechanical characterization of constituent materials are some of the most important aspects to be deepened. In-situ investigations, starting from non-destructive techniques (typological survey of masonry and materials, sonic and ultrasonic analyses, dynamic investigations, etc.), through minor destructive tests (single and double flat-jack tests) up to destructive investigations (compressive, diagonal and shear compression tests), lead to an improved knowledge of the building at different levels.
Similar documents were also previously adopted, at different international levels, by different committees [CEN - EN 1998-3, 1998; ICOMOS/ISCARSAH, 2003; ISO 13822, 2006].

Of all historical structural systems considered in recent guidelines and codes, this research focuses on multi-leaf stone masonry, which was a building technique widely employed for common historical constructions mainly to be found in the minor buildings of historical centres in the Italian territory as well as in other European countries, such as Slovenia [Tomaževič *et al.*, 1985] and Greece [Adami and Vintzileou, 2008]. Over the years, the special features and failure mechanisms of three-leaf masonries have been examined in depth [Adami and Vintzileou, 2008; Roberti *et al.*, 2004; Valluzzi, 2000; Vasconcelos, 2005; Vintzileou and Miltiadou-Fezans, 2008]. Firstly, this structural system is mainly characterized by a wide presence of voids in the inner core of the wall [Binda and Saisi, 2005; Binda *et al.*, 1999], which is constituted by stone fragments. Secondly, any transversal connection between opposite external layers is normally provided. These aspects make the masonry especially prone to brittle mechanisms of failure, such as detachment of external layers and out-of-plane collapse. These mechanisms are mainly caused by both compressive stresses, due to dead-loads, and horizontal actions, namely in-plane and out-of-plane forces, due to seismic loads. Nevertheless, investigations and knowledge of the overall behaviour of multi-leaf stone masonry is, nowadays, limited and needs to be improved.
In the light of this research, a few strengthening techniques have been examined, such as repointing of mortar bed joints, injections, insertion of transversal steel ties [Binda *et al.*, 1997a; Corradi *et al.*, 2008; Valluzzi *et al.*, 2005] and grout injection, having different chemical and rheological properties [Toumbakari, 2002; Valluzzi, 2000; Vintzileou and Miltiadou-Fezans, 2008]. Of these, the effects of hydraulic lime-based grout injection have been considered in the present research. This strengthening technique aims at limiting all the previously described failure mechanisms, which are typical for this type of masonry, assessing at the same time the compatibility among materials [Valluzzi *et al.*, 2004].
Since the '80s, studies and tests have been carried out to clarify the dynamic behaviour of historical masonry structures [Benedetti, 1980; Tercelj *et al.*, 1976; Turnšec *et al.*, 1978]. Furthermore, in the years to follow and up to the present, several researches, investigating the effects of a strengthening technique, focused on dynamic experiments

both on simple elements [Griffith *et al.*, 2003; Meisl *et al.*, 2007], such as masonry panels and piers, and complex structures [Benedetti *et al.*, 1998; Calvi *et al.*, 1996; Tomaževič and Weiss, 1994; Tomaževič *et al.*, 1992; Yi *et al.*, 2006], for instance substructures or whole buildings. These researches, mainly carried out through shaking table tests, had a direct correlation with the dynamic behaviour of strengthened masonry structures and led to an immediate interpretation of the obtained results.
Furthermore, quasi-static tests were also carried out to study the effectiveness of strengthening intervention techniques on stone masonries, particularly on multi-leaf structures. More interesting researches focused on diagonal and shear compression experiments, carried out through both in-situ investigations and laboratory campaigns [Corradi *et al.*, 2003, 2008; Oliveira *et al.*, 2006; Tomaževič, 2000; Vasconcelos, 2005; Vintzileou and Miltiadou-Fezans, 2008]. Differently, only few experiences are available on dynamic tests to study the effectiveness of strengthening interventions on stone masonry structures [Benedetti and Pezzoli, 1996; Benedetti *et al.*, 1998; Juhásová *et al.*, 2008; Tomaževič *et al.*, 1990, 1992] and, particularly, only a study concerns the employment of grout injections [Benedetti, 1980].

The present research, inserted in the afore-mentioned normative contest, is intended to thoroughly examine some aspects of grout injection of a single material, namely hydraulic lime-based mixture. This technique, widely applied by professional engineers and companies, seems to have been only partially studied and several aspects, particularly regarding its influence on the dynamic behaviour of structures to be strengthened, can not be found in literature.
On this basis, dynamic tests on strengthened structures seem to complete the knowledge of this aspect while quasi-static experiments will allow a more complete investigation program. A general overview of the aims and methods of the research is given in the next section.

Aim and methods of the research

The main aim of the present research is to contribute to the knowledge of the effects induced by the interventions of grout injection on the dynamic behaviour of stone masonry structures. Furthermore, the investigation involves a study of the effects of this intervention technique on the modification of failure mechanisms typical for the considered kind of masonry.
Of all the materials employed for structural injections and all historical building systems, this research focuses on the application of hydraulic lime-based grout injection on multi-leaf stone masonry.

The above-mentioned purposes were thoroughly examined thanks to an extensive experimental campaign involving both quasi-static and dynamic tests on single elements, such as masonry panels and piers, and complex structures, i.e. whole building models.

The first part of the whole experimental program involved shaking table tests on building models under different conditions. Unreinforced, strengthened and repaired structures were subjected to several seismic loads at the ENEA Research Centre ("la Casaccia") in Rome. The tests were carried out first on an UnReinforced building Model ("URM"), that constituted the reference sample to evaluate the effectiveness of intervening by injections. A further experiment was carried out on a structure injected before the test, named Strengthened Model ("SM"). This simulates an undamaged construction strengthened before the seismic event, allowing an examination of the

maximum increase in resistance. The third case is representative of a structural intervention performed on a previously damaged historical structure, which is the most common real situation of intervention, named Repaired Model (RM).
This test method allowed an evaluation of the modification of the failure mechanism and the increase in strength due to the injection of hydraulic lime-based grout. Furthermore, the dynamic characteristics of the three above described structures were thoroughly examined, such as natural frequencies, modes of vibration, damping factors and stiffness degradation.

A further dynamic experimental phase, which involves shaking table tests on sub-structural elements, was also designed. The high vulnerability of this masonry typology led to project also dynamic tests on masonry panels, subjected to an out-of-plane seismic load. In fact, this experimental set-up provides information of the effectiveness of the grout injection to avoid the local separation between the external load bearing layers and internal core. Furthermore, information on its capability to increase the overall masonry strength will be also achieved. However, the dynamic tests on these structural elements could not be performed within the present research. Nevertheless, the design, the construction and the strengthening phases of the panels will be presented, since the first analyses about the masonry injectability could be performed.

The second part of the experimental program focused on quasi-static tests on masonry panels. This experimental section was performed at the Laboratory of Materials and Structures of Department of the Structural and Transportation Engineering. Several undamaged panels could be recovered during the dismantling of building models subjected to seismic actions. Part of these specimens were tested under monotonic compression, while shear compression tests were performed on the remaining samples.
Monotonic compression tests allowed the characterization of the strength of injected masonry. Moreover, the failure mechanisms were also studied and a deeper knowledge was acquired of the difference between strengthened and repaired elements. Further mechanical parameters, such as elastic properties (Young's modulus and Poisson's ratio) were also investigated permitting a better understanding of the overall behaviour of the tested elements.

Shear compression experiments were performed on specimens having different slenderness. The application of different vertical stresses allowed an investigation of shear and flexural behaviour on both strengthened and repaired elements. This test method permitted an evaluation not only the strength but also the mechanical characteristics of injected specimens. Furthermore, stiffness degradation analyses and energetic considerations could be developed.

Tests on constituent materials were also carried out to characterize the basic mechanical properties of the masonry concerned in this study.

Finally, a numerical simulation of the monotonic compression tests is developed. The presented Finite Element analysis constitutes the first step of a process, that leads to obtain a simplified model. In fact, this would be employed for a subsequent development of more complex analyses, such as the numerical analysis of the in-plane shear compression tests on single structural elements and of the shaking table experiments on whole building models.

Thesis organization

The thesis is organized into 8 chapters. They are organized according to the logical path presented in the previous section. Furthermore, the order of chapters reflects the steps carried out during the research.

The first chapter focuses on the state-of-the-art of present and past studies carried out on topics similar to those approached in the present research. Shaking table tests on both single elements and whole building models were considered. Attention was mainly paid to testing methods, similar strengthening interventions and kinds of structures, namely multi-leaf stone masonry. Furthermore, works on other experimental parts developed in this thesis were found. Compression and shear compression tests on similar types of masonry were considered. Furthermore, also the experimental campaigns regarding different structures, employing a similar test rig, were regarded.

Chapter two provides a general overview of the whole experimental program, presenting the two main parts: shaking table tests and quasi-static experiments. For these parts, a detailed program and an overall introduction to the analyses, developed in the following chapters, are presented in order to direct the reader into the thesis.

Third chapter presents the preliminary characterizations carried out before the experimental campaign. In the first part, mechanical investigations of employed materials are summarized. The second part presents sonic investigations performed in order to study the feasibility and effectiveness of strengthening interventions.

In chapter four the performed shaking table tests are presented. Analyses are illustrated separately and, in the second part, a comparison of these leads to first conclusions concerning the effects of the employment of hydraulic lime-based grout.

Chapter five explains the results obtained from monotonic compression experiments. These tests permitted an examination of the modifications to failure mechanisms, strength and other mechanical aspects obtained through the use of lime grout injection. These results constituted the basis for the following experimental section.

In chapter six shear compression tests are described. As in the previous chapter, the analyses are performed separately, while a subsequent comparison of these permitted conclusions to be made concerning the effects induced by the lime grout mixture on the in-plane behaviour of injected masonry panels.

Chapter seven presents the results obtained from different FE models. These models are based on the results obtained during the experimental phases described in previous chapters. This study aims to reproduce both the stress-strain relationships of specimens and the stress distribution on the same panels during these tests. Furthermore, this allows the analyses made to be extended through parametric studies.

Finally, all the results obtained from the above-mentioned experimental and numerical analyses are summarized in chapter eight. In addition, an overall evaluation of these aspects leads to the conclusions regarding the effectiveness and limits of the studied strengthening technique. Moreover, the explored path has opened up issues and indicated further interesting experimental and numerical analyses.

Influence of Grout Injection on the Dynamic Behaviour of Stone Masonry Buildings

Chapter 1

Literature Review

The aim of this chapter is providing a critical overview on the main topics discussed in the present research. Nevertheless, the treated arguments will be presented in a different order with respect to that followed on the present research.
A general overview about the masonry typologies and both strengthening interventions and investigation techniques will be given firstly. The remarks will mainly be focused on the three-leaf stone masonry. Furthermore, among several techniques presented in the following, the injection of lime-based grout was considered. Great importance is also given to the sonic investigations, which allow to evaluate the effectiveness of this intervention technique.

A subsequent section will be dedicated to quasi-static experimental campaigns on structural elements. This part focuses on past researches, comprehending monotonic compression and shear compression experiments, to deepen the knowledge about the influence of the considered strengthening technique on the overall behaviour of multi-leaf masonry elements.

These studies constitute the basis to develop dynamic shaking table tests on both single structural elements and whole building models. Further researches will be presented with the aim to study both testing and analyses methods. Moreover, particular attention will be paid on experimental campaigns involving stone masonry structures and on further studies on grout injection.

Last part of the chapter provides an overview on different methods for the dynamic identification of the structures. Both the testing and analyses methodologies will be presented in order to select the most appropriate techniques to be employed to detect the dynamic characteristics of the models tested on the shaking table.

1.1 Masonry Elements: classification, interventions and investigations

The construction systems, based on the employment of masonry, are very numerous and diversified. Several and variegated examples can be found on historical buildings, whether they be monumental or applied to minor constructions. These differences are mainly related to their morphology, and to the typology and quality of employed materials [Binda and Saisi, 2001]. These aspects, together with the used construction system, characterize the different masonries and this results in a wide influence of their mechanical behaviour. In this sense a cataloguing of different masonry typologies become fundamental to identify and select a representative structural system.

Several factors, such as chemical or physical agents and further mechanical events, influence the durability of materials and cause the overall degradation of the masonry. Based on the analysis of the most typical damage for each typology [Binda *et al.*, 2000c], different strengthening intervention techniques were developed during the years, which aim at limiting and solving the most common problems that arise on different masonry typologies. On the other hand, these techniques should be validated before their large employment to avoid inducing further damages on structures [Corradi *et al.*, 2002; Modena, 1997].
In the light of these aspects, several investigation techniques may be applied to study the goodness of execution and the effectiveness of the applied strengthening interventions.

Finally, the representativeness of structures reproduced for experimental campaigns and the reliability of the consequent results, are deeply depending on the above mentioned aspects. Starting from these observations, the importance of a correct selection of the structural system, strengthening intervention and verification methodology becomes evident.

1.1.1 Masonry typology

The typological subdivision of existing masonries, which constitute the cultural heritage buildings, is a difficult topic. The variety of masonries that can be surveyed makes difficult a possible classification, which involves all the typologies. In fact, the employed materials, their combination and manufacture and the execution process are only few aspects among several important issues that should be considered.

Nevertheless, a correct definition of the existing masonry typologies allows to identify their overall mechanical characteristics, through in-situ investigations and laboratory tests. Furthermore, the obtained results and further information obtained by investigations would lead to the selection of the more appropriate intervention techniques.

A literature review on this topic shows that several classifications were already proposed, mainly depending on the final aim to be pursued. A more simple classification is based on the survey of masonry façade and it can be found on classical manuals of restoration [Carbonara, 1996; Giuffrè, 1990], while further divisions consider the seismic vulnerability of buildings and structures [AA. VV., 2006a,b, 2008]. Differently, considering a greater number of variables leads to a more complex classification [Binda *et al.*, 1999], which involves several goals.

A first classification of the existing masonries can be drawn on the basis of resisting elements [Carbonara, 1996] and of mechanical models [Giuffrè, 1990], that interpreter their overall behaviour. On the basis of the first aspect four main categories can be identified:

- stone masonry;
- brick masonry;
- raw brick masonry;
- rubble masonry;

Furthermore, under each item, a second order of division consider the assembling modality of these structural elements.

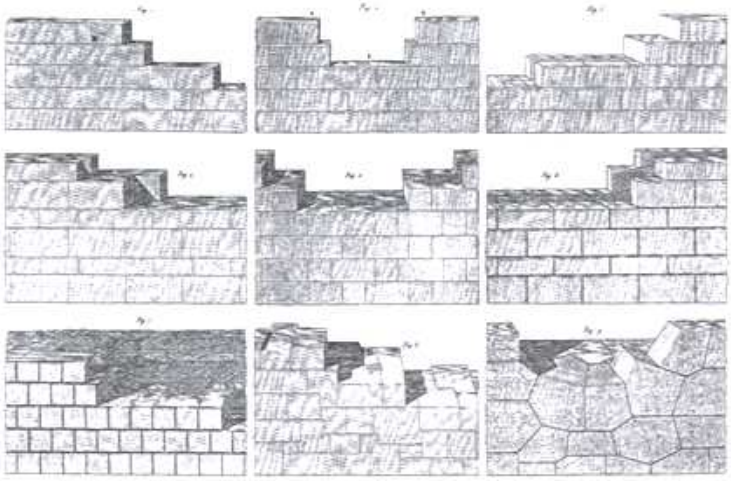

Figure 1.1: Examples of stone masonry made by blocks [Carbonara, 1996].

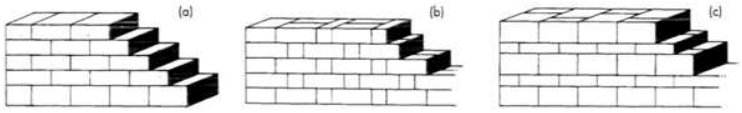

Figure 1.2: Examples of stone masonries made by squared blocks [Carbonara, 1996].

In the light of the final aim of the present research, involving the study of stone masonries, this category can be further divided as follows and as presented in figure 1.1:

- masonry with blocks with regular shape (ashlar masonry);
- masonry with blocks with irregular shape (rubble masonry);
- dry masonry;
- regular blocks or cobblestone with mortar;

Moreover, several mixed masonries are characterized by the presence of more than one material or by different composition on the masonry depth (figure 1.2) or still stone in-filled frames. Furthermore, as a consequence of the irregularity of stones, several construction system developed and, despite the detailed subdivisions, this can results in a difficult cataloguing of an existing masonry.
A similarly, further classification [Binda *et al.*, 2000d] consider the masonry texture and propose a first division on the basis of this element (figure 1.3).

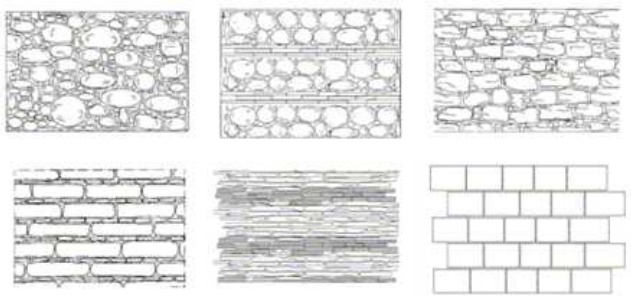

Figure 1.3: Examples of different textures [Binda *et al.*, 2000d].

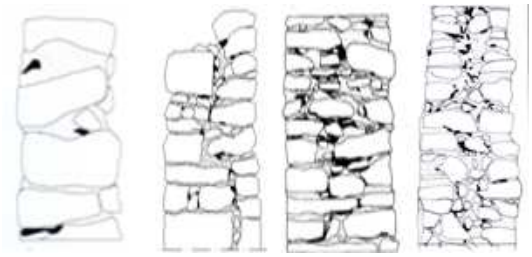

Figure 1.4: Classification of different cross sections of stone masonry: single-leaf, double-leaf without and with interlocking, three leaves [Binda, 1999].

However, further studies [Abbaneo *et al.*, 1996a; Binda and Penazzi, 2000; Binda *et al.*, 1999, 2006; Cardani, 2003; Egermann, 1993] also underlined the wide importance to characterize the transversal section of the investigated masonry. In fact, this aspect became one of the discriminating elements to identify the mechanical behaviour of the considered structural element. As a consequence, on the basis of this division, possible strengthening interventions may also be identified.
In the light of this relevant topic, Binda and Penazzi [2000] proposed an in-depth classification of the stone masonries. This identification is based on the survey of the leaves on the cross section of a wall. The most typical examples of transversal sections are presented in figure 1.4. Based on this classification, the main identified masonry typologies and their characteristics are:

- *Single leaf:* stone elements are bound together using mortar and single stones are disorderly disposed. Stones elements may be characterized by irregular shapes and the mortar joints are normally thick and horizontally or sub-horizontally disposed. Otherwise, stone elements can be regular, staggered and disposed on horizontal courses.

- *Double-leaf:* two different layers can be identified on the cross section. Nevertheless, this typology can be differentiated in two further sections:

  - accosted leaves, they are completely separated by a vertical joint, that can be made by mortar or voids;
  - interlocked leaves, where stones of subsequent courses of opposite layers are slightly overlapped.

- *Three-leaf:* two load-bearing external leaves with higher thickness and an internal core comprised stone fragments, normally on incoherent form and without any bound element. Thick mortar bed joints are horizontally disposed on external layers. In some cases, a transversal connection is provided by irregularly disposed and through passing elements.

Starting from this identified typologies, a recent and joined study between the Polytechnic of Milan and the University of Padova [Gardin, 2007] comprehends a general classification of a very large number of historical stone masonry buildings, considering their typical cross section among several further aspects. The Polytechnic of Milan developed first a data-base [Binda *et al.*, 1999] involving numerous study-cases collected during several years. This large collection was completed with further national [Polytechnic of Milan, 2004] and international [BAM, 2004; Bosiljkov, 2004a] study-cases, as well as with results of experimental campaigns [Binda *et al.*, 2004;

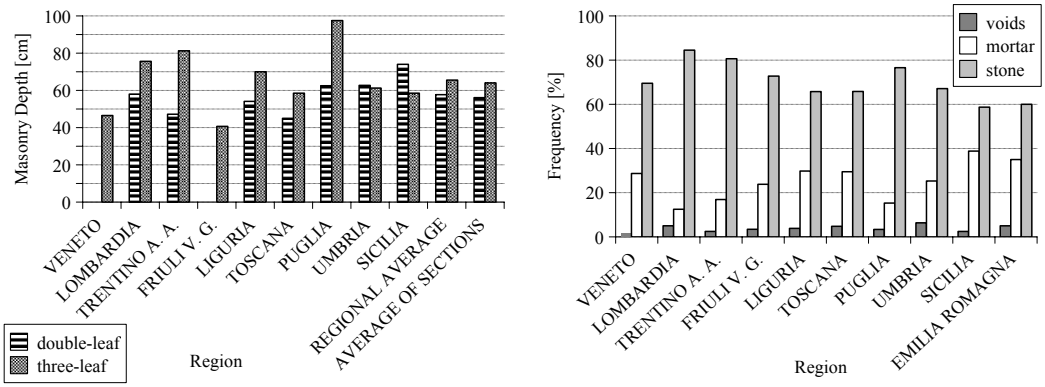

(a) **(b)**

Figure 1.5: Percentage of materials on typical cross sections (left) and kind of transversal typology (right).

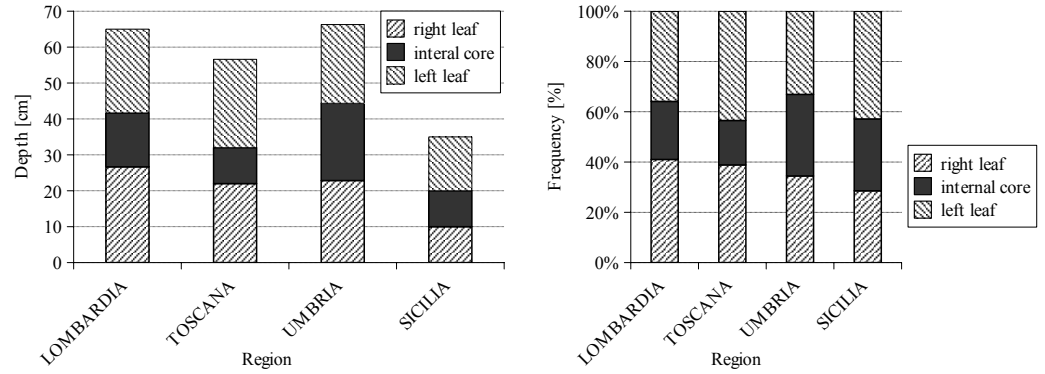

(a) **(b)**

Figure 1.6: Typical depth of each leaf (left) and percentage on the overall cross thickness (right).

Toumbakari *et al.*, 2003; Valluzzi, 2000]. Part of the main results are presented in figure 1.5 and figure 1.6.
As the chart clearly shows, double-leaf and three-leaf stone masonry are similarly distributed on each region with a limited predominance of this last case (figure 1.5a). Figure 1.5b indicates as the average percentage of voids settles at about 6%, while that of mortar range between 12% al 39%. As a consequence, the presence of stones settles in an interval between 60% and 80%. Furthermore, the thickness of both external layers is similar (figure 1.6a) and also their percentage on the overall thickness of the masonry is about constant (figure 1.6b).

As well described and represented by Giuffrè *et al.* [1993], the most common failure mechanisms for the three-leaf stone masonry are constituted by the separation of external layers and the out-of-plane failure of these elements (figure 1.7).

Furthermore, these mechanisms were confirmed also by experimental studies [Binda *et al.*, 2006; Valluzzi, 2000; Vintzileou and Tassios, 1995] and in-situ investigations [Beolchini *et al.*, 1997b; Chiostrini and Vignoli, 1994; Corradi *et al.*, 2002]. The earthquake occurred on Abruzzo (April 6^{th}, 2009) proved once again the reliability of these observations (figures 1.8 and 1.9).

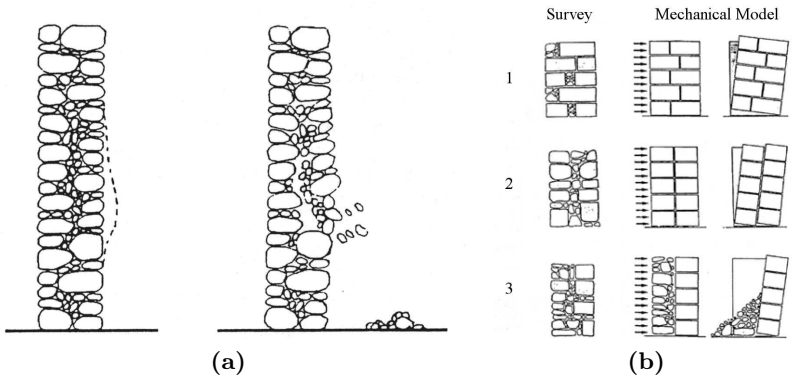

Figure 1.7: Out-of-plane failure (left) and simplified models (right) for multi-leaf stone masonry walls [Giuffrè *et al.*, 1993].

This collection of data, besides the analysis of the typical cross sections and the survey of different masonry typologies, involved also the study of the physical, chemical and mechanical characteristics of the employed materials, namely stones and mortar. The most common characteristics and their average values are presented in table 1.1 and table 1.2 (values obtained from Gardin [2007]).
As it can be seen, stones are characterized by a great dimensions of each single element and by high values of both the compressive (σ_{max}) and tensile strength (f_t). On the other hand, the mortar joints are very thick and they are characterized by a low compressive strength.
However, the experimental campaigns presented in section 1.2 validated the empirical observation that the overall strength of the multi-leaf stone masonry is mainly related to the global mechanisms of failure, namely separation of layers and out-of-plane damages, rather than to the strength of the single materials.
This way, the strengthening technique (compare §1.1.2) to be employed in order to avoid a structural damage should mainly consider the above mentioned mechanisms of failure and the main mechanical characteristics of historical materials above presented.

Table 1.1: Characteristics of most common stones in three-leaf stone masonry.

lithotype	Dimensions [cm]	Porosity [%]	Coeff. of absorp. [%]	σ_{max} [N/mm^2]	f_t [N/mm^2]
limestone	> 15	1.93	0.4	66.64	2.64

Table 1.2: Characteristics of most common mortar in three-leaf stone masonry.

Composition	Thickness of mortar joints [cm]	Porosity [%]	Coeff. of absorp. [%]	σ_{max} [N/mm^2]	f_t [N/mm^2]
Lime with calcareous binders	$1 \div 4$	21.93	12.09	3.34	1.48

(a) San Michele Arcangelo Church, Celano

(b) Castelnuovo village

(c) Castelnuovo village

Figure 1.8: Examples of separation of external layers on multi-leaf masonries after Abruzzo earthquake (April 6^{th}, 2009).

(a) Sant'Antonio de Nardis Church

(b) Santo Stefano Church, in Castelnuovo

(c) Castelnuovo village

Figure 1.9: Examples of out-of-plane failure on multi-leaf masonries after Abruzzo earthquake (April 6^{th}, 2009).

1.1.2 Strengthening interventions

Several techniques to strength different kind of masonry were developed during the years. Nowadays, both the traditional and innovative materials are currently employed in numerous ways to achieve this aim. The most common interventions, also advised on guidelines [D. M. 12/10/2007, 2007; ICOMOS/ISCARSAH, 2003; ISO 13822, 2006] and codes currently in force at national and international level [CEN - EN 1998-3, 1998; D. M. 14/01/2008, 2008], should firstly respect important requirements to guarantee the effectiveness and the feasibility of these techniques. These aspects are listed below:

- recovering of safety conditions at structural level;
- improvement of mechanical characteristics (not always easily pursuable since this depends on the initial condition of damage);
- mechanical and structural compatibility of materials and techniques to guarantee a minimum alteration of original characteristics;

- chemical and physical compatibility of materials;
- durability (employment of specific materials and technologies);
- reversibility and application of repairable interventions.

The present research will focus on strengthening interventions aiming at consolidating masonries and, among several typologies, particularly stonework. Actually, in both cases a fundamental topic is represented by the visibility of interventions. In effect, in several Cultural Heritage buildings strengthening should be not visible because of their artistic value, due to the presence of frescos, stuccoes or particular masonry textures.
The second fundamental requirement, which becomes indispensable in several cases, is represented by the reversibility of the interventions. This means that there should be the possibility to remove this, without any further damage to the structure, and substitute it with new and innovative technologies.
These topics also clarify since the study of strengthening interventions is an opened issue and their discussion is currently very active.

The most common techniques, applied to different structural masonry typologies and cited on the guidelines and codes above mentioned, are summarized in the following:

- *Substitution of deteriorated elements:* through local rebuilding and using new elements.This technique is normally applied in combination with further interventions;
- *Injection:* widely employed technique, realized through the introduction of fluid admixtures on multi-leaf masonries. The injection is realized using holes drilled in the mortar joints and aims at filling voids, stitching cracks and binding together the external leaves of multi-leaf masonries;
- *Deep repointing of mortar joints:* consists in the removal of the deteriorated mortar and its substitution with new materials, which have better characteristics in terms of strength and durability. It aims at increasing the overall strength and durability of the masonry;
- *Transversal ties:* applicable to multi-leaf masonries in order to bind opposite external layers through the insertion of steel bars in the masonry thickness. This technique aims to limiting the local separation of leaves;
- *FRP fabric:* recent technique which employs innovative materials. It has an increasing diffusion and it is realized through the application of strips of Fiber Reinforced materials (carbon, glass, aramid, etc.) with structural adhesives (resins). This technique has a limited applicability to stone masonry, since its natural irregularity of the surfaces.

The application of these techniques is limited to masonry elements and structures, without considering further problems related to the foundations or connections between vertical and horizontal elements.

On the light of observations developed on section 1.1.1 about the mechanisms of failure of the masonry typology investigated in this research study, namely three-leaf stone masonry, the most appropriate intervention technique are the injection of mixture, the repointing of mortar joints ans the insertion of transversal ties. All these

strengthening methodologies were deeply studied during last decades [Binda *et al.*, 1997b; Corradi *et al.*, 2008; Modena and Valluzzi, 2006, 2007; Valluzzi, 2000; Valluzzi *et al.*, 2005] and they are nowadays normally applied for structural restorations.

One of the most effective techniques able to limit the failure mechanisms of the multi-leaf masonry is represented by the grout injection. This strengthening methodology exploits the presence of voids inside the masonry to improve its overall behaviour. In fact, the injected admixture bind together the incoherent fragments contained in the masonry core, allowing an increase of the compressive strength. However, the main characteristic of this technique is given by its capability to bind the opposite external layers. Indeed, this consequence allows to improve the resistance of this masonry typology to the out-of-plane solicitations. As a consequence, the local problems due to the separation of layers, mainly caused by seismic loads, can be avoided or delayed.
However, this is one of the most complicate interventions, mainly because of the compatibility between the injected grout and the historical materials. Past studies involved the employment of different admixtures, such as resins [Doglioni *et al.*, 2009; van Gemert, 1987], materials with cementitious matrices [Toumbakari, 2002; Vintzileou and Tassios, 1995] or lime-based [Valluzzi, 2000; Vintzileou and Miltiadou-Fezans, 2008].

Recent studies carried out at the University of Padua [Bresolato and Pasin, 2008; da Porto, 2000; Valluzzi, 2000] in collaboration with Tassullo S.p.A. (Tassullo, Trento; `http://www.tassullo.it`) led to design and select a grout with a high compatibility with the main physical, chemical, rheological and mechanical characteristics identified by the great number of in-situ investigation presented in section 1.1.1.
The studies developed by Valluzzi [Valluzzi *et al.*, 2003; Valluzzi, 2000] led to choose a hydraulic lime-based grout, which exhibited the best characteristics, according to the above mentioned criteria.

All the specifications concening the considered strengthening technique, such as effects of injection, pressure and further detailed requirements of materials for admixtures can be found in these researches [Bresolato and Pasin, 2008; da Porto, 2005; Valluzzi, 2000].

Finally, the fundamental characteristics of all the grouts employed in different experimental researches and in-situ applications will be presented in section 1.2, where their main values will be related with the overall effects observed on the strengthened elements.

1.1.3 Investigation techniques

Several techniques were developed during the years to investigate the characteristics of the constitutive materials of masonries and whole elements. These methodologies mainly differ because of their degree of invasivity. Normally, the more invasive the tests, the more information and the more reliable data can be obtained [Binda *et al.*, 1997b]. However, different techniques can lead to different results and also less invasive investigation methodologies can provide important information. A first general classification is given in the following:

- Destructive tests;
- Minor Destructive Tests (MDT);
    - laboratory tests

  - in-situ investigations
- Non-Destructive Tests (NDT);
  - passive tests
  - active tests

The first grouping allows to quantify main mechanical characteristics of the materials and structures, such as compressive and tensile strength, elastic and shear moduli or failure mechanisms, as well as their dynamic characteristics, such as fundamental frequencies, damping factors and vibrational modes. The destructive investigations which allow the achievement of these results involve both the quasi-static tests, namely compression and shear compression experiments, and dynamic tests, which comprehend shaking table and pseudo-dynamic experiments. These arguments will be widely discussed in sections 1.2 and 1.3 respectively.

The Minor Destructive Tests (MDT) can provide only qualitative informations about the investigated structures. Few examples are the realization of core samples, visual inspections or sampling of materials. However, one of the most important and applicable MDT techniques to multi-leaf stone masonry are the flat-jack tests. This investigation method can provide information about the compressive strength and the elastic modulus of the analyzed element as well as the mechanical properties of the external load-bearing leaves of multi-leaf stone masonry. Since their low invasivity, these investigations are of great interest. Furthermore, a subsequent calibration of the obtained results with those achieved with further destructive tests is under developing [Baronio *et al.*, 2003; Binda and Tiraboschi, 1999; Binda *et al.*, 1997b, 2000c, 2003c]. This will result in both the improvement and diffusion of this investigation methodology.

Further interesting investigations, due their null invasivity, are the Non-Destructive Tests (NDT), such as sonic and ultrasonic or radar investigations, thermography and static or dynamic monitoring. Of all, the technique of the sonic investigations was employed since nineties to evaluate the quality of masonry [Abbaneo *et al.*, 1996b; Schuller *et al.*, 1995] but this was used also to evaluate the effectiveness of strengthening interventions [Binda *et al.*, 1997a; Schuller *et al.*, 1994; Valluzzi, 2000]. This method is based on the measurement of the velocities of sonic waves through the investigated specimen.

A common employment of this technique, as above mentioned, allows to evaluate the masonry quality. Nevertheless, several different classifications were proposed depending on the measured velocities. In fact, the higher the sonic velocities, the lower is the presence of voids and the better the masonry quality. Forde *et al.* [1985] and Berra *et al.* [1992] proposed two different categories, summarized in table 1.3, according to different ranges of sonic velocities.

Table 1.3: Classifications of masonry quality according to sonic velocities.

Masonry quality	Forde *et al.* [1985] [m/s]	Berra *et al.* [1992] [m/s]
good	>2500	>2000
discreet	1500 ÷ 2500	1000 ÷ 2000
poor	<1500	<1000

Furthermore, direct and tomographic sonic tests are nowadays also applied to evaluate the goodness and the effectiveness of grout injection on multi-leaf masonries [Berra *et al.*, 1988, 1992; Binda *et al.*, 2000a; Casarin *et al.*, 2007]. In fact, the main conclusions can be drawn starting from the comparison of the results obtained before and after the realization of the strengthening intervention. The wide presence of voids before injection leads to low overall velocities (figure 1.10a), while the intervention, using grout, allows to fill these, obtaining a more homogeneous section with higher velocities (figure 1.10b).
In conclusion, in a preliminary phase, sonic tests permit to check the injectability of masonry, detecting voids and further defects or peculiarities not visible from outside. Moreover, this investigation technique allows to validate the effective penetration and diffusion of the admixtures on the inner core of multi-leaf masonries after the strengthening. Lastly, also the homogeneity of the intervention can be also verified.

1.2 Quasi-Static Tests

The characterization of masonry structures under investigation can be developed at different levels. Actually, considering masonry as a composite material, where mortar, bricks and stones are the usual components, is a common acknowledgement. Furthermore, when strengthening interventions are considered, several other materials influence the overall behaviour of original structure. For this reason, studies should be developed both on single components and on composite elements.

On the basis of both the general overview, presented in section 1.1, and the aim of the present research, three-leaf stone masonry strengthened using injection of hydraulic lime-based grout are considered. A previous research, developed at the University of Padua [Valluzzi, 2000] refined the best material to be injected, according to rheological, chemical and physical requirements. Furthermore, mechanical tests on materials and structures were also performed.

Starting from the results obtained from these studies, this section aims at providing a general overview on further similar experimental campaigns, involving also different materials or masonry typologies. The attention will be focused on researches based on quasi-static tests, in order to collect methodologies and results to validate part of the experimental campaign developed in this study.

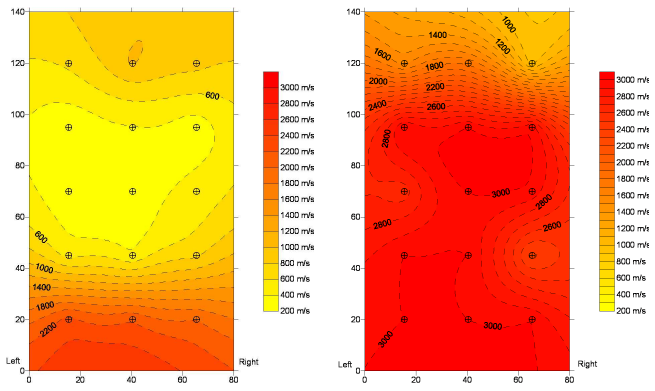

(a) **(b)**

Figure 1.10: Example of comparison of sonic velocities before (left) and after (right) injection of lime grout [Valluzzi, 2000].

Experiments aiming at investigating the compressive, shear and tensile characteristics of single structural elements, namely masonry piers, are considered. Studies involving compression tests provide important information about mechanical properties, such as compressive strength and deformation properties as well as failure modes. On the other hand, further testing methodologies supply fundamental information of the in-plane lateral strength, that can be related to the seismic resistance, and of other mechanical characteristics.

1.2.1 Compressive behaviour

A simple experimental test is constituted by compression experiments on masonry panels. This methodology allows to deepen the mechanical characteristics of considered specimens, particularly their elastic modulus and compression strength but also their Poisson's ratio and the deformation capability. Finally, the failure mechanisms can be also investigated.

In the following, some researches, carried out to evaluate the effectiveness of strengthening through injection of different grouts, are presented. The experimental campaigns are divided considering laboratory and in-situ experiments. Actually, some differences should be underlined between these categories. Among the most relevant aspects one should note as laboratory tests permit a more exact control of conditions but, on the other hand, specimens are often reproduced, while in-situ investigations allow to test existing structures and elements.

The laboratory experiments are normally carried out under a system constituted by a test frame and a jack (figure 1.11a). These investigations can be performed under displacement or load control and they often lead to the failure of specimens. In some cases, as for few campaigns presented in the following, the specimens are only damaged, permitting a repairing intervention, and subsequently led up to failure. Displacement control, even if less representative of the real situation than load control, allows to investigate the post peak phase, when the imposed displacement increases while the load decreases.
In-situ tests are more difficult to perform, since the testing system should be reproduced in the selected location. A panel is isolated from the whole structure and a distribution beam is posed to diffuse the load applied through actuators. In some cases only a compression test is carried out (figure 1.11b) and the panel is loaded up to failure. Often, a compression investigation constitutes the preliminary phase of a shear compression test. In this case, the specimen can be cyclically loaded, remaining in the elastic range, to study its elastic properties. After this phase the lateral load is imposed (compare §1.2.2)

1.2.1.1 Experimental campaigns

Tomaževič [1992] carried out an experimental campaign on two layered rubble stone masonry walls, employing materials typical of the Slovenian region. Panels had an irregular texture and thick mortar joints. A cement-based grout was employed, without and with addition of hydrophobic additives to reduce the environmental effects and the capillarity activity. The injection operations were executed at an about constant pressure of 0.2bar on holes spaced of 0.5-1.0m. These holes were drilled on the mortar joints and wetted before the injection. Main results are reported in table 1.4. Furthermore, the compressive strength of the injected grout is reported

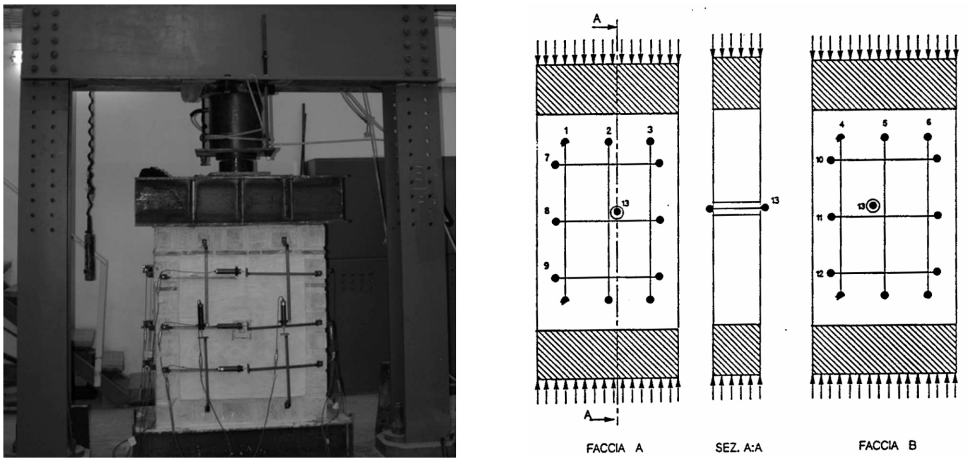

(a) [Vintzileou and Miltiadou-Fezans, 2008] **(b)** [Bettio *et al.*, 1993]

Figure 1.11: Examples of laboratory (left) and in-situ (right) compression test.

(f_{gr}). The tests exhibited the clear possibility to bound together the cracked parts of the stone masonry, obtaining a solid structure.

Table 1.4: Experimental results obtained by Tomaževič [1992].

Type of masonry	Description	f_{gr} [N/mm^2]	f_c [N/mm^2]	E [N/mm^2]
Uncoursed stone,	original	-	0.5	197
two layers, muddy sand	grouted	33	1	825
Uncoursed stone,	original	-	0.7	390
two layers, clean sand	grouted	33	2.14	2744

A wide series of in-situ tests was performed by Modena [Bettio *et al.*, 1993; Modena and Bettio, 1994] with the aim to compare the influence and the effectiveness of interventions through injections and jacketing. The considered panels are mainly constitute by two-leaf masonry with any transversal connection. Different grout were employed, mainly based on hydraulic lime and quicklime, hydraulic lime with crushed bricks and cementitious additives (without any sulphate). The injection operations were realized at low pressure (0.5bar) with a preliminary washing with water. The mesh was regular, considering 10 holes per squared meter, and it was realized only in one side of the wall. The strengthening increased of about 50% the compressive strength of the original masonry. The results are summarized in table 1.5. Elastic modulus are computed among different stress ranges[1].

Vintzileou and Tassios [1995] performed compression tests on three-leaf stone masonry with squared elements. The 8 specimens tested under compression had an overall dimension of 70x50x120cm; 2 of these were provided of a transversal interlocking (samples 1, 3; figure 1.12a), while any connection was inserted in the remaining specimens (samples 2, 4÷8; figure 1.12b). The high void presence allowed

[1] E_1 between 0.20[N/mm^2] and 0.40[N/mm^2]; E_2 between 0.40[N/mm^2] and 0.80[N/mm^2]; E_3 between 0.80[N/mm^2] and 1.20[N/mm^2];

Table 1.5: Experimental results obtained by Modena and Bettio [1994] (all quantities are expressed in [N/mm^2]).

		Before strengthening			After jacketing				After injection			
wall		E_1	E_2	$f_{wc,0}$	E_1	E_2	E_3	$f_{wc,s}$	E_1	E_2	E_3	$f_{wc,s}$
C1	A								210	130	70	1.50
	B								180	190	10	
C2	A								470	240	130	1.46
	B								530	500	400	
C3	A								800	430	250	1.71
	B								670	450	320	
C4	A	360	60	0.70					480	370	90	1.15
	B	2300	240						480	500	130	
C5	A							0.75				
	B											
C6	A	200	160	0.80	10400	7900	6700	1.85				
	B	550	400		11200	10800	9400					
C7	A				9300	10400	8600	1.8				
	B				9600	9400	6400					
R1	A	800	1100	0.90					3500	2500		1.00
	B	130	50						3400	2600		
R2	A	90	50	0.60	5300							
	B	240	100		19700							

the injection at a low pressure (0.07bar) of two cement grouts characterized by different compression strength, namely 30N/mm^2 (type A) and 13N/mm^2 (type B). The main damage involved sub-vertical cracks on the main sides of the specimens but also vertical cracks at the interface between internal core and external leaves, at bout the 50% of compressive strength. This caused wide out-of-plane displacements, as a consequence of a buckling effect, which lead to a premature failure. The grout injection demonstrated the ability to delay this mechanism, that manifested close to the failure. Nevertheless, the injection of cement-based grouts caused also a wide increasing of the elastic modulus of strengthened panels. Finally, despite the widely different compressive strength of grouts, injected samples manifested similar compressive strength. The results are summarized in table 1.6.

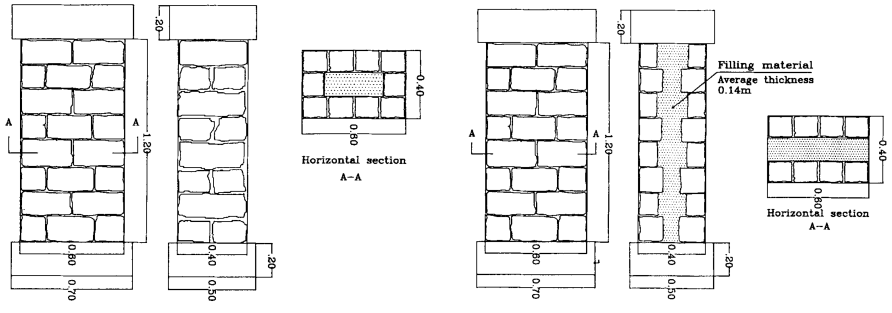

(a) With lateral interlocking **(b)** Without lateral interlocking

Figure 1.12: Specimens tested by Vintzileou and Tassios [1995].

Toumbakari and van Gemert carried out an experimental work [Pisano, 1999; Toumbakari and van Gemert, 1997] on four multi-leaf stone masonry panels. Specimens,

Table 1.6: Experimental results obtained by Vintzileou and Tassios [1995].

wall	grout	$f_{wc,0}$ [N/mm^2]	$f_{wc,s}$ [N/mm^2]	$\frac{f_{wc,s}}{f_{wc,0}}$ -	$E_{wc,0}$ [N/mm^2]	$E_{wc,s}$ [N/mm^2]	$\varepsilon_{wc,0}$ -	$\varepsilon_{wc,s}$ -
1	A	2.10	3.10	1.48	7000	6250	104	60
2	-	1.30	-	-	2706	-	-	-
3	A	2.40	4.30	1.79	5000	5971	141	110
4	A	1.60	-	-	4442	-	80	-
5	A	1.70	4.20	2.47	5670	7778	280	120
6	B	1.35	4.05	3.00	5625	8438	58	100
7	A	-	3.70	-	-	15413	-	90
8	B	-	3.00	-	-	3333	-	90

tested in laboratory, had overall dimensions of 60x120x40m. The external layers had calcareous stones and incoherent fragments in the central layer. Three different grout typologies were applied and injected at low pressure (0.08÷0.1bar) with a regular and dense mesh (holes at 20÷25cm). Also the influence of transversal connection was investigated, since in one panel (specimen 3) they were provided (4÷5 per m^2). The survey detected a percentage of about 15% of voids, allowing injection.
First damages occurred on main sides of samples and, only subsequently, cracks developed also on lateral side, at the interface between external layers and internal core. Furthermore, cracks mainly developed on mortar joints rather than of stones. The presence of transversal connections widely limits the out-of-plane deformation, even if the compression strength appeared very close to that of other samples. Finally, also the employment of grout with different strengths has a very limited influence on the overall behaviour of injected walls. Result are summarized in table 1.7.

Table 1.7: Experimental results obtained by Toumbakari and van Gemert [1997].

wall	f_{gr}	$f_{wc,0}$ [N/mm^2]	$f_{wc,s}$ [N/mm^2]	$E_{wc,0}$ [N/mm^2]	$E_{wc,s}$ [N/mm^2]	$\varepsilon_{wc,0}$ %	$\varepsilon_{wc,s}$ %
1	6.4	2.02	-	3670	-	1.42	-
2	14.6	2.1	3.3	4400	4500	1.6	2.3
3	5.2	2.6	3.5	5900	4000	1.7	2.4
4	5.2	2.7	3.3	5200	1900	2.1	3.5

Vignoli performed several in-situ compression tests in some sites located in Tuscany (Pieve Fosciana, S.Anastasio, Pognana, Canova, Castelletto e Merizzo). Some specimens were loaded up to the elastic limit, then unloaded, to realize a strengthening intervention, and finally loaded up to the failure. Other samples, as reference specimens, were only loaded up to the failure (samples in Pognana and S. Anastasio). The employed techniques were jacketing and grout injection [Modena, 1999]. The masonry was mainly constituted by two accosted leaves with irregular stones and cobblestones. The overall thickness was ranging between 44÷70cm, while hight and width ranged between 167÷205cm and 84÷101cm respectively. The applied techniques showed a considerable increase of both the strength and elastic modulus, as reported in table 1.8 (R=Repaired; C=Compression).

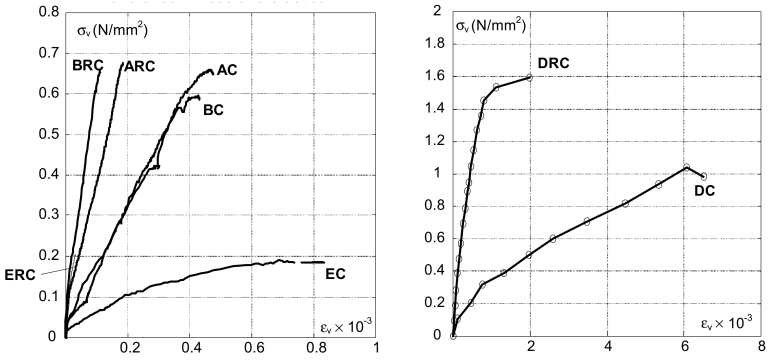

(a) **(b)**

Figure 1.13: Stress-strain relationship of tested specimens [Modena, 1999].

Table 1.8: Experimental results obtained by Vignoli [Modena, 1999].

	intervention	σ_{el} [N/mm^2]	σ_{max} [N/mm^2]	$E_{1/3}$ [N/mm^2]
Pieve Fosciana		0.654	-	1468
(A)	jacketing	0.698	-	3051
Pieve Fosciana		0.595	-	1333
(B)	jacketing	0.788	-	5169
Pognana		0.145	-	250
(E)	injection	0.205	-	4667
Pognana		0.158	1.041	376
(D)	injection	0.348	1.596	3012
S. Anastasio		0.158	0.236	1921

Valluzzi [2000] performed an experimental campaign on 16 three-leaf stone masonry panels to study the influence of different strengthening techniques, namely lime grout injection, repointing and insertion of transversal steel ties. In all cases, for grout as well as for mortar, lime-based materials were employed to ensure a better overall compatibility with historical materials. Nevertheless, two different types of admixtures were employed for the strengthening interventions. The experimental observation and results, reported in table 1.9, demonstrate the capability of injections to improve the mechanical characteristics of the multi-leaf masonry. Particularly, the out-of-plane deformations could be limited and the compressive strength improved. Moreover, the elastic properties were only slightly influenced by the injection, without a significant increasing of the elastic modulus. Further techniques manifested a lower influence on the strength. Nevertheless, tying allowed to avoid brittle failure modes, while repointing increased the durability of the considered element. The combination of these induced the best results in terms of overall behaviour of the specimens. Finally, results confirmed that the employment of different grouts, having higher mechanical properties, does not influence significantly the overall strength of the walls.

Toumbakari [2002] carried out an experimental campaign on nine three-leaf masonry specimens tested under compression. Four of these were realized using bricks, while stones were used for the remaining samples. The overall dimensions of all the

Table 1.9: Experimental results obtained by Valluzzi [2000].

Panel	intervention	$f_{wc,0}$ [N/mm^2]	$f_{wc,s}$ [N/mm^2]	$E_{wc,0}$ [N/mm^2]	$E_{wc,s}$ [N/mm^2]
5I1	injection	1.45	2.49	2390	2273
6I1	injection	1.95	2.49	2029	3093
13I1	injection	-	2.54	-	3992
1I2	injection	1.97	2.57	1450	3449
8I2	injection	1.91	1.82	1559	2367
16I2	injection	-	2.48	-	1223
2T	tying	1.95	1.77	1504	1789
9T	tying	1.65	1.34	2058	1932
11T	tying	-	1.26	-	474
10RT	repointing+tying	-	0.88	-	110
12I1T	repointing+tying	-	2.59	-	1336
14I1R	injecting+repointing	-	2.14	-	1617
17I1RT	injecting+tying+repointig	-	3.06	-	1772
3R	Repointing	0.99	1.34	-	538
7R	Repointing	1.50	1.17	1863	1781
15R	Repointing	-	1.32	-	395

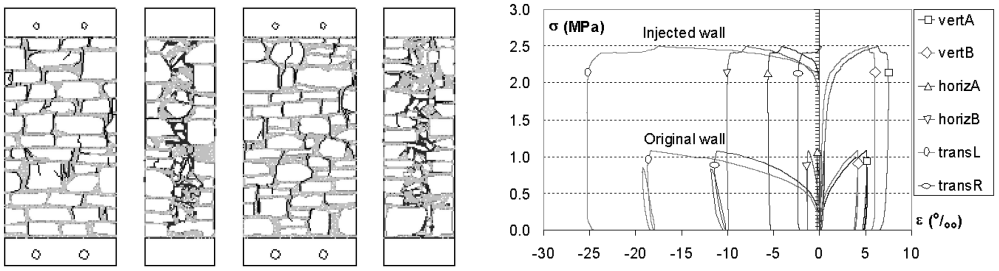

(a) **(b)**

Figure 1.14: Examples of specimen and stress-strain relationship [Valluzzi, 2000].

specimens were 60x40x120cm. Furthermore, different grouts were studied and injected, with similar injectability properties but different mechanical characteristics and reduced Portland cement content. The specimens were tested firstly in unstrengthened conditions and, after the interventions, they were subjected again to compression up to failure. The experimental observations confirmed that the main failure mechanism, in both cases, is the consequence of the bucking of external layers. Furthermore, results, showed in figure 1.15 and presented in table 1.10, highlight the capability of grout injection to improve the overall strength of the wall, even if the increase seems to be independent from the mechanical properties of injected grout. Differently, the stronger the grouts, the higher the increasing of elastic modulus of masonry samples. Finally, the great influence of different employed materials is mainly due to the shear bond strength of the grout-substratum interface.

At the University of Minho, Oliveira and Lourenço [2006] carried out first tests on three-leaf stone masonry walls. These experiments are part of a wide ongoing experimental campaign to deepen the mechanical behaviour of this masonry typology. Furthermore, several strengthening techniques will be investigated. First results, presented in table 1.11, are referred to unreinforced specimens and samples

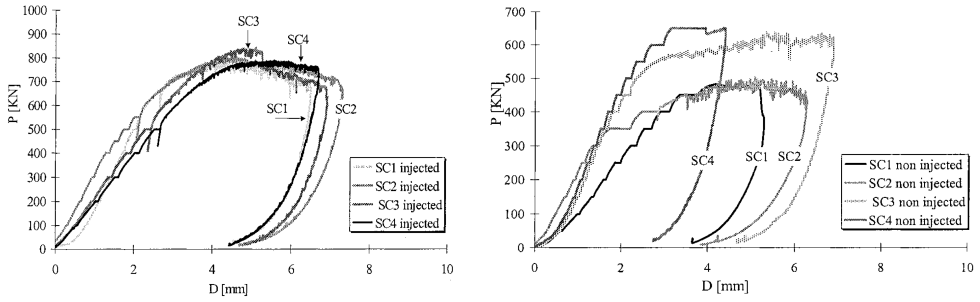

(a) Before injection **(b)** After injection

Figure 1.15: Load-vertical displacement curves of stone samples [Toumbakari, 2002].

Table 1.10: Experimental results obtained by Toumbakari [2002].

Panel	$f_{wc,0}$ [N/mm^2]	$f_{wc,s}$ [N/mm^2]	$E_{wc,0}$ [N/mm^2]	$E_{wc,s}$ [N/mm^2]	$\varepsilon_{wc,0}$ ‰	$\varepsilon_{wc,s}$ ‰
BC1	-	5.04	-	2238.2	-	2.42
BC2	2.41	3.15	729.6	1564.9	3.12	2.54
BC3	2.09	2.91	1018.3	1404.8	1.85	1.55
BC4	2.18	3.00	1097.6	1404.4	2.34	2.94
BC5	2.28	3.86	1144.9	1170.2	2.31	3.14
SC1	2.02	3.25	720.4	1622.2	1.42	3.55
SC2	2.09	3.36	1138.7	1558.6	1.65	2.33
SC3	2.65	3.51	1374.8	1187.6	1.73	2.45
SC4	2.71	3.29	1443.3	1014.5	2.11	3.49

strengthened through the insertion of transversal GFRP ties. These results highlighted that the application of these ties allow to sustain a load increasing of about 70% with reference to the unstrengthened conditions. Furthermore, the most typical failure mechanism, namely out-of-plane buckling of outer layer could be widely limited, allowing the development of vertical cracks, as in the case of a monolithic material.

Table 1.11: Experimental results obtained by Oliveira and Lourenço [2006].

Panel	f_{wc} [N/mm^2]	Panel	f_{wc} [N/mm^2]
1W1	2.40	2W2	3.30
1W2	1.70	2W3	2.60
2W1	1.40	2W4	3.50

Binda *et al.* developed an experimental campaign parallel to a numerical investigation [Binda *et al.*, 2006; Pina-Henriques and Lourenço, 2003], in order to deepen the knowledge of both the stress distribution and load-transfer mechanisms on three-leaf stone masonry. The whole program involved compression tests also on each singular leaf, while the results of the compression tests on whole masonry panels are reported hereafter (table 1.12). Figure 1.16 shows the local behaviours of each single layer during the test of two samples. Experimental observations led to note the influence of interlocking between external leaves and internal core on specimens. Furthermore, different stone typologies led to different failure modes.

Table 1.12: Experimental results obtained by Binda *et al.* [2006].

Panel	f_{wc} [N/mm^2]	E_{wc} [N/mm^2]
NS3	5.8	1770
SS33	>15.1	2940
NO3	6.4	2085
SO3	>15.1	2725

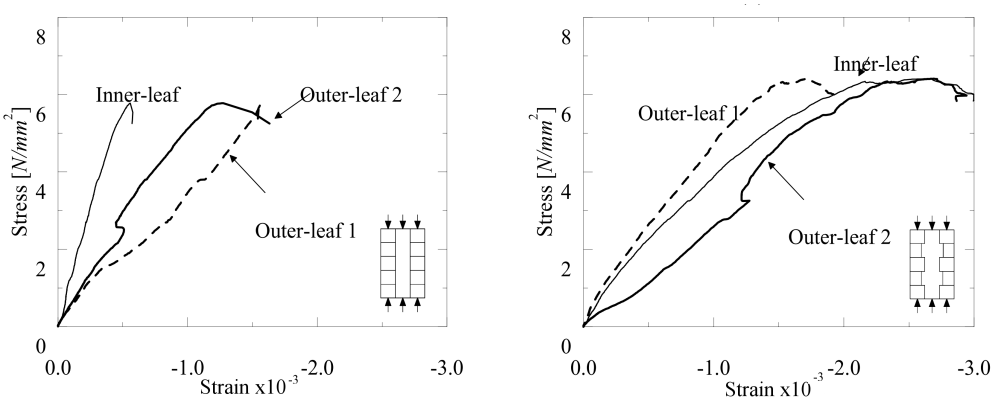

(a) straight collar joints **(b)** keyed collar joints

Figure 1.16: Stress-strain curve on different masonry layers [Binda *et al.*, 2006].

Vintzileou and Miltiadou-Fezans [2008] carried out a further laboratory campaign to study the typical strength of a three-leaf stone masonry with courses of solid bricks. The program was developed to study the effectiveness of ternary grouts (cement, pozzolan and hydrated lime) and hydraulic lime-based grouts on the compressive strength of masonry. These mixes were expressly designed to be applied in the case of panels with frescos, mosaics and decorative elements, with the aim to avoid any problem of durability and compatibility, as observed with high contents of cement. Obtained results, reported in table 1.13, confirmed that the main failure mechanism in compression of this masonry typology is due to an early separation of outer layers. Nevertheless, both ternary and hydraulic lime-based grouts could induce a substantial enhancement of the masonry compressive strength. Finally, further analyses confirmed the capability of these grouts in filling the voids and homogenize the whole masonry.

Table 1.13: Experimental results obtained by Vintzileou and Miltiadou-Fezans [2008].

Masonry texture	$f_{wc,0}$ [N/mm^2]	$f_{wc,s}$ [N/mm^2]	$E_{wc,0}$ [N/mm^2]	$E_{wc,s}$ [N/mm^2]	$\varepsilon_{wc,0}$ ‰	$\varepsilon_{wc,s}$ ‰
three-leaf stone and solid bricks masonry	1.82	3.00	1000	1200	-	1.76
three-leaf stone and solid bricks masonry	1.74	3.75	1440	1550	1.60	2.50
three-leaf stone and solid bricks masonry	2.26	3.73	1500	1300	2.25	3.39

Corradi *et al.* [2008] performed an experimental in-situ campaign on several panels of buildings to be dismantled. The preliminary phase involved compression tests on two panels. These were firstly tested in unstrengthened conditions and, subsequently, again subjected to compression after a combined intervention applying deep repointing and injection. The results are presented in table 1.14.

Table 1.14: Experimental results obtained from compression tests by Corradi *et al.* [2008].

masonry texture	intervention	σ_{max} [N/mm^2]	E [N/mm^2]
Double-leaf roughly cut stone masonry	Unstrengthened condition	0.201	1289
	Deep repointing + grout injections	0.286	4153
Double-leaf roughly cut stone masonry	Unstrengthened condition	0.215	306
	Deep repointing + grout injections	0.286	1770

Galasco *et al.* [2009a] realized a laboratory campaign on double-leaf stone masonry elements subjected to compression. This constitutes a preliminary phase to subsequent dynamic program involving shaking table tests on building models, realized with the same masonry typology. The aim was the mechanical characterization of the structural elements and, for this reason, masonry piers (80x120x32cm) were realized. The compression tests were performed with subsequent cycles at increasing load levels. The final strength of panels is summarized in table 1.15. Data show a limited scattering and values are aligned with other obtained during similar laboratory researches.

Table 1.15: Experimental results obtained by Galasco *et al.* [2009a].

Panel	f_{wc} [N/mm^2]	ε_{wc} ‰	E_{wc} [N/mm^2]
V1	3.09	0.0040	2400
V2	3.14	0.0035	3000
V3	3.76	0.0080	2600
V4	3.18	0.0060	2200
V5	3.13	0.0040	2900
V6	3.36	0.0050	2200

1.2.2 Shear behaviour

The knowledge of both shear and tensile strength appears as fundamental, among other aspects, to deepen the study about the seismic resistance of a building system and to evaluate the effectiveness of strengthening interventions carried out in a structure.
Two different methodologies are currently applied to investigate these aspects: diagonal compression tests and shear compression tests. In the following a brief overview on these testing methodologies is proposed and is not to be intended as exhaustive.

1.2.2.1 Diagonal compression tests

Two different standards were developed to perform diagonal compression tests: ASTM E 519-02 [2002] and RILEM TC 76-LUM [1991].

Testing methods provided by both standards are very similar. Specimens should have a squared shape with a side of about 1.2m. The specimen should be placed rotated of 45° with reference to the horizontal level and the load, vertically applied, is provided along the diagonal of the specimen (figure 1.17a). This configuration induces vertical compression and horizontal tensile stresses in the specimens and, for this reason, the corresponding strains are measured with the aim to obtain a stress-strain relationship. Both codes provide the same method to compute the shear strength of the tested material:

$$\tau_{max} = \frac{\sqrt{2}}{2} \cdot \frac{P}{A_w} \tag{1.1}$$

where P is the vertical applied load and A_w the net area of the specimen. On the hypothesis, proposed by codes, of an homogeneous pure shear stress distribution in the middle of the panel, the tensile strength of the material results equal the shear stress. On the basis of computed stress and strain, also the shear modulus can be obtained as ratio between these quantities. Nevertheless, the hypothesis of homogeneous pure shear stress distribution is not accepted by all the researchers and further formulations were proposed. In the case of experimental tests presented in section 1.2.2.3 one should refer directly to the original work, while hereafter only results are reported and commented.

This methodology, normally applied in laboratory, can be also adopted in the case of in-situ campaigns. In this case a panel is isolated from the whole structure and, differently from that previously described, the testing system is rotated (figure 1.17b) to obtain the same configuration above discussed.

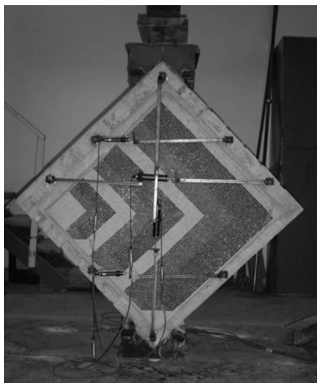

(a) [Vintzileou and Miltiadou-Fezans, 2008]

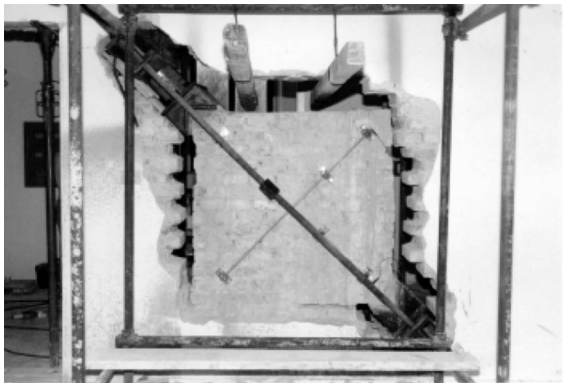

(b) [Corradi *et al.*, 2002]

Figure 1.17: Examples of laboratory (left) and in-situ (right) diagonal compression tests.

1.2.2.2 Shear compression tests

The shear and tensile strength of a material can be investigated employing this second methodology. The technique consists in subjecting a panel to a vertical load, reproducing the precompression level normally acting in a building, which is

kept constant during the whole experiment. After this preliminary phase, a lateral displacement is imposed cyclically at increasing values.
Furthermore, this testing system allows to deepen the knowledge about the stiffness and the energy dissipation capacity of the specimen and this can be interpreted as the structural response to a seismic load (figure 1.18) . Finally the maximum drift capacity can be detected.

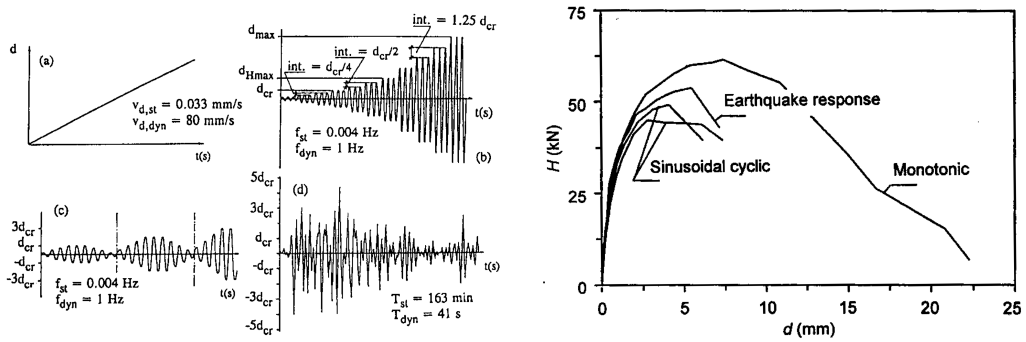

Figure 1.18: Loading patter (left) and related analyses (right) [Tomaževič *et al.*, 1996].

The experimental aspects, such as level of vertical stress and displacement history, are widely depending on the aim of the test. Furthermore, also boundary conditions and results are widely depending on the experimental set-up. Moreover, the masonry specimen can be tested as cantilever or double fixed end wall. For both boundary conditions a large variety of test rigs have been designed and used [da Porto, 2005].

This methodology allows to study more failure mechanisms: shear, flexure and sliding. In fact, the overall behaviour of the specimen is depending on applied conditions, such as vertical load and lateral displacement, which can be controlled through the testing system, and on mechanical properties of materials.

As in the case of diagonal tests, this testing method is normally performed in a laboratory (figure 1.19a). In this case, tested specimens can be expressly realized or taken from an existing structure. Nevertheless, this test is also often performed in-situ (figure 1.19b), where a real structure can be directly tested.

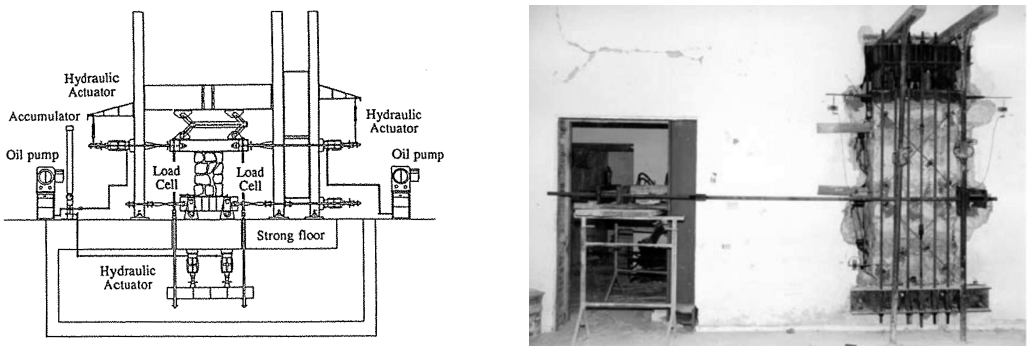

(a) [Tomaževič and Apih, 1993] **(b)** [Corradi *et al.*, 2002]

Figure 1.19: Examples of laboratory (left) and in-situ (right) shear compression tests.

1.2.2.3 Experimental campaigns

Tomaževič [1992] performed also an experimental campaign aiming at studying the shear resistance of the multi-leaf stone masonry. These were executed on masonry panels similar to those previously presented and tested under monotonic compression. In this case, experiments were performed on samples having a slenderness ratio equal to 2. Furthermore, both in-situ and laboratory tests were realized. Results are reported in table 1.16.

Table 1.16: Experimental results obtained by Tomaževič [1992].

Type of masonry	Description	f_{gr} [N/mm^2]	f_t [N/mm^2]	G [N/mm^2]
Uncoursed stone, two layers, muddy sand	original	-	0.02	70
	grouted	33	0.12	100
Uncoursed stone, two layers, clean sand	original	-	0.1	87
	grouted	33	0.25	145

A further experimental campaign was carried out by Tomaževič and Apih [1993] on two-leaf masonry walls, constituted by stones and crumbled bricks, with sub-horizontal mortar joints. Different cement-based grouts were employed with the insertion of pozzolana or hydrophobic additives. The execution details are similar to those of previous experiments performed by the author, namely, low pressure of injection (0.2-0.3bar) and regular mesh or holes (distance of 30÷50cm).
The program involved shear compression tests on 11 samples divided between both in-situ and laboratory experiments. The specimens tested in the ZRMK laboratories were subjected to a constant precompression of 1N/mm^2, considered about the 25÷30% of the masonry compressive strength after injection. Results, summarized in table 1.17, demonstrate as the insertion of additives widely decreased the compressive strength of the grout without affecting the shear strength of the walls. Nevertheless, the addition of sand lowered the chemical incompatibility. The failure mechanisms highlighted as the injection allows the homogenization of the section and the improvement of the overall behaviour. This led to exploit the tensile strength of materials and to delay further failure mechanisms. Actually, all samples failed in shear at a lateral deformation of 3.0÷4.0mm and, close to the failure, vertical cracks occurred also on the transversal sides.

Table 1.17: Experimental results obtained by Tomaževič and Apih [1993].

Masonry wall	f_{gr} [N/mm^2]	f_t [N/mm^2]	K_e [kN/mm]	G [N/mm^2]
A-1	32.5	0.3	64.69	160
A-2	32.5	0.3	83.85	200
B-1	19.7	0.36	48.85	117
B-2	19.7	0.37	52.31	122
C-1	6.8	0.2	53.85	137
C-2	6.8	0.42	57.98	142
D-1	12.8	0.33	57.25	148
D-2	12.8	0.39	60.89	148

Modena and Bettio [1994] completed the experimental campaign of compression tests with further shear compression tests employing a Sheppard testing system [dal Farra, 1992]. Masonry specimens were consolidated through the hydraulic lime-based grout injection, drilling about 10 holes per squared meter on both sides of samples. Results showed as the intervention induced an increasing of both strength and stiffness. However, despite the great diffusion of holes, the panels were not uniformly injected and a poor adherence to the stones was noted. In the case of panels preventively wetted these aspects could be improved as table 1.18 shows.

Table 1.18: Experimental results obtained by Modena and Bettio [1994] (all quantities are expressed in [N/mm^2]).

	Before strengthening					After strengthening				
panel	σ_0	τ_u	f_t	G	E	σ_0	τ_u	f_t	G	E
1	0.048	0.043	0.040	43.1	258.9	0.061	0.055	0.052	56.1	336.6
	0.041	0.037	0.034	37.8	226.5	0.044	0.040	0.037	39.9	239.5
2	0.046	0.046	0.043	45.3	271.8	0.049	0.049	0.046	48.5	291.3
	0.028	0.028	0.026	28.0	168.3	0.046	0.046	0.043	45.3	271.8
3	0.025	0.026	0.024	24.8	148.9	0.038	0.039	0.035	37.8	226.5
	0.028	0.029	0.026	28.0	168.3	0.042	0.042	0.039	41.0	246.0
4						0.077	0.071	0.066	71.2	427.2
						0.077	0.071	0.066	71.2	427.2
5	0.030	0.031	0.028	30.2	181.2	0.048	0.049	0.044	46.4	278.3
	0.030	0.031	0.028	30.2	181.2	0.048	0.049	0.044	46.4	278.3
6						0.089	0.064	0.052	57.2	343.0
						0.081	0.059	0.058	65.8	394.8

The completion of the experimental campaign performed by Vintzileou and Tassios [1995], presented among the compression experiments, included also diagonal tests on two masonry panels without lateral interlocking (figure 1.20a) with overall dimensions of 80x80x40cm. Due to the brittle failure induced by this testing method, the specimens were tested only after injection. Both samples provided a tensile strength equal to 0.64N/mm^2 (figure 1.20b). This confirms the capability of injection to widely increases the original mechanical characteristics, that can be assumed as: $f_{wt,0} = 0.1 \cdot f_{wc,0} = 0.15 N/mm^2$.

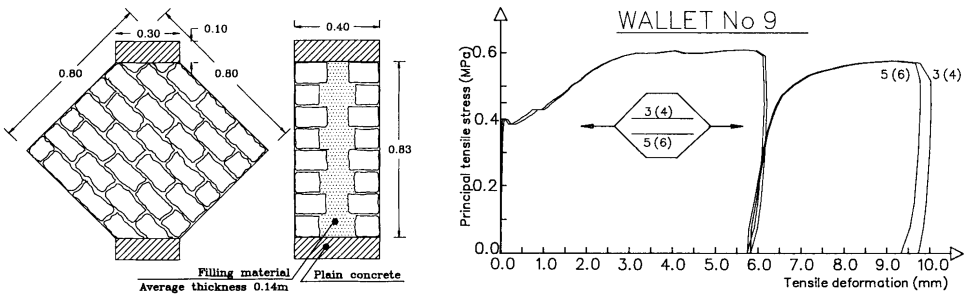

(a) Diagonal test set-up **(b)** $f_t - \varepsilon$ relationship

Figure 1.20: Specimens tested by Vintzileou and Tassios [1995].

Beolchini *et al.* [1997b] carried out an experimental campaign of diagonal tests on stone masonry panels initially strengthened by cementitious grouts. After a first series of cyclic tests, the samples were repaired again through reinforced injections (inserting steel bars) parallel to the masonry surface. A synthesis of results is presented in table 1.19. Data demonstrate that a noticeable increase is induced in all the considered mechanical parameters, such as strength, shear modulus and ductility ratio. This was particularly evident in the case of reinforced injections, that also showed a higher dissipation capacity close to the collapse.

Table 1.19: Experimental results obtained by Beolchini *et al.* [1997b].

test	intervention	τ_{max} [N/mm^2]	G [N/mm^2]	μ -
1	unstrengthened	0.040	4.6	>2.1
	injection	0.222	111.15	5.55
	r. injection (4 bars)	0.297	66.05	4.7
2	unstrengthened	0.066	8.2	>2.6
3	unstrengthened	0.057	12.6	>1.9
	r. injection (2 bars)	0.252	66.5	8.95
4	unstrengthened	0.056	7.6	>2.8
	r. injection (2 bars)	0.204	120.1	>9.9

Subsequently, Beolchini *et al.* [1997a] designed also a further experimental campaign on some masonry panels of a building to be dismantled. Cyclic tests were performed imposing a lateral displacements to the whole structure at floor levels, as presented in figure 1.21. A first test was carried out up to the maximum lateral strength, without inducing the collapse, and the structure was subsequently repaired by means of widespread cementitious injections. The results demonstrated the capability to increase the overall original strength (figure 1.22) of about 80%, in the case of lateral displacement applied only to the roof level, and of about 50% in the case of lateral displacement imposed at both floors levels.

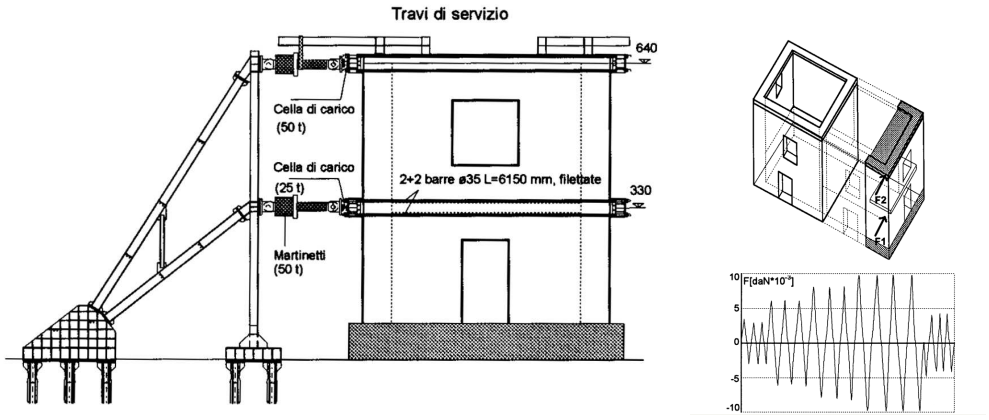

(a) Load application **(b)** Displacement history

Figure 1.21: Experimental set-up designed by Beolchini *et al.* [1997a].

Within the experimental campaign proposed by Toumbakari and van Gemert [1997] also diagonal compression tests were carried out on three panels strengthened by

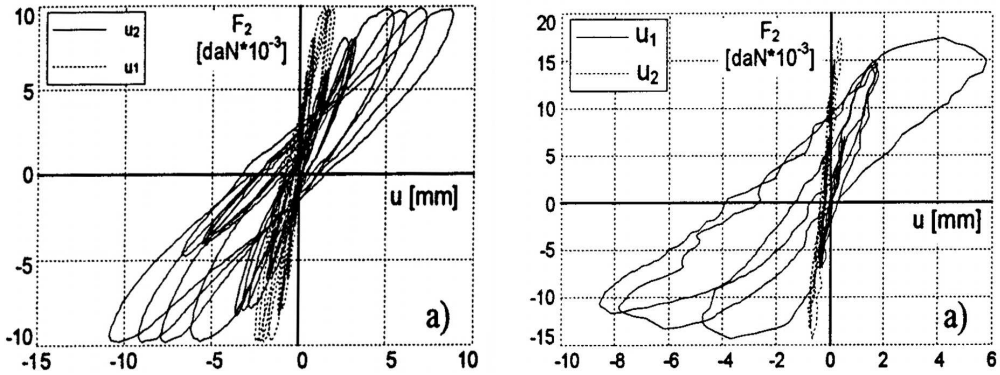

(a) Before strengthening **(b)** After strengthening

Figure 1.22: Experimental results obtained by Beolchini *et al.* [1997a].

grout injections, with the same characteristics presented for the compression tests. The specimens had overall dimensions equal to 80x80x40cm and transversal connections between external layers could be also surveyed. Experimental observations underlined as cracks occurred because of sliding of mortar joints and only in a limited way on stones. As mentioned by Tomaževič and Apih [1993] yet, the results, summarized in table 1.20, highlighted a substantial invariance of shear strength from the strength of injected grout.

Table 1.20: Experimental results obtained by Toumbakari and van Gemert [1997].

panel	f_{gr} [N/mm^2]	τ_{max} [N/mm^2]	$\varepsilon_{h,\tau_{max}}$ ‰	$\sigma_{\tau_{max}}$ [N/mm^2]	$\varepsilon_{v,\tau_{max}}$ ‰
1	6.4	0.45	1.41	0.52	0.87
		-	-	-	-
2	14.6	0.30	-	-	-
		0.7	-	-	-
3	5.2	0.30	2.00	0.30	1.50
		0.60	3.10	0.70	2.60

Vignoli completed the in-situ compression tests with a further experimental campaign involving experiments in the same location with the aim to study the influence of injections also in the shear behaviour [Modena, 1999]. Also in this case, as for compression tests, jacketing and injections were applied to the masonry panels. Two different experimental set-up were considered, namely shear compression tests and diagonal tests. First method involved samples similar to those tested in compression, while for the second methodology a mean thickness of 43÷50cm was considered. Results, summarized in table 1.21 and in figure 1.23 (R=Repaired; T=Shear), demonstrated as the interventions reduced both the overall ductility ratio and the shear modulus.

The experimental campaign proposed by Toumbakari [2002] was completed with further diagonal compression tests on samples similar to those tested under compression. Results, presented in table 1.22, highlight as the injection appeared most

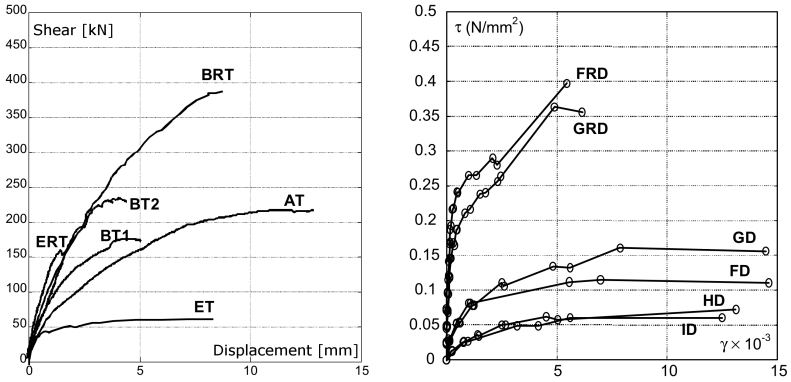

(a) Shear compression tests **(b)** Diagonal tests

Figure 1.23: Results of specimens tested by Vignoli [Modena, 1999].

Table 1.21: Experimental results obtained by Modena [1999].

	intervention	τ_u [N/mm^2]	μ -	G [N/mm^2]
Pieve Fosciana	unstrengthened	0.379	5.30	179
(A)	jacketing	0.573	-	-
Pieve Fosciana	unstrengthened	0.491	-	435
(B)	jacketing	0.664	2.82	274
Pognana	unstrengthened	0.114	5.74	102
(E)	injection	0.237	2.34	268
Canova	unstrengthened	0.114	-	285
(G)	jacketing	0.397	-	-
Canova	unstrengthened	0.16	-	102
(F)	jacketing	0.364	-	-
Castelletto	unstrengthened	0.072	-	36
Merizzo	unstrengthened	0.061	-	74

effective in the increasing of tensile strength rather than on the compressive one. Furthermore, this intervention allowed to decrease up to 70% the horizontal deformations. As a consequence, when damages occurred in the specimens, the crack developments resulted accelerated.

A wide in-situ campaign was performed by Corradi *et al.* [2003] in several buildings, to be dismantled, in the regions struck by the Umbria-Marchigiano earthquake of 1997-1998. All the selected panels were constituted by multi-leaf stone masonry, in some cases with brick courses at regular distance. Any strengthening intervention was applied, since the aim of the research was the mechanical characterization of historical multi-leaf stone masonry structures. Two different tests were carried out: shear compression and diagonal compression. In the first case, specimens had a dimension of 90x180cm, while in the second one squared samples with 120cm per side were obtained. Before the initiation of the shear compression tests, three cycles of compression were performed up to 0.1, 0.2 and 0.3 N/mm^2 respectively. This allowed to estimate the elastic modulus of masonry. After this preliminary phase, lateral displacements were imposed and the results are presented in table 1.23.

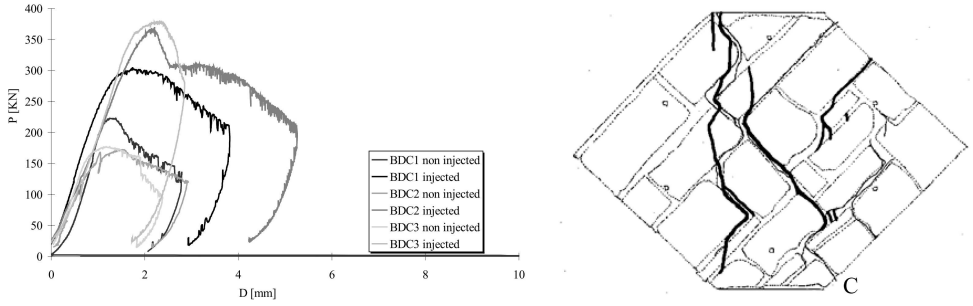

(a) Diagonal compression tests **(b)** Typical crack pattern

Figure 1.24: Results of specimens tested by Toumbakari [2002].

Table 1.22: Experimental results obtained by Toumbakari [2002].

Panel	$f_{t,0}$ [N/mm^2]	$f_{t,s}$ [N/mm^2]
BDC1	0.44	0.60
BDC2	0.34	0.73
BDC3	0.35	0.75
SDC1	0.47	0.50
SDC2	0.34	0.68
SDC3	0.28	0.59

Further investigations involved diagonal compression tests on similar masonry typologies and results are summarized in table 1.24.
The set of results highlight as the scattering of the obtained shear strength values is very low and the average is higher than the highest shear strength recommended by the Italian Standards. On the contrary, elastic properties and shear modulus are very scattered. Finally, the execution of both kind of tests on the same masonry typology highlighted as these set-ups lead to significantly different results and rising the problem of which test is representative of the real masonry behaviour.

The investigation on shear strength about multi-leaf stone masonry was deepened by Corradi *et al.* [2008] through further in-situ tests. As for the previous campaign, also in this case both shear compression and diagonal tests were performed. Results of shear compression experiments, reported in table 1.25, show a great scattering but shear strength, as well as shear modulus, manifests a large increase.
Results of diagonal compression tests showed (table 1.26) as the strengthening uniquely

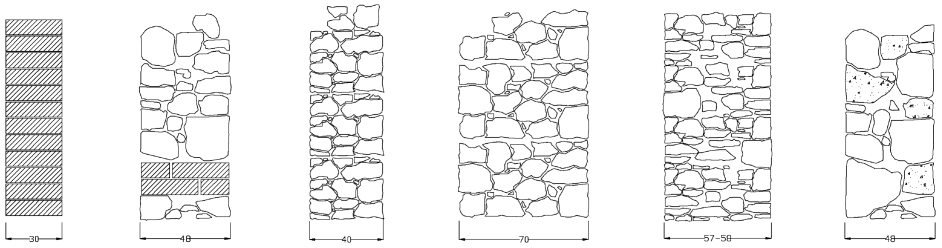

Figure 1.25: Survey of the thickness of testes masonry panels [Corradi *et al.*, 2003].

Table 1.23: Experimental results from shear compression tests [Corradi *et al.*, 2003].

masonry texture	E [N/mm^2]	τ_{max} [N/mm^2]	σ_0 [N/mm^2]	G [N/mm^2]
Double-leaf roughly cut stone masonry with two solid brick courses at intervals of 80-120 cm	917	0.219	0.3	546
Double-leaf roughly cut stone masonry with two solid brick courses at intervals of 80-120 cm	1814	0.225	0.3	450
Double-leaf roughly cut stone masonry	471	0.172	0.3	216

Table 1.24: Experimental results from diagonal compression tests [Corradi *et al.*, 2003].

masonry texture	τ_{max} [N/mm^2]	$G_{1/3}$ [N/mm^2]	$\gamma_{1/3} \times 10^{-3}$
Double-leaf roughly cut stone masonry with two solid brick courses at intervals of 80-120 cm	0.072	30	0.791
one leaf only bricks	0.069	131	0.136
Double-leaf roughly cut stone masonry	0.047	19	0.824
Double-leaf roughly cut stone masonry	0.072	25	0.942
Double-leaf roughly cut stone masonry	0.068	60	0.370
Double-leaf roughly cut stone masonry	0.053	26	0.642
Double-leaf roughly cut stone masonry	0.059	37	0.533

by the execution of deep repointing induced an increasing of shear stiffness, while the shear strength can be improved only using injections.

Table 1.25: Experimental results from shear compression tests [Corradi *et al.*, 2008].

masonry texture	intervention	τ_{max} [N/mm^2]	σ_0 [N/mm^2]	G [N/mm^2]
Double-leaf roughly cut stone masonry	Unstrengthened condition	0.083	0.147	38
	Deep repointing + grout injections	0.412	0.272	281
Double-leaf roughly cut stone masonry	Unstrengthened condition	0.089	0.184	65
	Deep repointing + grout injections	0.196	0.268	196

The experimental campaign of compression tests carried out by Vintzileou and Miltiadou-Fezans [2008] was completed the execution of three diagonal compression experiments. These were realized to evaluate the effectiveness of ternary grouts in the increasing of tensile and shear strengths of multi-leaf stone masonry panels. Figure 1.26 shows as the injected panels could suffer a mean tensile stress of about 0.22N/mm^2 in two cases and about 0.34N/mm^2 in the third panel, demonstrating its contribution in increasing the overall strength of the masonry.

Table 1.26: Experimental results obtained from diagonal tests by Corradi *et al.* [2008].

masonry texture	intervention	τ_{max} [N/mm^2]	$G_{1/3}$ [N/mm^2]	$\gamma_{1/3}$
Double-leaf roughly cut stone masonry	Unstrengthened condition	0.059	37	0.533
	Deep repointing + grout injections	0.157	731	0.070
Double-leaf roughly cut stone masonry	Unstrengthened condition	0.045	80	0.190
	Deep repointing	0.054	232	0.076

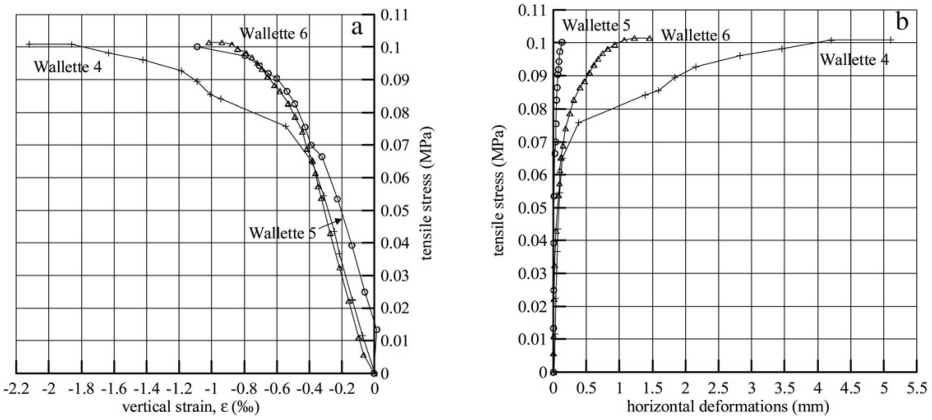

(a) Tensile stress-vertical strain curve **(b)** Tensile stress-vertical cracks

Figure 1.26: Results of diagonal compression tests [Vintzileou and Miltiadou-Fezans, 2008].

The experimental campaign developed by Galasco *et al.* [2009a] involved also diagonal compression tests on panels similar to those previously presented for the compression part. The tests were performed cyclically at increasing load levels up to the failure. In all cases the manifest a linear behaviour up to quiet high loads, but results show a greater scattering than that obtained for compression tests. Results are reported in table 1.27.

A further part was designed and performed by Galasco *et al.* [2009b], completing the experimental program of quasi-static tests on double-leaf stone masonry. Five shear compression tests were realized on slender samples (250x125cm) and on squat specimens (250x250cm). They were subjected to two different precompression level equal to 0.2N/mm^2 and 0.5N/mm^2. These represent two realistic stress states normally present on historical buildings. The tests were designed to obtain two most typical failure modes, namely shear and flexure, depending on the slenderness ratio and on the precompression level. Results, presented in table 1.28, are in accordance with those obtained from diagonal compression tests.

1.2.3 Resume of experimental results

The methodical cataloguing of mechanical parameters presented in the previous sections is summarized in the following. Table 1.29 and table 1.30 resume respectively

Table 1.27: Results of diagonal compression tests [Galasco *et al.*, 2009a].

Panel	τ_{max} [N/mm^2]	f_t [N/mm^2]	$\gamma_{1/3}$ x10^{-5}	G [N/mm^2]
D1	0.135	0.090	5.46	820
D2	0.183	0.128	8.78	700
D3	0.243	0.169	1.17	700
D4	0.197	0.137	6.72	950
D5	0.174	0.121	5.66	1000
D6	0.249	0.174	9.49	850

Table 1.28: Results of shear compression tests [Galasco *et al.*, 2009b].

Panel	f_t [N/mm^2]	σ_0 [N/mm^2]
CS00	0.20	0.2
CS01	0.16	0.5
CS02	0.10	0.2
CT01	0.13	0.5
CT02	0.10	0.2

the values collected from in-situ and laboratory experimental campaigns. Parameters are listed separately to underline the source of tested specimens. Actually, in-situ tests are clearly representative of the real situation, while experiments performed in laboratory were carried out on samples, whose overall characteristics should be representative of the real condition and this condition needs to be verified.

The mean values for each considered campaign are reported. Furthermore, the average is computed, considering the whole number of tested specimens, and also maximum and minimum values are provided, to give an indication of the range of variability. The values reported in the tables, for strengthened elements, consider only the injected specimens.
Concerning the admixtures, the most diffuse grout typologies were cement-based or cement-content, while a lower number of experimental campaign employing lime-based admixtures could be found.

For all the considered mechanical parameters, values appeared as widely scattered, actually a wide difference between minimum and maximum values can be noted in both resuming tables.
In the case of in-situ studies, the average compressive strength of the unreinforced specimens is about 1N/mm^2, with peak values more than doubled. Furthermore, in this case the mean increase due to injection can be quantified around 30%.
Again, table 1.30 underlines as the compressive strength of unreinforced laboratory specimens results higher than that obtained from in-situ tests. Nevertheless, even if this average results higher, the mean increase consequent to injections settle around 30% also in this case. However, also the remaining mechanical parameters show values higher than those computed in table 1.29. Moreover, a wider discrepancy can be noted in the case of computed shear strength. Actually, while the mean increasing due to grout injection is very limited in the case of in-situ tests, a very high improvement of this mechanical parameter is found, when laboratory tests are analyzed.

Finally, several considered experimental campaigns, comprehending both in-situ and laboratory experiences, lead to note how the main effect of the injected grout is to bind together the external layers of multi-leaf masonries, thus delaying their buckling. On the other hand, the compressive strength of employed admixtures resulted less relevant in the final improvement of the masonry compressive strength, while the overall compatibility of materials appeared as a more relevant aspect.

Lastly, table 1.31 summarizes the composition of different grout typologies employed on the presented experimental campaigns. Furthermore, also their mechanical characteristics are reported and the mean pressure adopted during injection operations. Descriptions and values reported on the table underline the wide variability on the composition of adopted admixtures and the consequent great difference on their overall strength. Actually, values of compressive strength vary from about $3N/mm^2$, in the case of pure lime admixture, up to more than $30N/mm^2$, when pure cement grout is adopted. Nevertheless, as previously observed, this wide variation of the characteristics of grouts does not have a significant influence on the overall strength of the injected walls.
The pressure of injection operations is generally low and any difference can be noted in the case on in-situ or laboratory applications.

1.3 Shaking Table Tests

The dynamic experimental campaigns allow to deepen the knowledge about the dynamic behaviour of tested elements or structures. If quasi-static tests provide results concerning the mechanical characteristics (compare §1.2.1) and first information about the seismic resistance, particularly to the in-plane actions (compare §1.2.2), shaking table tests lead to a better knowledge concerning both the overall dynamic behaviour and specific aspects of the tested structures.

Since eighties, pseudo-dynamic and dynamic experimental campaigns were performed [Benedetti and Castellani, 1980; Chen and Shah, 1988; Clough *et al.*, 1990; Popov, 1986; Tercelj *et al.*, 1976; Tomaževič *et al.*, 1989; Turnšec *et al.*, 1978] in order to study the influence of the retrofitting techniques on the dynamic behaviour of masonry structures, since this leads to evaluate both the feasibility and effectiveness of their employment. In fact, this can reflect on several effects, such as the variation of fundamental frequencies, of mode shapes and of damping values, as well as on the modification of the mass and the stiffness distribution.

On the following decades, up to nowadays, the experimental researches widely increased in number, providing tests on both single structural elements and complete building models.
Furthermore, the requirement to limit the costs, the physical limits of the testing facilities and further practical difficulties often led to realize specimens employing a reducing scale factor [Tomaževič and Velechovsky, 1992], particularly in the case of whole building models.

1.3.1 Single structural elements

The design and the execution of simple shaking table experiments can provide important information about the dynamic behaviour of the tested elements.

Starting from the basic idea that the less complex the considered specimens the easier will probably be the interpretation of the results and of the consequent

Table 1.29: Synthesis of mechanical parameters obtained from in-situ investigations.

Author	$f_{wc,0}$ [N/mm^2]	$f_{wc,s}$ [N/mm^2]	$E_{w,0}$ [N/mm^2]	$E_{w,s}$ [N/mm^2]	$\tau_{w,0}$ [N/mm^2]	$\tau_{w,s}$ [N/mm^2]	$G_{w,0}$ [N/mm^2]	$G_{w,s}$ [N/mm^2]
Bettio *et al.* [1993]	0.750	1.370	248	791				
dal Farra [1992]			190	352	0.029	0.049	32	53
Modena [1999]	0.639	1.596	1149	3012	0.199	0.237	173	268
Beolchini *et al.* [1997b]					0.055	0.222	8	111
Beolchini *et al.* [1997a]	1.125		167		0.137		36	
Chiostrini and Vignoli [1994]	2.243		1288		0.227		245	
Tomaževič [1992]					0.120	0.165	40	275
Corradi *et al.* [2003]			1067		0.11		166	
Corradi *et al.* [2008]	0.208	0.286	798	2962	0.069	0.203	52	239
Average	1.038	1.315	428	940	0.120	0.123	115	154
Maximum	2.243	1.596	1288	3012	0.227	0.237	245	275
Minimum	0.208	0.286	167	352	0.029	0.049	8	52.6

Table 1.30: Synthesis of mechanical parameters obtained from laboratory investigations.

Author	$f_{wc,0}$ [N/mm^2]	$f_{wc,s}$ [N/mm^2]	$E_{w,0}$ [N/mm^2]	$E_{w,s}$ [N/mm^2]	$\tau_{w,0}$ [N/mm^2]	$\tau_{w,s}$ [N/mm^2]	$G_{w,0}$ [N/mm^2]	$G_{w,s}$ [N/mm^2]
Tomaževič and Apih [1993]	0.635	1.570	294	1785	0.060	0.304	79	142
Vintzileou and Tassios [1995]	1.742	3.725	5074	7864				
Toumbakari and van Gemert [1997]	2.354	3.367	4792	3467	0.349	0.650		
Valluzzi [2000]	1.671	2.398	1836	2733				
Toumbakari [2002]	2.304	3.486	1083	1463	0.370	0.642		
Oliveira and Lourenço [2006]	1.833	3.133						
Binda *et al.* [2006]	6.100		2380					
Vintzileou and Miltiadou-Fezans [2008]	1.940	3.493	1313	1350	0.100	0.260		
Galasco *et al.* [2009b]	3.277		3550		0.137		837	
Average	2.423	3.173	2308	2818	0.144	0.523	542	142
Maximum	6.100	3.725	5074	7864	0.370	0.650	837	142
Minimum	0.635	1.570	294	1350	0.060	0.260	79	142

Table 1.31: Synthesis of composition and mechanical characteristics of employed grouts.

Author	Grout characteristics	Strength [N/mm^2] comp	flex	Pressure [bar]
dal Farra [1992]	hydraulic lime mortar/cocciopesto 1:2; fluidifying; anti-shrinkage, w/b 1:5	–	–	gravity
Tomaževič [1992]	cement/pozzolana 9:1, w/b 1:1, 0,9:1	30.3	–	2.0
	cement/pozzolana 9:1, w/b 0,7:1	32.5	1.9	2.0-3.0
	cement/pozzolana 9:1, hydrophobic additives, w/b 0,7:1	19.7	1.6	2.0-3.0
	cement/pozzolana 7:1, hydrophobic additives, w/b 0,75:1	6.8	0.6	2.0-3.0
	cement/pozzolana 7:1, sand, hydrophobic additives, w/b 0,75:1	12.8	1.7	2.0-3.0
	cement/pozzolana 14:1, sand, hydrophobic additives, w/b 0,9:1	15.9	4.2	2.0-3.0
Vintzileou and Tassios [1995]	cement 74%; Silica fume 24,7%; fluidifying1,3% w/b=0,89	30.0	–	0.07
	cement 53,7%; Silica fume 20,2%; lime 24,6; fluidifying1,5% - w/b=0,89	13.0	–	0.07
Beolchini *et al.* [1997b]	w/cement 0,54,	–	–	1.5-2.0
Toumbakari and van Gemert [1997]	cement/lime 4:1, fluidifying, w/b 0,85:1	14.6	5.6	0.8-1
	cement/lime 2:1, Silica fume, pozzolana, fluidifying, w/b 0,67:1	6.4	1.6	0.8-1
	cement/lime 2:1, pozzolana, fluidifying, w/b 0,83:1	5.2	1.8	0.8-1
Valluzzi [2000]	lime 100%, superplasticizer additives	3.23	0.35	0.5
	lime 100%	5.10	–	0.5
Toumbakari [2002]	cement 30%; pozzolana 52,5%;lime 17,5% w/b=0,85	7.3	1.7	
	cement 30%; pozzolana 42,5%; Silica fume 10%; lime 17,5% - w/b=0,85	9.0	1.1	
	cement 100% - w/b=0,85	19.5	4.5	
Corradi *et al.* [2003]	lime, kaolin lime, carbonates micronized -w/b =0,45	8.0	–	1.0
Vintzileou [2007]	white cement 30%; lime 25% pozzolana 45,7%; fluidifying1% w/b=0,80	8.2	2.2	0.7
	grout NHL5 100%; fluidifying1% - w/b=0,80	4.5	2.5	0.7
Corradi *et al.* [2008]	Albaria grout 100	7.0	3.0	1.0

considerations, researches on single structural elements were developed during years. Actually, these experimental campaigns allow an in-depth knowledge concerning the tested elements and eventually applied strengthening techniques. A further advantage of this method is represented by the possibility to perform tests on full-scale specimens, avoiding scale factors, which induce unavoidable problems on the realization of elements and in the interpretation of results.

An extension of this investigation methodology, not considered in the following overview, is represented by experimental campaigns on substructures. This can be assumed as the intermediate point between tests on single elements and on complete models. Actually, tests on single elements or substructures often precede the experimental campaigns on whole structures. Furthermore, laboratory investigations on substructures allow to study both the behaviour of single elements and also the mutual interaction among these. In this field, particularly interesting are the researches focused on the study of the influence of connections, such as between vertical and horizontal structures as well as between orthogonal vertical elements. As in the case on single elements, substructures can be often realized at full scale, due to their limited extension.

In the following sections some experimental works on single structural elements will be presented for completeness, even if this part of experimental campaign was only designed in the present study and will be next performed.
The researches are organized considering the methodology of solicitation of elements, namely in-plane or out-of-plane dynamic action, even if most of the subsequently described works were performed using this second configuration.
Lastly, one should consider as the mentioned experiments were all carried out on masonry panels. Furthermore, they were principally performed on brick samples.

1.3.1.1 In-plane dynamic tests

The study about dynamic behaviour of masonry elements subjected in-plane seismic excitation provide important information concerning their in-plane strength and the consequent typical failure mechanisms. Furthermore, this loading methodology can be considered well representative of the real structural condition, where connection elements and horizontal structures redistribute the seismic action among the resisting elements parallel to the seismic action.
Furthermore, one should consider that the shear compression experiments are able to provide informations similar to those achievable via in-plane shaking table tests [Elgawady *et al.*, 2004; Tomaževič, 2000], that result more complex and expensive. This probably induced several researchers to design and develop experimental campaigns in the quasi-static field, considering also that these testing facilities are more diffuse than those to perform dynamic tests and this results in a restricted number of in-plane dynamic tests.

At the University of British Columbia, Turek [2002] performed a series of shaking table tests on eight full scale concrete-masonry walls. These specimens were tested in both the unreinforced and strengthened conditions, with the application of FRP strips. Furthermore, different configurations of reinforcement were tested and their effectiveness was investigated.
The experimental program validates the possibility of increasing the shear strength of Unreinforced Masonry Walls by applying FRP strips. The results showed as the thickness of the vertical strips provided improved results, even if the best enhancement

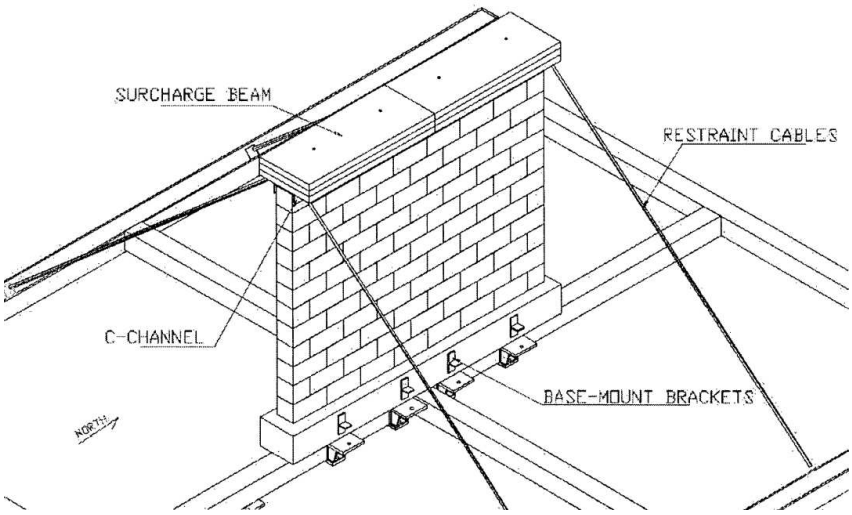

Figure 1.27: Schema of set-up used for in-plane dynamic tests [Turek, 2002].

was obtained through the coverage of the wall with horizontal reinforcing elements. However, the most applicable methodology resulted with an X-pattern of strips. All configurations permitted to control the failure modes and anchor details resulted important to control the stiffness of strengthened elements as well as their overall capacity.

ElGawady *et al.* [2005] designed and performed an experimental campaign in order to evaluate the shear strength of brick masonry panels strengthened using FRP. At the ETH Research Centre, in Zurich, five panels were realized at half scale, employing reduced brick to respect the scale ratio. All of these were subjected to in-plane seismic actions (figure 1.28), even if they were different because of unlike slenderness ratio. Masonry specimens were strengthened through the application of FRP only in one side of the panels.
The tests validate the effectiveness of the applied strengthening technique. Actually, the strength increased of an average value ranging between 1.3 and 2.9, while the increasing of the lateral drift capacity was less significant. Finally, authors underlined as the employment of two different methodologies, namely fabrics and grids, is useful to delay the typical failure mechanism of the masonry panels.

1.3.1.2 Out-of-plane dynamic tests

Out-of-plane experiments on single structural elements, namely masonry panels in this case, are more diffused than the testing methodology proposed in the previous section and a greater number of laboratory campaigns could be found. However, also in this field, the collected experimental works provide an incomplete overview and any reference test on stone masonry could be find.
Only Liberatore and Spera [2001] performed experimental shaking table tests on monolithic marble blocks to evaluate the influence of the slenderness ratio through the input of two different time histories. However, this tests aimed at studying the overall behaviour of non-structural elements, such as building façades, parapets and more generally non load bearing walls.

Nevertheless, during nineties Giuffrè deepened the out-of-plane behaviour of stone masonry walls yet. From in-situ observations of most common damages and

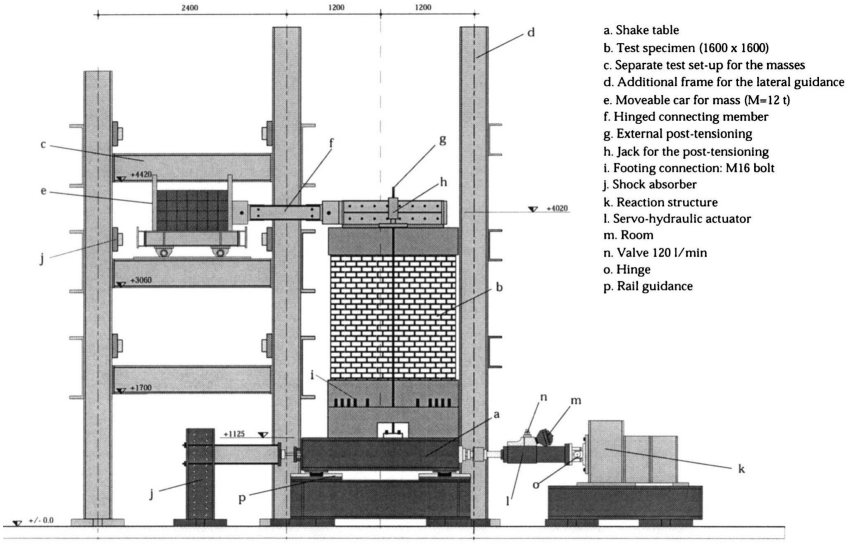

Figure 1.28: Set-up of dynamic tests employed by ElGawady *et al.* [2005].

mechanisms, Giuffrè [1990] concluded as prevalent failure modes are the consequence of an out-of-plane seismic solicitation. Particularly, observations were developed also in the case of multi-leaf stone masonry elements, where damages occurred mainly because of buckling of external layers and overturning of whole masonry portions. This study started from the observation of typical failure mechanisms occurred during earthquake [Giuffrè *et al.*, 1993] and not carrying out laboratory tests.

Starting from above mentioned considerations, the research focused, more generically, on experimental laboratory tests performed on the out-of-plane behaviour of masonry panels. Some relevant works are briefly summarized as follows.

One of the earlier experimental campaigns performed in this topic was carried out at ABK [1981] (Agbabian & Associates, S.B. Barnes & Associates, Kariotis & Associates) on 1981. This study involved several masonry typologies and, among these, the most similar to multi-leaf stone masonry was a multi-wythe brick masonry. This investigation aimed at defining the slenderness limit and the boundary conditions of single panels to determine their resistance and evaluate the effectiveness of possible strengthening interventions.
20 full scale masonry panels were subjected to about 200 seismic inputs (figure 1.29) comprehending the full range of USA seismicity. Besides for the study of interventions, results obtained from these tests were thus employed for the development mathematical model for collapse prediction as well as of guidelines for strengthening. Finally, the collapse mechanism resulted more dependent on the peak velocities input at the top and at the bottom of panels than the relative deformation induced by the top and bottom relative displacement.

Subsequently, Bariola *et al.* [1990] designed and realized dynamic tests (figure 1.30) on seven masonry panels, having different slenderness ratios and different overall dimensions. The research focused on the study about the influence of the slenderness ratio and the masonry thickness on the out-of-plane dynamic behaviour and main failure mechanisms of a not load bearing wall.
Tests underlined as, having equal slenderness, specimens with higher thickness mani-

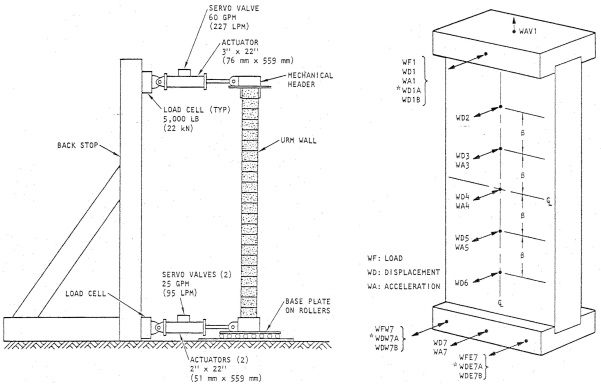

Figure 1.29: Experimental set-up (left) and sensor location (right) [ABK, 1981].

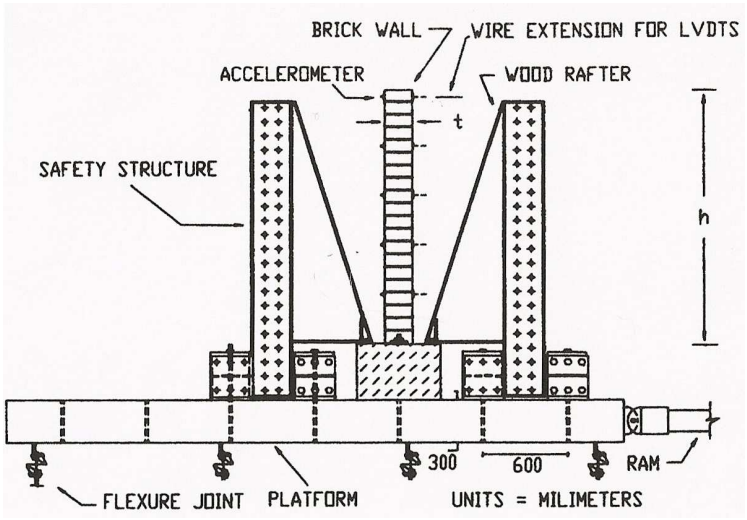

Figure 1.30: Equipment for shaking table tests [Bariola *et al.*, 1990].

fested a more stable behaviour, while squat panels suffered higher seismic input, independently from the overall depth.

In more recent years, Griffith *et al.* [2004] developed experimental and numerical studies on the stability of unreinforced masonry walls. The experimental dynamic campaign (figure 1.31) performed on fourteen specimens underlines as the large displacements are the main cause for the collapse of walls rather than the inertial force amplitude. Finally, the results led to drawn an empirical force-displacement relationship to predict the wall collapse.

Simsir *et al.* [2004] carried out a dynamic campaign on four half-scale lightweight concrete hollow blocks. The experimental set-up allowed to test contemporary all walls in the free-standing boundary conditions (figure 1.32). As a consequence, two of these were tested in-plane, while the remaining in the out-of plane direction. A relevant aim of the experiment was the investigations about influence of boundary conditions, namely horizontal structures at top and constrain at the bottom of wall panels in the real situation. Differently from other similar tests, specimens did not

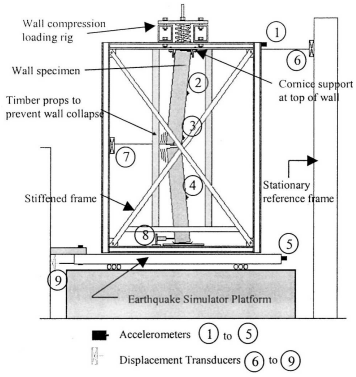

Figure 1.31: Experimental set-up employed by Griffith *et al.* [2004].

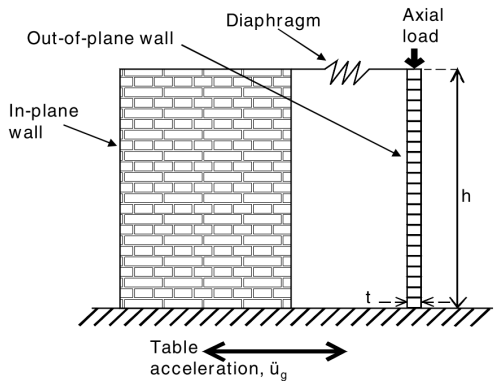

Figure 1.32: Test set-up [Simsir *et al.*, 2004].

exhibit a mid-height failure, causing the subsequent collapse, except when the axial load was reduced. Furthermore, the flexibility of diaphragms can significantly enhance the out-of-plane displacements.

Meisl *et al.* [2006] tested four multi-wythe URM walls, as in the case of ABK [1981]. Two were realized with good quality of mortar, while the remaining with poor quality. The study focused on the influence of the ground motion input and on the quality of the wall construction on their out-of-plane strength. Obtained results, demonstrated as URM walls on soft soils present higher out-of-plane damages and failures than those located on firmer substrate. Furthermore, the quality of the mortar seems to have a limited influence on the overall behaviour and on the mechanisms of failure of tested specimens.

Wilhelm *et al.* [2007] carried out a series of shaking table tests on six brick masonry panels at IBK Institute in Zurich (ETH). The specimens are realized at full scale but with different thickness values, ranging between 12.5cm to 20cm. The main objective of the experimental program was the evaluation of the effect induced by boundary conditions on the overall out-of-plane behaviour of masonry panels. For this reason two different test set-ups were designed and reproduced by a steel frame (figure 1.33). The first testing configuration reproduces a fix constrain at the base, while the top of the specimen can both rotate and vertically translate. This represents the case of a last floor of a building, with low vertical stress. In the second condition also the top of the walls was prevented to translate and rotate, namely was double-fixed,

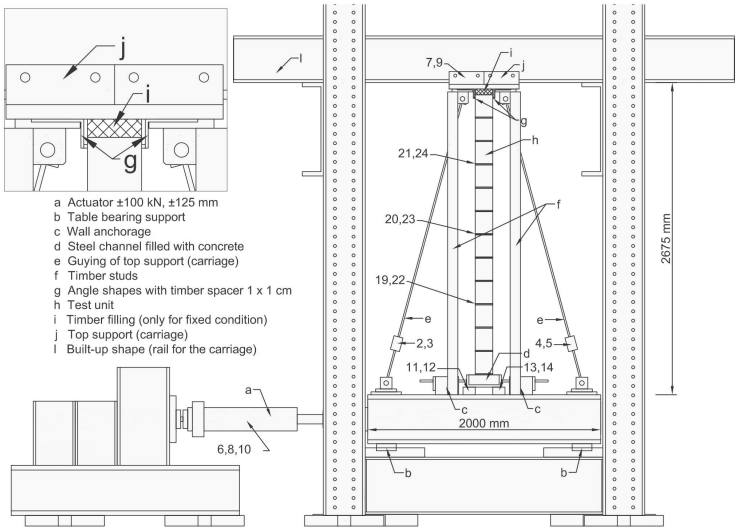

Figure 1.33: Set-up for dynamic tests with detail of the top support [Wilhelm *et al.*, 2007].

representing a typical internal wall with concrete slab, that prevents displacements and rotations. The experimental program led to conclude that, if a correct connection among vertical and horizontal structures is provided, damages concentrated at two third of the panel height. Furthermore, three subsequent phases could be identified during the tests: elastic, stable rocking and rocking with moving of cracks.

1.3.2 Complete models

This section presents some experimental campaigns, carried out on whole buildings models via shaking table facilities. Despite the reference works, presented in the following sections, were performed on different specimens, in terms of employed materials, geometrical dimensions, applied strengthening techniques and several other characteristics, some aspects are remarkable. These can be compared among the considered campaigns and may lead to develop important basic considerations to design part of the experimental dynamic program, main argument of the present research.

Performing experimental campaign on whole structures, instead of single elements, allows to deepen the knowledge about the overall behaviour of complete models. This provides important information, complementary to those achievable from experiments presented in the previous section. As drawback, one should consider that perform experiments on whole models often induce to consider scale factors to realize the specimens. Nevertheless, this topic will be discussed in section 1.3.3.1.

The experiments described thereon can be divided in three main categories, even if they will be presented following a different logical order.
Some experimental programs provided the realization of a single model, tested on unreinforced conditions and after the strengthening, employing a unique technique. This methodology allows to verify the effectiveness of the performed intervention.
Other experiments comprehended two building models realized with the same materials but with different configuration, to study different geometrical and morphological properties, or equal floor plain in unreinforced and strengthened cases, in order to investigate its influence.

Lastly, a series of specimens, different for geometrical configurations, materials and strengthening techniques, can be considered. This approach is surely more expensive and complex but it allows to provide a large quantity of informations and a more extensive database.

1.3.2.1 Tests on stone masonry buildings

The bibliographic research about shaking table tests on stone masonry models reveals as a restricted number of experiments were performed on this kind of buildings. On the other hand, the widespread diffusion of historical buildings, realized with these materials (compare §1.1, [Binda and Saisi, 2005; Bresolato and Pasin, 2008; Gardin, 2007]), and more and less recent earthquake events (Lunigiana and Garfagnana, 1995; Reggio Emilia, 1996; Umbria and Marche, 1997; Piedimonte, 2000; Molise, 2002; Piedimonte, 2003; Salò 2004; Abruzzo,2009) underline the need to deepen the knowledge about their seismic behaviour and strengthening possibilities.

Benedetti [1980] performed a wide experimental campaign of 12 multi-leaf stone masonry building with the aim to verify the effectiveness of different strengthening and repairing interventions. All the models had a single storey and they were realized with the same geometry, considering a reducing scale factor equal to 1:2 with reference to the prototype building.
Two building were tested in unstrengthened conditions and they constituted the reference samples to evaluate and quantify the modifications induced by the applied interventions. Two further building models were respectively partially and fully grouted by a cement admixture, with a water/cement ratio equal to 1:1, injected at about 2bar.
The remaining building models were strengthened using a different number of vertical and horizontal tendons, placed in different positions of the structure with two main aims: providing a vertical prestress in the piers and preventing the out-of-plane failure of the masonry. Furthermore, horizontal ties prevented also the separation of the transversal walls.
After the tests, an unstrengthened and the fully grouted models were repaired, by local grouting and insertion of horizontal steel rods, and tested again. All these structures were subjected to a set of static forces, thus simulating the seismic load through a pseudo-dynamic test.

Both grouted models manifested a good performance. The resistance of the fully grouted model exceeded the measurement range of the adopted instrumentation, thus no data are available at the ultimate state. Furthermore, any crack could be seen on the building model. Actually, it showed a tendency to a rigid rotation, manifesting a separation from the foundation slab.
Differently the model strengthened with a partial grouting could sustain an increasing of about 20% of seismic forces, attaining about 0.45g.
Finally, the models repaired employing cement grout injections showed a likewise good behaviour, since the interventions allowed not only to restore the original strength but also to increase it. Actually, the ultimate load manifested an increasing of about 20% in both repaired models.
Nevertheless, any information is provided about the overall stiffness of the models, even if one should remember as cement admixtures normally induce a noticeable increasing of the stiffness (compare §1.2), thus inducing also a considerable change in the overall dynamic behaviour of the injected structure.

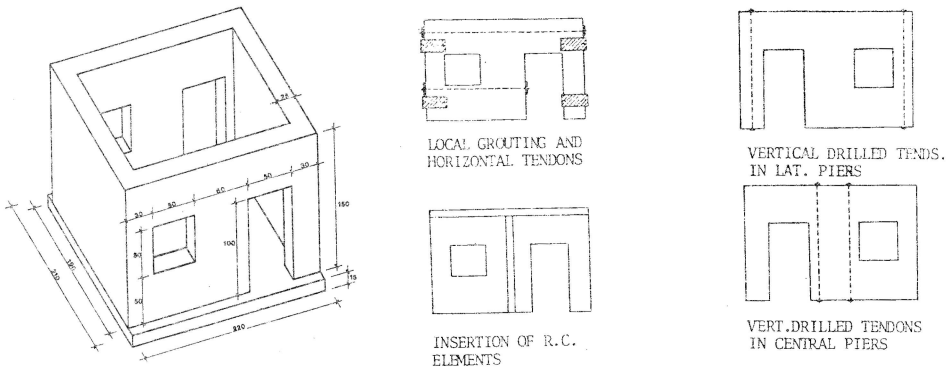

(a) **(b)**

Figure 1.34: Geometry of models and examples of strengthening interventions [Benedetti, 1980].

Several experimental programs were performed at Slovenian national Building and Civil Engineering Institute [Tomaževič *et al.*, 1990, 1992]. Seismic events, even if of a limited intensity, occurred on the Slovenian region [Tercelj *et al.*, 1976; Tomaževič *et al.*, 1985] highlighted as the loss of adequate connections between horizontal elements and vertical structures prevent the possibility to develop the whole resistance of masonry, due to the premature failure of vertical elements caused by out-of-plane mechanisms.

Starting from these considerations, four building models, with a geometrical reducing scale factor equal to 1:4 and two storeys, were realized and subjected to seismic solicitations in order to study the influence of different floor stiffness on the overall dynamic behaviour of structures. Rough limestones were employed for vertical elements. The considered prototype building has a rectangular floor dimension of 3m by 3m, with wooden floors, and the masonry depth is equal to 50cm. Load bearing walls are parallel and without openings; the seismic load was applied in this direction. All models had different horizontal structures:

- double planking wooden floors;
- concrete floors with external RC tie beams;

without any further structural detail. Differently, further two floor systems involved:

- brick vaulted floors;
- double planking wooden floors;

These structures were strengthened using pre-stressed external steel tie rods, to prevent out-of-plane mechanisms.
All tests were performed at increasing amplitude of PGA, considering the Montenegro earthquake (April 15, 1979) as seismic input.
The experiments underlined the importance of providing adequate connections between masonry piers and horizontal structures to avoid undesired out-of-plane mechanisms. Furthermore, a too much massive RC floor element induced a brittle collapse of model at first level, leaving undamaged the second storey.
First considerations were developed on the amplification of accelerations recorded during the tests. Subsequently, the analysis of this accelerations and those obtained from the impact hammer input led to the evaluation of dynamic characteristics of the considered building models. The most important parameters considered

to evaluate the effectiveness of the applied strengthening interventions were the analysis of frequency decay and the variation of the related fundamental mode shapes. furthermore, also the damping values were analyzed to evaluate the energy dissipation capacity of models before and after the strengthening. Starting from the information of the involved masses, the base shear coefficient could be computed. Finally on this basis and relating the actual displacements, the hysteresis loops could be obtained and the analysis of the stiffness variation was also performed.

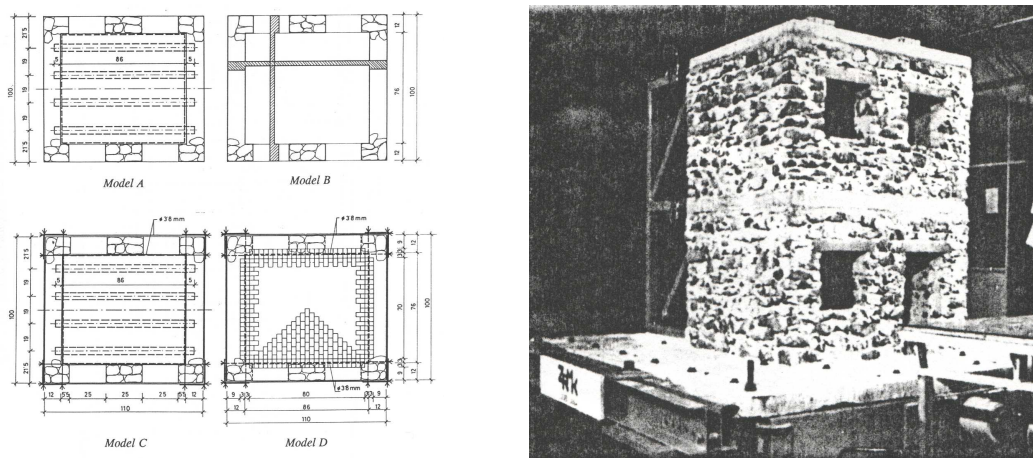

(a) **(b)**

Figure 1.35: Design of different floor typologies (left) and test of a building model (right) [Tomaževič *et al.*, 1992].

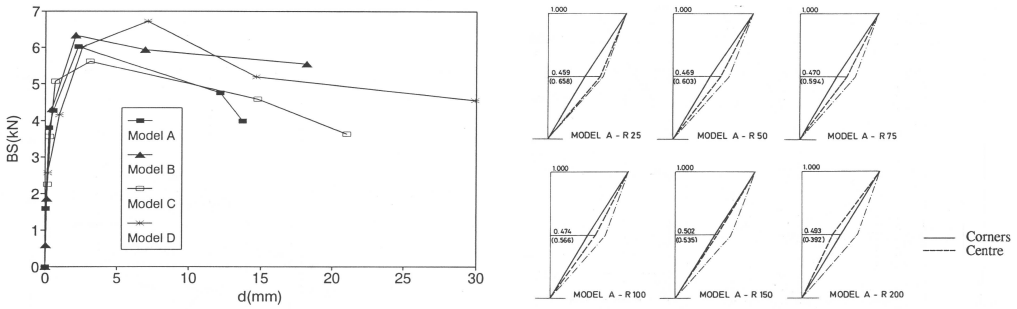

(a) **(b)**

Figure 1.36: Analysis of Base Shear (left) and mode shapes (right) [Tomaževič *et al.*, 1992].

Benedetti *et al.* [Benedetti and Pezzoli, 1996; Benedetti *et al.*, 1998] realized a further wide experimental campaign testing 14 masonry building models between ISMES Research Centre (Bergamo, Italy) and LEE Institute (Athens, Greece). Among these, 6 buildings were realized using stone masonry.
The chosen scale factor was equal to 1:2 and the seismic inputs were applied at increasing PGA for an overall number of 119 tests. The high number of tests and models distinguishes this experimental program, that allowed to study several strengthening interventions[2] (table 1.32) and edit a scale of effectiveness.

[2]lsg: sealing with gypsum-based materials; sc: steel profiles fixed to timber beams; rb: steel

All models had a rectangular floor dimension of 2.20m by 2.75m and an overall depth of masonry of 0.40m. Bricks had reduced dimensions, while stone masonries had a weak connection between orthogonal walls and between walls and floors. Mortar had poor qualities in all cases.
Benedetti *et al.* performed several analyses on the obtained dynamic results. First analyses focused on the study of amplification factors to obtain information about the monolithic behaviour of tested structures. Moreover, the identification of fundamental frequencies was performed and the evaluation of their overall decreasing after subsequent seismic inputs allowed an evaluation on the effectiveness of applied strengthening techniques. Furthermore, the analysis of damping factors led to a comparative analysis of the different dissipation capacity induced by each intervention technique. These quantities were analysed considering the recorded accelerations during the seismic inputs applied, contemporary, in both orthogonal horizontal directions. Finally, the analysis of induced forces and related displacements led to consider the stiffness degradation of the structure (figure 1.38).

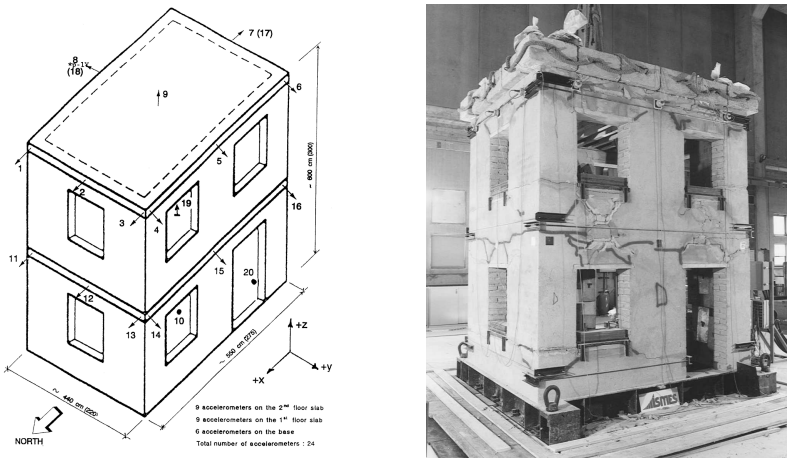

(a) **(b)**

Figure 1.37: Design (left) and test (right) of the building model [Benedetti *et al.*, 1998].

At LNEC (Laboratório Nacional de Engenharia Civil, Portugal), Juhásová *et al.* [2008] carried out an interesting experimental campaign on a stone masonry building. This model was realized at full scale, with a single storey, for an overall mass of 30tons. A 6DOF shaking table was employed with a bi-directional seismic input.
The model had maximum floor dimensions of 3.58m by 4.01m and an heigh of 3.6m and it was unprovided of floor (figure 1.39). The model had an asymmetric plan to study also torsional effects.
The model was initially tested in unstrengthened conditions while, when damage could be seen on the structure, it was repaired with vertical grids and fibre plaster. Impact tests, ambient vibrations, seismic tests on two orthogonal directions and harmonic sweep sine tests were the main inputs employed for the analysis of dynamic characteristics of the tested structure. Furthermore, a numerical simulation was

grid wrapping the whole building, covered by a cementitious matrix; ht: horizontal steel ties; hb: horizontal steel beams posed along the walls; vb: vertical steel beams posed along the walls; a1: curved steel plates posed at intrados and extrados of arches; wp: wooden plankings externally fixed at mid-height to redistribute the stress of ties.

Table 1.32: Intervention techniques applied to stone masonry models [Benedetti and Pezzoli, 1996].

Model	Number of Inputs	Applied technique
E1	5	sc - rb
F1	4	sn 1, 2
G1	4	
H1	3	sc - ht
N1	2	
N2	5	lsg - vb - ht
O1	2	
O2	6	lsg - vb - ht - a1
P1	3	
P2	5	lsg - wp - ht - a1 - hb

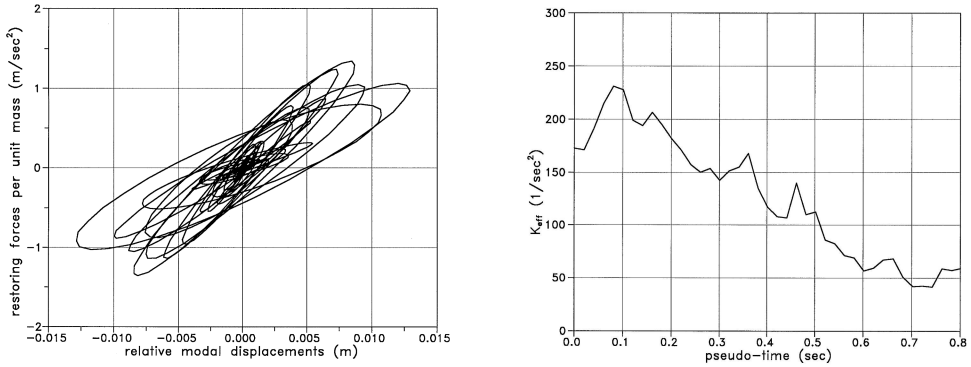

(a) Restoring forces (x-mode, system E1) **(b)** Stiffness variation (x-mode, system E1)

Figure 1.38: Study of hysteretic and stiffness behaviour at ultimate shock [Benedetti *et al.*, 1998].

performed and the mode shapes and frequencies could be compared with those of the tested model (figure 1.40).

As this brief overview summarize, laboratory studies on dynamic behaviour of stone masonry structures are very limited in number. Furthermore, among these examples, any test was performed with the aim to study the strengthening technique considered in this study, namely injection of hydraulic lime-based grout. This prevents a direct comparison with previous investigations.

1.3.2.2 Tests on different structures

The limited number of experimental campaigns carried out on stone masonry buildings led to research further relevant studies performed on similar structures, namely brick masonry models. This extension of the state-of-art, about shaking table tests, allowed a better comparison on the relevant aspects, such as selected input and method of scale, presented in the following sections (§1.3.3). However, few further studies were selected, even if performed on structures realized with different materials, due to their similarities with both previously presented researches and the actual one.

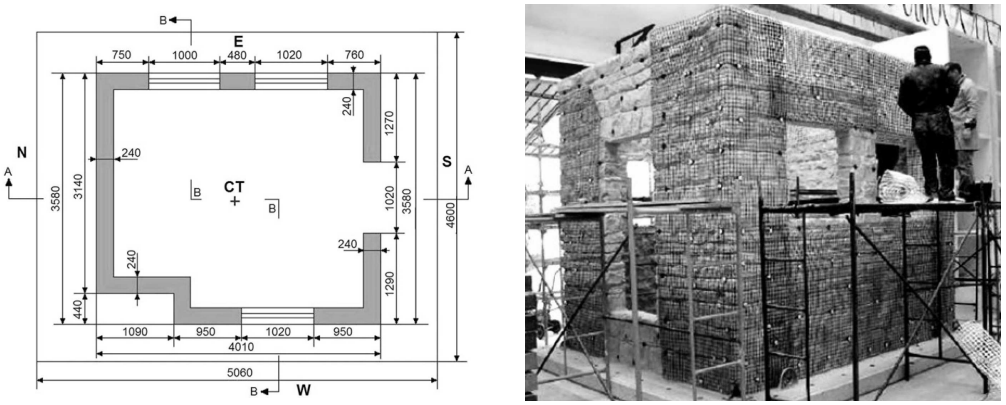

(a) **(b)**

Figure 1.39: Floor plan of model tested by Juhásová *et al.* [2008] and strengthening intervention.

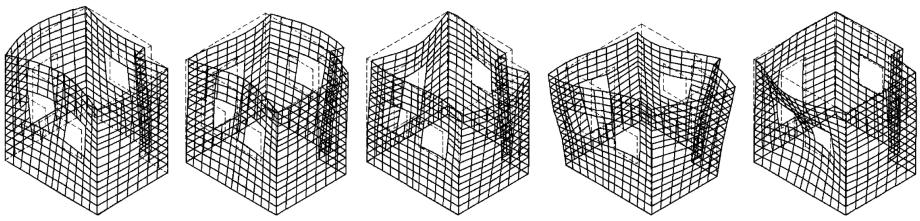

Figure 1.40: Numerical analysis of natural modes of vibration Juhásová *et al.* [2008].

Juhásová *et al.* [2002] performed a further experimental campaign on a brick masonry building at ISMES Research Centre. The model had two storeys and it was realized with a scale factor of 1:2. The floor plan was regular but with different elevation: brick vault and timber floor on two halves of specimen at first floor, while the second storey had a unique timber floor (figure 1.41). This confers an asymmetric behaviour that allows to understand its influence on the overall dynamic behaviour. The masonry had an overall depth of 23cm. Mortar was characterized by poor quality to simulate an historical situation.
Firstly, the specimen was tested on unstrengthened conditions whilst, after the beginning of a heavy damage, it was strengthened using a special lime cement fibre plaster reinforced by plastic grids.

A series of were tests performed at ZRMK Institute in Ljubljana [Tomaževič *et al.*, 1990] and at ENEA Research Centre in Rome [Modena *et al.*, 1992] on similar models with three storey and a scale ratio of 1:5 and 1:3 respectively. These studies were developed to study the dynamic behaviour of a typical Italian residential building, realized with a mixed structure of concrete frames and bricks.
Four models, having two different geometrical configurations, were tests by Tomaževič *et al.* [1990] and their results compared. Two models had a central RC column (2 and 4) while the others had load bearing brick walls (1 and 3). These structures were tested in unstrengthened conditions (3 and 4) and strengthened in both vertical and horizontal directions (1 and 2).
Only one model was tested by Modena *et al.* [1992] and a wide preliminary characterization and comparison among prototype buildings and realized model was carried out.

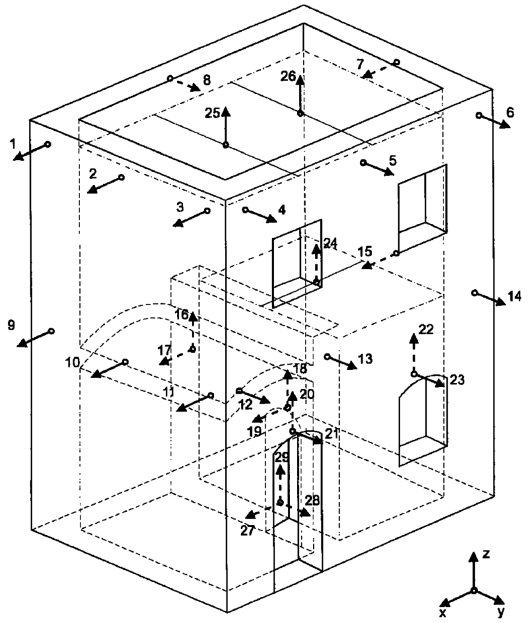

Figure 1.41: Axonometric view of tested building specimen [Juhásová *et al.*, 2002].

Three four storeys models were realized and tested by Jurukovsky *et al.* [1992]. First experiment was realized on unstrengthened conditions, while the remaining models were strengthened by injection of a special cement mortar on brick walls, in one case, and insertion of external RC jacketing panels in the other one. All models had a reducing scale factor equal to 1:3 and they were realized with concrete frames and brick panels at first floor while upper storeys had load bearing brick walls, representing a typical mixed structure in Italy.

A great number of the reported studies were performed on structures with RC load bearing elements and infilling brick walls. This represents the most common situation of modern residential buildings. To deepen the study of this typology, Žarnić *et al.* [2001] carried out an experimental campaign at the University of Bristol.
Two reduced models, with a scale ratio of 1:4, were built. First model (B) had regular floor plan and a single storey, while second structure (H) had a symmetric plan and two levels. The comparison of results allowed an in-depth study of the effect of the out-of-plane solicitations in both configurations. FE models to predict the expected overall behaviour were also developed.

A more recent research, developed at the University of Berkeley [Hashemi and Mosalam, 2006], was developed on a portion of model, representing a multi-storey building with RC frames and brick walls. The specimen was realized with a limited reducing scale factor of 3:4 and the resulting overall dimensions are 4.88m by 4.42m, with an height of 3.43m. The choice of studying only a portion of the prototype building allowed to test a model with dimension close to full scale. The asymmetrical design led to investigate the stress distribution of RC frames before and after the beginning of damage on the infilling brick panels.

Further campaigns, relevant for this study in terms of testing procedures, were performed on structures realized with different materials and aiming at investigating the overall behaviour and effects of both seismic isolation and dissipation devices.

Chung *et al.* [1999] carried out dynamic tests on two reduced steel structures. A first model was tested in normal conditions, while the second one was provided with isolation devices at the base. The study allows a direct evaluation of the effectiveness of this safety methodology but led also to a subsequent assessment concerning the capability of pseudo-dynamic experiments in providing reliable results on these structures. Finally, data collected allowed a comparison with the elaborations obtained by a FE model.

A second relevant experiment was carried out by Dolce *et al.* [2005]. The tested models represents an ideal portion of a building with a RC frame structural system. The specimens was realized with a scale factor of 1:3.3 in original conditions, with filling brisk panels and employing two different devices for energy dissipation based on shape memory alloys.

1.3.3 Design of experimental campaigns on whole models

Past experimental studies on shaking table tests constitute an important reference point about several aspects for the experimental campaign developed and presented in the present research.
The first important aspect deepened in this section is the similitude laws employed to realize the models, to design and chose the materials as well as for all other remaining aspects involved by the scale factors.
The second developed topic focuses on the choice of the adopted input for dynamic test. Particularly, the applied time histories and the motivations which led to the choice.
Lastly, different testing procedures were compared with the aim to obtain an overview on design aspects of practical execution of the experimental program, further important phase to obtain reliable results.

The experimental researches presented in the previous section were considered and, particularly, the few works performed on stone masonry building, having a direct relation with the campaign of tests presented in the following chapters. However, further interesting studies were thus considered to extend this overview and to provide a more complete information on these topics.

1.3.3.1 Similitude laws and Scale Factors

The easiest methodology to design and realize an experimental campaign based on shaking table tests is represented by the realization of specimens at full scale. This allows to employ materials commonly used to build the structure to be investigate, without further problems about their mechanical characteristics, excepting their representativeness of the real situation.
However, many aspects often prevent the realization of full scale models of real structures under study. The geometrical and pay load limits of testing facilities, the impossibility to realize a full scale model, due to the too much greater dimensions of the original structure, and the restraint of cost are among the most relevant causes. This considerations lead to two different solutions: considering only a part of the structure at full scale or realizing a whole model with a geometrical reduced scale factor. This second option, investigated in this section, introduces further problems related to the capability of realizing models representative of the real situation in terms of both mechanical and dynamic characteristics of materials, but also of the whole structures.

All the considerations about Scale Factors carried out during experimental campaigns presented in the following are summarized and compared in table 1.33.

The problem of the geometrical reduction of models, compared to the prototype structure, involves the application of the same similitude laws to all the considered quantities of materials and also to the seismic input. Tomaževič *et al.* [1992] considered a geometrical reduction of models equal to 1:4 and proposes two different methodologies to apply this also to other quantities. The Complete Model entails the use of the materials with reduced mechanical characteristics. Their scale factor can be computed starting from fundamental magnitudes and calculating those derived. As a consequence, also strength and elastic properties of employed materials should be reduced to respect the similitude. This implies the design of proper materials to realize the reduced models with the wide difficulty in respecting the correct scale factor for all the quantities.
Furthermore, also the seismic input should be scaled to induce a correct solicitation on the specimens to be tested. As a consequence of the considered ratios, the time is reduced on the basis of the square root of geometrical scale factor, while the acceleration of the original signal can be considered.

A different method to realize a correct reduction of magnitudes is proposed by the same Tomaževič *et al.* [1992]. This Simple Model starts from the same geometrical scale factor proposed in the Complete Model. However, this methodology is based on the hypothesis to employ the original materials also on the reduced model. This implies that both strength and elastic properties of the specimens are equal to that of the prototype, as well as for its specific weight. This reflects on the processing of the seismic input, that should be reduced in the time with the geometrical scale factor and whose accelerations must be amplified of the same quantity. These considerations involved the employment of steel plates to increase the weight of structure with the aim to respect the correct ratios.

The same methodology of scale reduction was employed by Zonta *et al.* [2001]. In his experimental campaign a geometrical reduction of 3 times was considered and the same materials of prototype building were employed.

Benedetti *et al.* [1998] carried out an experimental campaign on 14 building models, considering a reducing scale factor equal to 2. The considerations developed about properties of materials led to use the same elements employed on the prototype building, simplifying the realization of models. However, to respect the correct stress distribution on materials and to reflect a correct dynamic behaviour with that of original structure, masses were added at floor levels of building specimens. This methodology of reduction allowed to consider the original seismic signal in terms of acceleration, that were not reduced, while the time should be lessen respecting a scale factor equal to the square root of geometrical ratio between model and prototype. Nevertheless, Benedetti *et al.* underlined as the models exhibited an overall behaviour different from than that of the prototype buildings, probably due to the incorrect mass distribution.

A different method, to scale the specimens to be tested, was followed by Jurukovsky *et al.* [1992]. The models were realized with a geometrical reduction of 1:3 and the quantities were computed in accordance with a complete model of similarity. Actually, The elastic properties and the consequent stress are halved, while the specific weight of material of models was properly designed. With the aim to respect a correct overall dynamic behaviour of specimens, the seismic input was considered constant in the acceleration level, while the time was reduced with the square root of geometrical ratio.

As a consequence, also velocities and displacements resulted modified. Furthermore, about the 30% of the overall self-weight was added on the structure to respect the correct stress ratio. Finally, further considerations were developed about the energy amount introduced by the dynamic solicitation.

The models realized by Chung *et al.* [1999] considered a geometrical reduction of 4 times. The employed materials had mechanical characteristics equal to that of the originals structure, resulting in an unavoidable mass reduction that not respect the correct ratio. As a consequence of these considerations, the seismic signal had a time reduction with the square root of geometrical scale factor, while the accelerations were unaltered. Further considerations were developed about the stiffness decrease on the building models.

Žarnić *et al.* [2001] employed an equal geometrical reduction, namely 1:4, but considering a reduction about mechanical characteristics of used materials. This reflects on a reduction of masses, and consequently of forces, that follows the cube of the applied scale factor. The selected and input time histories maintained the accelerations of original earthquake record, while the time domain was reduced following the square root of applied scale factor. Also in this case, masses were added to obtain correct failure modes.

As example of higher scale factor, Li *et al.* [2006] considered a geometrical reduction equal to 20 times of a high-rise building. Due to the high ratio employed on the law of similitude, the materials were accurately designed. Furthermore, to respect the effective stress distribution on the building model, masses were added, even if the high employed factor induced heavy problems in respecting the weight ratio and, as a consequence, also the related magnitudes. Differently, time and acceleration values were elaborated considering the inelastic response of the employed materials.

1.3.3.2 Seismic Input

The results of experimental campaigns carried out via shaking table tests are widely depending also on the applied time history. Furthermore, a correct choice of signals, coherently with the aims of the research, yields more reliable the obtained results. Finally, the possibility of applying a certain time history is widely depending also on the capability of testing facilities to correctly reproduce this. For these reason, the selection of the seismic input should be carefully evaluated and elaborated before its employment.

The experimental program carried out by Tomaževič *et al.* [1992] made use of the North-South component of the Montenegro earthquake, occurred in 1979 and recorded in Petrovać. The attained PGA is 0.43g and this time history was reproduced at 8 different intensity levels, considering percentage of the maximum recorded acceleration varying between 50% and 200%. All inputs had a constant duration of 6s.

Jurukovsky *et al.* [1992] employed four different natural accelerograms: El Centro, 1940; Parkfield, 1966; Friuli, 1976 (recorded in Breginj, Slovenia); Montenegro, 1979 (records of Petrovać and Bar). The aim of using several and different records is mainly the study of the response of the investigated structure when subjected to ground motions, differing because of energy and frequency content. Only natural inputs were employed, since the spectra have a real pattern. Furthermore, two categories of signals were employed: strong earthquakes (El Centro, 1940; Parkfield, 1966) and records of seismic events occurred on the region where the considered prototype building is typical and widely diffused (Friuli, 1976; Montenegro, 1979).

Table 1.33: Similitude laws and Scale Factors employed on some considered studies.

Quantity	Tomaževič *et al.* [1992]		Tomaževič *et al.* [1992]		Benedetti *et al.* [1998]		Zonta *et al.* [2001]	
	law	S. F.	law	S. F.	law	S. F.	law	S. F.
Length (L)	S_L	4	S_L	4	S_L	2	S_L	3
Strain (ε)	1	1	1	1	1	1	-	-
Strength (f)	S_L	4	1	1	-	-	-	-
Stress (σ)	S_L	4	1	1	S_F/S_L^2	1	E_r	1
Elastic Modulus (E)	S_L	4	1	1	1	1	1	1
Sp. Weight (Γ)	1	1	1	1	-	-	1	1
Mass (m)	-	-	-	-	-	-	$S_\Gamma \cdot S_L^3$	$27/8$
Force (F)	S_L^3	64	S_L^2	16	S_L^2	4	L_r^2/E_r	9
Time (t)	$\sqrt{S_L}$	2	S_L	4	$\sqrt{S_L}$	$\sqrt{2}$	$S_L\sqrt{E_r/\Gamma_r}$	3
Frequency (Ω)	$1/\sqrt{S_L}$	$1/2$	$1/S_L$	$1/4$	$1/\sqrt{S_L}$	$1/\sqrt{2}$	$1/S_t$	$1/3$
Displacement (d)	S_L	4	S_L	4	S_L	2	S_r	3
Velocity (v)	$\sqrt{S_L}$	2	1	1	$\sqrt{S_L}$	$\sqrt{2}$	$\sqrt{S_r/\Gamma_r}$	1
Acceleration (a)	1	1	$1/S_L$	$1/4$	1	1	$1/S_L$	$1/3$
Energy	-	-	-	-	-	-	-	-
Stiffness	-	-	-	-	-	-	-	-

Table 1.33: Similitude laws and Scale Factors employed on some considered studies.

Quantity	Jurukovsky *et al.* [1992]		Chung *et al.* [1999]		Žarnić *et al.* [2001]		Li *et al.* [2006]	
	law	S. F.	law	S. F.	law	S. F.	law	S. F.
Length (L)	$L_r = L_r$	3	L	4	L	4	L_r	20
Strain (ε)	1	1	1	1	1	1	-	-
Strength (f)	-	-	-	-	L	4	-	-
Stress (σ)	$\sigma_p = E_r$	2	1	1	-	-	1	-
Elastic Modulus (E)	$E_r = 1/2$	2	-	-	L	4	-	5.650
Sp. Weight (Γ)	$\Gamma_p = E_r/L_r$	2/3	-	-	1	1	$m_m/m_p \cdot 1/L_r^3$	0.282
Mass (m)	-	-	L^2	16	L^3	64	-	-
Force (F)	$F_r = E_r \cdot L_r^2$	1/18	L^2	16	L^3	64	L^2	-
Time (t)	$T_r = \sqrt{L_r}$	1.733	$\sqrt{L}$	2	$\sqrt{L}$	2	$L_r\sqrt{\Gamma_r/E_r}$	4.464
Frequency (Ω)	$f_r = 1/T_r$	0.578	-	-	$1/\sqrt{L}$	0.5	$(\sqrt{E_r/\Gamma_r})/L_r$	0.224
Displacement (d)	$d_r = L_r$	3	L	4	L	4	-	-
Velocity (v)	$V_r = (L_r)1/2$	1.733	-	-	$\sqrt{L}$	2	$\sqrt{L}$	-
Acceleration (a)	1	1	1	1	1	1	$E_r/(L_r \cdot \Gamma_r)$	1
Energy	$W_r = E_r \cdot L_r^3$	54	-	-	-	-	-	-
Stiffness	-	-	L	4	-	-	-	-

An overall number of 28 inputs were applied to the models. One should underline as the non-linear range of the structure was investigated only applying the Montenegro (1979) time history, while the remaining accelerograms were employed during the linear phase of the structures.

Synthetic inputs with a sinusoidal content were employed by Žarnić *et al.* [2001] on both building models. The signal was applied only in one direction, despite the symmetrical configuration of models, with the aim to facilitate the damage identification and the study about the influence of the considered elements. The input was designed with three phases, differing because of acceleration amplitude. This signal was then reduced and amplified in percentage during the experimental campaign.

A single natural record was considered in the laboratory program jointly developed by Italy and Greece [Benedetti *et al.*, 1998]. However, two different elaboration were performed starting from the record of Irpinia earthquake (1980, recorded in Calitri). Firstly, the whole duration of the seismic event was considered, namely about 90s, while the second input comprehends only the first part of this, namely about 40s, characterized the same frequency content.
The time history was contemporary applied on all three orthogonal directions, imposing that a peak of 70% on the vertical acceleration with reference to the horizontal one.

The structures investigated by Chung *et al.* [1999] were provided with seismic isolators. This reason and the fact that models had different fundamental periods led to select and employ more seismic records. Among several possibilities, three time histories were chosen, namely El Centro (1940), Taft (1952) and Mexico City (1985). First two earthquake records are characterized by a wide amplification of accelerations for periods lower than 0.4s÷0.5s and a values clearly lower for periods higher than 0.6s, as the case of isolated structures. This consideration led to apply also the Mexico City record (1985), whose response spectrum shows high values also for higher periods.
Further three synthetic signals were considered. They were realized in accordance with the Uniform Building Code and high values of acceleration can be found in a wide range of frequencies. Even if this situation moves away from the real condition of a natural seismic event, this allows to verify the efficiency and the reliability of the testes devices.

Fardis *et al.* [1999] designed two different synthetic time histories, both characterized by a length of 10s and by a mean damped elastic spectrum of 5% up to a period of 1.3s. Higher period components were filtered out to avoid problems during its replication with the shaking table. Singe the model resulted overstrength, with reference to the characteristics of prototype building, the structure was subjected to a multi-directional seismic input. Both horizontal directions were considered, with an effective peak acceleration three times that of the design motion.

The experimental campaign performed at ISMES by Juhásová *et al.* [2002] considered a natural seismic signal. The input was selected among several time histories, reported in the American Catalogue comprehending the accelerograms and characterized by a magnitude (M) higher than 7.5. The applied signal is that recorded during the Alaska earthquake, occurred on 1972.
All three components of the record were applied contemporary. This accelerogram was selected, due to its adequate frequency content. Actually, the considered seismic input properly solicits a rigid structure as that realized.

Hashemi and Mosalam [2006] selected two different natural time histories, namely Northridge (CA, 1994) and Duzce (Turkey, 1999). Both accelerograms were input only in a single direction, parallel to the filling panel of brick masonry, in order to study their in-plane effects on the RC frame. These records were selected on the basis of their frequency content. The main characteristics were compared with the average between fundamental periods of typical RC frame with and without masonry filling panels. The first input was divided in 6 different PGA levels, while the second considered record was input only at two percentage values.

A single artificial time history was generated by Dolce *et al.* [2005] to test RC frames without and with passive control systems. This input had a spectrum compatible with that proposed for design by CEN - EN 1998-1 [1998], considering a soil typology "B", for an overall duration of 20s. The synthetic accelerogram was divided in 16 increasing levels, that were subsequently applied to the structures, up to attain a maximum value of 1.0g.

A second experimental campaign proposed by Juhásová *et al.* [2008] involved a single time history, selected among several natural records. The chosen accelerogram, namely the record of earthquake occurred in Herceg Novi (1979), was selected as the typical seismic signal at which the investigated structure can be subjected. Both components of the record were employed, even if the structure is already asymmetric. The maximum seismic input acceleration attained values equal to 0.36g and 0.34g, for directions X and Y, respectively.

Zonta *et al.* [2001] proposed the employment of a synthetic time history with a spectrum in accordance with the CEN - EN 1998-1 [1998], considering a soil typology "B". The overall length was 8s and its initial PGA was fixed at 0.06g. 33 subsequent exponentially increasing levels led to the attainment of a maximum acceleration equal to 0.9g. Several tests were executed at low acceleration levels, since one of the main aims was the study concerning the evolution of damage due to subsequent seismic events of medium-low intensity.

The experimental program carried out by Li *et al.* [2006] employed more seismic inputs to simulate rock sites, medium soil sites, and soft soil sites. These time histories were synthetically generated in accordance with the Chinese code [GB 50011-2001, 2001] and also obtained from the elaboration of a natural record. Five different levels of PGA were employed.

The seismic inputs selected by Gülkan *et al.* [1990] are based on a consideration developed also by further authors. Actually, the three considered natural records, namely El Centro (1940), Taft (1952) and Pacoima Dam (1971), were chosen as representative of a seismic event of the selected region.
The ground motion was input parallel to the load bearing elements and only in one direction, due to the limits of testing facility. However, in the second part of the testing program, the models were rotated of 30° with reference to the main direction, inducing in this manner a bidirectional solicitation on the structure.

1.3.3.3 Testing Procedure

The experimental program on shaking table is normally preceded by further laboratory phases with the aim to characterize materials and structure to be dynamically tested.

A first characterization is carried out on quasi-static field. In all cases mechanical characteristics of components are investigated, such as compression strength and elastic properties. Subsequently, dynamic campaigns are often anticipated by com-

Table 1.34: Seismic inputs applied on different experimental campaigns.

Authors	S. F.	Laboratory	Seismic Input	Direction
Tomaževič *et al.* [1992]	1:4	ZRMK	N-S Petrovać, Montenegro 1979	X
Tomaževič *et al.* [1990]	1:5	ZRMK	Synthetic time histories	X
Tomaževič *et al.* [1990]	1:4	ZRMK	N-S Petrovać, Montenegro 1979	X
Modena *et al.* [1992]	1:5	ENEA	Synthetic time history	X,Y
Jurukovsky *et al.* [1992]	1:3	IZIIS	El Centro 1940, Parkfield 1966, Montenegro 1979, Friuli 1976	X,Y
Žarnić *et al.* [2001]	1:4	Bristol University	Sinusoidal input	X
Benedetti and Pezzoli [1996]	1:2	ISMES-LEE	Calitri, Irpinia 1980	X,Y
Chung *et al.* [1999]	1:4	LSSTL	El Centro 1940, Taft 1952, Mexico City 1985	X
Fardis *et al.* [1999]	1:1	ISMES	Synthetic time histories	X,Y
Juhásová *et al.* [2002]	1:2	ISMES	Sitka, Alaska 1972	X,Y,Z
Hashemi and Mosalam [2006]	1:1	Berkeley University	Northridge, CA, 1994 Duzce, Turkey, 1999	X
Dolce *et al.* [2005]	1:3.3	University of Athens	Synthetic time history (compatible with EC8)	X
Juhásová *et al.* [2008]	1:1	LNEC	Herceg Novi 1979	X,Y
Zonta *et al.* [2001]	1:4	ENEA	Synthetic time history (compatible with EC8)	X
Li *et al.* [2006]	1:20	Seismology Bureau, Harbin	Synthetic time histories (compatible with GB-50011-2001)	X,Y
Gülkan *et al.* [1990]	1:1	EERC Berkeley University	El Centro 1940, Taft 1952, Pacoima Dam 1971	X

Table 1.35: Mechanical characteristics of masonry piers, in [N/mm^2] [Benedetti, 1980].

		central pier		lateral pier	
	τ	σ_0	σ_x	σ_0	σ_x
model 13	0.095	0.10		0.132	
model 15	0.150	0.10	0.10	0.164	0.10

Table 1.36: Mechanical characteristics of masonry panels, in [N/mm^2]; values in parentheses indicate properties after strengthening [Tomaževič *et al.*, 1992].

Compressive Strength	σ_c	$0.3 \div 0.9$	$0.6 \div 3.7$
Tensile Strength	f_t	$0.02 \div 0.15$	$0.19 \div 0.33$
Elastic Modulus	E	$200 \div 1000$	$800 \div 3000$
Shear Modulus	G	$70 \div 90$	$100 \div 450$

pression tests on panels to know the strength of structural elements constituent the models. These can be followed by studies about the shear strength and more general shear properties through diagonal or shear compression experiments.

Similarly, dynamic researches on complete models can be anticipated by further shaking table tests on single structural elements constituent the whole building specimens.

This series of experimental tests leads to a complete knowledge of the materials and structures under investigations, permitting to drawn specific conclusions.

Concerning the shaking table tests on whole building models, structures are dynamically loaded at increasing peak accelerations, as discussed in previous section. Furthermore, between two subsequent inputs, dynamic characteristics of models are investigated in different manners to evaluate their modifications.

The experimental campaign designed by Benedetti [1980], even if performed via pseudo-dynamic test and not using shaking table facilities, was relevant since bith the employed materials and structures were similar to those considered in the present research. As a first remark, the models were tested in unstrengthened, strengthened and repaired condition, distinguishing the intervention performed on a damaged or undamaged structure. The interventions were mainly performed using cement grout (water/cement ratio 1:1), which was injected at about 2bar. The main mechanical properties of the unstrengthened and injected masonry is reported in table 1.35, where σ_0 is the vertical stress acting on the wall and σ_x is the horizontal precompression stress. The values of τ range between 0.03N/mm^2 and 0.08N/mm^2 in the first case, while the strengthening increases these limits up to 0.08N/mm^2 and 1.2N/mm^2.

The whole experimental program, designed by Tomaževič *et al.* [1992], involved a preliminary mechanical characterization of employed materials. In this case, mechanical properties of masonry panels were investigated, as well as those of employed lime mortar. The mean values are presented respectively on table 1.36 and table 1.37.

The dynamic experimental program performed by Tomaževič *et al.* [1992] was carried out at increment of 25% of the original signal, from 25% up to 200%. Further investigations about dynamic properties of models, namely fundamental frequencies, mode shapes and damping factors, where developed hitting the models at the top floor level with an hammer and measuring the resulting free vibrations. A comparison with the survey of crack pattern complete the studies.

Table 1.37: Mechanical characteristics of employed mortar, in [N/mm^2] [Tomaževič *et al.*, 1992].

Models		A & B	C & D
Compressive strength	σ_c	1.23	0.94
Tensile Strength	f_t	0.34	0.35

Table 1.38: Mechanical characteristics of materials, in [N/mm^2] [Benedetti *et al.*, 1998].

Element	Compressive Strength	Diagonal Strength
Mortar	0.80	-
Stone	0.27	0.043
Brick	2.20	0.151

The experimental campaign developed by Benedetti *et al.* [1998] on 14 models involves both stone and brick masonry elements. A preliminary mechanical characterization of materials was performed only on mortar while further compression and diagonal tests were carried out on masonry panels (100cm x 150cm x 22.5cm). Mean values are summarized in table 1.38.

The dynamic tests on shaking table were performed at increasing load levels but preventing their collapse with the aim to allow a subsequent repairing intervention. The identification of more relevant dynamic quantities was performed during the tests simplifying the whole structure as an equivalent linear system and the system as "single input-single output" problem. First ten modes were identified even if one should note the difficulty in detecting some modes when heavy damages occurred on models.

Shaking table tests performed on stone masonry buildings by Juhásová *et al.* [2008] were anticipated by a mechanical characterization of materials used on models (table 1.39). Further investigations were carried out through in-situ studies, such as flat-jack tests, and other chemical experiments.

Subsequently to the preliminary characterization phase, dynamic tests were carried out on the unreinforced model using a bidirectional input at increasing PGA, up to a maximum values of 0.36g. Over this solicitation the structure was strengthened and tested again up to about 1.30g.
The identification of relevant dynamic characteristics was performed after each subsequent seismic input. These quantities were obtained from records of several different methods of solicitation: hitting the model in several points with an hammer, and using sinusoidal inputs at constant amplitude as well as ambient and white-noise vibrations. These monitoring was repeated twice, with shaking table facility operatives and switched off, to study the influence of basement vibration.
Lastly, one should note as the strengthening intervention allowed to sustain higher seismic loads but also modified the crack pattern, that concentrate at the basement of the model. Furthermore, the intervention induced modifications also on dynamic properties, particularly permitting a better dissipative quality and a more monolithic behaviour.

Table 1.39: Mechanical characteristics of employed materials [Juhásová *et al.*, 2008].

	test	[N/mm^2]
Stone	σ_c (stone kind A)	67.31
	σ_c (stone kind B)	67
	E (stone kind A)	37478
	E (stone kind B)	35000
Mortar	σ_c (mortar prisms)	0.8045
	E (plaster mortar)	1125
	σ_c (plaster mortar)	10-14
	f_t (plaster mortar)	1.6-1.9
Grid	(ε at 3%)	2.5 kN

1.4 Identification Methods

Dynamic monitoring and the subsequent dynamic identification of structures represent one of the most important non-destructive techniques to deepen the knowledge about their seismic behaviour. Furthermore, the application of different modal identification techniques to models subjected to laboratory tests allows to detect their structural damage as well as provide informations about the influence of strengthening techniques on the dynamic behaviour of the considered elements.

Dynamic identification, was firstly developed and applied on the aeronautic and aerospace fields [Kennedy and Pancu, 1947]. Several studies were performed on following decades [Allemang, 1984] and on seventies, with the development of transducers, sensors and acquisition system, modal testing was established [Ewins, 1984]. Only on eighties, this methodology was also adopted to characterize civil structures [Cawley and Adams, 1979]. Particularly, different methodologies of testing, mainly based on the analysis of the response of a structure subjected to the application of an external force (Input-Output methodology) either on the study of its natural vibrations (Output-only methodology).
These analyses lead to investigate fundamental frequencies, mode shapes, values of damping factors and further modal parameters. On the basis on their variation, structural damages can be detected and a comparative study can also allow their localization.

Earlier and also nowadays most diffuse applications on the field of Civil Engineering are those applied to steel or reinforced concrete structures. A wide overview on these arguments and on methodologies of application is provided by Doebling *et al.* [1996], while further and more recent researches focus on specific topics, such as the application of structural damage identification and localization to RC structures [Zonta, 2000], the variation on dynamic characteristics on different structural elements at increasing damage [Garaygordóbil, 2003] and detection of structural damages on precast RC elements [Franchetti, 2004], deepening also the effects of prestressing procedure.
The above mentioned studies and further researches demonstrate as dynamic tests are a potentially highly-effective investigation methodology to obtain several informations

about the whole structure as well as on local damage.
The application of these methodologies to Cultural Heritage buildings and, more generally, to historical structures is an argument which started to be developed during last decades and which is currently under deep development.

Casarin [2006] carried out an experimental study about the structural assessment and vulnerability of Cultural Heritage buildings. Modal analysis techniques were applied to the Cathedral of Reggio Emilia with the aim to identify its dynamic characteristics. Furthermore, the obtained results were employed to develop and calibrate a complex FE model. This study highlights the possibility in employing dynamic monitoring systems to detect both overall and local behaviours. This knowledge leads to the choice of a correct intervention, if needed, and enables the study of effects of these strengthening on the considered structure.

A further relevant study [Ramos, 2007] deepens and develops a damage identification methodology to be applied specifically on masonry structures. Laboratory experimental tests were performed on masonry arches and panels to study, through vibration signatures, the damage propagation at low intensity levels with the aim to perform increasing damage scenarios. This method, on the basis of developed observations, was applied also to real study cases, namely the Clock Tower of Mogadouro and the Church of Jerónimos Monastery, in Lisbon.

Garaygordóbil [2003] performed a series of laboratory experiments on masonry walls, stone piers and both RC beams and slabs. Furthermore, the simple-layout experiment employed allowed to demonstrate the usefulness of dynamic assessment on structural elements. An extensive numerical simulation was also developed to simulate the real condition. The combination of these analyses resulted suitable to study the correlation between the occurrence of damage and the variation of the dynamic properties of considered structural elements. Finally, the methodology was validated by its application on masonry building components of Historical Constructions in Spain and Belgium.

Besides these researches, completely dedicated to the development of new methodologies of identification and relation with the dynamic and mechanic characteristics of investigated constructions, several further studies were developed about the application of dynamic identification of masonry structures. Most of these applications are study-cases in which a dynamic monitoring was performed and modal parameters were identified.

The dynamic behaviour of an existing masonry building was investigated by De Sortis *et al.* [2005]. Low vibration levels were particularly studied, as in the case of [Ramos, 2007]. Sinusoidal and sweep vibration input were applied to the structure in order to detect structural damages. Probably due to weak non-linearities, the measurements obtained from sinusoidal tests appeared more reliable and suitable than those achieved through sweep tests. Very good agreement between numerical and experimental frequency response functions was found, allowing to conclude that well-established identification techniques can provide useful information about the dynamic properties of existing masonry structures.

An interesting application of operational modal analysis for damage detection was performed by Ramos *et al.* [2005]. The identification methodology was applied to a one-storey masonry building model subjected to shaking table tests Juhásová *et al.* [2008] and presented in previous section. Besides the identification and localization of structural damages, one of the main objectives of this study was the comparison of classical modal analysis with the ambient-based modal analysis. This allowed

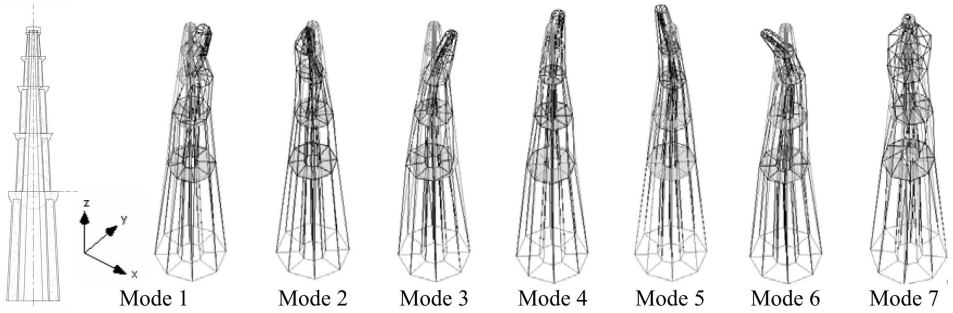

Figure 1.42: Identified modes on the Qutb Minar [Ramos *et al.*, 2006].

the validation of the use of this technique particularly for damage detection in early phases of development.

Ambient vibration tests were employed to define the dynamic properties of the Qutb Minar tower [Ramos *et al.*, 2006]. The developed analysis led to identify seven different mode shapes (figure 1.42). Furthermore, some FE models were realized to simulate its structural response and the obtained results manifested a good relation with modal identification values. These models were also used to evaluate the overall performance of the structure and to define the maximum allowable seismic solicitation.

Further applications for large employment of dynamic monitoring are those presented by De Stefano and Clemente [2006]. Wireless systems and optical sensors were employed in the structural monitoring of Historical Constructions. Particularly, the author underlines the great advantages, the low cost and the possibility of acquiring high quality and "real-time" information on the dynamic behaviour of considered structures, allowing a probabilistic safety assessment and their structural control.

Several further application to real study cases were presented by several authors [Gentile and Saisi, 2004, 2007; Jaishi *et al.*, 2003; Modena *et al.*, 2001]. In all cases the main aim was the study of dynamic characteristics of a damaged structure, mainly the study of frequencies and mode shapes. Starting from the results obtained from these monitoring analyses, authors could drawn observations on the structural conditions of investigated elements and this led to the design of proper interventions. The persist of monitoring also after the strengthening allowed to validate both its effectiveness and influence.

As emerged by researches previously mentioned, the application of modal identification to historical buildings represent a difficult topic due to the wide variability of mechanical properties of masonry, differently from other typological structures, such as RC or steel constructions. However, it is also clear that this technique can be very usefully and effectively applied in the survey of Historical Constructions. Actually, this methodology allows to obtain global information about the investigated structure in a non-destructive way, providing also informations not achievable by further non-destructive techniques (compare §1.1.3).

1.4.1 Dynamic investigation of the structural behaviour

Dynamic modal testing can be defined as a methodology of investigation about dynamic characteristics of structures with the main objective of obtaining a mathematical description of their dynamic parameters [Ewins, 1984]. Three different requirements

control the reliability and the feasibility of analysis and they are influenced by further elements, such as practical aspects and elaboration methodologies:

- the theoretical basis of vibration - experimental modal analysis techniques;
- accurate measurement of vibration - acquisition equipments;
- realistic and detailed data analysis - modal extraction methods;

Therefore, the dynamic identification is an experimental process from which it is possible to extract the modal properties of the structure, namely frequencies, mode shapes and modal damping. These properties are inherent characteristics of the structure and are directly related to its physical properties (mass, damping and stiffness) and to the boundary conditions. This way, this methodology presents itself as a very interesting NDT for the acquisition of important quantitative information on the structure's modal properties, allowing to constitute an accurate mathematical modal model which can be very important for validation and calibration of previous mathematical models over the structure, as well as for damage detection by the analysis over the changes of the modal properties.

Regarding the experimental modal analysis techniques, there can be defined two main groups, according to the type of excitation: the Input-output techniques, also called as Classical Structural Identification techniques, and the Output-only techniques, also called as Operational Modal Analysis (OMA). Furthermore, free vibrations tests can be performed to acquire the dynamic properties of the structure, by measuring the dynamic response of the structure after releasing it from an initial deformation. Nevertheless, for in-situ applications, and especially when Historical Constructions are involved, the Input-output and Output-only techniques are more adequate. The basic fundamentals and associated modal extraction methods, for each one of the presented techniques, will be further detailed in section 1.4.2.

1.4.1.1 Basic Measurement Systems

This section presents the experimental equipments normally employed to perform modal identifications and is not intended to be an exhaustive description (figure 1.43). Further and more detailed aspects and updated informations can be found in the works of Cunha and Caetano [2005] and Ramos [2007].
Different methodologies of experimental extraction of structural modal parameters can be obtained through determined, even if not yet standardized, test procedures. These systems are based on a set of equipments that can be summarized in three different categories:

- support and excitation of the considered structure;
- signal transduction of acquired quantities, as input and response;
- acquisition systems and data processing.

Structural support and excitation

In the first category two main aspects can be distinguished, that need some specifications, and should be considered when approaching to the modal identification of a structure. These are: (i) the support of the structure; (ii) the excitation method.

When a structure is investigated, the first important information regard the support and the boundary conditions of the considered element. These can be

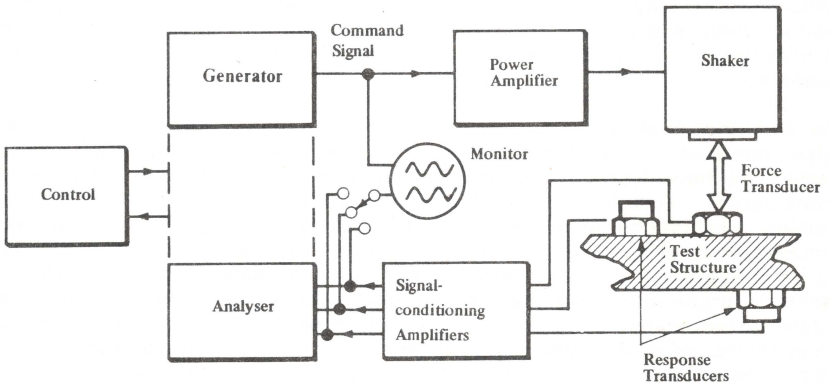

Figure 1.43: Basic components for experimental dynamic identification [Ewins, 1984].

distinguished in three main categories: unrestrained, grounded or in-situ condition. Free boundaries represent the easier situation to be investigated, since this can be clearly identified and defined, while remaining situations are more difficult to describe and to represent [Ewins, 1984].

A second important aspect to be deepened is constituted by the excitation mechanism. Actually, this induces vibrations on the structure to be investigated, allowing the identification of its modal parameters, through subsequent analyses. The most common excitation methodologies, in the field of civil structures, are structural shakers and impact hammers. Further excitation methodologies are represented by drop weight methods, step relaxation, consisting in releasing the structure from a determined deformation state, and ambient vibration, commonly induced for example by wind, traffic and vehicles, among others.

Among several excitation techniques and methods, structural shakers are commonly employed to induces a solicitation in a structure (figure 1.44). These equipments are characterized by different working configurations, mainly based on mechanical, electro-magnetic or electro-hydraulic nature. These techniques normally induce large forces in structures, being used to investigate dynamic properties of large structures, such as bridges or towers. Furthermore, their employment is a difficult topic and they need of a wide test preparation (correct fixing to the structure, interruption of its use, etc.). For these reasons, their employment on masonry structures should be avoided, at least for small or medium elements. Actually, the large applied excitation can induce both damages and instability problems or produce non-linear response of the structure.

The most commonly used technique to induce a force on small structure, and particularly on masonry structures, is represented by the impact hammer. Actually, this method allows to induce a force in the studied structure in a very simple way and this is able to provide a wide-band input. This constitutes an important point, since several and different mode shapes can be investigated. Among major disadvantages, the relatively low spectral estimates frequency resolution should be noticed. This can induce some inaccuracy in the estimation of modal damping factors and in the lack of energy to excite some relevant modes of vibration [Cunha and Caetano, 2005].

Signal transduction

During the years, several different transduction systems were developed to perform experimental measurements of the dynamic response of structures. Nowadays, most

Figure 1.44: From left to right: Impulse hammer; Impulse excitation device for bridges; Electrodynamic shaker over three load cells; Eccentric mass vibrator [Cunha and Caetano, 2005].

commonly employed and representative equipments are piezoelectric, piezoresistive, capacitive or force balanced accelerometers (figure 1.45). Each accelerometer typology can be applied to different structural elements, due to its own particularities and advantages or disadvantages in each particular case. Recently, wireless sensors were developed and started to be applied in the field of dynamic identification and monitoring. These equipments allow to obtain an extensive and continuous set of structural response data with a minimum cost, even if even if they should well calibrated and noise problems can arise in the acquired signals. More detailed information about this type of sensors can be found in De Stefano and Clemente [2006] and Ramos [2007].

Sensor equipments allows to acquire physical data and transform them in equivalent electrical signals. Devices normally employed are displacement and acceleration transducers, in order to known the corresponding typical quantities of the selected structure. These signals are received by a Data Acquisition Systems and subsequenly transformed into digital data. Accelerometers usually provide signals with a rather low intensity, thus condition amplifiers are included in these acquisition systems. These equipments are also designed to provide anti-aliasing, low-pass filtering (allowing lower sampling rates) and analogue integration to velocities or displacements [Cunha and Caetano, 2005].
The reliability of results of dynamic identification procedures is widely depending on both quantity and quality of dynamic informations on the structure. Better results can be obtained by placing as much transducers as possible. Furthermore, their disposal should be studied, depending on the structure typology, to obtain correct and relevant data. Having an idea about the range of frequencies and acceleration levels to be measured is also an important topic and this is depending on the sensitiveness of the operator. Further aspects that influence the analysis are economic factors, aim of the data and periodicity of measurements.
These considerations lead to the choice of the types of sensors to be employed, their number and location, the mounting system, duration of the signal recording and definition of the data acquisition and storage software.

Acquisition System

Last important aspect that allows to obtain reliable results is represented by the data acquisition device. This equipment analyses data collected from the vibration of the structure, starting from both excitation and response signals. Actually, the device receives the electrical signals, from transducers, and processes these, transforming them into digital data, to be analytically analysed. These operations are possible

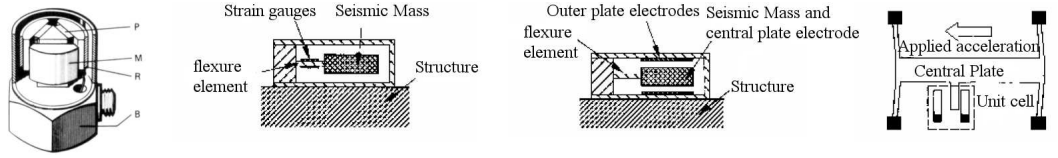

Figure 1.45: Schematic cross-section of (a) piezoelectric, (b) piezoresistive, (c) capacitive and (d) force balance accelerometers [Cunha and Caetano, 2005].

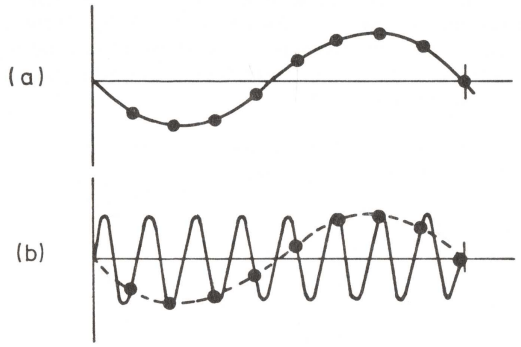

Figure 1.46: Aliasing phenomenon [Ewins, 1984].

through the use of a converter device, normally included in the equipment (Analog-to-digital converter, ADC).
Furthermore, the acquired signals should be firstly conditioned and, only subsequently, processed to obtain results about dynamic characteristics of the investigated structure. Most common conditionings automatically performed on acquired signals are: (a) amplification of the low levels signals to increase resolution and reduce noise; (b) filtering signal data to prevent aliasing phenomena (low-pass filter and anti-aliasing filter should be used to remove spectral measurements approaching the Nyquist frequency [Ewins, 1984]) and also reduce noise; (c) isolation of the transducers signals from the computer; (d) exciting transducers, that need external voltage or excitation; (e) linearisation of the non-linear transducers response in case of changes during the measures [Ramos, 2007].

Among these conditionings, anti-aliasing techniques is underlined. Actually, aliasing phenomena can induce heavy errors (figure 1.46): two different continuous signals can become indistinguishable when sampled, since two signals of different frequencies can produce identical digital signals. The anti-aliasing filter technique allows to remove from signal the frequency components higher than the one which is able to be properly resolved by the sampling device. It is clear as an adequate choice of sampling rate is fundamental. This sampling rate should be at least twice than the maximum signal in the analogue signal, according to the Nyquist frequency [Ewins, 1984].

1.4.1.2 Data processing

The processing of acquired signals is a sensitive process and special cares should be paid in order to avoid errors in the analysis of data and consequent results. Furthermore, one should consider as the normally acquired signals, such as accelerations, displacements or forces, are in the time domain, while most common analyses, as well as spectral properties, are in the frequency domain.

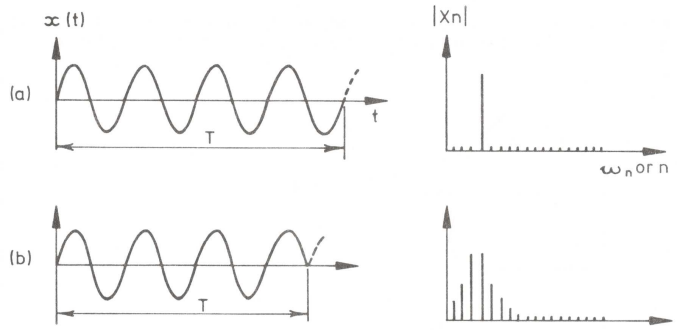

Figure 1.47: Leakage phenomenon [Ewins, 1984].

First important phenomenon to prevent is leakage. This problem is a direct consequence of the basic hypotheses of analysis of acquired data. Actually, recorded signals have a finite length, while this is assumed as periodic when processed (figure 1.47). As mentioned, this can occur when the signal is transformed from time to frequency domain, through the Fast Fourier Transform (FFT). The FFT is a variation of the well known Fourier Transform algorithm and relates to a finite sampling interval (which must be a value of 2^n where n is an integer. i.e. 2, 4, 8, 16, ..., 512, 1024):

$$X_k = \sum_{n=0}^{N-1} x_n \cdot e^{\frac{2\pi i}{N} \cdot n \cdot k} \qquad \text{k} = 0, \ldots, \text{N-1} \tag{1.2}$$

This analysis methodology, namely FFT, is commonly employed in signal processing because it makes use of an algorithm characterized by a low computational cost, assuming a periodic signal in the sampled window. When this is not verified, which is normally the case for experimental modal data, leakage can occur and cause serious errors in the frequency domain data. Furthermore, this can also result cause in a limited amplitude of the signal with reference to the true value.
This error can be minimized superimposing a predetermined function to the real time signal by windowing. This process consists in applying weighting functions to acquired signal with the aim to guarantee periodicity requirements of the FFT, namely inducing a continuous and periodic waveform sample. The common signal discontinuities, normally at the beginning and end of the sampling period, are forced to be equal to zero, by the use of these weighted functions or windows. Several types of windows can be employed (figure 1.48), each one with its one particularities and applicability to the type of signal, most common functions are the Rectangular and Hanning windows, flat-top and exponential windows.

The filtering process is a technique normally applied in the time domain field and this is normally applied to solve the aliasing problems. Similarly to the weighting functions, filtering modifies the spectrum signal removing unwanted parts of the signal, such as random noise, or extract useful parts of the signal. The most commonly used filters for signal processing are the low-pass, high-pass and band-pass, that reduce signals with frequencies higher, lower or within a certain range respectively. Band-stop and notch filters (a band-stop filter with a narrow stop-band) are further less common signals.

Decimation is a process allowing to resample the rate of acquired signal. This is a low-pass digital filter used over the spectrum signal, whose output sample rate is less

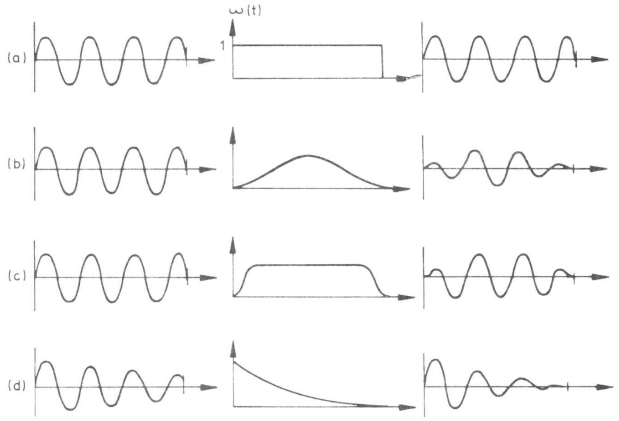

Figure 1.48: Different types of window: (a) without windowing; (b) Hanning window; (c) Cosine Taper; (d) Exponential window [Ewins, 1984].

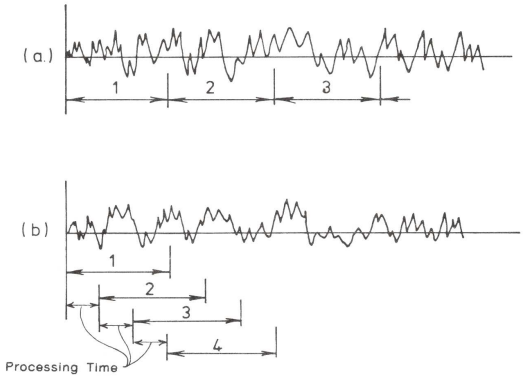

Figure 1.49: Sequential (a) and Overlap (b) averaging [Ewins, 1984].

than the filter's input sample rate. However, this results in a loss of accuracy and quality of original signal. In order to avoid aliasing problems, the output sample rate must not violate the Nyquist criteria. Furthermore, a low-pass filter with a cut-off frequency of about 40% of the new sample frequency should be applied [Ramos, 2007].

Finally, an overlap averaging can be considered during the signal processing. This methodology is commonly applied in the case of random processes, for which spectral densities and correlation functions should be computed instead of Fourier Transforms. The method consists in considering subsequent samples with a certain percentage of overlap and this results in an extra processing of collected data. As a consequence, this shrewdness allows to obtain smoother spectra. Furthermore, statistical properties of this analysis are obviously different than those obtained from samples without overlap (figure 1.49).

1.4.2 Techniques of modal identification

During last decades, several methods to perform a modal identification of a structure were developed ans subsequently refined. Among these methodologies two main groups can be identified:

- Input-Output techniques;
- Output-only techniques.

Most relevant difference between these techniques is given by the type of excitation considered as input in the structure. The chosen method obviously influences the measurement settings employed to detect the dynamic response of investigated structure and the mathematical approach to extract modal parameters.
On the following section a general overview on main theoretical principles of Input-Output and Output-only methodologies is provided. A list of commonly employed techniques for modal extraction of parameters is also given.

1.4.2.1 Input-Output techniques

The Input-Output techniques is based on the knowledge of both the force induced in the structure to be investigated and its dynamic response. This methodology considers the analysis of transfer functions, to control the output response of the structure. These techniques represent the earliest developed methods on the Dynamic Identification field. Nevertheless, nowadays this method is less employed, due to the development of algorithms based on FFT, that allows a faster processing. Furthermore, the transition from time to frequency domain and vice-versa results easier.

As expressed, the modal identification based on the Input-Output technique is focused on the analysis of the structural response to a given and known excitation. As a consequence, the commonly applied analysis methodology is based on the estimation of a set of Frequency Response Functions (FRF), that provide informations on the response of the system subjected to an input [Ewins, 1984].

The Frequency Response Function ($H_{(I,J)}(\omega)$) is computed starting from the FFT analysis of the acquired signals of structural response. Collected data are normally measured in terms of accelerations (defined also as Inertance, when a ratio between the acceleration and the applied force is considered) and they are transformed from time to frequency domain. The FRF represents the ratio of the FFT functions of the response signal and that of the excitation (equation 1.3). Otherwise, this elaboration can be intended as the transformation of the acquired accelerations data into a series of sinusoidal waves, from the lowest possible frequency (when a cycles crosses the entire time record), up to as many cycles as possible (one-half of the sampling rate, per Nyquist) [Shust, 2001].

$$H_{(i,j)}(\omega) = \frac{Y_i(\omega)}{U_j(\omega)} \tag{1.3}$$

The estimation of modal parameters can be also developed in the time domain, employing similar techniques based on the Inverse Fourier Transform (IFT) to obtain an Impulse Response Function (IRF).

The Frequency Response Function can be also computed through stochastic input-output analyses of the cross-spectra density functions, of excitation and response signals, and of Power Spectral Density (PSD) functions, of the response to the excitations [Ramos, 2007]. The PSD is computed as an FFT analysis of set of data in which the original signal can be divided. Results are thus averaged and divided by the frequency resolution.
The PSD is the adequate methodology to analyse random data, since direct FRF technique can not be applied. On the contrary, this method is appropriate for deterministic and periodic time histories.

The reliability of FRF analyses results can be verified through the studying of further modal parameters, such as natural frequencies and mode shapes, as well as

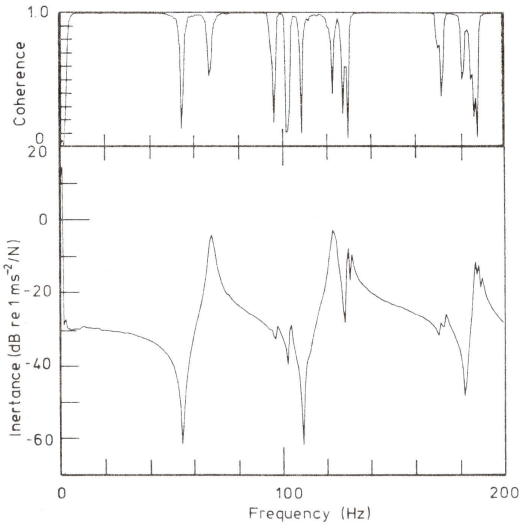

Figure 1.50: Examples of inertance and phase of a dynamic identification [Ewins, 1984].

by the computation of adequate estimators, namely the Coherence and the Phase functions.

The Coherence function (γ) is an estimator which gives a measure of the quality of the data, by performing a ratio between receptance estimators of the response and of the excitation signals. The Coherence can be defined as follows:

$$\gamma^2_{i,j}(\omega) = \frac{H_1(\omega)}{H_2(\omega)} = \frac{\left|S_{y(i,j)}(\omega)\right|^2}{S_{y(i,i)}(\omega) \cdot S_{y(j,j)}(\omega)} \tag{1.4}$$

where $S_{y(i,i)}$ and $S_{y(j,j)}$ are, the PSD of response and excitation signals respectively, while $S_{y(i,j)}$ is the cross spectrum between same signals [Ewins, 1984]. The more close to the unit the Coherence values, the more reliable the performed analysis, since a good relation between signals was found.

The second indicator of reliability is constituted by the Phase function. This compares two sinusoidal components, obtained from previous FFT analyses. Its overall trend can be intuitively related to the overall behaviour of the structure. Actually, when both sinusoidal components of considered signals attain their maximum value at the same frequency, the Phase is close to zero. On the contrary, when components manifest an opposite behaviour, the phase attain 180 degrees [Shust, 2001].

Modal extraction methods

The theoretical bases, previously and briefly exposed, led to several different methodologies of analysis. Actually, a great number of extraction methods were developed during the years by several researches. Modern computational instruments improved the algorithms of analysis for the structural Dynamic Identification, evolved from aeronautical and mechanical engineering fields.

Each developed method is properly indicated in some situations, such as depending on input signal and typology of structure. Furthermore, the choice of the most adequate method to be applied significantly depends also on the modal parameters which are intended to be extracted.

These analyses methodologies can be categorized in very different forms; the classification proposed by Cunha and Caetano [2005] is reported in the following:

- Domain of application (Time or Frequency domain);
- Type of identified dynamic properties (Indirect or Direct);
- Number of modes analyzed (Single-degree-of-freedom (SDOF) or Multiple-degree-of-freedom (MDOF));
- Number of inputs and output locations (single-input single-output (SISO), single-input multiple-output (SIMO), multiple-input single-output (MISO) and multiple-input multiple-output (MIMO));
- Types of estimates (Local or Global).

A schematic list of most important and effective modal extraction methods is reported in table 1.40, obtained from the overviews presented by Ewins [1984] and Ramos [2007]. The most common subdivision among all methods is provided by their domain of application, namely Time or Frequency domain.

Frequency domain methods provide a quite accurate, quick and almost direct modal estimation. This can be performed by the simple identification of the peaks of FRF's functions, if a non-noisy input is used and if the structure to be investigated is characterized by well separated structural natural frequencies. The extracted parameters should be validated through a comparative evaluation of other modal parameters, namely phase angle, magnitude and coherence functions.

Methods operating in the time domain are normally more robust even if also more complex than algorithms working on the frequency domain. Furthermore, both data processing and development of considerations result in a more difficult interpretation. Their development was a need to overcome leakage errors and limitations of frequency domain methods. Lastly, time domain methods are more accurate, when a large frequency range is analyzed and a considerable number of modes are present [Cunha and Caetano, 2005].

The local or global definition is related to the analysis method of FRF's. Actually, while the local estimation is characterized by a separate analysis of the computed FRF's, in the global one all these functions are considered in an analysis.

1.4.2.2 Output-only techniques

The Output-only techniques had a wide enhancement during recent years, due the important advances made on the experimental equipments technology. Actually, this guarantees a higher accuracy on the dynamic response measurement and a consequent reliability of results. Furthermore, the accuracy of results obtainable through the employment of Input-Output techniques is widely depending on the methodology of exciting the structure, with the aim to obtain the most important mode of vibrations in a low range of frequencies. On the contrary, the analysis of modal properties of the structure based on their simply ambient vibration results easier. Actually, the Output-only techniques, namely Operational Modal Analysis, provide the dynamic response of the investigated structure, excited only by ambient and operating forces. This can be considered as a stationary white noise stochastic process in a frequency range of interest [Ramos, 2007]. This particular input allows the excitation of a widespread band of frequencies, larger than other excitation methods, and make

Table 1.40: Resume of most important modal extraction methods for Input-Output analyses [Ramos, 2007].

	Method	Formula	DOF	Type of estimates	Number I/O
Frequency Domain	Peak Peaking (PP)	Indirect	SDOF	Local	SISO
	Circle-fit				
	Inverse				
	Dobson				SISO MIMO
	Nonlinear LSFD		MDOF	Local Global	SISO
	Orthogonal Polynomial				MIMO
Time sinusoid	Mau		SDOF	Local	SISO
	Asher's		MDOF	Global	MIMO
Time domain	Complex exponential		SDOF	Local	SISO
	LSCE		MDOF	Global	SISO MIMO
	Ibrahim (ITD)				MIMO
	ERA				
	ARMA	Direct			

easier the identification of the most important vibrational modes as well as other modal parameters.
In the case of most structures, the excitation, due to their regular operating conditions, can be considered as a stochastic input, namely ambient vibrations that produce noise signals. In some other cases, the fundamental modes of a structure can be superimposed by harmonic components, caused by external factors. These components should be carefully identified and removed from the modal analysis, providing in this way the real structural modes [Jacobsen *et al.*, 2006].

Modal extraction methods

The methodologies for modal extraction of properties, in the case of Output-only techniques, are different and widely sensible to the input. Actually, a random excitation induces responses due to real structural modes and, contemporary, responses due to undesired sources and this contaminates the sample with noise. This is one of the main challenges of this methodology, since the output data can deal with very small magnitudes.

Algorithms of the classical modal analysis, that is based on impulse response functions, can be employed to the output-only cases, which base their analysis on response correlations functions [Cunha and Caetano, 2005]. Some examples of this

Table 1.41: Chart of most important modal extraction methods for Output-Only analysis [Ramos, 2007].

	Method	Characteristics
Frequency Domain	(PP)	Classical SDOF non-parametric method
	(FDD)	MDOF non-parametric method; Application of SVD to reduce noise
	(EFDD)	MDOF non-parametric method; Application of SVD to reduce noise
	Polimax	MDOF method
Time Domain	(RD)	Operates on time domain series, leading to a free decay curve analysis
	(ARMA)	Time series modelling using recursive algorithms
	Maximum Likelihood Methods	Stochastic methods based on the minimization of a covariance matrix (parametric method)
	(SSI)	Stochastic methods based on the project of state vector on a vector of past realizations (parametric method)

can be found in the use of the methods of ITD, the Multiple Reference Ibrahim Time Domain (MRITD), the LSCE, the Polyreference Complex Exponential (PRCE), the Covariance-Driven Stochastic Subspace Identification (SSI-COV) or the ERA, among others.

Several Output-only methods have been recently developed and each one is characterized by its own advantages, disadvantages and particularities. A brief resume of the most important and used methods for civil engineering structures, and specially for historical structures is provided in table 1.41 [Cunha and Caetano, 2005; Jacobsen *et al.*, 2006; Ramos, 2007; Rodrigues *et al.*, 2004].
As in the case of Input-Output methods of extraction, two main groups can be identified: parametric and non-parametric models. The substantial difference is, once again, the domain in which the analyses are performed, namely time and frequency domain.
Among all listed methods, Brincker and Andersen [2000] proposed the non-parametric methods of the Frequency Domain Decomposition (FDD) and the Enhanced Frequency Domain Decomposition (EFDD), working in the same line of the Peak-Peaking method, but with several enhancements. Further informations about these methods will be provided in the next section since they will be applied in part of the experimental campaign carried out in the present study.

1.4.2.3 Adopted modal identification methodologies

Several extraction methods can be applied for the modal identification of structures, as presented in previous sections. However, each one has its own particularities and applicability. For this reason, this section provide a brief and general overview on methodologies that constitutes the base of the employed commercial software, namely ARTeMIS Extractor [SVS].

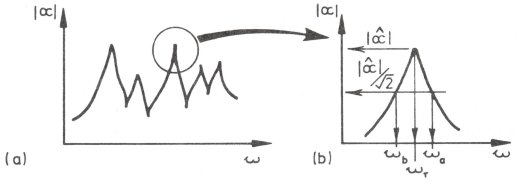

Figure 1.51: Peak Peaking method: (a) summation of single modes and (b) damping estimation through the Half Power Bandwidth Method [Ewins, 1984].

Peak-peaking method (PP)

The Peak-Peaking method (PP) is one of the most popular, simplest and used methods to identify modal parameters of a considered structure. This methodology is applicable in the case of an excitation as ambient vibrations. This method starts from the consideration that the FRF reaches extreme values near the resonant frequencies of the structure. Actually, in the vicinity of a resonance, the total response is dominated by the contribution of the mode whose natural frequency is closest, this means that the response is dominated by the resonant frequency mode shape, being the contribution of other resonant modes annulled. Lastly, one should consider as this method can be satisfactory applied in the case of structures whose FRF is characterized by modes clearly identifiable and separated. Furthermore, the system should be correctly damped, to avoid difficulties on the identification (lightly-damped) and influences of other modes (heavily damped) [Ewins, 1984].

Considering the ambient vibration measurements, the input is characterized by a constant PSD function and the FRF is replaced by the auto spectra of the ambient outputs. Since all frequencies are equally exited, this causes the natural frequencies can be simply identified by the peaks on the plots of the averaged normalized power spectral densities. These can be obtained starting from the Discrete Fourier Transform (DFT), allowing a conversion of acquired acceleration data from the time domain to the frequency domain. Nevertheless, an analysis of the coherence functions is needed for a correct identification, as well as the amplitude and phase relations between the records.

The Peak-Peaking method does not have in itself a procedure to compute the damping estimation. Nevertheless, damping values, related to each identified mode, can be obtained with different methods. One among the most easy and suitable methods for this analysis is the Half-Power Bandwidth method. Further techniques consider the whole structure as a SDOF system and compute values from the isolated peaks of the spectral density functions. These methods of damping estimation provide a first indication of values, that should be verified and validated by other more stable and reliable methodologies, especially in the case the Half-Power Bandwidth method [Rodrigues *et al.*, 2004]. Their accuracy is widely depending on the quality of acquired data [Ramos, 2007].

Main problems of this method can be summarized in the subjective selection of peaks on the FRF, the hill conditioned method for damping estimation and operational deflection shapes are obtained instead of mode shapes. Furthermore, only real modes or proportionally damped structures can be correctly identified.

Frequency Domain Decomposition (FDD)

The Frequency Domain Decomposition (FDD) method can be considered as an extension of the Peak-peaking method. The main idea is based on the decomposition

of the spectral density matrix on Singular Value Diagram (SVD). Actually, the method is based on an approximate decomposition of the system response into a set of independent SDOF systems, one for each mode [ARTeMIS Extractor, SVS]. The algorithm considers that, at each frequency, the spectral density matrix can be decomposed into SVD, that concentrates the information from all spectral density functions and the contributions of the different modes of a system. The FDD method was presented by Brincker and Andersen [2000] and, following this interpretation, any system response can be written in modal coordinates as it follows:

$$y(t) = \varphi_1 \cdot q_1(t) + \varphi_2 \cdot q_2(t) + \cdots = \Phi \cdot q(t) \tag{1.5}$$

where φ_i corresponds to i-th mode shape of the system and Φ is the mode shape matrix. Furthermore, considering that the covariance of the acquisitions is related to the covariance of the modal coordinates through the mode shape matrix, and after a Fourier transform, the equivalent relation in frequency domain is obtained by:

$$G_{yy}(f) = \Phi \cdot G_{qq}(f) \cdot \Phi^H \tag{1.6}$$

This way, if the modal coordinates are not correlated, the power spectral density matrix ($G_{yy}(f)$) of the modal coordinates will be diagonal, and thus, if the mode shapes are orthogonal, the equation 1.6 is a SVD of the response spectral matrix [Brincker and Andersen, 2000]. As a consequence, the Frequency Domain Decomposition method is the Singular Value Decomposition (SVD) of the response spectral density matrix, given by:

$$G_{yy}(f) = U(f) \cdot [S_i] \cdot U(f)^H \tag{1.7}$$

where $[S_i]$ is the diagonal matrix of the singular vectors, positive and real eigenvalues of the matrix $G_{yy}(f)$, and $U(f)$ is the orthogonal complex matrix where each column contains the mode shape vectors of each spectral peak. The singular vectors are orthogonal to each. Plotting the singular values of the spectral density matrix will result in an overlaid plot of the auto spectral densities of the modal coordinates [Brincker and Andersen, 2000].

From the analysis of the singular values spectra, it is possible to identify the auto power spectral density functions corresponding to each mode of a system, which may include parts of several singular values spectra, depending on which mode is dominant at each frequency. The mode shapes are estimated as the singular vectors at the peak of each auto power spectral density function corresponding to each mode [Rodrigues *et al.*, 2004].

Enhanced Frequency Domain Decomposition (EFDD)

The Enhanced Frequency Domain Decomposition (EFDD) is an extension and an improvement of the FDD method developed by the same author. The basis are thus very similar, presenting some additional procedures that allow the estimation of damping values and enhanced capacities for the identification of frequencies and mode shapes, specially for closest modes.

In the case of EFDD method, the selection of peaks on the auto power spectral density function is followed by the identification of a modal peak around the selection, making use of the MAC factor in a certain frequency range around the spectral peak. The SDOF power spectral density functions are then taken back to time domain by the Inverse Discrete Fourier Transform (IDFT).

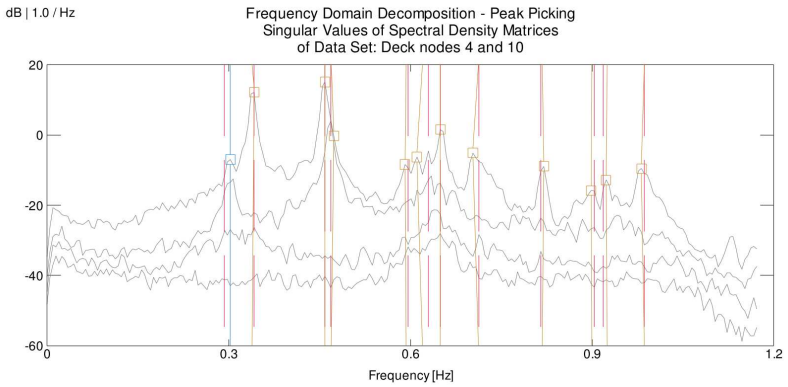

Figure 1.52: plot of the singular values of the spectral density matrices by the FDD method [Cunha and Caetano, 2005].

The natural frequencies are obtained by an enhanced estimation of the number of zero-crossing as a function of time. The damping coefficients are obtained by the logarithmic decrement of the corresponding SDOF normalized auto-correlation function [Jacobsen *et al.*, 2006]. The estimation of the mode shapes is done by considering all the singular vectors within each SDOF auto-spectral density function, weighted with the corresponding singular values [Rodrigues *et al.*, 2004].

Special attention must be given to the influence of harmonic excitations and other dominant deterministic signals in the measured responses, which can have an important influence in the results of the EFDD method. The deterministic signals can be seen as a forced vibration excitation with very low damping. Nevertheless, by the use of the Kurtosis parameter, these contributions can be identified and removed by linear interpolation from the results of the EFDD [Jacobsen *et al.*, 2006].

1.5 Conclusive Remarks

The literature survey, presented in this chapter, involves several basic aspects for the subsequent development of the experimental program.

An introductory overview on the classification of historical masonry typologies identified as multi-leaf masonries are very diffused in the Italian regions as well as in other Countries [Binda and Saisi, 2001; Carbonara, 1996; Giuffrè, 1990]. Actually, this building system is mainly employed in minor buildings of historical centres, even if it can be found also on more relevant structures. Nevertheless, these studies highlight also the great vulnerability of this masonry typology, mainly due the independent behaviour of load bearing layers [Giuffrè *et al.*, 1993]. This characteristic induces buckling problems on the outer leaves and to a consequent overall out-of-plane failure mechanism.

Further studies focused on the mechanical characterization of most diffuse materials [Binda *et al.*, 2003a; Valluzzi, 2000], constituent a multi-leaf masonry, as well as their physical and chemical properties. The typological characterization of the masonry texture and of its most common transversal section allowed to identify a typical and most representative example of this building system [Binda, 1999; Binda and Penazzi, 2000]. These observations and considerations led to the design of masonry to be employed in the experimental research presented in this study.

The typical composition of the multi-leaf masonry led to identify the grout

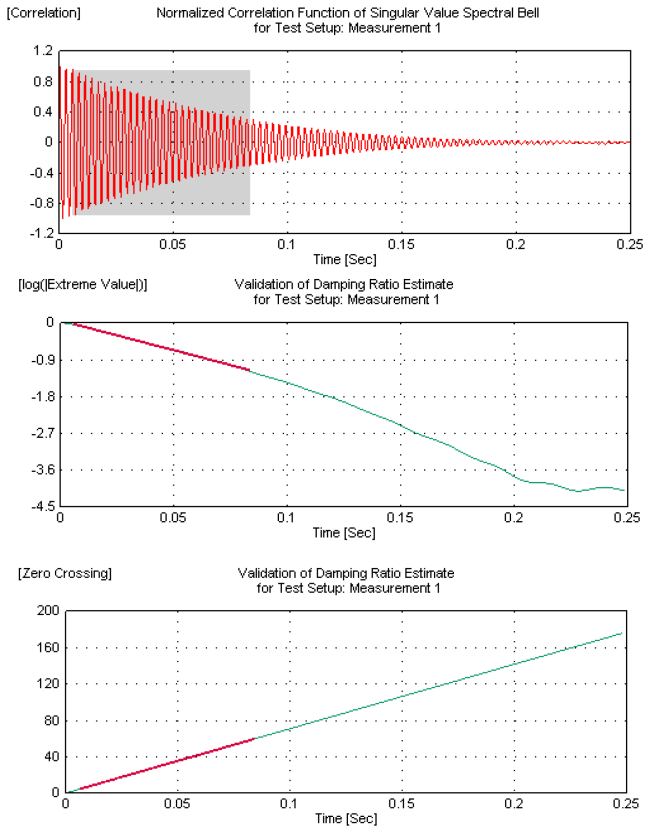

Figure 1.53: Plot of the normalized correlation function (top); damping ratio estimation from the decay of the correlation function (centre); natural frequency identification by zero-crossing counting (bottom); [Jacobsen *et al.*, 2006].

injection as one of the most appropriate strengthening intervention techniques to increase the overall strength of the structure and to prevent or delay most common structural problems [Valluzzi *et al.*, 2003; Valluzzi, 2000; Vintzileou and Miltiadou-Fezans, 2008]. Actually, several experimental studies, carried out quasi-static tests on multi-leaf masonry, aimed at quantify the increasing of strength employing injection of different typologies of admixture [Doglioni *et al.*, 2009; Pina-Henriques and Lourenço, 2003; Toumbakari, 2002; Valluzzi *et al.*, 2004; Vintzileou and Tassios, 1995]. These researches allowed to investigate the influence of this technique on the compressive behaviour as well as on the shear and tensile strength of injected structural elements, among further mechanical parameters.

A subsequent literature survey underlines the importance on carrying out shaking table experimental campaigns for a deeper understanding about the dynamic behaviour of structures and, particularly, to investigate the influence of a strengthening technique on their overall behaviour. In this field, simpler studies involved tests on single structural elements, while more complex experimental campaigns include experiments on whole building models.
The choice about the more correct testing method appeared to be widely depending on the aim of the study. Investigations on single elements, such as masonry panels, led to a complete knowledge about their out-of-plane behaviour, even if this is limited to a unique structural part, without any information on its interaction with the remaining part of the building. On the other hand, experiments on whole structures

provide informations about the effects of the applied strengthening technique on the overall behaviour of the model and not only a knowledge of its local influence. Moreover, this methodology allows to deepen more structural aspects and can be considered as the final validation point of a strengthening intervention technique.
Only an experimental campaign, studying the effects of the grout injection on the seismic resistance of a whole building model, was found. However, this research was performed through pseudo-dynamic tests, while any further shaking table test, focusing on the application of this strengthening intervention to single structural elements or to whole building models, could be found. Moreover, any experimental campaign on stone masonry elements could be gathered, while only few shaking table experiments on whole stone masonry buildings could be presented [Benedetti and Pezzoli, 1996; Juhásová *et al.*, 2002, 2008; Tomaževič *et al.*, 1992], even if they consider different structural interventions.

The great diffusion of this structural system and, on the contrary, the limited number of experimental studies on its dynamic behaviour, on fitted and effective strengthening intervention, as well as the effects of most recent and destructive seismic events, underline the wide importance on deepening a field in which many issues are still opened.

On these bases three main aspects appeared as important to be deepened with the aim to validate the injection of hydraulic lime-based grouts as effective strengthening technique on multi-leaf stone masonry buildings: (i) the study about its effects on the overall dynamic behaviour of a whole structure, (ii) its influence on the out-of-plane dynamic behaviour of a single structural element and (iii) deepening the knowledge about its effectiveness on improving the compressive strength as well as the resistance to in-plane forces. These aspects, considering the investigated masonry typology, lead to a complete and exhaustive knowledge, that would allow the employment of this intervention for the preservation of historical and Cultural Heritage buildings.

The design and execution of an experimental dynamic campaign on a whole building model allows to verify if the local improvements of injections, studied by some authors on the static field, are effective also when subjected to a seismic load. Moreover, several further aspects, not mentioned in any study, need to be deepened. Investigation about the influence of lime-based grout injections on the dynamic characteristics of the whole structure appears as a topic of primary importance. Particularly, its effect on the fundamental frequencies and vibrational modes as well as on the stiffness characteristics but also its effectiveness on the dissipation of seismic energy should be studied. Furthermore, this testing methodology would lead to important consideration about the interaction among different structural elements and, particularly, among those injected, but also the influence on further structural details, such as the connection between vertical and horizontal structures.
The analysis of failure mechanisms and the survey of most important and typical damages on multi-leaf stone masonry, as well as the state of preservation of minor buildings on historical centres lead to distinguish different conditions: structures well preserved and without any substantial damage and structures characterized by different damage conditions. In the first case, the intervention can be identified as *strengthening*, since any damage is present and the applied technique only improve the overall behaviour of the structure. Differently, in the second case, the intervention can be defined as *repairing*, since the structural integrity should be re-established firstly and, thus, the improvement effects would result limited or partial. This aspect should also be deepened to study the application limits and the possibilities of injections.

The study about the influence of the selected strengthening technique on the dynamic behaviour of multi-leaf stone masonry elements, when subjected to the out-of plane seismic excitation, appears as an important topic to complete the knowledge about its effectiveness. Actually, while previous studies particularly deepened this aspect through quasi-static tests and, only in a case, with a pseudo-dynamic study, any evidence is provided in the case of dynamic excitation. This would constitute a further important point in the validation process, since this evidence would confirm the observations and the analyses performed in the static investigations.

Lastly, the mechanical characterization of unreinforced and strengthened structures through quasi-static tests would lead to a further important confirmation of observations obtained from previous researches. Moreover, the design and the execution of laboratory experiments, to study the effectiveness of injections on the improvement of the in-plane mechanical behaviour, would also provide further informations about the capability in dissipating seismic energy and the influence on the stiffness of structural elements.

Chapter 2

Experimental Program

The research presented in this thesis includes a wide experimental phase aimed at investigating the static and dynamic behaviour of historical stone masonry buildings. Attention will be mainly focused on a specific typology of construction building system, namely three-leaf rubble stone masonry. This building system is fairly common in the minor buildings, widespread in the historical centres of Italy and in other European Countries. This structural typology is particularly vulnerable to the seismic actions and seems interested by a certain percentage of voids. This allows to consider the grout injection as one of the most suitable intervention techniques for its rehabilitation and for the improvement of both its mechanical characteristics and strength.
The main characteristic of this stonework is the presence of two external leaves, made of rough hew stones bound by mortar, and an internal core, comprising fragments of the same materials. As a consequence, the external layers are load bearing, while the inner coat is just a filling. The total absence of transversal connection is its second feature. These characteristics cause the main mechanisms of collapse, namely the out-of-plane failure and the disconnection of the external leaves, for this kind of masonry [Binda and Saisi, 2005; Binda *et al.*, 2003b; Giuffrè *et al.*, 1993].

In order to study the effects of hydraulic lime-based grout injection, a detailed test program was defined.
Two main laboratory phases were carried out: the first part focused on dynamic tests, employing the shaking table facilities provided by the ENEA Research Centre in Rome ("la Casaccia"), while the second part involves quasi-static experiments at the Laboratory of Department of Structural and Transportation Engineering in Padua. Dynamic tests were performed on stone masonry building models with the aim of studying the effects of lime grout injection on the entire structure. Differently, quasi-static experiment were carried out on structural elements, such as masonry piers. In this chapter, the whole experimental campaign will be presented.

2.1 Shaking table tests

One of the main objectives of the present research focused on the study of the dynamic effects of employing injection as a strengthening technique. This admixture, developed by Tassullo S.p.A. and the University of Padua [Valluzzi, 2000], is lime-based to guarantee a higher compatibility with historical construction materials, particularly in the case of multi-leaf masonry. In fact, the injection of hydraulic lime-based grout mainly aims at avoiding or limiting the typical failure modes of this masonry typology when subjected to earthquakes (compare §1.1).

Two different structures were designed and realized with the purpose of thoroughly examining the effects of this strengthening intervention: whole building models and masonry panels. The main objectives for each specimen typology, their design and realization will be described in the following paragraphs.

2.1.1 Masonry buildings

The first part of this shaking table experimental campaign aims at investigating the overall behaviour of whole structures strengthened using hydraulic lime-based grout injection. Actually, an examination of the influence of this intervention technique on the dynamic behaviour of a structural system appeared as fundamental. This experimental section allows to evaluate the effectiveness of this technique and also to underline its possible limits and undesired effects. Starting from these observations, a simple historical construction was selected as a prototype to design the building models to be tested.
The reference historical construction is a typical structure, widely diffused in Italy, with limited dimensions and comprising two storeys. Floors and roofs are normally made of timber, so they do not represent a rigid diaphragm for the whole structure.

2.1.1.1 Experimental Program

Two different building models were built in order to study the effects of grout injection, comparing the different situations and conditions of structures to be tested. The models had the same geometrical characteristic and were constructed with different purposes. The first model can be considered the reference specimen and it is representative of a minor historical building. This model, named Unreinforced Masonry model (URM), was subjected to seismic load, without being strengthened by grout injection. Instead, the second building specimen, named Strengthened Masonry model (SM), was injected with a hydraulic lime-based mixture before the shaking table test.
These specimens describe two different real situations. The URM model is representative of an unreinforced historical masonry structure subjected to seismic action. The SM model describes the overall behaviour of an old building, characterized by a good state of conservation in terms of the mechanical characteristics of materials and structures, strengthened before a seismic event.
A third intermediate situation was simulated. Since the URM model was prevented from collapsing, it was possible to repair this structure by injection in order to test it again. Therefore, this case is representative of the most common situation: an old structure, damaged by previous earthquakes and other mechanical, physical and chemical events that have weakened the masonry, on which to intervene in order to provide "seismic improved" overall behaviour. Finally, the URM model, repaired by injections after a series of shaking table tests, led to testing a third specimen called Repaired Masonry model (RM). A brief summary of the test matrix is given in table 2.1.

2.1.1.2 Scale factors

The test facilities did not allow full scale realization of specimens, mainly because of geometrical dimensions and pay load limits of the test rig employed (table 2.2). Therefore, the building models were built with a reduced scale factor. Nevertheless,

Table 2.1: Test matrix: Shaking Table Test.

Model	Injection	Description
URM	no	Tested without strengthening injection
SM	yes	Injected before Shaking Table Test
RM	yes	Resulting from URM model after repairing by injections

Table 2.2: Shaking table characteristics

Geometrical dimensions	[m]	4 x 4
Degree of freedom	-	6
Frequency range	[Hz]	0 - 50
Peak acceleration	[g]	3
Peak velocity	[m/s]	0.5
Maximum displacement	[m]	0.25
Reaction Mass	[ton]	2000
Mass and gravity center	[ton]	10
for hard structures	[m]	1

the limited dimensions of the prototype building enabled quite a high scale factor to be considered, equal to 2:3. As a consequence, this value allowed the realization of a building model with overall measurements similar to the real ones.

The scale factors in question were calculated on the basis of the method proposed by Tomaževič and Weiss [1994], among several other analyzed methodologies (compare §1.3.3.1). The relationship between the quantities characterizing the prototype and the building model are presented in table 2.3. This method involves the reduction of the geometrical dimensions of the specimen to be tested and keeps constant both the Young's modulus and the specific weight of the materials employed. This allows the original materials to be used, thus avoiding further complications caused by the necessity to scale other characteristic parameters of different constituents.
The typological analysis of most diffuse multi-leaf masonries (compare §1.1) led to identify an overall typical thickness of about 50cm, divided in three main parts: two external leaves and an internal core. The mean depths are respectively equal to about 18cm and 14cm. Thus, these measures were considered for the masonry of the prototype building. As a consequence of the reduction factors, the overall masonry thickness of the building models is 33cm, divided as 12cm, for the external layers, and 9cm, for the internal core. Furthermore, also the dimensions of the constituents, namely stones, were reduced to respect the considered scale factor. Nevertheless, this masonry, realized with the overall dimensions geometrically reduced and characterized by the original mechanical properties, can also be considered as representative of a real structure with limited dimensions.

Finally, the chosen method of similitude implies a reduction in time and an amplification of the accelerations of the seismic signal considered as input. Furthermore, this method guarantees a correct reproduction of the mechanisms and failure modes typical for the prototype building in the model with a reduced scale. Nevertheless, one should consider as this similarity also depends on both quantity and distribution of the additional masses added to the building model during the experiments [Tomaževič, 2000].

Table 2.3: Employed scale factors (simple model).

Quantity	General Equation	Simple model	
Length (L)	$S_L = L_P/L_M$	S_L	3/2
Strain (ε)	$S_\varepsilon = \varepsilon_P/\varepsilon_M$	1	1
Strength (f)	$S_f = f_P/f_M$	1	1
Stress (s)	$S_s = f_P/f_M$	1	1
Young's modulus (E)	$S_E = S_s/S_\varepsilon$	1	1
Specific weight (Γ)	$S_\Gamma = \Gamma_P/\Gamma_M$	1	1
Force (F)	$S_F = S_L^2 S_f$	S_L^2	9/4
Time (t)	$S_t = S_L\sqrt{(S_\Gamma S_e/S_f)}$	S_L	3/2
Frequency (Ω)	$S_\Omega = 1/S_t$	$1/S_L$	2/3
Displacement (d)	$S_d = S_L/S_e$	S_L	3/2
Velocity (v)	$S_v = S_e\sqrt{(S_f/S_\Gamma)}$	1	1
Acceleration (a)	$S_a = S_f/S_L \cdot S_\Gamma$	$1/S_L$	2/3

2.1.1.3 Design of specimens

The models had a rectangular floor plan, with dimensions of 2.40m by 2.80m, and two storeys, with an overall height of 3.60m. All prospects were different (figure 2.1), conferring a strong asymmetric behaviour to the structure. This aspect was designed to induce greater loads on masonry walls, due to the additional torsional effects. A typical cross section of masonry models is presented in figure 2.2.
Steel ties were designed at both floor levels to avoid global out-of-plain behaviour of masonry and, therefore, to emphasize the in-plane grout effect. This will lead to a better understanding of injection influence.
Wooden floors allow the behaviour of a non-rigid diaphragm to be simulated, mainly found in historical masonry buildings. As a consequence, orthogonal walls mainly behave independently, also as the floor beams are arranged just in one direction while no connection with masonry is perpendicularly provided.

2.1.1.4 Construction phases

A reinforced concrete base was cast to support the masonry structures. The concrete base was provided with two pairs of rectangular holes placed in opposite positions. This configuration allowed the insertion of two HE steel beams, used first to move the specimens and after to fix them to the shaking table (figure 2.3).

Rough limestone and lime mortar were employed to build the three-leaf stone masonry with the overall thickness of 33cm (figure 2.4). The characteristics of the masonry section, in terms of volume of stone, mortar, stone fragments and voids, are listed in table 2.4. On the basis of previous research into similar masonries [da Porto, 2000; dal Farra, 1992; Valluzzi, 2000], the specific weight was evaluated as 2300kg/m^3 for an overall calculated mass of 18000kg for each non-injected specimen.
Floors were built employing timber beams with a cross section of 9cm by 12cm. Double wooden planking, with an overall thickness of 4cm, was wrapped in orthogonal directions and nailed to the beams. Timber lintels were also positioned.
Six steel tie beams were inserted for each level: three were fixed to the timber beam heads and the remaining were positioned in the orthogonal direction.

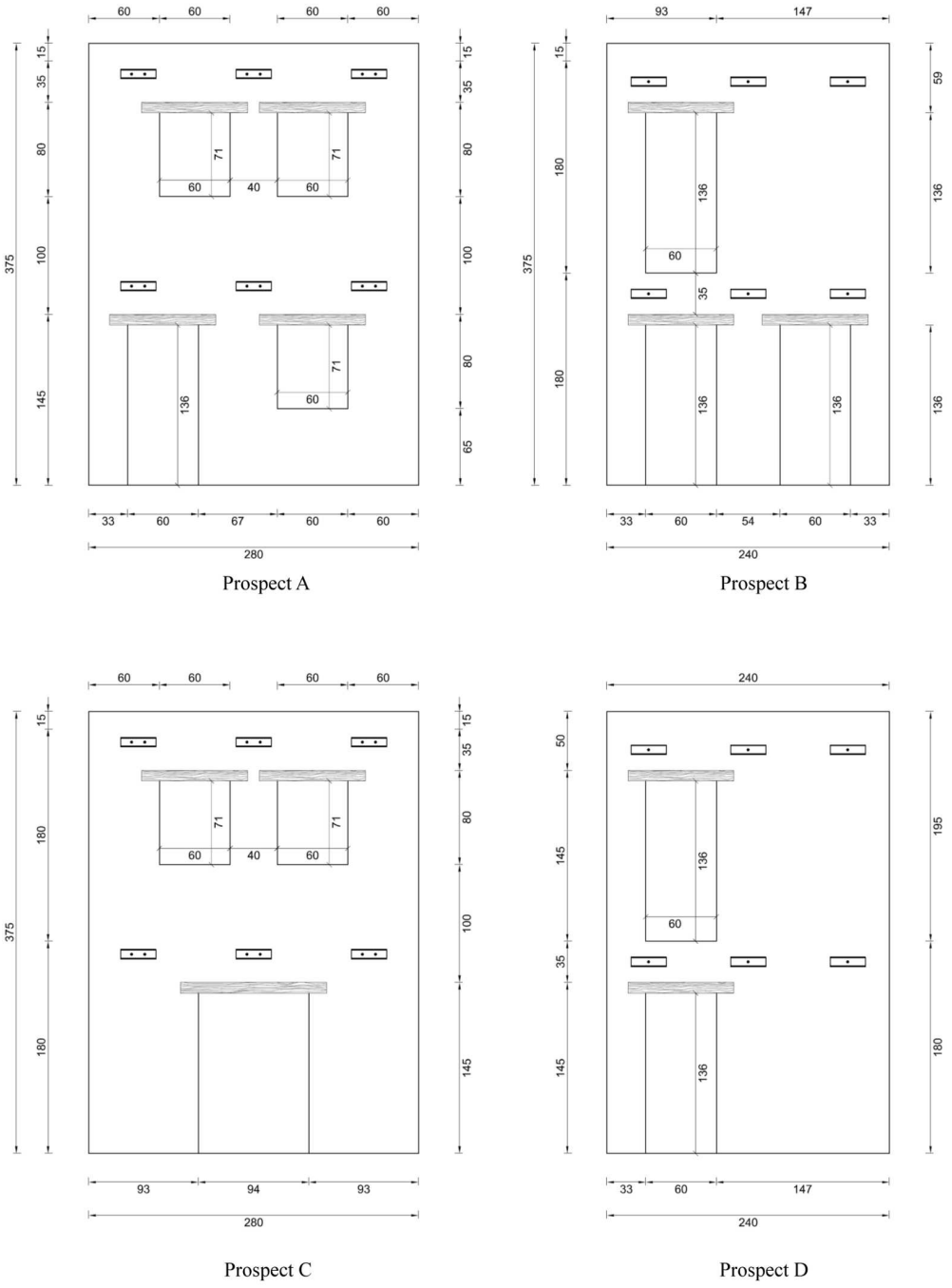

Figure 2.1: Prospects of models.

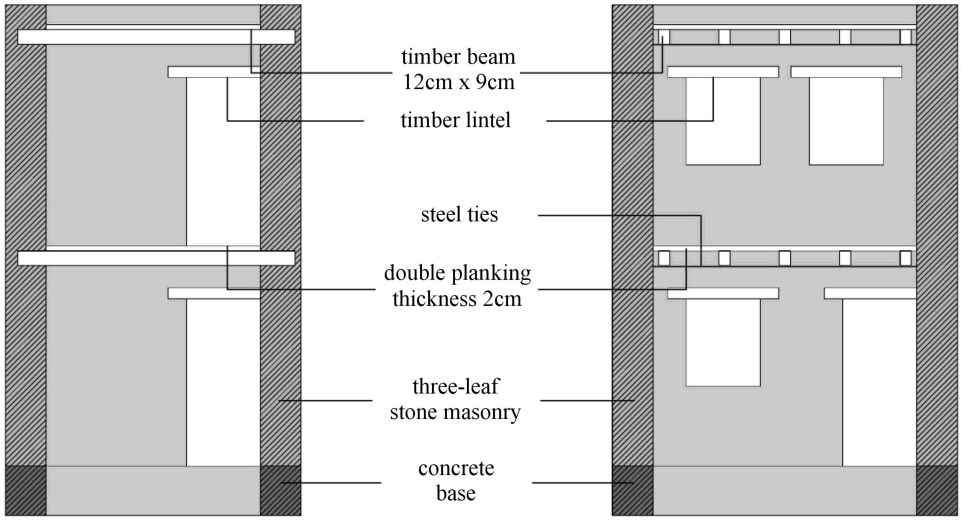

Figure 2.2: Orthogonal sections of models.

Table 2.4: Multi-leaf stone masonry: percentage of constituent materials

Material	**Percentage** %
Rough limestone	52
Stone fragments	16
Mortar	20
Voids	12

2.1.1.5 Grout injection

The preparation and the execution of injection operations were performed after the mortar curing. Holes were drilled at the external side of the wall (figure 2.5) respecting a triangular mesh with 30cm per side, to allow a better distribution of mixture in the masonry core. Lime grout was injected across plastic tubes fixed in the external sides of the models. Holes in the internal side of the masonry were also made to check the grout path during injection. The strengthening intervention was accomplished progressing from the bottom to the top of the specimens.
A low and constant pressure, ranging from 0.5atm to 1.0atm, was applied by means of a hand pump to avoid damaging the masonry.
The introduced grout quantity was monitored to evaluate the injectability of the realized masonry and the effectiveness of the intervention method. During the execution of this phase, the leak of admixture from holes and masonry cracks was also observed, to study the free diffusion of grout within the masonry core.

2.1.1.6 Test rig and experimental set-up

This experimental phase was carried out at the Laboratory of Structural Dynamic and Vibration Control at ENEA Research Centre ("La Casaccia", Rome). The main characteristics of the shaking table employed have been presented in table 2.2.

The whole construction and strengthening or repairing phases for both masonry building models were executed off the shaking table. Afterwards the specimens were

Figure 2.3: Detail of the concrete base and building construction.

Figure 2.4: Transversal section of the masonry wall.

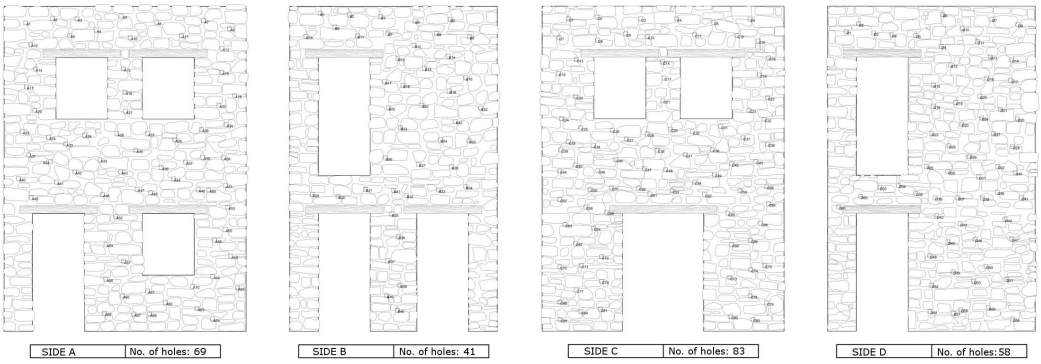

Figure 2.5: Scheme of holes executed to realize the injection.

moved onto the test rig using a bridge crane. The concrete base, on which the masonry structures were built, was doubly fixed to the shaking table. Horizontal movements were inhibited by means of 14 L-shaped steel plates, arranged along the perimeter of the concrete base and fixed to the strong steel base of the shaking table. Pre-stressed steel bars, binding two long HE steel beams passing horizontally through two pairs of holes provided in the concrete base, prevented vertical displacements. The fixing system is shown in figure 2.9.

2.1.2 Masonry panels

The second part of the dynamic experimental research focused on sub-structural elements. Actually, testing simple elements makes it easier to study the effectiveness of lime grout injection. Due to the considered masonry typology and its typical mechanisms of failure, as previously introduced, one of the most suitable structural elements to be studied is represented by out-of-plane tests on masonry panels. Some similar experiments were presented and discussed in the section 1.3.

Dynamic tests on these structural elements could not be performed within the present research and only the design, the construction and the strengthening of specimens was accomplished. Nevertheless, first analyses concerning the injectability of the masonry and the verification of the quality of intervention could be performed.

Figure 2.6: Hand pump for grout injection.

Figure 2.7: Grout injection.

Figure 2.8: Grout leak from a masonry crack.

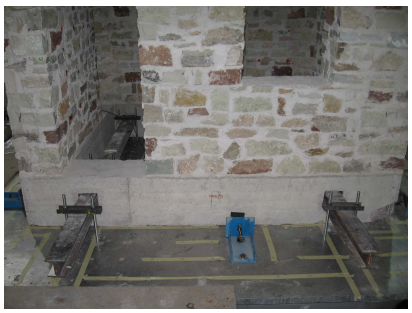

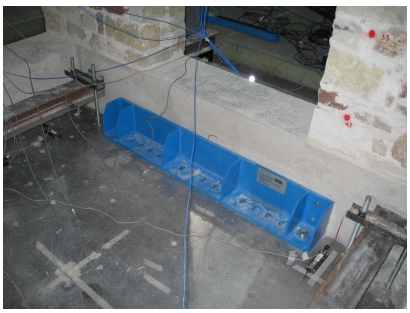

Figure 2.9: Fixing system for anchoring building models to the shaking table: external (left) and internal (right) view.

2.1.2.1 Experimental Program

Few experimental campaigns, investigating the dynamic behaviour of masonry panels, were found during a review of existing literature (compare §1.3.1). For instance, no experimental dynamic study about the out-of-plane behaviour of stone masonry panels could be found. Furthermore, no dynamic test about the influence of grout injection employment was noticed. Consequently, starting without any reference campaign, eight panels were built with the aim of investigating the influence of two different strengthening interventions: the application of transversal tie rods and the injection of hydraulic lime-based grout. These masonry panels aim at simulating the out-of-plane behaviour of a portion of a stone masonry wall on the upper floor of an old building. In fact, it is the most stressed part in relation to a typical mechanism for this masonry typology, namely the out-of-plane failure. Seismic accelerations, amplified on the top floor because of the height of the structure in question, induce a strong force in a portion with a very low compressive stress. In fact, the weight of the roof is the only acting load on this masonry portion. Furthermore, one should consider as in the case of a historical building, the covering structures were normally made by timber. As a consequence, this induces a very low vertical compressive stress on the wall below.
This is one of the worst conditions for the stability of masonry elements and thus a very interesting case to study: low compressive stress combined with high horizontal seismic load.

In order to reproduce the real behaviour of this building part, the effective constraints in the case of the historical building considered as a reference prototype should be studied, namely the floor elements. In the case of historical buildings, both floors and roofs were typically built using timber. These structural elements, realized with this material, are not able to fixedly constrain the inter-floor masonry, preventing the rotation of its lower and upper part. For this reason, two hinges were considered as constraints at the top and bottom of the panels to be tested. A specific test rig was designed, which was able to reproduce the previously described real effective behaviour on the shaking table. An overview of this testing system is given in section 2.1.2.5.

The design of masonry panels and their test set-up enable an investigation of the overall out-of-plane behaviour in four different situations. Two masonry specimens were strengthened using lime grout injection while, on another two samples, transversal steel tie rods were placed. On two further panels, the two afore-mentioned strengthening techniques were applied together. On the last pair of samples, no intervention was applied and these were the reference panels to evaluate the effectiveness of the previously described interventions. A brief summary of the realized panels is given in table 2.5.

Table 2.5: Strengthening techniques applied to realized masonry panels.

Panel No.	Acronym	Strengthening Technique
2		No strengthening intervention was provided
2	T	Insertion of transversal steel tie-rods
2	I	Injection of hydraulic lime-based grout
2	IT	Combination of tie-rods and lime grout

2.1.2.2 Design of specimens

Masonry panels to be tested were built at full scale, considering that the limited weight and the restricted geometrical dimensions of each specimen enabled them to be tested on the shaking table. As presented for the building models, the typological study of the multi-leaf masonries (compare §1.1) led to consider a typical section of about 50cm (18cm and 14cm for external leaves and internal core respectively). The overall height is 2.60m, which simulates a real inter-floor element. Furthermore, with the aim to obtain a slenderness ratio equal to 2, the width of panels was assumed as 1.3m. The design of the specimens is presented in figure 2.10.

2.1.2.3 Construction phase

A reinforced concrete base was cast as a support on which the specimens were built (figure 2.11). A wall with an overall length of about 12m, as a sum of all the specimens, was realized (figures 2.12 and 2.13). Furthermore, after the ripening of materials and the realization of strengthening interventions, it was sawed in order to obtain the eight panels (2.10). This was done to avoid any problems during the strengthening phase, as after explained.
Both heads of the wall were inserted as throwaway parts. Actually, panels extracted from the central part of the wall are free from any transversal connection between the opposite external layers neither in the middle nor at the hedges, since any leaf is provided in the short sides of each panes. As a consequence, also panels 1 and 8IT (figure 2.10) can be considered as an internal part of the wall, since both heads will be eliminated. This way, all panels will have the same characteristics, without any transversal connection. Finally, a further concrete beam was cast on the top of the wall to complete the specimens (figure 2.14).
Furthermore, employing the value of density as computed for the building models, an overall mass of about 4000kg for each non-injected panel should be considered.

2.1.2.4 Grout injection

The grout injection was performed after the mortar ripening and following the procedure described in the case of building models. About 60 holes per prospect were realized (figures 2.15 and 2.16), respecting the triangular mesh with 30cm per side.

Also in this case the strengthening intervention was realized from the bottom to the top of the wall (figure 2.17) and the quantity of injected grout was monitored.

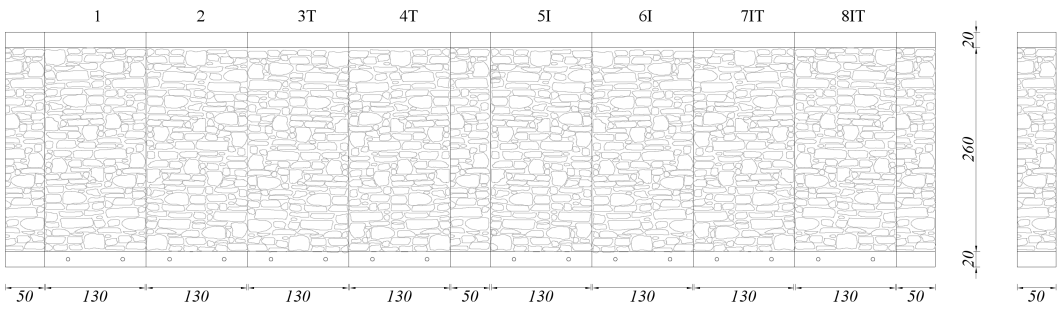

Figure 2.10: Design of panels with relative acronym.

Figure 2.11: Detail of the concrete base.

Figure 2.12: Construction of walls.

Figure 2.13: Detail of the cross section of the wall.

Figure 2.14: Completed wall before cutting.

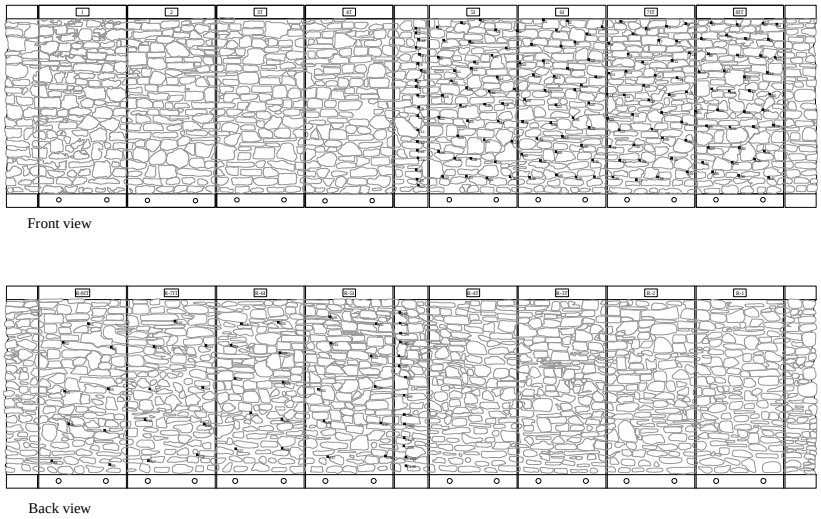

Figure 2.15: Scheme of holes executed to realize the injection: front and back view of wall.

Figure 2.16: Drilling holes in the wall.

Figure 2.17: Injecting lime grout.

2.1.2.5 Test rig and experimental set-up

The masonry panels were realized at the Laboratory of Structural Dynamic and Vibration Control at the ENEA Research Centre ("La Casaccia", Rome).

The panels will be subjected to out-of-plane dynamic loads through the shaking table, whose characteristics were presented in the section 2.1.1.6 (table 2.2), while the design of the test rig to be employed in order to perform the experiments, is described in the following.
A steel frame was expressly projected to reproduce the real boundary conditions and to allow the formation of two hinges at the top and bottom of the panel (figure 2.18). Vertical displacements, occurring in the real situation, are also permitted, since the upper part of the testing system binds the top of the masonry sample, preventing only horizontal displacements. Furthermore, steel buffers, bolted to the shaking table platform, restrain the base of the masonry panel, precluding any displacement.
Finally, a FE model was created to study stresses induced in the steel frame by the masonry specimen and to deepen the knowledge of its dynamic characteristics, to obtain natural frequencies far from those typical of the panels.

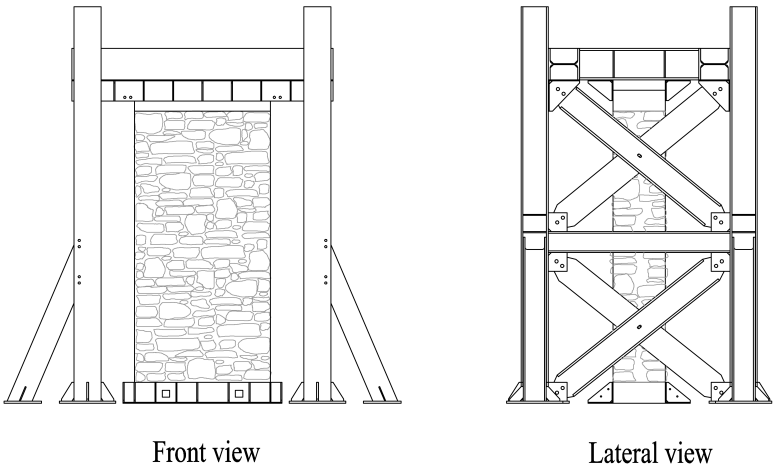

Figure 2.18: Design of the steel frame: front (left) and lateral (right) view.

2.2 Quasi-Static tests

Important information, concerning the mechanical characteristics of multi-leaf stone masonry and the influence of the investigated strengthening technique, can also be obtained from quasi-static tests, as demonstrated by several authors [da Porto, 2005; Lourenço *et al.*, 2005; Magenes and Calvi, 1997; Mosele, 2009; Oliveira *et al.*, 2006; Tomaževič, 2000; Tomaževič *et al.*, 1996; Valluzzi *et al.*, 2004] and presented in section 1.2. Many of these studies provide further knowledge of the dynamic behaviour of tested structures, even if the experiments were statically carried out. On this basis, two different kinds of test were specifically planned and designed:

- Monotonic compression tests,
- Cyclic in-plane shear compression tests.

The experimental program, the description of specimens and the test rig for each experimental typology will be presented in the following paragraphs.
Since the building models, described in section 2.1.1, were prevented from the collapse during the shaking table tests, it was possible to recover several undamaged and slightly damaged masonry panels from building specimens. These samples were employed for static tests presented in this section. The masonry panels were extracted, after the execution of dynamic tests, from RM and SM building models. As a consequence, all the specimens presented in the following were injected. Figure 2.19 shows the position from where the panels for quasi-static tests were taken.

2.2.1 Monotonic Compression tests

A series of specimens were tested under uniaxial monotonic compression. The two main aims, that led to the design of these experiments, are listed in the following:

(i) Investigating the effective compressive strength of the multi-leaf stone masonry strengthened by grout injection.
(ii) Studying the effects of the admixture in terms of the overall deformability of specimens and deepening the knowledge of the influence of lime grout on the failure mechanism due to the buckling of external layers.

Moreover, it should be considered that these panels can be interpreted differently. Firstly, the specimens can be considered as geometrically reduced, as in the case of

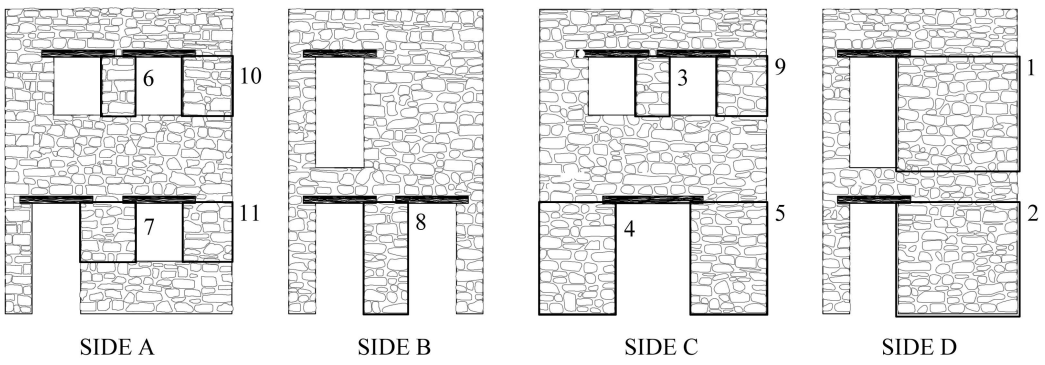

Figure 2.19: Scheme of position from where specimens for quasi-static tests were obtained.

Table 2.6: Origin of specimens for uniaxial compression tests.

Source building model	Identification code	No. of panels
RM	R	5
SM	S	7

the building models from which they derive. On the other hand, they can also be considered full scale panels, representative of a real structural element, even if with limited dimensions.

2.2.1.1 Experimental Program

Monotonic compression tests were carried out on 12 panels, with different slenderness ratios. This experimental phase allowed to estimate the mean values of mechanical characteristics, such as compression strength, Young's modulus and Poisson ratio. In addition, the results achieved in this part represent the basis for the subsequent FE analysis developed in chapter 7.

2.2.1.2 Description of specimens

The specimens, being obtained from building models, have a mean overall thickness of 33cm and are characterized by different slenderness ratios, ranging about between 1.0 and 1.8. Chart 2.6 summarize the original structure from which the specimens for uniaxial compression were obtained. Furthermore, the geometrical characteristics of each panel are presented in table 2.7.

2.2.1.3 Test rig and experimental set-up

Uniaxial compression tests were carried out by means of a universal Amsler machine, whose maximum load is 10000kN (figure 2.20). Two layers of Teflon were placed under the bottom and over the top of each specimen to allow a uniaxial stress state. The tests were performed in displacement control. After achieving maximum stress, the test progressed up to achieve a decreasing of 20% of the load peak value, in order to study the overall behaviour of specimens in the decreasing branch of the characteristic compression curve. Tests were carried out under monotonic loading with an incremental loading rate of about 0.5kN/s [EN 1052-1, 1998]

Table 2.7: Compression test matrix.

Position			3	6	7	8	9	10	11
R series	thickness	[mm]	322		335		324	322	318
	width	[mm]	397		664		608	587	599
	height	[mm]	710		726		837	724	852
	slenderness	-	1.79		1.09		1.38	1.23	1.42
S series	thickness	[mm]	323	323	335	330	327	323	332
	width	[mm]	399	402	654	513	590	596	584
	height	[mm]	700	700	610	1269	765	734	631
	slenderness	-	1.76	1.74	0.93	2.48	1.30	1.23	1.08


Figure 2.20: Compression experiment: test rig (left) and equipped specimen (right).

2.2.2 Cyclic Shear compression tests

The main aims of this experimental section, involving cyclic shear compression test, are:

(i) Estimating the typical mechanical properties, such as the shear modulus, the stiffness decrease, the maximum achievable shear stress and the related shear strain;
(ii) Developing energetic considerations.

2.2.2.1 Experimental Program

The shear compression tests were performed on 6 masonry panels. As considered for monotonic compression tests, one should regard that results, obtained from these panels, can be considered representative of two different structures: geometrically reduced, as in the case of building models from which they were obtained, and full scale elements, representative of a real structural element.

2.2.2.2 Description of specimens

The specimens, as introduced in this section, were obtained during the dismantling of the masonry buildings described in section 2.1.1. Table 2.8 illustrates the origin of the panels to be tested. The specimens, obtained from building models, have a mean overall thickness of 33cm and are characterized by two different slenderness ratios, respectively equal to about 0.9 and 1.5. The geometrical characteristics of each panel are presented in table 2.9.

Two different slenderness ratios were chosen in order to force both the shear behaviour, when the ratio h/b is close to the unit, and the flexural behaviour, when this ratio is approximately 1.5. Other aspects influencing the failure modes of specimens will be discussed in chapter 6.

2.2.2.3 Test rig and experimental set-up

The proposed test set-up was adopted to obtain a series of mechanical parameters, such as stiffness degradation and energy dissipation, fundamental to understanding the seismic behaviour of multi-leaf structures injected by hydraulic lime-based grout.

Table 2.8: Origin of specimens for shear compression tests.

Source building model	Identification code	No. of panels
RM	R	3
SM	S	3

Table 2.9: Shear Compression test matrix.

Position			2	4	5
R series	thickness	[mm]	320	320	321
	width	[mm]	1463	913	930
	height	[mm]	1221	1236	1381
	slenderness	-	0.8	1.4	1.5
S series	thickness	[mm]	325	331	328
	width	[mm]	1453	923	929
	height	[mm]	1370	1275	1381
	slenderness	-	0.9	1.4	1.5

Moreover, this type of test, previously adopted at the University of Padua, firstly by Modena and Bernardini [1984] and Bernardini *et al.* [1997] and, more recently, by Mosele [2009] and da Porto [2005], allows specimens under cantilever boundary conditions to be tested. A deeper presentation of the employed test rig (figure 2.21) can be found in Mosele [2009], while the hydraulic system and control used during the tests discussed in this thesis are those developed by da Porto [2005].

The base for the specimen was doubly fixed: vertical displacement is stopped using four anchor bars, bound to the strong floor of the laboratory; horizontal movements are prevented by two L-shaped steel plates, fixed to the strong floor of the laboratory. Free rotation of the top was ensured by a steel track, which allowed free displacement of the upper part of the specimen. Two vertical actuators were connected to the sledge sliding on a frictionless linear guide, fixed at the top of a horizontal steel beam for the load distribution, and impressed the pre-load during the test. The horizontal

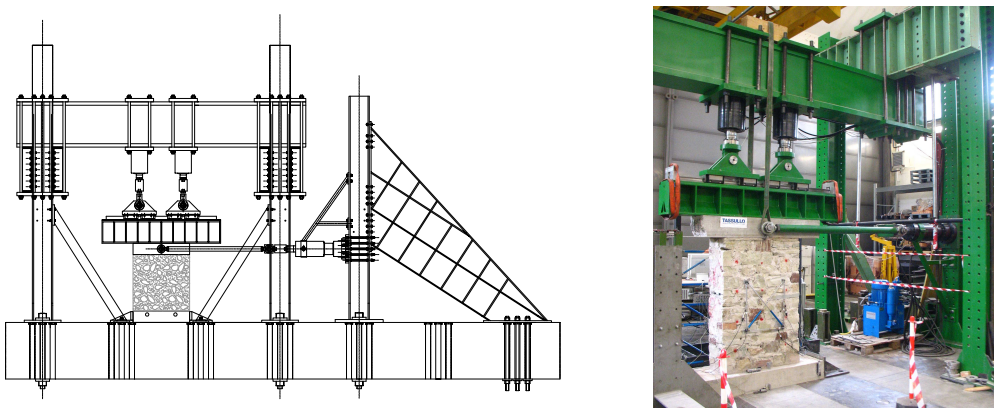

Figure 2.21: Cyclic shear compression test set-up and rig: drawing (left) and view (right)

displacement was applied by a further actuator, fastened to a stiffening steel structure. The horizontal actuator was connected with a forked beam for load redistribution. Two horizontal steel arms linked this to the concrete beam, placed at the top of the masonry specimen. Both rods were connected to a hole, positioned in the middle of the concrete beam, with a steel pin.

2.3 Layout of the research

An overall layout of the whole experimental program is presented in figure 2.22. On the right, the main aims rof the specific parts of the research are listed.

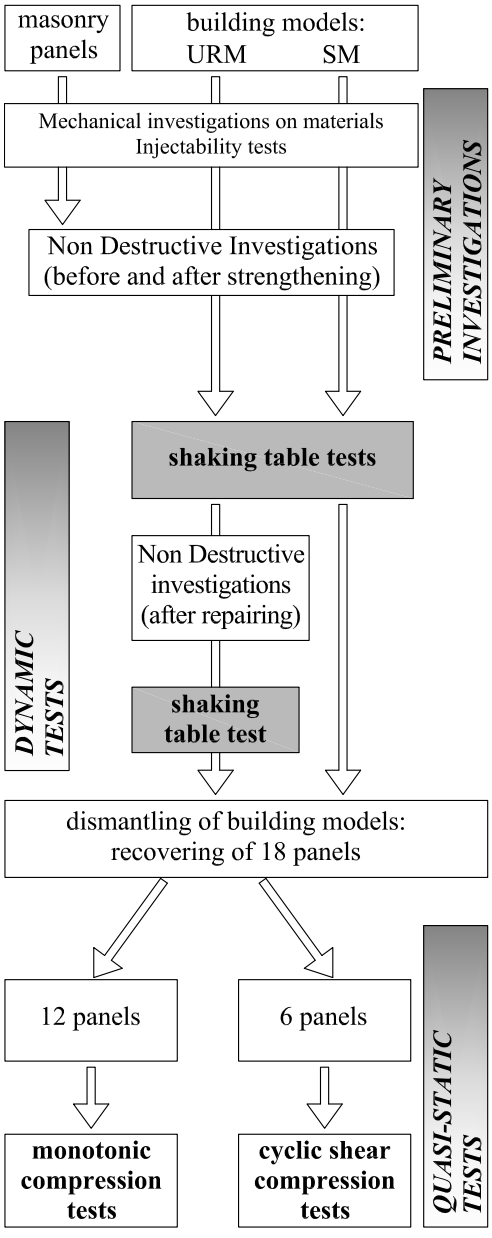

Objectives

Preliminary investigations:
- Mechanical characterization of basic materials;
- Characterization of internal masonry core (Injectability test);
- Evaluation of the feasibility of injections;
- Examination of the homogeneity and effectiveness of grout injections;

Shaking table tests:
- Examination of the influence of grout injection on the dynamic behaviour of a structure;
- Evaluation of *strengthening* improvement, (intervention performed on an undamaged structure);
- Evaluation of *repairing* improvement, (intervention performed on a damaged structure);
- Evaluation of differences between strengthened and repaired structures;

Monotonic compression tests:
- Study of the overall behaviour of injected panels;
- Evaluation of compressive strength of injected elements;
- Evaluation of failure mechanisms;
- Estimation of difference between strengthened and repaired structures;

Shear compression tests:
- Study of the overall behaviour of injected panels;
- Evaluation of shear strength of injected elements;
- Evaluation of failure mechanisms;
- Estimation of difference between strengthened and repaired structures;
- Evaluation of energy dissipation capacity of injected elements

Figure 2.22: Layout of the research.

Chapter 3

Preliminary Characterization of Materials and Structures

The whole experimental program is preceded by an initial phase constituted by several tests on materials and constituents. This preliminary part results widely important to guarantee the similarity concerning mechanical and physical properties of basic materials, employed on masonry panels and building models, with those of historical constructions.

The chapter is divided into two main parts, involving both destructive and non-destructive investigations.

The first section focuses on the preliminary mechanical and physical characterization of the materials employed. However, these tests were performed again in conjunction with the experiments carried out on the shaking table for a better examination of their mechanical values.

The second part of this chapter proposes the results of sonic investigations carried out on both realized structures: masonry panels and building models. These analyses were performed in two subsequently phases. Firstly, the sonic tests were carried out before injection and allowed the void presence and the feasibility of injecting the masonry, as well as the masonry quality to be verified. Secondly, they were applied again after the strengthening operations to check the effectiveness of injections and, particularly, the homogeneity of the intervention.

An outline of the organization of this chapter is provided hereafter:

1. Mechanical characterization of materials:
    - Mortar;
    - Stone;
    - Grout;
    - Injectability test;
2. Non-destructive investigations on whole structures:
    - Panels;
    - Building models;

3.1 Mechanical characterization of materials

The specimens were built employing materials with mechanical characteristics similar to those found during in-situ and laboratory tests on constituents or structural

elements of historical constructions [Binda and Saisi, 2005; Binda *et al.*, 1999, 2001, 2007]. The main results concerning the mechanical characteristics of all the basic materials are presented in the following sections.

3.1.1 Mortar

All the specimens were built using a mortar expressly designed to have low mechanical characteristics similar with that normally found on historical buildings. As previous researches demonstrated [Binda *et al.*, 2003a; Faria *et al.*, 2008; Lanas and Alvarez-Galindo, 2003; Rodrigues and Henriques, 2004; Valluzzi, 2000], a natural hydraulic lime-based material results more similar with historical mortars than cement-based ones. The insertion of an airing material allowed a reduction in typical strength of mortar to be compatible with the historical ones (table 3.1).
Tests were carried out following the prescriptions given by UNI EN 1015-11 [2007] about methods of test for mortar for masonry.

Table 3.1: Mechanical characteristics of mortar.

Test		
Compression Strength	(28days)	3.7N/mm^2
Flexural Strength	(28days)	1.3N/mm^2
Young's Modulus	(28days)	6130N/mm^2

(a) **(b)**

Figure 3.1: Flexural and compressive tests on mortar specimens.

3.1.2 Stone

All the stones used are calcareous. Although this similarity, they appeared different in colour and in chemical composition, even if any deeper analysis was performed concerning its chemical origin. These differences reflect in their mechanical characteristics as confirmed by typical values reported in table 3.2. Nevertheless, one should consider as the overall behaviour of the masonry will widely depend on the characteristics of the weakest component material, in this case mortar.
Tests were carried out following the prescriptions given by UNI EN 12372 [2007]; UNI EN 14580 [2005]; UNI EN 1926 [2007]; UNI EN 1936 [2007] about methods of test for natural stones.

Table 3.2: Mechanical characteristics of stone.

Test	Typology 1	Typology 2
Compressive Strength	265N/mm^2	159N/mm^2
Flexural Strength	31.6N/mm^2	25.2N/mm^2
Young's Modulus	72300N/mm^2	56380N/mm^2
Real Volumic Mass	2659kg/m^3	2669kg/m^3
Apparent Volumic Mass	2654kg/m^3	2654kg/m^3
Open Porosity	0.84%	1.68%
Total Porosity	0.19%	0.56%

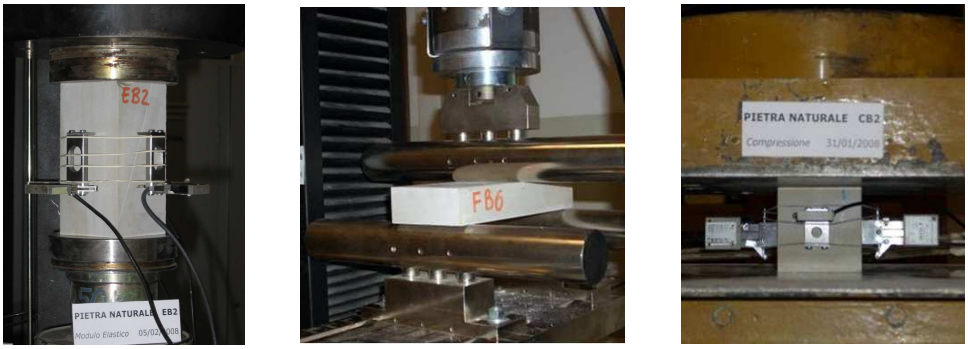

(a) **(b)** **(c)**

Figure 3.2: Determination of elastic modulus and of flexural and compressive strength of stone specimens.

3.1.3 Grout

The investigated strengthening intervention technique is based on the injection of hydraulic lime-based grout to bind the incoherent fragments existing in the inner part of multi-leaf masonry. The chemical composition, the mechanical characteristics and rheological aspect of this mixture were refined and calibrated by Valluzzi [Valluzzi *et al.*, 2003; Valluzzi, 2000]. This grout typology is characterized by high fluidity, a low water-soluble salts content and resistance to the lime-based sulphates.
The mechanical values reported in table 3.3 confirm a high compatibility between grout and mortar, showing a similar Young's Modulus. The grout also showed an unusually high compression strength that, as confirmed by several studies [Toumbakari, 2002; Valluzzi *et al.*, 2004; Vintzileou and Miltiadou-Fezans, 2008; Vintzileou and Tassios, 1995], does not influence the overall compression behaviour of the strengthened structure. Since neither standard nor recommendations are given for testing on grouts, in this case the procedure provided by UNI EN 1015-11 [2007] is followed.

Table 3.3: Mechanical characteristics of grout.

Test		
Compressive Strength	(28days)	12.8N/mm^2
Flexural Strength	(28days)	3.8N/mm^2
Young's Modulus	(28days)	6580N/mm^2

(a) **(b)** **(c)**

Figure 3.3: Determination of elastic modulus and of flexural and compressive strength of grout specimens.

3.1.4 Injectability test

In addition to the test on material specimens, the mechanical characterization was also carried out on composite elements. Following the UNI EN 12390 Standard [UNI EN 12390-1, 2002; UNI EN 12390-2, 2002; UNI EN 12390-3, 2003; UNI EN 12390-4, 2002; UNI EN 12390-6, 2002] for concrete cylinders, plastic moulds (diameter 15cm and overall height of 30cm) were filled with stone fragments (figure 3.4a) employed to built masonry panels (full scale) and building models (reduced scale). Subsequently, they were injected with grout (figure 3.4b) to simulate the behaviour of the strengthened internal core of multi-leaf walls.
Although fragments were taken from both full and reduced scale structures, any noticeable influence about their dimensions could be seen on the overall mechanical characteristics on cylinders. On this basis, the presented average was computed considering all the specimens.

(a) **(b)** **(c)** **(d)**

Figure 3.4: Preparation of specimen: (a) and (b); determination of indirect tensile (c) and compressive strength (d).

These specimens were made and subsequently tested respectively in conjunction with the construction of building models and the execution of the shaking table tests. Table 3.4 shows that the compression strength is widely lower than that exhibited by grout, due to the presence of incoherent stone fragments that influence the Young's Modulus values, resulting higher than that of admixture.

Table 3.4: Mechanical characteristics of cylinders (grout and stone fragments).

Test	
Compressive Strength	2.12N/mm^2
Indirect Tensile Strength	0.20N/mm^2
Young's Modulus	11094N/mm^2

3.2 Non-destructive investigations on whole structures

The strengthening technique investigated by the present research work, namely the injection of hydraulic lime-based grout, is applicable to masonries that are characterized by a wide presence of voids in their internal part. The masonry typology employed to build all the specimens to be dynamically tested, i.e. panels and building structures, usually presents a percentage of voids ranging between 10% and 12% [Binda, 1999; Binda *et al.*, 2003a; Gardin, 2007]. Nevertheless, this range can vary quite significantly depending on the masonry typology.

Direct and tomographic sonic tests were performed on masonry panels and building models before and after the strengthening interventions, allowing the development of several observations presented as follows. Furthermore, while direct sonic tests gave information about wider zones of specimens, sonic tomographies provided a deeper knowledge in a single section of the wall. The comparison of the results with the classifications proposed by Berra *et al.* [1992] and Forde *et al.* [1985] (compare §1.1.3) will also allow a qualitative evaluation of the masonry quality.

An instrumented impact hammer with hard tip, producing stress waves with frequency up to 1kHz, was used as excitation source. Piezoelectric accelerometers with a measurement range of ±0.5g and a frequency range between 0.05 and 4000Hz were employed as sensors. A National Instruments PXI was used as a system acquisition combined with LabVIEW commercial software for analyses and results of direct sonic tests. Successively, a software developed at the University of Padua [Monteforte, 1997] was employed to elaborate sonic tomographies.

The position of sonic tests and the results will be presented and discussed in the following paragraphs.

3.2.1 Masonry panels

The first part of the sonic investigations focuses on the analyses performed on the masonry panels. The adopted investigation grids and the analysis of results obtained both before and after the strengthening interventions are presented in the following.

3.2.1.1 Investigation grid

Two direct sonic tests were performed on a rectangular mesh with an overall width of 1.0m and a height of 2.0m. This mesh was centred on each masonry panel. Points of measure were spaced 25cm apart, which corresponds to half of the masonry thickness. This led to a mesh comprising 45 acquisition points, which provide in-depth information on the entire surface of panels.

Furthermore, four tomographic sonic tests were carried out in a horizontal and vertical directions on both investigated panels. These tests were performed in the middle of the panel, allowing more exact information to be obtained on zones that will

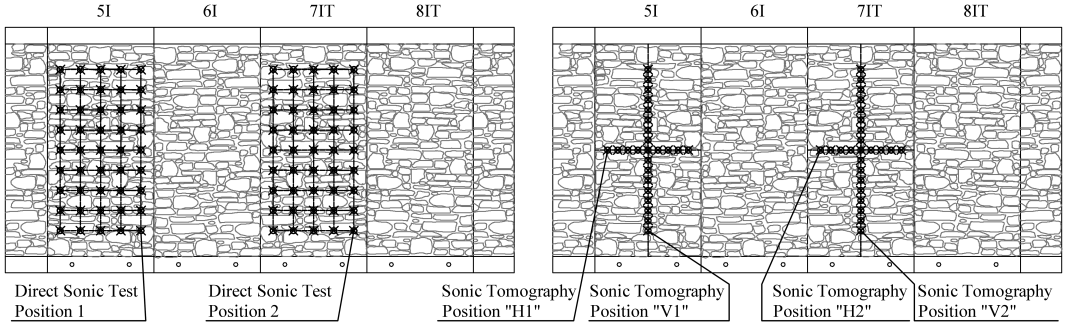

Figure 3.5: Position of sonic grids on masonry panels: direct tests (left) and tomographies (right).

be most stressed during the shaking table tests. The overall length of tomographies is 2.0m. The mesh was thickened, with reference to direct sonic tests, and was settled at 12.5cm. This step corresponds to a quarter of the overall depth of the specimen, thus obtaining 34 acquisition points. Since vertical tests had a higher number of acquisition points and the length of some paths is particularly large, the analyses were performed separately in three parts, namely upper, central and lower ones.

the position and grids of both direct sonic tests and tomographies are presented in figure 3.5.

3.2.1.2 Results before strengthening

Direct sonic tests carried out on both investigated masonry panels underlined that the mean velocities range between 770m/s and 1000m/s (figures 3.6 and 3.7). Comparing these results with reference values [Berra *et al.*, 1992; Forde *et al.*, 1985], the quality of masonry can be classified as poor. Low sonic velocities can be ascribed to the wide presence of voids in the inner part of masonry. Higher velocities range between 1600m/s and 1800m/s and are positioned in the lowest part of investigated panels.
This overall behaviour can be explained by some construction details of this masonry typology:

- The lowest stone courses are characterized by a greater regularity than the upper ones, since they lean on the concrete base.
- The self-weight of the upper part of the wall causes a compacting of the lowest one.

This leads to a decrease in voids and a consequent greater density of materials, explaining the increasing of sonic velocities.

Vertical tomographic sonic tests (figures 3.6 and 3.7) confirm the results obtained from direct sonic tests. Two different zones, characterized by different behaviours, can be clearly identified. Low velocities can be found in the upper part, over 1.5m, where sonic values range between 500m/s and 1000m/s, and are compatible with those obtained by direct sonic tests. Secondly, the results concerning the bottom part seem to confirm the analysis obtained by direct sonic tests. Also horizontal sonic tomographies (figures 3.6 and 3.7) provide values comparable with those of direct tests. However, the four performed tomographies are not able to emphasize the dissimilar textures of different masonry layers: a more compact external parts

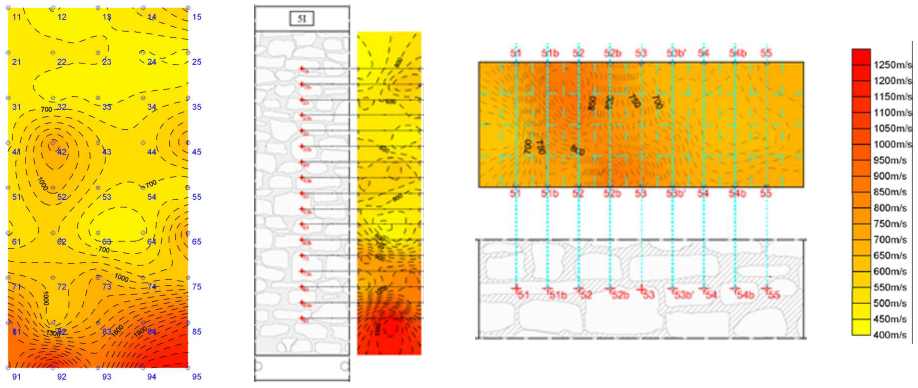

Figure 3.6: Position 1, before injection: direct sonic test (left); vertical (centre) and horizontal (right) sonic tomographies.

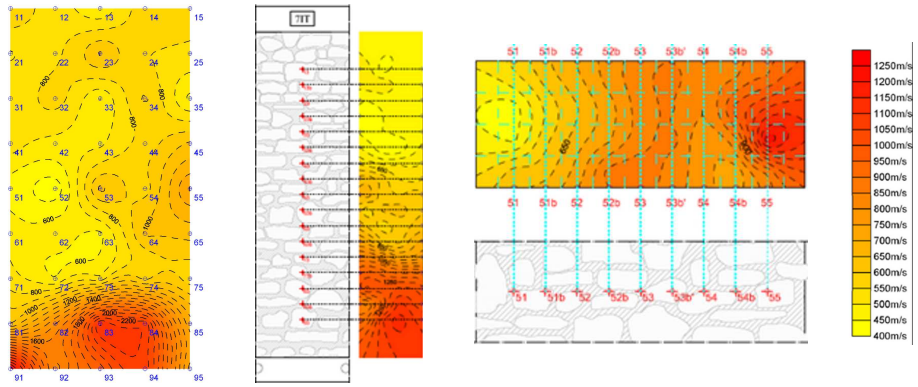

Figure 3.7: Position 2, before injection: direct sonic test (left); vertical (centre) and horizontal (right) sonic tomographies.

and an internal core with a wide presence of voids. The isovelocity curves follow the sonic paths, developing perpendicularly to the surface and not on a parallel plane.

Results obtained from sonic tomographies are in agreement with those obtained with direct sonic tests. The inability of tomographies to identify different masonry layers can be ascribed to the larger dimension investigated, which for the longest path exceeds 2m, invalidating the final result. The lack of in-depth information on horizontal tomographies suggests the need to increase the number of the acquisition points, to obtain a better knowledge of masonry.

3.2.1.3 Results after strengthening

The quantity of injected lime grout was monitored during the strengthening intervention phases. For instance, the number of litres introduced to each hole was recorded. The quantity ranges from $4 \cdot 10^{-3}\text{m}^3$ to over $30 \cdot 10^{-3}\text{m}^3$. This check allows a mapping of quantities to be obtained for each panel and this can be related to the results of sonic tests performed after the lime grout injection.

After the strengthening operations, direct sonic tests were performed again. Figure 3.8 shows a significant increase in velocity. Results on panel "5I" range between 2000m/s and 3000m/s, while velocities on panel "7IT" are generally higher than 2800m/s. These high values of sonic velocities, obtained after injection, allow it to be claimed that most voids were filled by the grout. However, velocities lower than

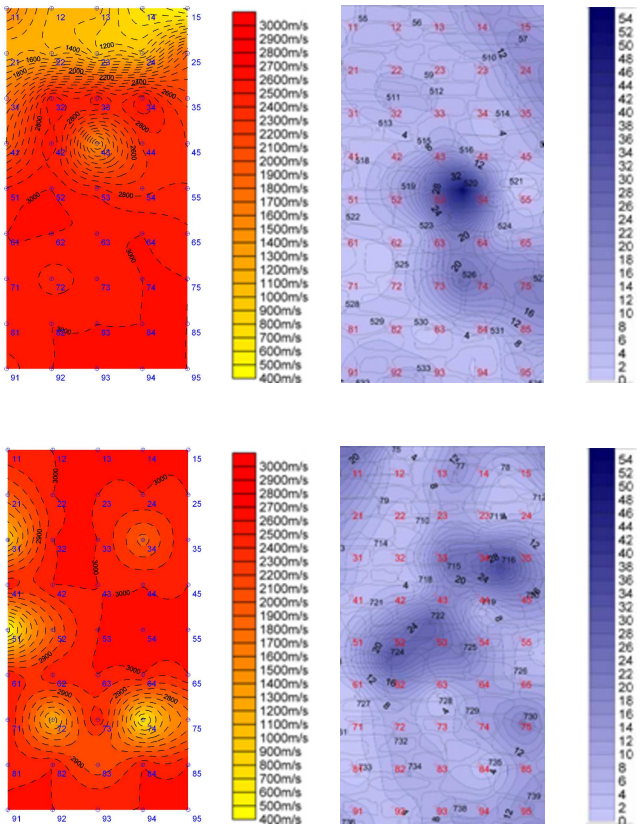

Figure 3.8: Position 1 (top) and 2 (bottom), after injection: direct sonic tests (left) and quantity of injected grout (right) in litres.

1500m/s were identified in the upper part of the first panel. Similarly, some isolated points on the second panel showed velocities of about 2500m/s. The difference of velocities among these points and the remaining part of the panels can be ascribed to an irregular distribution of grout in the masonry core, causing an incomplete permeation of the voids. Indeed, these velocities are higher than those calculated before the injection but they are clearly lower than the main values obtained in different zones of the panel.

The comparison of velocities before and after strengthening confirms the wide presence of voids in the masonry core. Furthermore, one should note as, notwithstanding the great lack of homogeneity in the quantity of injected grout for each hole (figure 3.8), the final velocity is quite high and uniform on the whole surface. This result confirms the wide diffusion of the admixture in the zones characterized by widely present voids.

3.2.2 Building models

Direct and tomographic sonic tests were also performed on several portions of the building models for the confirmation of the previously drawn hypotheses and a validation of the effectiveness of the investigation technique.

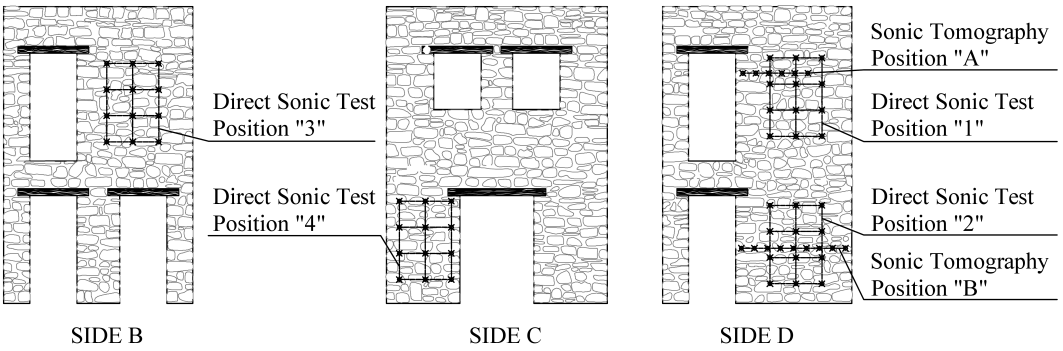

Figure 3.9: Position of sonic grids on masonry buildings: direct tests and tomographies.

3.2.2.1 Investigation grid

Four direct sonic investigations were planned in the same number of panels of each specimen. A rectangular mesh of 66cm by 99cm was employed with a step of 33cm, equal to the overall masonry thickness. This set-up allowed 12 acquisition points per each test. Direct sonic tests were performed by measuring the transit time in all of the corresponding sonic paths, that are between corresponding the pairs of points positioned at the same location on opposite sides of the wall section. Investigations were carried out in the largest parts of the structure: positions 1 and 3 are placed on the second floor while 2 and 4 on the first one. Locations 1 and 2 are vertically aligned to control likenesses and differences of masonry characteristics, due to dissimilar storeys.

Two sonic tomographies were also carried out in the same pier to control and compare results with those obtained from direct sonic investigations. Tomography "A" was realized placing sensors on three sides, using a two by six mesh. Tomography "B" involved four sides, with a two by nine mesh. In both cases the acquisition points were equally spaced at 16.5cm, corresponding to half of the overall masonry thickness. Sonic tomographies were realized by measuring the transit time in all of the possible sonic paths in the identified horizontal cross-section, according to the considered acquisition grid. Results were elaborated considering simultaneously all the recorded transit times [Monteforte, 1997]. It was therefore possible to detect the fastest and slowest paths and, consequently, the most compact and loose areas of the masonry section in question.

The positions and grids of both, direct sonic tests and tomographies are presented in figure 3.9.

3.2.2.2 Results before strengthening

Direct sonic tests, carried out before strengthening interventions on both URM and SM models, highlight sonic velocities under 1000m/s. This result denotes weak masonry conditions, according to the proposals of Forde *et al.* [1985] and Berra *et al.* [1992]. In particular, positions 2 and 4, on the first storey, presented higher velocities than positions 1 and 3, situated on the second floor (figures 3.10 and 3.11). This difference is due to masonry dead loads, which caused a natural compacting of material in the lower storeys. These weak conditions are related to the wider voids present in the masonry core.
Position 4 is of particular interest, where sonic velocities are also higher than 2000m/s.

This fact is due to the mesh position. In fact, higher velocities can be found on the lateral sides corresponding to the pier edges, where stones are positioned transversally to the section. Existing lower velocities of about 1000m/s on the middle of the pier, where no transversal connection is provided, confirm this thesis. Other tests, carried out away from the pier edges do not present this unusual behaviour. Figures 3.12 and 3.13 demonstrate that at the pier edges, where stone and masonry continuity is present, velocities are greater than 1800m/s while, in the central zone, higher transit times confirm the incoherence of the masonry core. Time records between points on opposite long sides are predominant with reference to those obtained from juxtaposed faces, making it difficult to detect a central core, characterized by weak conditions, and reaching a mean velocity greater than that calculated from direct sonic tests.
All the results of sonic tests carried out on URM and SM models are therefore similar, confirming that it is possible to strengthen masonry by injection.

3.2.2.3 Results after strengthening

Sonic direct tests, performed after injections on the SM model, denote how the mean velocity widely increased: all sonic velocities range between 2200m/s and 2900m/s, indicating quite good masonry quality.
Figure 3.14 shows how the quantity $[10^{-3}m^3]$ of injected lime grout in each panel was not uniform, confirming the great variability of the masonry core. Nevertheless, figure 3.15 highlights how the free diffusion on lime grout can lead to an homogeneous distribution of sonic velocities. Slight differences were found in limited parts of the investigated panels. Particularly, low values found on the bottom of position 2 can be ascribed to local problems of lime grout penetration, because of too small core fragments. Furthermore, position 4 (figure 3.15) shows that on lateral zones a limited increase can be found, indicating that not many voids are present in the pier edges, while they are obviously concentrated in the middle. This conclusion can also be deduced from an analysis of the injected quantities, concentrated in the centre of the panel, confirming the previous comments. Moreover, no velocity increase was found between the second and the first storey.

Sonic tomographies confirmed the analysis obtained from direct tests. For instance, the sections in question are homogeneous, successfully eliminating differences between pier edges and the central zone as highlighted before strengthening (figure 3.16). Tomographies carried out after injections indicate lower velocities than those obtained from direct sonic tests due to the alternative elaboration of different signals in the same areas.

By considering the overall sonic results after strengthening, it can be confirmed that lime grout is freely distributed and has permeated a large percentage of voids, and that homogeneity and improved compacting (figure 3.15) can be achieved, even starting from worse and heterogeneous conditions (figure 3.11).

3.2.3 Conclusive Remarks

The values concerning sonic velocities, obtained from investigations carried out on laboratory specimens and presented in the previous sections, indicate that the realized models are quite representative of a real situation. However, the absolute velocities of specimens, ranging between 900m/s and 1100m/s (figures 3.6, 3.7, 3.10, 3.11, 3.12 and 3.13), are lower than those obtained from in-situ tests (1932m/s). Nevertheless, this fact does not invalidate the reliability of experimental models since the comparison

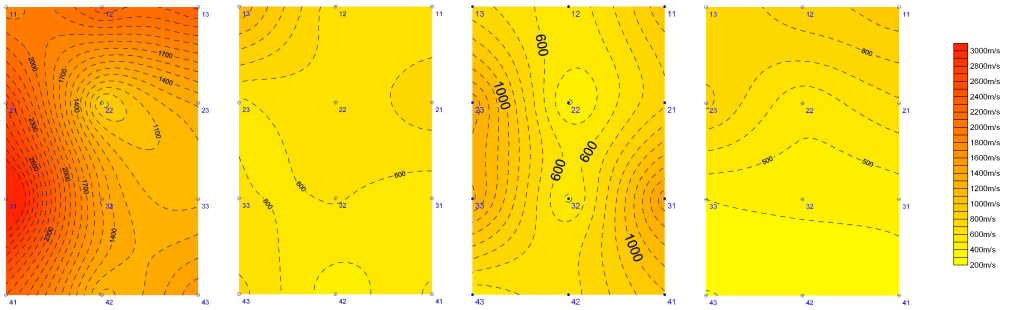

Figure 3.10: URM model: direct tests before injection. From left to right: position 1 to 4.

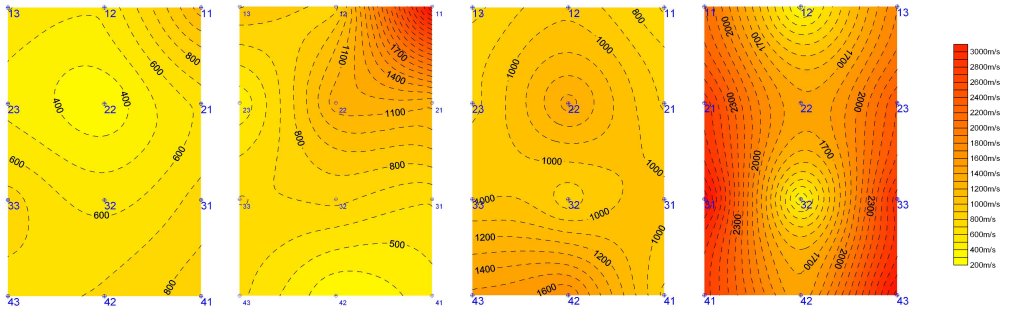

Figure 3.11: SM model: direct tests before injection. From left to right: position 1 to 4.

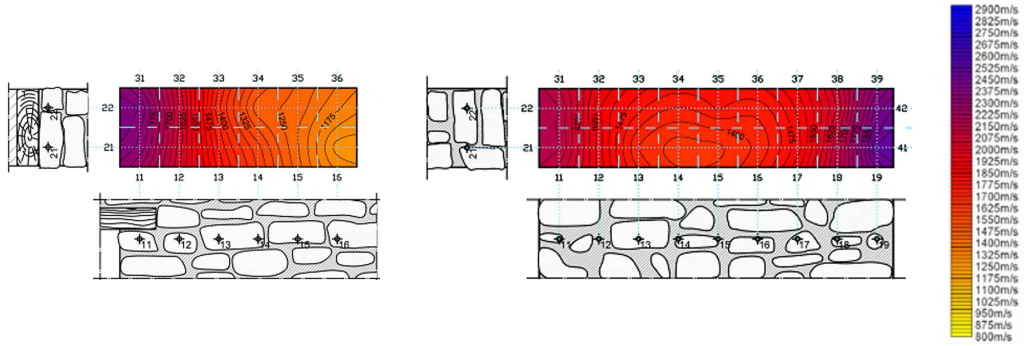

Figure 3.12: URM model: sonic tomographies before injection. Position A (left), B (right).

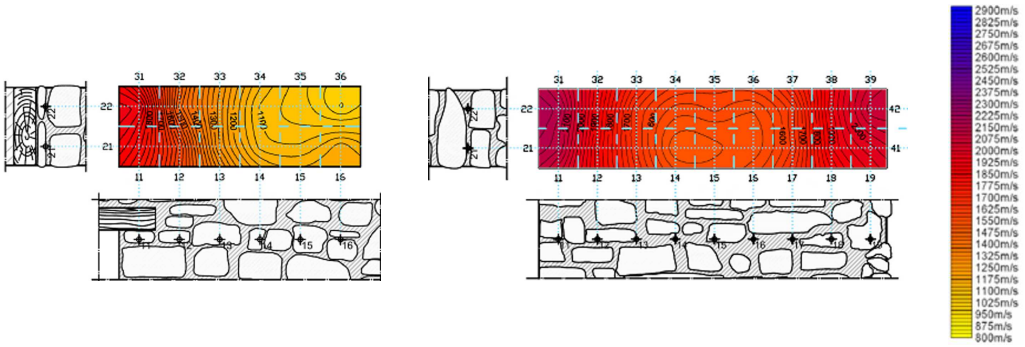

Figure 3.13: SM model: sonic tomographies before injection. Position A (left), B (right).

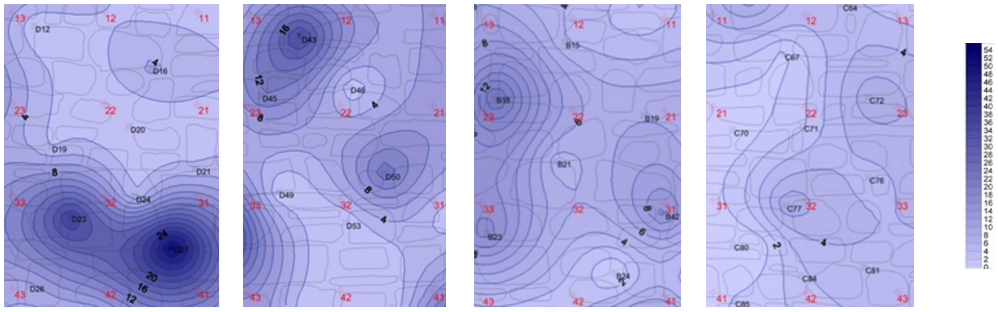

Figure 3.14: SM model: Maps of injected grout (litres). From left to right: position 1 to 4.

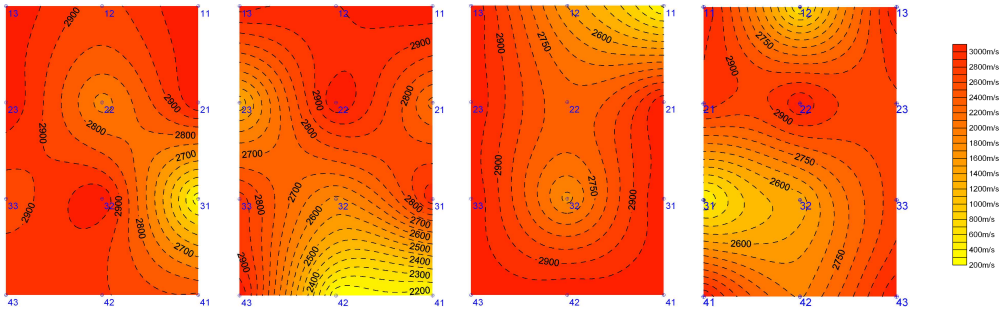

Figure 3.15: SM model: direct tests after injection. From left to right: position 1 to 4.

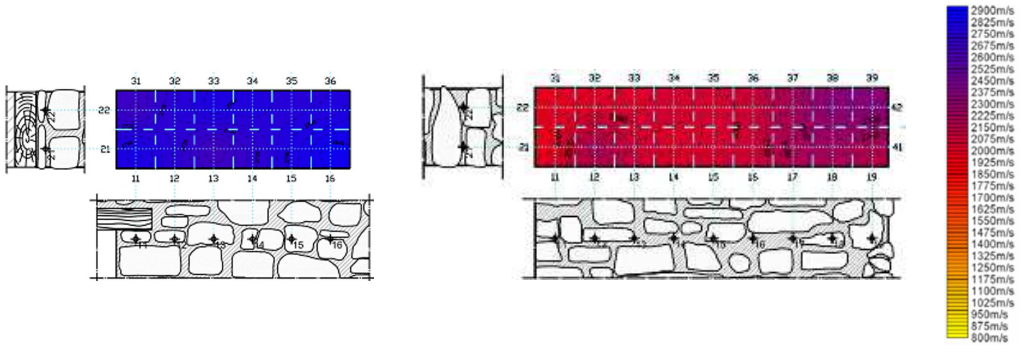

Figure 3.16: SM model: sonic tomographies after injection. Position A (left), B (right).

between results calculated before and after injection reflects the overall behaviour showed during in-situ investigations: low sonic velocity before intervention and a significant increase after strengthening. This confirms that the usefulness of direct and tomographic sonic tests is based on comparative evaluation and not in absolute results [Binda *et al.*, 1997b, 2000a; da Porto *et al.*, 2004].

The comparative analysis of velocities, obtained from direct sonic tests before and after injection, remains highly significant for all categories of masonry and building types. Moreover, sonic tomographies provide a deeper knowledge of masonry, even if an adequate thickness should be accounted. This fact is clearly validated by laboratory tests carried out on building models. For instance, the monitoring of the injection process and the use of sonic tests after the intervention lead to an evaluation of the strengthening effectiveness. Finally, the areas where injection more difficultly penetrated can be detected, as the uniformity of intervention can be verified.

In conclusion, the limited application of direct sonic tests at a point of the structure cannot provide sufficient elements to detect its characteristics. On the

contrary, the application of the technique to different parts of the model and the comparison of its results help to qualitatively understand masonry characteristics and detect voids.

Chapter 4

Shaking Table Tests on Masonry Buildings

Dynamic tests carried out on whole stone masonry buildings constitutes the core of this research. The experimental section described in this chapter allows direct investigation of the influence of grout injection on the dynamic behaviour of injected structures. Furthermore, as the the state-of-the-art outlined (compare §1.3), previous experimental campaigns, carried out by other researchers on the same technique applied to similar masonry typologies, focused on tests on single structural elements. On the other hand, only a case of an experimental campaign, which involved tests on building models strengthened by cement-based injections, could be found [Benedetti, 1980]. The results, obtained from shaking table tests, provided information on both the local and overall effects of grout injection. This chapter presents preliminary observation and advanced analyses developed to study the effectiveness of the injection technique and the possible differences between strengthening and repairing, where *strengthening* indicates interventions on an undamaged structure, while *repairing* denotes an intervention carried out on a previously damaged structure.

4.1 Test procedure and instrumentation

The three shaking table tests were realized in several steps characterized by an increased seismic load. The test rig employed and all further devices have already been presented in section 2.1.1. A more detailed description of the experimental set-up can be found in Modena *et al.* [2009], technical report on this campaign.

4.1.1 Instrumentation systems

Several devices were fixed to the structures to monitor both accelerations and displacements on crucial points of buildings.
Two series of sensors were employed to record accelerations and they were placed in different positions:

- Externally, in the corners of structures, fixed in both horizontal directions and at both levels (figure 4.1);
- Internally, in the central timber beam in both horizontal directions and at both levels (figure 4.2);

- To the shaking table, to control the seismic input in both horizontal directions and a vertical one, to control further induced movements.

Both instrumentation systems employed PCB sensors, while for the external positions piezoelectric accelerometers were employed (models 393B12 and 393A03, figure 4.3), for internal ones capacitive accelerometers were fixed (model 3701, figure 4.3). A layout of the positions and directions of sensors is given in figure 4.1.

Furthermore, an optical system was employed to monitor the displacement of about a hundred of points (figure 4.4). This instrumentation is based on the survey of the position of markers using triangulation of the directions recorded by several isolated optical cameras placed all around the structure. This allowed both to deepen the knowledge of local mechanisms and to link relative displacements and accelerations.

Moreover, displacements of the concrete base were monitored using four LVDT's to control the boundary conditions at the bottom of the models.

4.1.2 Additional masses

The theory selected and employed for the scale reduction of models (simple model, proposed by Tomaževič and Velechovsky [1992]) imposes to verify the stress level at the bottom of walls on the models. In fact, a comparison of the floor to wall mass ratios at each floor level, in the case of the prototype and model structures, underlines how the theoretical value is not respected.

$$m_{Floor,P} : m_{Wall,P} = 1 : 14.1 \tag{4.1}$$

The floor mass can be estimated equal to:

$$\begin{aligned} m_{Floor_P} &= q_{Floor,P,acc} \cdot A_{Floor,P} + s \cdot A_{Floor,P} \cdot \Gamma_{Planking} + \\ &\quad + 5 \cdot A_{Beam} \cdot l \cdot \Gamma_{Planking} \\ &= 200 \cdot 3.2 \cdot 2.6 + 0.04 \cdot 3.2 \cdot 2.6 \cdot 600 + \\ &\quad + 5 \cdot 0.18 \cdot 0.14 \cdot 2.6 \cdot 600 = 2060\text{kg} \end{aligned} \tag{4.2}$$

and the mass of masonry equal to:

$$m_{Wall,P} = V_{Wall,P} \cdot \Gamma_{Wall,P} = 12.65 \cdot 2300 = 29095\text{kg} \tag{4.3}$$

The masonry density, evaluated during the handling of models on the shaking table, was computed to be equal to $\Gamma_{Wall,M} = 2466\text{kg/m}^3$.
As a consequence of the equation 4.1, the floor mass, considering both the self-weight and the live loads, should be equal to:

$$m_{Floor,M} = 8976 : 14.1 = 637\text{kg} \tag{4.4}$$

By subtracting the self-weight, equal to 168kg, one deduces that the load to be added at each floor level is equal to 468kg. Subsequently, the stress level at the base between the prototype ($\sigma_{0,P}$) and the model ($\sigma_{0,M}$) can be compared. In the case of the URM model the stress level is equal to:

$$\begin{aligned} \sigma_{0,M} &= \sum Q_{Floor,M}/A_{Wall,M} + \Gamma_{Wall,M} \cdot h_M = \\ &= \frac{(2 \cdot (468 + 168) \cdot 9.81/2)}{330 \cdot 2140} + 2.466 \cdot 10^{-5} \cdot 3600 = \\ &= 0.009 + 0.089 = 0.098\text{N/mm}^2 \end{aligned} \tag{4.5}$$

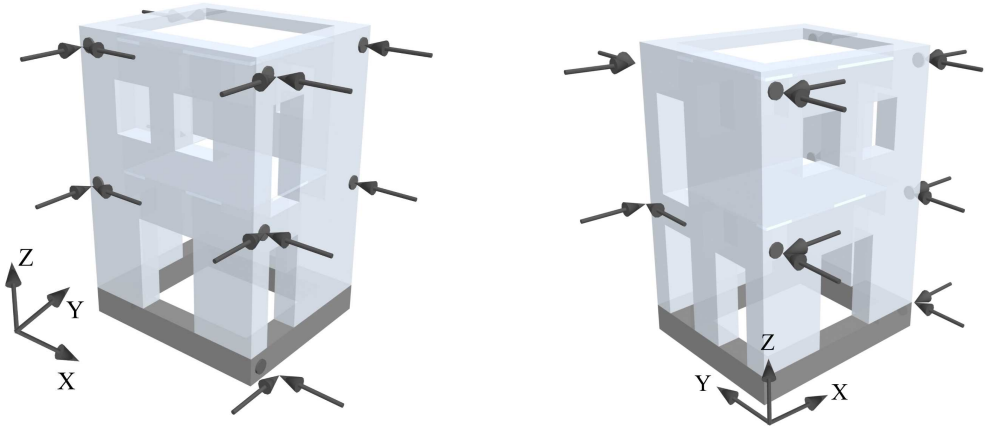

Figure 4.1: Disposition and directions of externally fixed accelerometers.

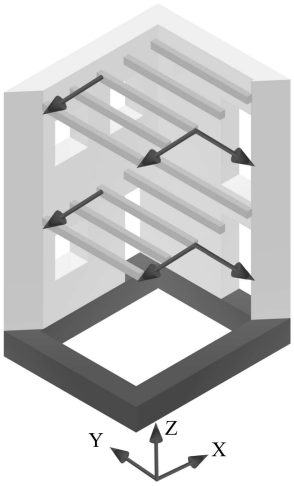

Figure 4.2: Disposition and directions of internally fixed accelerometers.

Figure 4.3: Examples of the capacitive (top) and piezoelectric (bottom) accelerometers.

Figure 4.4: Disposition of markers to monitor the displacements.

Figure 4.5: Examples of additional masses.

While, in the case of the prototype building, the stress level is equal to:

$$\begin{aligned}\sigma_{0,P} &= \sum Q_{Floor,M}/A_{Wall,M} + \Gamma_{Wall,M} \cdot h_M = \\ &= \frac{(2 \cdot (2060) \cdot 9.81/2)}{500 \cdot 3240} + 2.3 \cdot 10^{-5} \cdot 5400 = \\ &= 0.012 + 0.083 = 0.137\text{N/mm}^2\end{aligned} \tag{4.6}$$

It should be noted that the stress ratio, $\sigma_{0,P}/\sigma_{0,M}$, is equal to about 1.5, highlighting that this ratio is almost constant on both structures. In the case of injected models the result is similar, since the density of masonry increases proportionally on the prototype and models.

For the above mentioned reasons, steel plates for an overall mass of 500kg were added per each floor of all models (figure 4.5). These masses were fixed to the floors using pins. Furthermore, one should remember that the correctness of the overall dynamic behaviour of models can be obtained mainly providing a correct mass distribution rather than a correct simulation of the compressive stress at the bottom of the walls [Tomaževič, 2000].
Considering the specific weight of the masonry and timber, the mass distribution for each model can be obtained. Table 4.1 summarizes the overall masses of models.

Table 4.1: Mass distribution on models.

		First Floor [kg]	Second Floor [kg]
URM Model	Masonry	8808	10139
	Planking and beams	168	168
	Additional mass	500	500
	Total	9476	10807
SM Model	Masonry	9467	10897
	Planking and beams	168	168
	Additional mass	500	500
	Total	10135	11565

4.1.3 Seismic input

The seismic input employed in this experimental program was selected at the University of Pavia, where ongoing research, focusing on shaking table tests on old masonry structures in order to study further structural aspects and intervention techniques, employs the same time history. This will allow a comparison to be made of methodologies and results for the carried out experiments and will provide further information on the dynamic behaviour of old masonry structures and the influence of strengthening techniques. The main characteristics and reasons, which led to the choice, have been presented by Penna *et al.* [2007] and are summarized as follows.

The employed time history was based on an a priori choice of records of natural events, so that the shape of the signal is realistic also in the time domain. This consideration, combined with the selection of a seismic input compatible with the spectrum provided in the Italian code [D. M. 14/01/2008, 2008], led to seven alternatives presented in figure 4.6.

The experiment will be carried out at increasing levels of Peak Ground Acceleration (PGA). As a consequence, the structures will be progressively damaged, causing an increase in the fundamental period of the building model. This consideration led to a choice of signals with less variation between 0.1s and 0.5s on the spectral shapes. This interval fits well into the range of frequencies typical for the studied structure.

All the above mentioned observations led to a choice of the time history (figure 4.7) of earthquake that occurred in Montenegro (15/4/1979).

The elaboration of the original seismic signal, considering the scale theory proposed in section 2.1.1.2, led to a time reduction and an amplification of accelerations as shown in figure 4.8.
As a consequence, the interested interval period in question changed, varying within the range between 0.1s and 0.5s, that corresponds to the interval between $0.0\bar{6}$s and $0.\bar{3}$s of the processed signal.

4.1.4 Testing procedure

The employed time history, whose selection is presented in section 4.1.3, was performed with a peak increasing by 0.05g at each successive execution. The experiments were performed until sever damage occurred to specimens and the stability of the models was compromised. In all cases the collapse of structures was avoided.

The test procedure was repeated at each step and it consists of three different phases:

- Preliminary dynamic characterization through ambient vibration;
- Preliminary dynamic characterization through white noise input;
- Execution of seismic input at increased peak amplitude.

Obviously, both characterizations were also performed at the end of each experiment, before the models were dismantled. Tables from 4.2a to 4.2d list the steps performed on each tested structure and the direction of the seismic input.

Some considerations of the performed steps are given as follows.
The seismic excitation was input in two orthogonal directions at all steps carried out on the URM model. After the beginning of heavy damage to the structure, during the step at 0.25g, the following test was repeated at the same peak amplitude, named 0.25g (bis). This allowed to verify if the damaged model would sustain the same

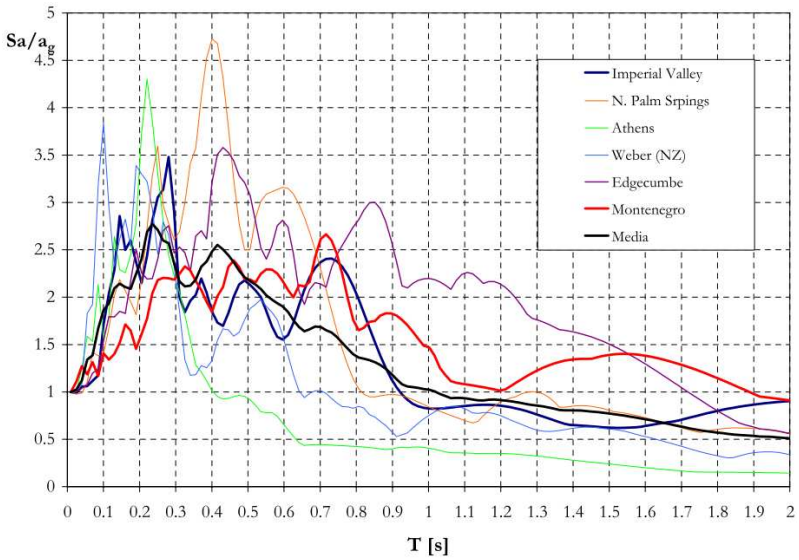

Figure 4.6: Response spectra of selected time histories [Penna *et al.*, 2007].

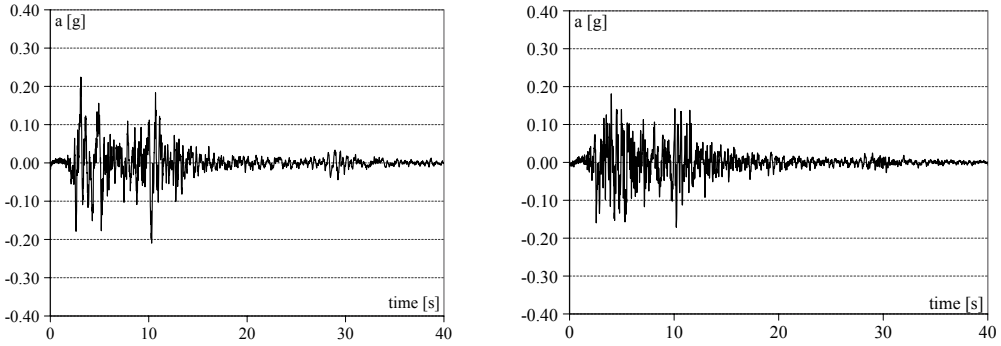

Figure 4.7: Time history of Montenegro earthquake on X (left) and Y (right) directions.

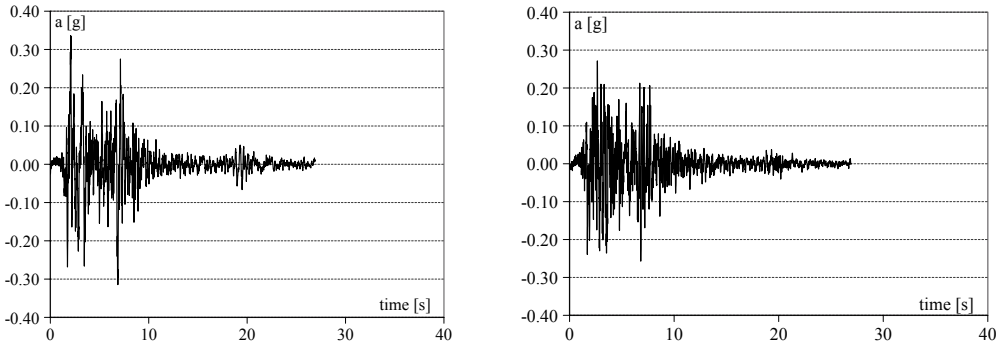

Figure 4.8: Processing of the the Montenegro earthquake on X (left) and Y (right) directions, considering the scale factor of 2:3.

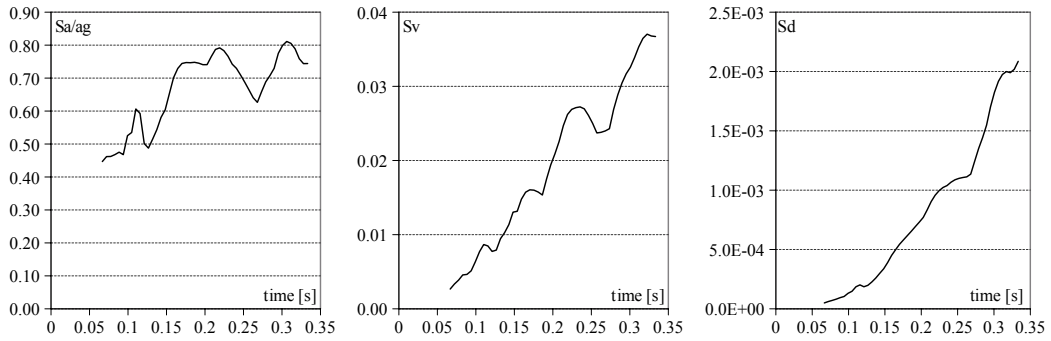

(a) Acceleration spectrum **(b)** Velocity spectrum **(c)** Displacement spectrum

Figure 4.9: Spectra of elaborated signal.

seismic load.
The RM model was normally tested with the seismic input, having two components, at all steps.
Instead, on the SM model the standard procedure was applied up to 0.55g, when heavy damage occurred and the stability of the structure was impaired. In order to carry on with the experiment, St. Andrew's timber cross-bracing were placed in the opening along the X direction. Over this step, the seismic load was input only in the X direction. Since the SM model could sustain the maximum acceleration applicable by the shaking table to this model, the last step of 0.70g was repeated twice.
Table 4.3 summarizes the maximum attained accelerations for each model.

4.2 Crack pattern and damage development

The First important considerations concerning the effects of lime grout on the behaviour of the injected models can be drawn from an observation of crack pattern development of damage to the structures. The comparison between the unstrengthened and injected building models, as well as the relation between the strengthened and repaired specimens, will be useful to highlight the divergences and effectiveness of the different applications. The surveys, presented as follows, show the crack pattern with different damage occurring during the last step (red line) from that appearing during the previous steps (black line).

4.2.1 URM model

The preliminary movement of the model on the shaking table induced few and limited cracks that did not develop during the first steps of the experiment. Damage could be seen before the attainment of 0.25g, when cracks opened particularly at the second floor and the formation of macro elements took place. Furthermore, the detachment of fragments from the top of the model was noticed. Before this step the model can be considered as intact.

A following sudden movement of the shaking table caused the initial damage particularly around the openings at the second floor. Further damage appeared at the first floor level. At this step, the local separation of external masonry layers could be seen, particularly at the corners of the upper floor. Moreover, the out-of-plane mechanism of limited portion of the stonework took place (figure 4.10).

Table 4.2: Tests performed on models

(a) Tests performed on URM model.

URM MODEL	
Input direction	Intensity
Montenegro XY	0.05g
Montenegro XY	0.10g
Montenegro XY	0.15g
Montenegro XY	0.20g
Montenegro XY	0.25g
Montenegro XY	0.25g (bis)
Montenegro XY	0.30g
Montenegro XY	0.35g
Montenegro XY	0.40g
Montenegro XY	0.45g

(b) Tests performed on RM model.

RM MODEL	
Input direction	Intensity
Montenegro XY	0.05g
Montenegro XY	0.10g
Montenegro XY	0.15g
Montenegro XY	0.20g
Montenegro XY	0.25g
Montenegro XY	0.30g
Montenegro XY	0.35g
Montenegro XY	0.40g
Montenegro XY	0.45g
Montenegro XY	0.50g
Montenegro XY	0.55g
Montenegro XY	0.60g

(c) Tests performed on SM model, Part I.

SM MODEL. Part I	
Input direction	Intensity
Montenegro XY	0.05g
Montenegro XY	0.10g
Montenegro XY	0.15g
Montenegro XY	0.20g
Montenegro XY	0.25g
Montenegro XY	0.30g
Montenegro XY	0.35g
Montenegro XY	0.40g
Montenegro XY	0.45g
Montenegro XY	0.50g
Montenegro XY	0.55g

(d) Tests performed on SM model, Part II.

SM MODEL. Part II	
Input direction	Intensity
Montenegro X	0.55g (bis)
Montenegro X	0.60g
Montenegro X	0.65g
Montenegro X	0.70g
Montenegro X	0.70g bis

Table 4.3: Maximum attained accelerations.

Model	Acceleration [g]
URM	0.45g
RM	0.60g
SM	0.70g

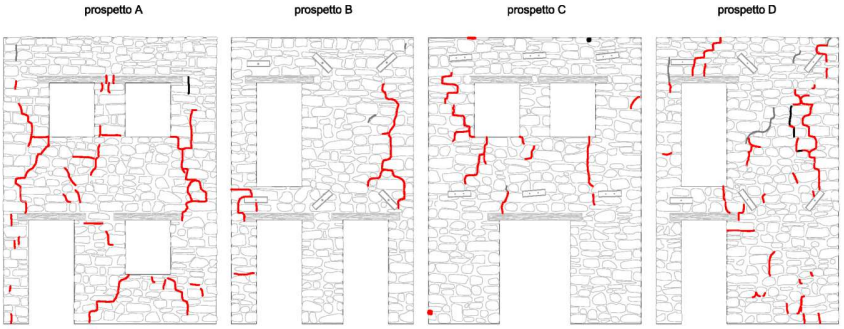

Figure 4.10: URM, Crack pattern after step 0.25g.

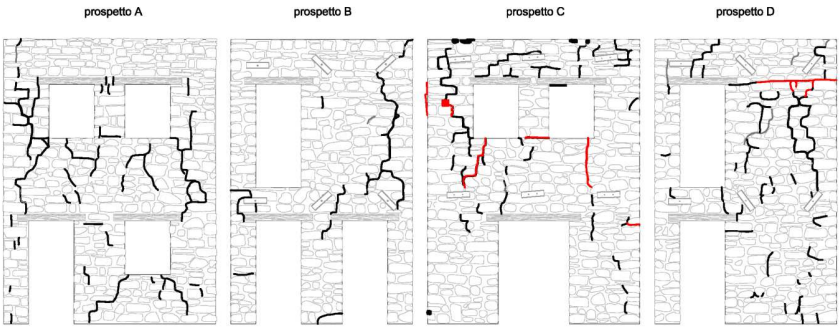

Figure 4.11: URM, crack pattern after step 0.45g, end of experiment.

To verify the changes occurred in the model, after the execution of ambient and random excitations, which allowed the monitoring of dynamic characteristics, the following step was repeated at an intensity equal to 0.25g. This step induced further limited damage and an overall settlement of the masonry.

The following step, namely 0.30g, the monolithic behaviour was completely lost and the most severe damage occurred in the upper part of the model. Local separation of masonry layers at corners became worse and further heavy damage was done to larger parts of the structure.

The damage continued to spread with an input equal to 0.35g. A widespread crack pattern occurred in the mortar bed joints of the whole model while stones showed no signs of damage.

Several masonry parts of prospect C were noticeably damaged and their stability was only guaranteed by the self-weight of the structure. The most damage is mainly due to the great diffusion of cracks, even if the presence of a few macro-elements could be seen.

The last performed step attained a peak acceleration of 0.45g. The second floor was completely damaged while the first floor revealed concentrated cracks. Figure 4.11 shows the crack pattern at the end of experiments on the URM model (compare also figures from A.1 to A.6).

4.2.2 RM model

The RM model, as previously presented, results from the repairing interventions on the URM model. This was tested again after the curing of the grout and demonstrated monolithic behaviour during the first steps of this second experiment. Any opening of the repaired cracks could be seen up to an intensity of 0.25g. During this execution,

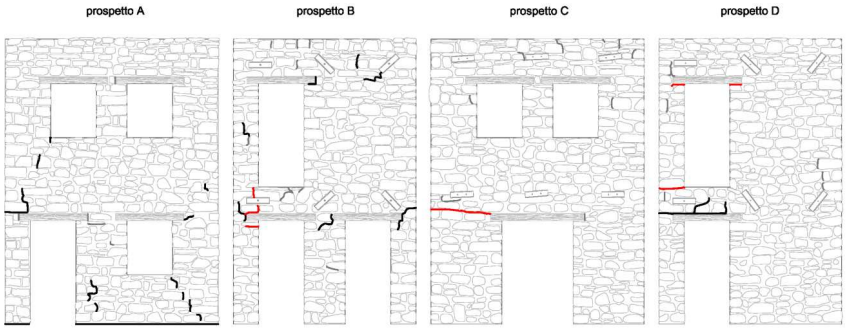

Figure 4.12: RM, crack pattern after step 0.45g.

initial damage occurred to mortar joints. In particular, this damage occurred in the same positions observed for the URM model.

The following steps, namely 0.30g and 0.35g, increased the extension and width of the cracks but without inducing further and new damage. However, during the test with a peak acceleration of 0.35g, the mortar joint at the bottom of the pier on prospect D crushed. Because of this occurrence, the structural element involved started to rise during the tests. Steel profiles (UNP200), fixed on both sides of the concrete base, prevented this phenomenon from worsening (figure A.7). Related to this, a horizontal crack started to appear at the first floor level.

The model started to manifest a loss of monolithic behaviour and the formation of macro-elements can be noted at both levels. The horizontal crack on the previously considered pier increased and, after this seismic level, this structural element behave independently from the building model. Figure 4.12 shows the crack pattern up to a peak amplitude of 0.45g and, compared with the end of the experiment on the URM model, limited damage is established.

With increased seismic loads, namely 0.50g, the macro-elements manifested large displacements, particularly at the second level, even if they return to the original position at the end of the seismic input. The monolithic behaviour is completely absent and widespread damage occurred. Mortar and stone fragments fell from the upper part of the model.

Further damage appeared to have increased at the first floor level and a new horizontal crack appeared at the second floor level on prospect D, above that previously described for the seismic input at 0.55g.

The model was widely damaged and it was highly unstable. For this reason, and to avoid its collapse, the last performed step attained a maximum acceleration equal to 0.60g. Cracks at the second floor level increased and further damage occurred at the corners (compare also figures from A.7 to A.12).

4.2.3 SM model

The experiment on the SM model was divided into two parts as a consequence of the heavy damage occurred during the tests. As for the previous models, the input of the first phase, up to 0.55g, was characterized by two components.

Up to a seismic load equal to 0.25g no substantial damage could be seen on the model. Only limited and small cracks appeared homogeneously on the surface and a few mortar fragments fell from the model, probably due to their inadequate adhesion.

The following steps, namely 0.30g, 0.35g and 0.40g, showed the appearance of a

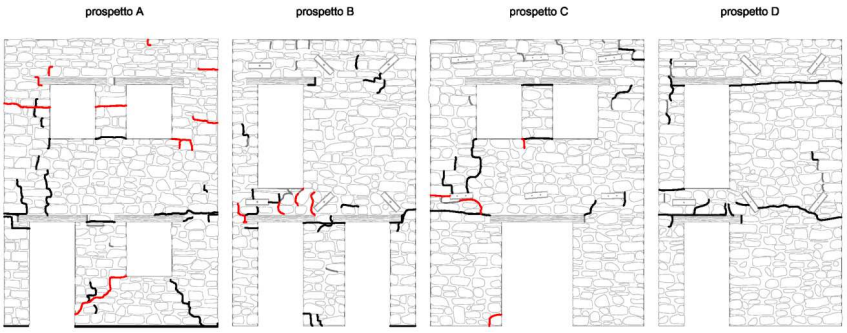

Figure 4.13: RM, crack pattern after step 0.60g, end of experiment.

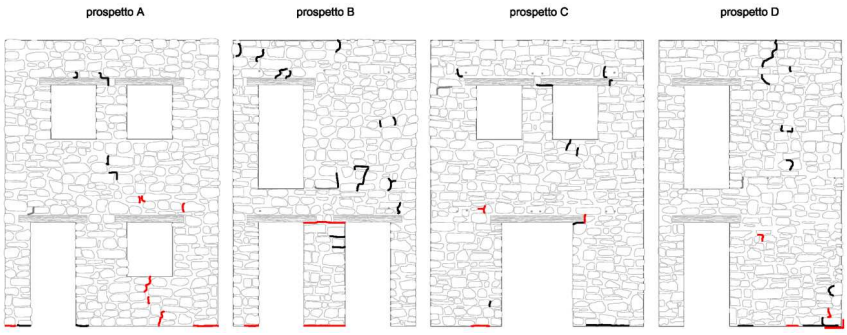

Figure 4.14: SM, crack pattern after step 0.45g.

few further cracks and the overall behaviour of the model was monolithic. However, starting from the step at 0.35g, the partial detachment of the bottom of the pier on prospect D occurred.

At the seismic excitation level at which the experiment on the URM model ended, at 0.45g, no separation of the external layers or out-of-plane failure could be seen. Nevertheless, the bottom of the pier on prospect D moved of few millimetres, due to the slight rise in the model during the tests, and some macro-elements start to appear (figure 4.14).

After the seismic test at 0.50g and 0.55g, the only extra damage was a displacement of 3cm at the bottom of the previously mentioned pier (figure A.13). Moreover, this mechanism induced a deeper crack at the first floor level. This required, over 0.55g, the insertion of steel profiles (UNP200) to stop this movement, since the overall stability was impaired. A similar device was employed for the pier at the first level on prospect B. Nevertheless, the overall behaviour of the SM model was good and only further limited cracks could be seen in the masonry.

The second part of the test started with a repetition of the seismic input at 0.55g in the X direction only, parallel to prospects A and C. In fact, the limited stability of a masonry pier requires the insertion of timber brace elements (figure 4.15 and figure A.14). This intervention widely limited the displacements, even if the overall behaviour was almost similar to that observed during the previous step. The blocked piers behave independently from the remaining part of the structure and further cracks started to appear. Also the subsequent seismic loads were applied only in the X direction.

Further seismic input denoted the beginning of additional cracks and the consequent formation of further macro-elements. These elements returned to their original

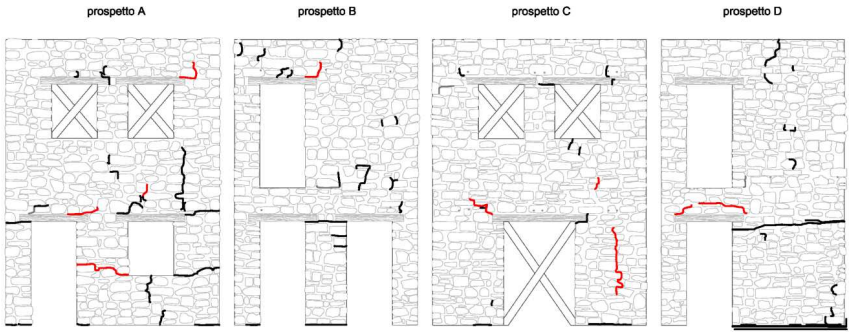

Figure 4.15: SM, crack pattern after step 0.55g in the X direction.

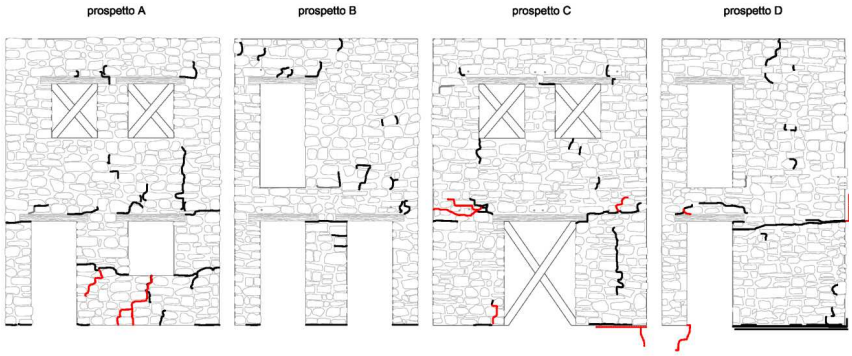

Figure 4.16: SM, crack pattern after step 0.70g in the X direction, end of experiment.

position at the end of each step, without denoting a residual displacement. The worst damage is concentrated at the first floor level.

Seismic input at a peak amplitude of 0.70g was repeated twice, since the shaking table could not input higher accelerations, due to the mass of the model. Most damaged sides, A and C, also denoted heavy damage at the second floor level at the end of the experiment. Any further new cracks opened while existing ones increased and it was necessary to stop the experiment to avoid the collapse of the whole structure (compare also figures from A.15 to A.17).

4.2.4 Observations

The overall behaviour of the building models observed during the tests is very clear. For instance, the biggest differences can be seen between the URM model and the injected structures. Actually, the Unreinforced Model exhibited only initial monolithic behaviour up to 0.25g, when heavy damage occurred to the structure. This caused the formation of a widespread crack pattern, involving the whole model, particularly on the second storey.
Moreover, both injected models exhibited a localized appearance of cracks, characterized by a longer length and opening. This damage was localized at floor levels and occurred at higher seismic loads. Thus, monolithic behaviour could be sustained up to higher solicitations.
Furthermore, the local separation of external layers could be seen in the URM model, while it could be avoided using lime grout. Finally, no out-of-plane damage was seen on the injected models, while it occurred on the Unreinforced one.

A comparison of the injected models indicates how the SM structure manifests

damage at higher loads than the RM one. Furthermore, the Repaired building Model exhibited the re-opening of cracks previously noticed on the URM one.

4.3 Amplification Factor of accelerations

In this section the results of the recorded accelerations will be presented. In short, the performed elaborations are intended to deepen the knowledge of the overall dynamic behaviour of unstrengthened and injected structures.

The first relevant analysis regards the Amplification Factors (AF) of recoded accelerations. This value was computed as the ratio between the acceleration at each floor level and the Peak Ground Acceleration and it is expressed in the equation 4.7. The values in question are the average of accelerations measured by sensors presented in figure 4.1.

$$AF = \frac{a_{floorlevel}}{PGA} \tag{4.7}$$

This factor provides an indication of the overall behaviour of building models. Actually, the ratio varies when damage increases, and it gives an indication of the monolithic behaviour of masonry.

4.3.1 URM model

The Amplification Factor can be considered constant during the first steps in the X direction, as table 4.4 and figure 4.17a show. This overall behaviour can be observed for both, the first and second levels. The result confirms how the structure can be considered monolithic. Moreover, the trend in the Y direction decreased even in the same range, characterized by very low seismic loads. The comparison of graphs in figure 4.17 indicates how the values in X are higher than those in the Y direction, probably due to the openings on prospects A and C, which caused their higher stiffness.
The values at 0.25g II do not show any clear difference from the previous steps, even if heavy damage occurred at this seismic level. It can only be noticed in the Y direction as the values are lowest at this step.
With higher seismic loads, up to 0.35g, the Amplification Factors increased in both directions and, over this step, they decrease until the end of experiment. In fact, the highest decrease in values takes place at the second floor level, where most heavy damage was noted during the tests.

4.3.2 RM model

The RM model, resulting from the repairing intervention of the URM structure, exhibits values lower than the initial ratios computed for the URM model. On the other hand, one should note how, in both directions, the values during the last step on the URM structure are lower than the initial ratios for the RM model. This can be considered the positive effect induced by the lime grout injection, which is able to recover and improve the Acceleration Factors of URM model in undamaged conditions.
In both directions, over the first step, a huge decrease can be noted. During subsequent

Table 4.4: URM, Amplification Factors in X and Y directions.

Test	X direction		Y direction	
	AF_{floor1} [-]	AF_{floor2} [-]	AF_{floor1} [-]	AF_{floor2} [-]
0.05g	1.179	1.667	1.380	1.510
0.10g	1.317	1.750	1.227	1.648
0.15g	1.284	1.858	1.213	1.443
0.20g	1.235	1.748	0.910	1.131
0.25g I	1.432	2.068	0.765	1.050
0.25g II	1.236	1.899	0.675	0.840
0.30g	1.576	2.053	0.656	1.081
0.35g	1.552	2.555	0.996	1.174
0.40g	1.472	2.286	0.787	1.244
0.45g	1.663	2.103	0.792	0.828

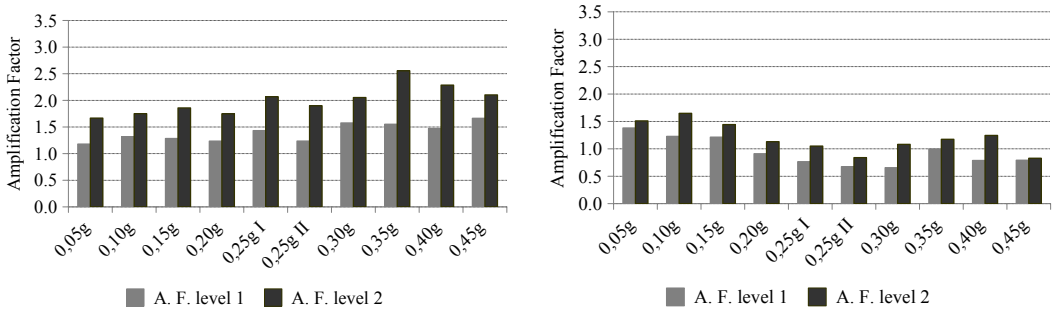

(a) X direction **(b)** Y direction

Figure 4.17: URM, trend of Amplification Factors in both directions.

seismic excitations and up to 0.30g, values show a slight increase in the X direction, while perpendicularly they are almost constant. Furthermore, the ratio between the values on the first and second floor are almost constant. This leads to an evaluation of the effectiveness of injection, which guarantees good and monolithic behaviour up to 0.30g.
Higher seismic loads caused different overall behaviours. While the Amplification Factor at the first level increases up to 0.50g, the one for the second floor becomes constant over 0.55g. These trends, considering the scattering due to experimental conditions, can be observed in both directions.

A similar behaviour can be seen in the orthogonal direction, even if differences are noted in the first steps and up to 0.30g. Over this seismic load, the Amplification Factor of accelerations increased, probably due to the insertion of steel profiles, which block the bottom of a masonry pier, as described in section 4.2.2.
In this direction, the second level indicated higher values, between 0.30g and 0.40g. Over this step, the Amplification Factor decreases, particularly at the second floor level.
During the last step, as in the case of the X direction, no further amplification can be seen, denoting the heavy damage occurred to the model, which does not exhibit monolithic behaviour.

Table 4.5: RM, Amplification Factors in X and Y directions.

Test	X direction		Y direction	
	AF_{floor1} [-]	AF_{floor2} [-]	AF_{floor1} [-]	AF_{floor2} [-]
0.05g	1.855	2.242	2.273	3.455
0.10g	1.075	1.610	1.243	1.888
0.15g	1.398	1.723	1.198	1.781
0.20g	1.512	1.884	1.213	1.899
0.25g	1.540	2.109	1.013	1.662
0.30g	1.863	2.694	0.979	1.246
0.35g	1.706	2.286	1.108	1.751
0.40g	2.002	2.394	1.483	2.626
0.45g	2.101	2.190	1.131	1.615
0.50g	2.331	2.412	1.219	1.473
0.55g	2.178	2.481	1.251	1.870
0.60g	1.994	2.142	1.181	1.363

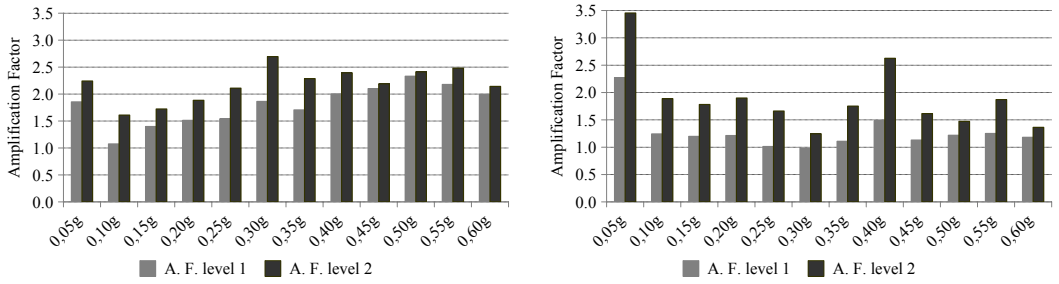

(a) X direction **(b)** Y direction

Figure 4.18: RM, trend of Amplification Factors in both directions.

4.3.3 SM model

The values of Amplification Factors computed for the SM model are presented in table 4.6 and their trend is presented in figure 4.19 for both directions.

Figure 4.19a shows that, up to 0.40g, Amplification Factors slightly increase with increasing seismic input. Furthermore, this range can be divided into two phases with the same trend, up to 0.20g and up to 0.40g. Also in this case the ratio between values computed at the first and second floor level are almost constant.
For higher seismic inputs, up to 0.55g, a wide increase in both values in the X direction can be noticed. The last part of the experiment shows how the acceleration ratio at the second floor level drastically decreased in both directions, denoting the development of heavy damage to this part of the model. Instead, values at the first level increased up to 0.65g, while over this seismic threshold they suddenly decreased.

The orthogonal direction, represented in figure 4.19b, shows a similar trend. The first part presents a limited variation, underlining the monolithic behaviour of the structure. Also in this case, values are lower and presented a limited variation if compared with those in the X direction.
The ratio of accelerations shows a slight reduction at 0.40g, while at higher seismic

loads the factor increased. In the last steps a notable decrease takes place confirming the development of damage, which caused the loss of monolithic behaviour.

The overall trend, presented in figure 4.19, well represents the visible damage noted during the execution of the experiment. The strengthened model showed monolithic behaviour up to accelerations higher than those suffered by both the URM and the RM models. Furthermore, the damage occurred in concurrence with the above described decrease in the Amplification Factors.

Table 4.6: SM, Amplification Factors in X and Y directions.

Test	X direction		Y direction	
	AF_{floor1} [-]	AF_{floor2} [-]	AF_{floor1} [-]	AF_{floor2} [-]
0.05g	1.210	1.629	1.174	1.698
0.10g	1.167	1.417	1.208	1.460
0.15g	1.301	1.712	1.141	1.621
0.20g	1.367	1.958	1.292	1.718
0.25g	1.154	1.412	1.372	1.535
0.30g	1.168	1.747	1.026	1.478
0.35g	1.103	1.831	0.870	1.241
0.40g	1.272	1.969	0.748	1.042
0.45g	1.386	2.527	1.067	1.491
0.50g	2.030	2.526	1.501	1.940
0.55g	1.493	3.416	1.267	1.798
0.55g X	1.703	3.232	2.535	2.822
0.60g X	1.972	3.062	1.794	2.286
0.65g X	2.158	2.991	1.050	1.650
0.70g X I	1.195	1.985	1.289	1.334
0.70g X II	0.895	1.426	1.073	1.328

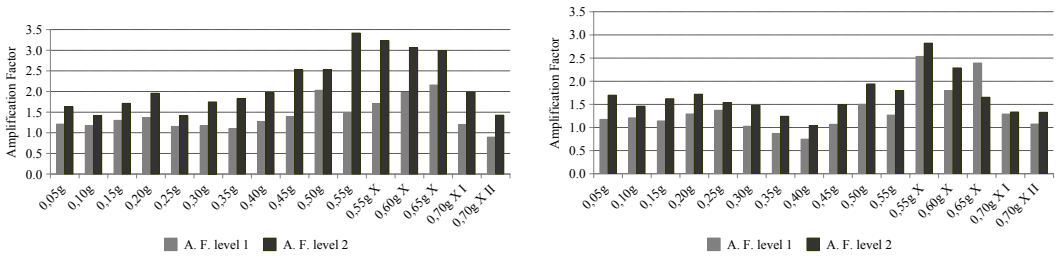

(a) X direction **(b)** Y direction

Figure 4.19: SM, trend of Amplification Factors in both directions.

4.3.4 Observations

Figures 4.20 and 4.21 lead to a comparison of Amplification Factors manifested by all models in both orthogonal directions.

The URM model behaves similarly to injected structures during the first steps, up to 0.20g and 0.15g in the X and Y directions respectively. Over these seismic ac-

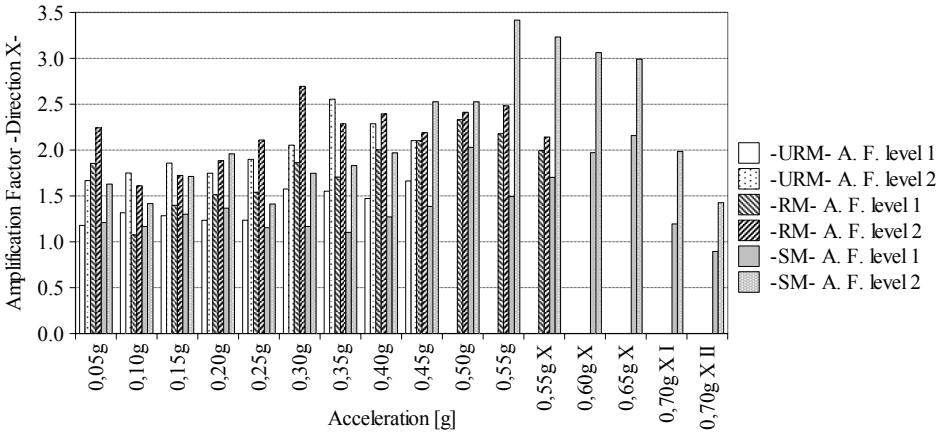

Figure 4.20: Comparison of Amplification Factors of Models, X direction.

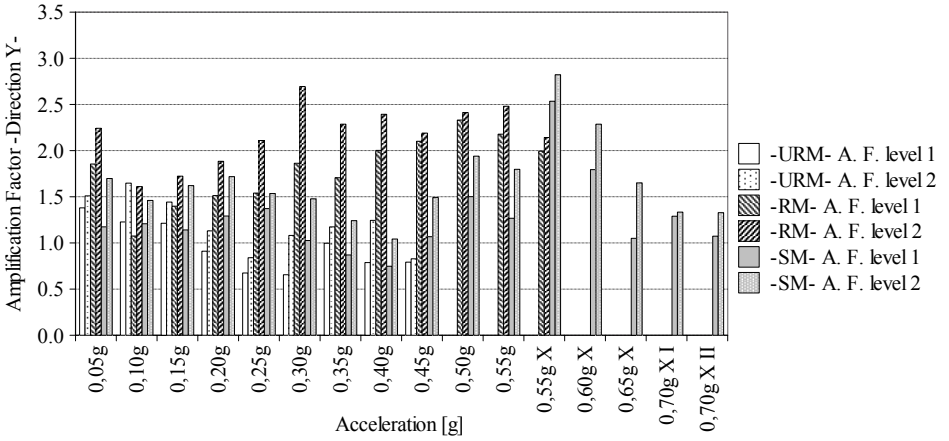

Figure 4.21: Comparison of Amplification Factors of Models, Y direction.

celerations, the Unreinforced Model manifests an overall decrease, while both injected structures could sustain an invariance up to a mean value of 0.35g. Consequently, structural intervention allows monolithic behaviour to be maintained also at higher seismic loads. The grout injected models behave similarly in both directions, with few differences in the load that causes the reduction in amplifications. Furthermore, one should note how the injection is able to recover and improve, on the RM model, the initial condition exhibited by the URM structure. Besides, this recovery can be sustained up to high lateral loads, allowing a monolithic behaviour on the Repaired specimen when the URM model was already seriously damaged.

A further comparison, of results obtained for injected models, highlights how the strengthening intervention allows a correct ratio between the Amplification Factors of the first and second floor to be maintained up to 0.50g, while repairing allows this behaviour up to 0.40g in both directions. Moreover, both injected models exhibit four subsequent phases: an initial increase, followed by a reduction in the Amplification Factors and by a second growth, while during the last part a final decrease can be seen. These phases are contracted in the RM model, demonstrating how the SM structure has the best characteristics in terms of Amplification Factors.

4.4 Dynamic Response of the Models

Analyses based on the acquired accelerations are developed separately in the case of each building model and will be presented in this section. The performed elaborations aim at deepening the knowledge of the overall dynamic behaviour of unstrengthened and injected structures. The parameters involved in these analyses are:

- Frequencies;
- Mode shapes;
- Damping factors.

All dynamic analyses were mainly performed in the Frequency Domain, employing ARTeMIS Extractor [SVS] commercial software and the results will be discussed in the following.

4.4.1 Analysis of Frequencies

The frequencies of the building models, on the basis of the Nyquist-Shannon sampling theorem, were analysed up to 50Hz. Nevertheless, only the first three characteristic modes were considered, namely the first bending modes in both orthogonal directions and the first torsional mode, due to the wide difficulty in identifying higher modes. For the frequency analysis, two different methodologies, based on the same theoretical approach, were exploited with ARTeMIS Extractor [SVS]: Frequency Domain Decomposition (FDD) and Enhanced Frequency Domain Decomposition (EFDD).

In order to provide greater reliability for the obtained results, a further computational method was employed. This analysis was performed in collaboration with Professor Aoki T. [Mazzon *et al.*, 2009], from the Nagoya City University (Nagoya, Japan). This second dynamic identification was carried out on the time domain, using a software developed by Prof. V. Denoel, University of Liege [Denoel *et al.*, 2007], based on Stochastic Subspace Identification (SSI) method.

For all the building models, the trend of frequencies and their reduction during the test were studied. Two different decreases were accounted: secant decrease, as difference between values at two successive steps of the test, and tangent decrease, as difference between the actual and the initial frequencies.

4.4.1.1 URM model

An observation of the obtained values underlines how the frequencies of the unreinforced model are characterized by a monotonic decreasing trend (table 4.7). Furthermore, all trends behave similarly, showing amplified effects at higher frequencies (figure 4.22a). Finally, the accordance of all performed elaborations (figure 4.22a), namely FDD, EFDD and SSI, provides a highly reliable results.

The overall decrease of the first identified frequency, namely the first bending mode in the Y direction, amounts to about 1.20Hz (figure 4.22b). The most relevant decrease can be seen at 0.20g and 0.25gII. Furthermore, the trend shows two different behaviours for seismic solicitations up to and over 0.25gII. For lower intensities of seismic input, a considerable decrease can be noted, while, over this step, the frequency reduction appears limited. This overall behaviour can be linked to the development of the crack pattern. In fact, during the first steps, the masonry gradually became

damaged. This also reflects on the change in the overall behaviour of the URM model during the whole experiment. Beyond 0.25gII, a widespread crack pattern was almost completely developed. Instead, higher seismic inputs induced larger displacements and worsened the already existing damage but only few further cracks took place.

The second fundamental frequency is related to bending in the X direction. The overall decrease, higher than that of the first frequency, attains 2.00Hz. As in the previous case, an initial appreciable reduction can be seen up to the sudden drop that occurred at 0.25gII while, over this step, frequency values manifested a limited variation and they stabilize at about 6.00Hz (figure 4.22c).

The third frequency is due to the torsional mode and exhibits the highest overall decrease, slightly less than 4Hz, as reported in table 4.7. The trend is very similar to the one manifested by lower modes with an emphasis on the previously described behaviours. These aspects confirm the above mentioned observations.

4.4.1.2 RM model

The sequence of identified frequencies is completely similar to the one computed for the URM model. From the lowest to the highest frequency: the first bending mode in the Y direction, the first bending mode in the X direction and the torsional mode. The corresponding values for all frequencies are reported in table 4.8, while figure 4.23a provides a graphical view. Also in this case, the three identified frequencies behave similarly and all methods of analysis provide very similar results, validating the elaborations made.

Computed values, corresponding to the first frequency, exhibit a total reduction of about 0.80Hz. The overall trend is decreasing, even if local increments can be seen. Particularly, during the first steps, the frequency decreases, up to 0.20g. Otherwise, values can be considered nearly constant between 0.30g and 0.35g (figure 4.23b). This behaviour can probably be imputed to the settlement of materials and particularly to the influence of injection. This is also reflected at higher seismic loads: a sudden drop, as at 0.40g and 0.55g, followed by a phase with constant frequencies. In this case, each drop corresponds to an increase in damage and, particularly, to the further formation of macro-elements. Furthermore, the localised decrease, occurred during the first steps, has a lower slope than that observed in the last part of the experiment.

The second considered frequency is characterized by an overall decrease of about 1.40Hz (table 4.8), being double than that of the previous one. The overall trend (figure 4.23c) confirms the above described observations, even if the most notable decrease is concentrated at seismic loads different from those previously mentioned. The 0.15g, 0.30g and 0.55g are the steps which induce the heaviest damage. Finally, in both intervals, between the beginning and the first drop but also between the first and second drop, frequencies exhibit a local increase, while over 0.30g there is a substantial decrease up to the end.

The highest identified frequency corresponds to the torsional mode and it has an overall reduction of 3.60Hz, widely larger than that of the lower modes. The third frequency (figure 4.23d) emphasizes the trend exhibited by the lower modes. Moreover, in this case, no localised increase could be seen and the frequency reduction was more constant along the overall execution of the experiment, without any sudden and evident drop.

Table 4.7: URM, Frequency values after each dynamic test.

Step	1^{st} Frequency [Hz]	2^{nd} Frequency [Hz]	3^{rd} Frequency [Hz]
0.00g	6.45	7.87	13.10
0.05g	6.34	7.78	12.72
0.10g	6.30	7.69	12.68
0.15g	6.23	7.59	12.48
0.20g	5.88	7.23	11.74
0.25g I	5.93	7.25	11.47
0.25g II	5.35	6.25	9.45
0.30g	5.27	6.20	9.18
0.35g	5.15	6.13	9.18
0.40g	5.20	6.01	8.84
0.45g	5.13	5.88	8.89

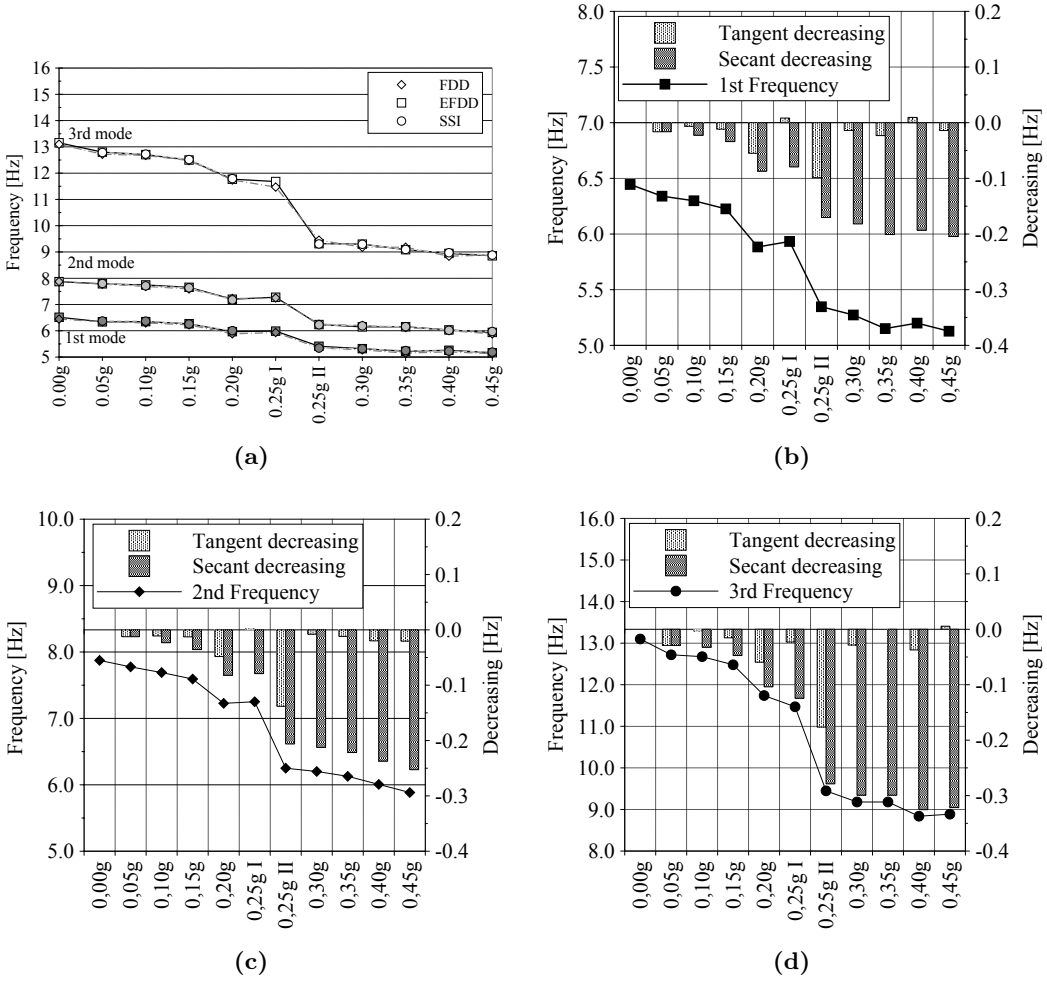

Figure 4.22: URM, Trend and decreasing of frequencies.

Table 4.8: RM, Frequency values after each dynamic test.

Step	1^{st} Frequency [Hz]	2^{nd} Frequency [Hz]	3^{rd} Frequency [Hz]
0.00g	6.37	8.23	14.16
0.05g	6.20	8.35	13.87
0.10g	6.23	8.42	13.70
0.15g	6.05	7.98	13.55
0.20g	5.98	8.15	13.35
0.25g	6.08	8.28	13.33
0.30g	6.03	7.71	12.57
0.35g	6.08	7.45	12.38
0.40g	5.79	7.59	11.74
0.45g	5.79	7.45	11.55
0.50g	5.84	7.40	11.40
0.55g	5.52	6.88	10.67
0.60g	5.52	6.81	10.26

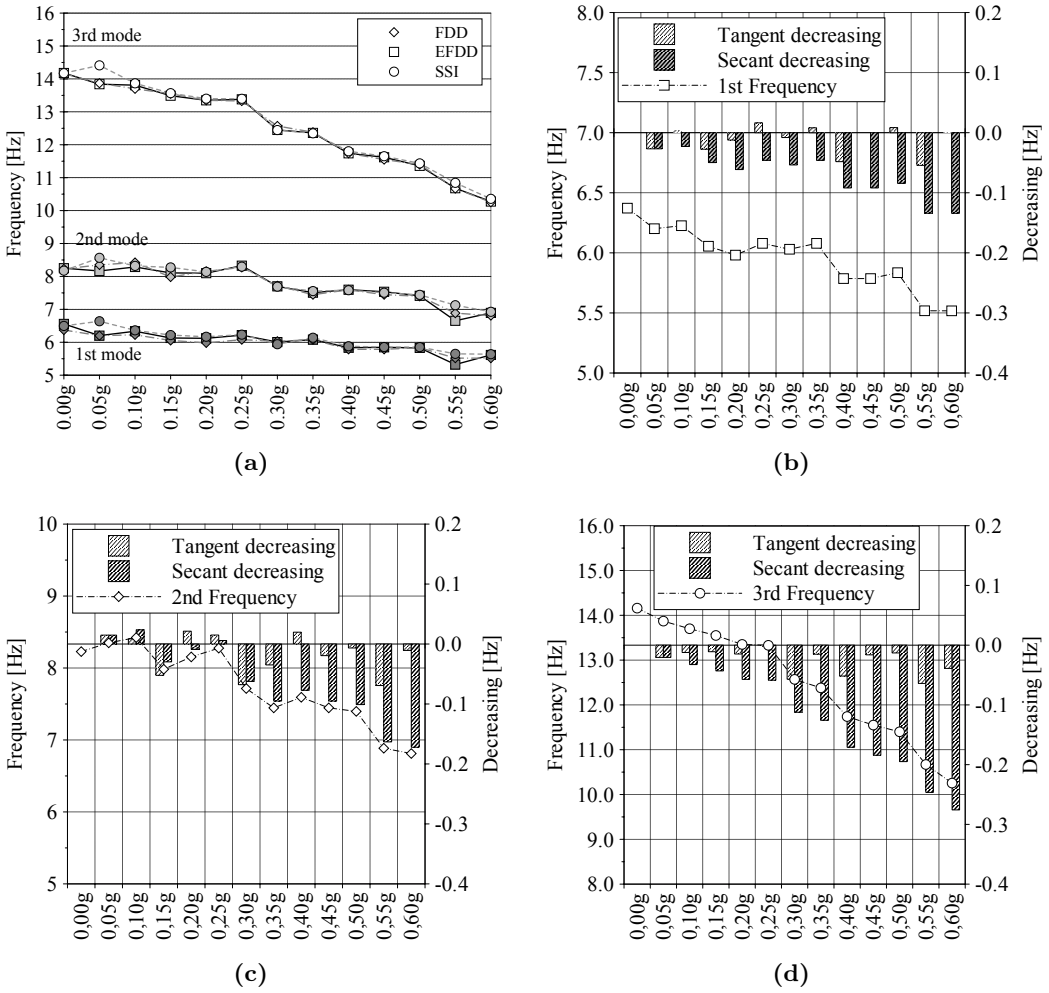

Figure 4.23: RM, Trend and decreasing of frequencies.

4.4.1.3 SM model

The dynamic identification performed on the last masonry model shows that the overall trend of frequencies behaves slightly differently from the URM and RM models.

The maximum decrease in the first frequency is about 1.20Hz, even if the behaviour is ascending and descending. In fact, over a slight increase at 0.05g, a wide frequency reduction took place up to 0.20g. Over this value, as in the case of the RM model, a localised increase in values can be seen up to 0.30g, while over this seismic load a second deep reduction can be seen, followed by the last notable positive variation, up to 0.55g. Starting from this step, wooden bracing elements were placed (figure 4.15) to avoid the occurred problems of stability (compare §4.2.3). This intervention increased the overall stiffness of the model, comparing values between 0.55g and 0.55g X, and this is clearly evident in figure 4.24b, even if these elements were placed in the orthogonal direction to that actually investigated. As in the case of the Repaired building Model, some drops followed by subsequent increases characterize the overall behaviour. At the beginning, this can be imputed to the settlement of materials, since previously the structure was never subjected to dynamic solicitations. For higher seismic loads this may be due to the formation of macro-elements, as confirmed by direct observation during the experiment. Over 0.55g X, the decrease is very quick and notable.

The second identified frequency, related to the bending mode shape in the X direction, shows an overall decrease of 2.30Hz. The trend behaves similarly to that of the first frequency, showing an overall decease with few localised increases. Despite the lower identified mode, these local trends are very limited in the first part of the experiment, up to 0.55g. The second part shows an overall decrease higher than the one occurring during the first phase and this developed in a lower number of steps, denoting how the models are completely damaged.

The third identified frequency manifested the highest decrease of about 4.60Hz. The overall behaviour is similar to that of the first frequency, even if the trend appears amplified. Actually, as figure 4.24d shows, the most considerable localised increase persists during four steps, from 0.25g up to 0.40g, followed by a noticeable decrease. The insertion of stiffening elements caused a limited and temporary growing in frequency, which is quickly lost. Unlike from lower modes, the overall decrease during the second phase has the same slope as that manifested during the first part of the experiment.

The highly compatible results (figure 4.24a), obtained from all methods of analysis, guarantees the reliability of the identified overall behaviours. For instance, the consistent localised increases are confirmed by both time and frequency domain analyses.

4.4.1.4 Observations

The comparison of frequencies of all models should be developed considering that the URM and RM structures are the same physical model, thus values can be directly related, while SM is a different specimen. Therefore, in this second case, only the trend and overall behaviour can be compared with those of the URM model.

The first significant difference between the unstrengthened and injected models is the sudden decrease in all frequencies of URM at 0.25g, while both injected models show a gradual decrease during the whole experiment (figure 4.25). On the contrary, the SM model manifests a wide localised increase, while the URM model has a

Table 4.9: SM, Frequency values after each dynamic test.

Step	1^{st} Frequency [Hz]	2^{nd} Frequency [Hz]	3^{rd} Frequency [Hz]
0.00g	7.15	8.74	15.60
0.05g	7.28	8.57	15.38
0.10g	6.93	8.40	14.65
0.15g	6.74	8.54	14.16
0.20g	6.45	8.25	14.06
0.25g	6.69	8.57	14.45
0.30g	6.81	8.32	14.89
0.35g	6.47	8.37	14.60
0.40g	6.42	8.30	14.23
0.45g	6.03	7.89	12.74
0.50g	6.84	8.86	13.28
0.55g	6.37	7.45	12.13
0.55g X	7.25	8.25	13.01
0.60g X	6.64	7.64	12.04
0.65g X	6.47	7.37	11.55
0.70g X I	6.29	7.06	11.19
0.70g II	6.84	6.40	10.99

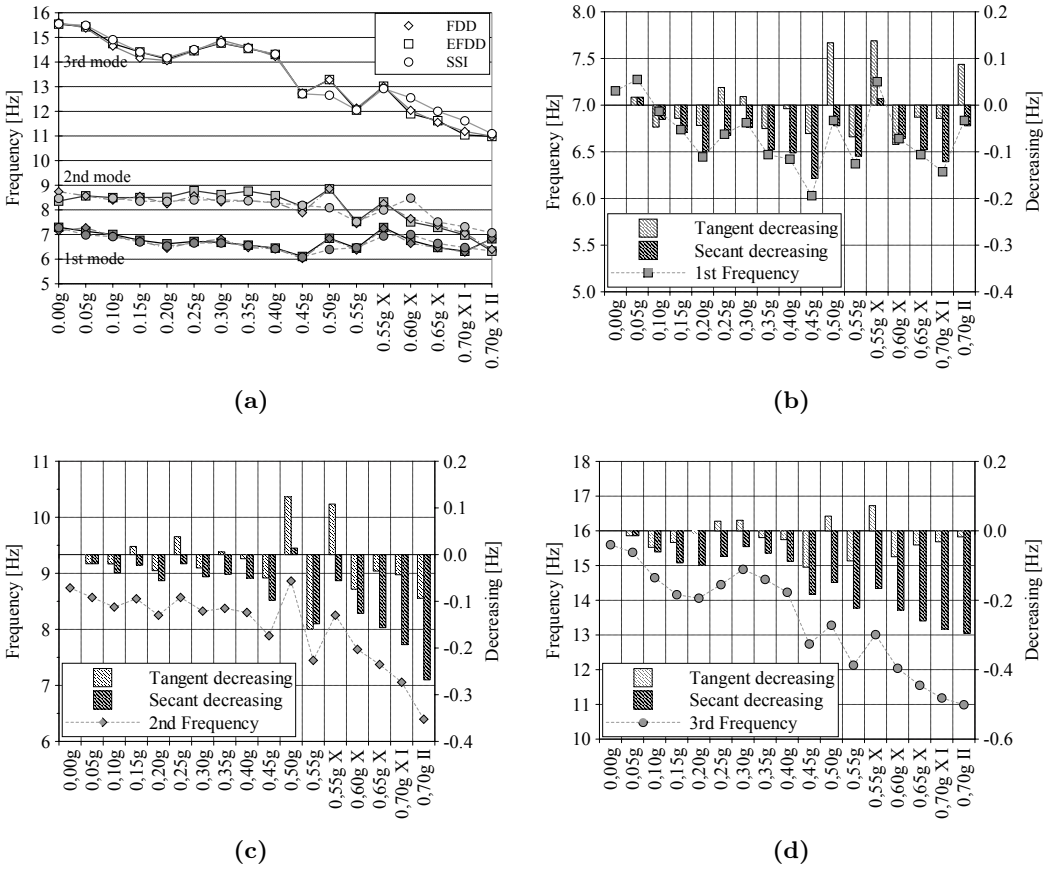

Figure 4.24: SM, Trend and decreasing of frequencies.

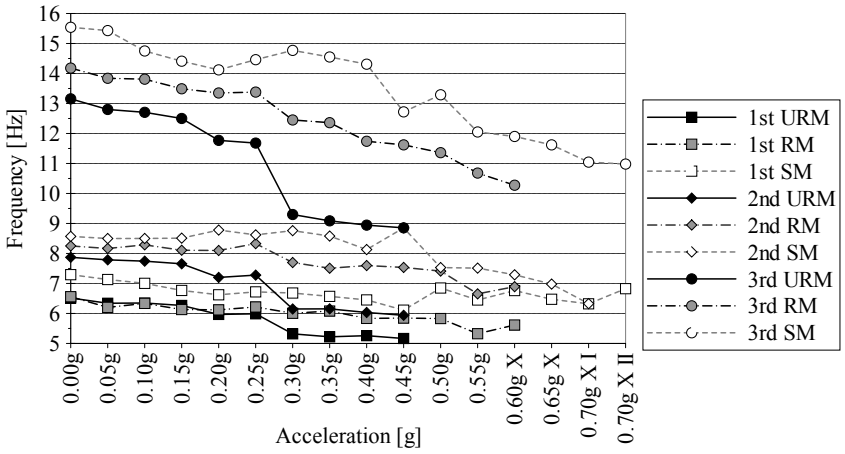

Figure 4.25: Comparison of the first three frequencies of all building models.

monotonic decrease. The RM building behaves similarly to the SM one, even if the localised increase is lower.

A significant effect of lime grout injection is that it allows the recovery of the original starting frequencies of the URM model in the Repaired structure. Therefore, injection causes an increase in frequencies, since the final values of the URM model return to the initial values thanks to the use of lime grout. Moreover, in the case of higher frequencies, they can also be slightly increased.
These considerations, related to those developed during the analysis of crack patterns and Amplification Factors, further underline again how the URM model suddenly exhibits the occurrence of damage and, after this, only few further mechanisms could be developed. Instead, injected models manifest several damaged parts of the structure, occurred at different load levels.

A comparison of decreasing frequencies at the same seismic level (figure 4.26a) was performed at 0.45g, corresponding to the last step of the URM model. This analysis clarifies how structural intervention, using lime grout, helps to limit the degradation of the dynamic characteristic in question. Furthermore, one should note how also between the RM and SM models a difference can be highlighted. Actually, strengthening intervention proved to be the best type of intervention, since it is able to provide the lowest frequency decrease. On the other hand, repairing also shows a good overall behaviour, similar to that of the SM model but slightly worse.
Lastly, figure 4.26b confirms the above presented observations and increases the significance of these. Actually, comparing the frequency decrease at the end of the experiments, the SM model manifested the lowest values, even if it sustained higher loads and more seismic steps than the other structures. The Repaired Model exhibits an intermediate situation, more similar to that of the strengthened building.

4.4.2 Analysis of Mode Shapes

A second analysis, providing important information about the dynamic behaviour of unreinforced and injected models, involved a study of the typical mode shapes of structures. The results were achieved through analyses in the frequency domain, using ARTeMIS Extractor [SVS] commercial software. Furthermore, the results presented in the following were elaborated considering the normalized deformation related to each identified frequency. Reflecting the identified frequencies, the first identified

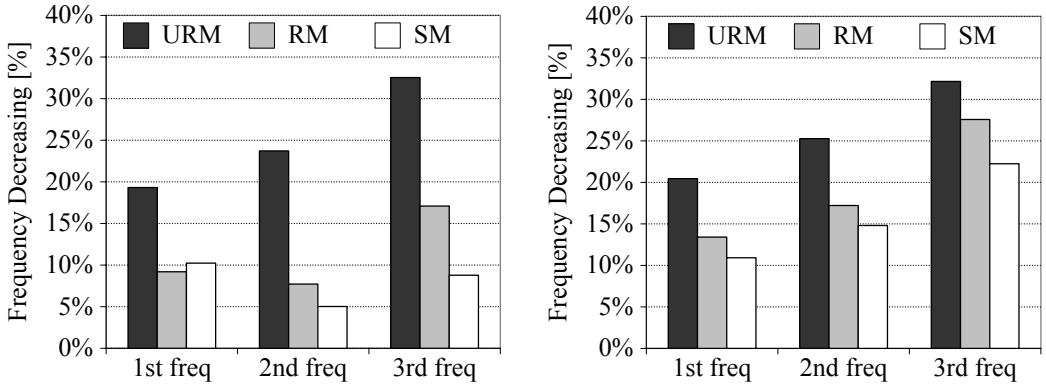

(a) Comparison at 0.45g **(b)** Comparison at the end of the experiment

Figure 4.26: Comparison of decreasing of frequencies.

mode is related to the first bending mode in the Y direction, while the second mode to the first bending mode in the X direction.

4.4.2.1 URM Model

Figure 4.27 shows the first bending modes in the two orthogonal directions. Both analyses manifest an initial condition of approximately a ratio of 0.6. The range of variation for both modal deformations is very limited up to 0.25g I, when the appearance of the first heavy damage manifested. The following step caused a sudden drop, that reflects an increase in normalized deformations at the first floor level in the Y direction (figure 4.27a) while the second mode showed a decrease at the same level (figure 4.27b).
This behaviour highlights how the first mode shape the absolute displacement of the first floor increases more than that of the second floor, while the second mode shape manifests a diametrically opposite situation. This leads to the conclusion that in the first case the damage in the Y direction is specifically concentrated especially at the first floor level, while the increase in displacements at the second floor level indicates an increase of the crack pattern at this storey. These deductions are confirmed by the observations carried out during the survey of crack patterns (compare §4.2.1).

Over the sudden drop occurred at 0.25g I, the following steps showed a limited variation in modal shapes. This confirms how subsequent seismic loads did not induce further substantial damage but only increased the existing ones, which made the model unstable.

4.4.2.2 RM Model

Both mode shapes computed for the Repaired Masonry model (figure 4.28) behave similarly and are characterized by similar starting values, namely 0.6.

The first normalized modal deformation manifested a limited variation during the whole experiment (figure 4.28a). However, the higher the seismic load, the higher the reduction in mode shape at the first floor level. This remark, combined with the observation of absolute modal displacement, also revealed a relative increase in the modal deformation on the second storey, where the most important damage was detected.

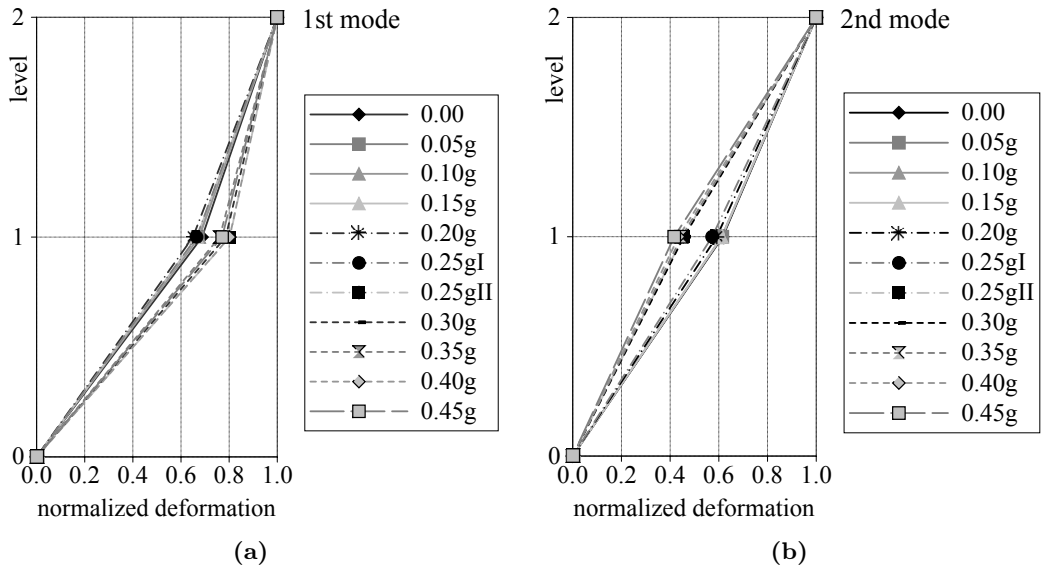

Figure 4.27: URM, first (left) and second (right) mode shape.

As mentioned above, the second mode shape behaves similarly to the first one and manifests a larger overall decrease in normalized deformation at the first floor level. This induces to observe as, also in this case, damage occurred on different storeys, depending on the analysed direction.

The RM model showed a gradual variation oin mode shapes, without any notable and sudden drop in its overall dynamic behaviour, regarding modal deformations. In conclusion, the Repaired Model manifests a monolithic behaviour up to high loads while only at 0.50g a slight variation in the computed quantities becomes evident.

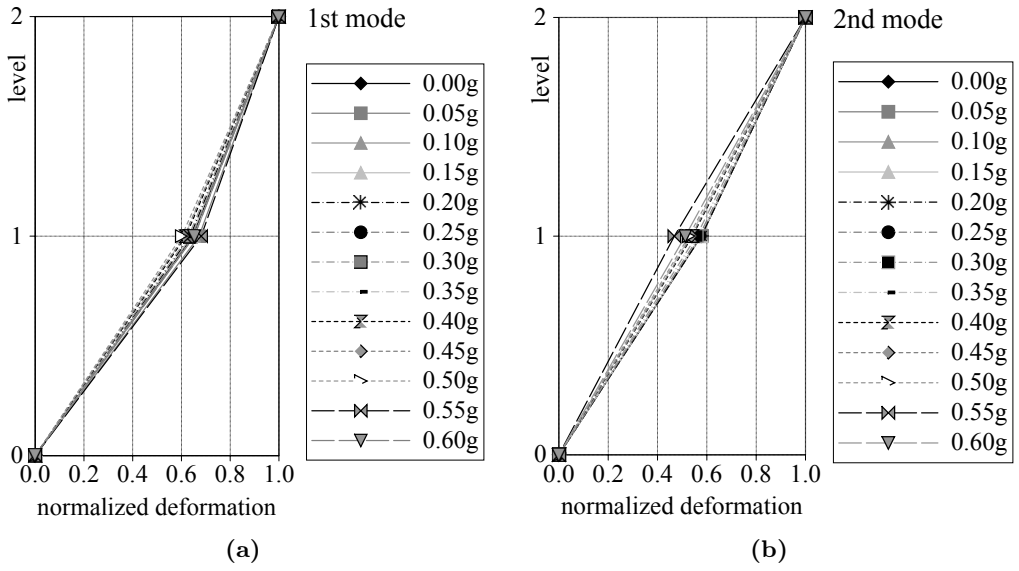

Figure 4.28: RM, first (left) and second (right) mode shape.

4.4.2.3 SM Model

Mode shapes related to the Strengthened Model are presented in figure 4.29: both normalized deformations manifest a wide variation, if the whole experiment is considered.

The identified bending mode shapes in orthogonal directions behave similarly. The overall normalized deformations present a limited variation up to 0.45g. This confirms how the Strengthened Model is able to preserve unaltered its dynamic characteristics up to this seismic load. Over this solicitation level, normalized deformations increased at the first floor level, particularly for the first identified mode. Furthermore, figure 4.29a clearly underlines other phases during the experiment, beyond the first one up to 0.45g.

The second part of the test is characterized by the insertion of stiffening elements and this reflects on a change of the normalized mode shape at the first floor level, consequence of an increase of the modal deformation at the second floor level. The last phase shows a wide amplification of this same behaviour, with a reduction leading to a ratio of 0.4, underlining as the structure is completely damaged and the second level risks collapse.

As figure 4.29 shows, the insertion of the brace elements in the X direction reflects both mode shape trends. Furthermore, the modes related to the orthogonal directions behave differently. In fact, on the first identified mode the modal deformation at the first floor level decreases, while on the second one this quantity increases.

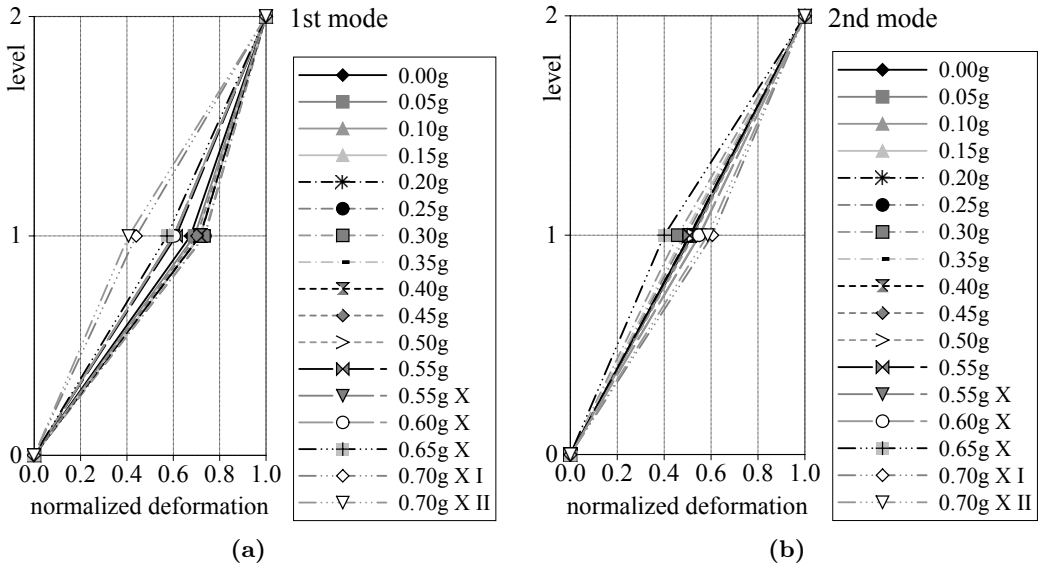

Figure 4.29: SM, first (left) and second (right) mode shape.

4.4.2.4 Observations

The analysis of the mode shapes of all models confirms the observations performed for the previously presented elaborations.
Both the identified mode shapes of the URM model show a sudden change, when heavy damage arose (figures 4.27a and 4.27b). Differently, both injected structures exhibit a gradual variation in normalized modal deformations, once again emphasizing

as the use of lime grout is able to induce a gradual damage to masonry.
However, repairing intervention on the RM model can only partially recover the initial deformations of the URM structure, unlike frequencies. Nonetheless, the RM model could sustain higher seismic loads than the URM one, limiting the overall degradation of both identified mode shapes.
The best overall behaviour is exhibited by the Strengthened Model, since a larger and gradual variation in modal deformations is allowed (figures 4.29a and 4.29b).

4.4.3 Analysis of Damping Factors

The acquired accelerations also allowed an examination of the dissipation capacity of the tested models. Processing data with the ARTeMIS Extractor [SVS] program, the damping factors could be computed on the Frequency Domain, based on Enhanced Frequency Domain Decomposition. Furthermore, to provide greater reliability for the obtained results, data were also processed in the Time Domain [Mazzon *et al.*, 2009]. Professor Aoki T., from Nagoya University (Japan), collaborated on this analysis, using software developed by Prof. V. Denoel, University of Liege [Denoel *et al.*, 2007], based on Stochastic Subspace Identification method (SSI). Damping factors, computed employing both methods of extraction, are presented and compared in the following sections. Finally, one should note as a restricted number of damping values could not be computed, due to difficulty in processing noisy data in the time domain.

4.4.3.1 URM Model

All damping factors computed for the URM model, starting from the three identified modes presented in previous sections, are characterized by a limited variation and low values. These damping factors range between 1.5% and 4%, as figure 4.30 shows. Furthermore, higher values are provided by the first and second identified modes, contrarily to the values of computed frequencies.
During the first phase of the experiment, the overall trend increases, even if this growth is limited and a localised decrease can be seen. This behaviour continues up to 0.20g and it is more clearly manifested by the second identified frequency, namely the first bending mode in the X direction. Subsequently, a drop in damping factors can be highlighted at the seismic acceleration of 0.25g I and, also in this case, this is more evident for the second mode.
Over this load level, all damping factors can be considered as a constant equal to about 2.5%-3.0% for both the first and second mode. The third mode settles at 2.0%, even if one should note how this mode manifested a very limited variation during the whole experiment.
Damping values increase until the model is undamaged, namely 0.25g I. Instead, over this load level, when damage could also be seen during the experiment, they decrease and become constant with low values (figure 4.30).

Lastly, one should note how both employed methods provide similar results and the overall trends are very similar. The corresponding between values obtained from Frequency and Time Domain analyses guarantees the reliability of the analyses and validates the previous observations.

4.4.3.2 RM Model

Damping factors computed for the Repaired Masonry model are characterized by a wide range of variation. Actually, values vary between 2% and 10%. Three different

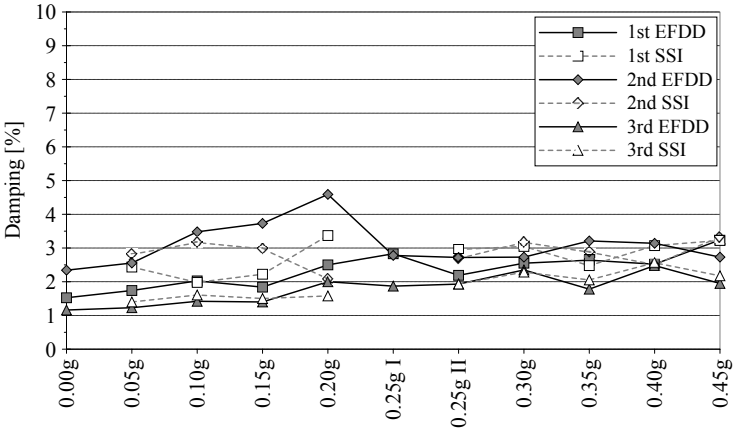

Figure 4.30: URM, Damping Factors.

phases can be identified and these are more clearly evident in the second mode in question. The first part involves the lowest seismic loads, up to 0.10g, and its special feature is a considerable increase in values. During the second phase, an overall decrease can be seen, followed by the last constant trend, when values manifest a very limited variation (figure 4.31).

In the first identified phase, the damping factor related to the second mode attains values slightly lower than 10%, while others range between 2% and 4%. At higher seismic loads, the second mode shows a high decrease, while the first and third ones manifest a very limited variation. The last part underlines a slight decrease, more evident for the second mode, with values settled between 2% and 3%.
At load levels causing sudden changes in damping factors, no evident damage could be seen, confirming that some dynamic characteristics start to deteriorate before the occurrence of observable damage.

Time Domain analysis provides values of damping factors similar to those presented above and computed in the Frequency Domain. Only the second mode highlights damping slightly different factors, even if in all cases the trend of both elaborations is very close, particularly for the second part of the experiment.

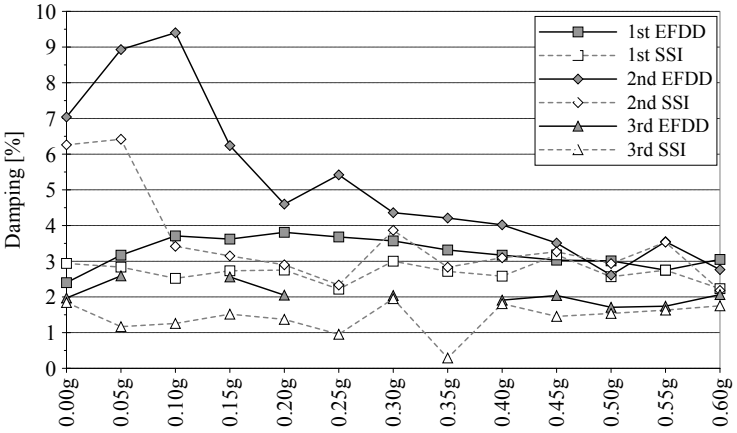

Figure 4.31: RM, Damping Factors.

4.4.3.3 SM Model

Damping factors manifest, also in this case, a wide variation during the experiment and they range between 2% and 9%. The second mode exhibits a marked increase with reference to damping factors related to the remaining modes.
As in the case of the Repaired Masonry model, three different phases can be distinguished: an initial increase, followed by a decrease and a final part characterized by constant damping factors of about 2% and 4% (figure 4.32).

Second and third modes manifest an increase in values up to 0.25g, at a load level at which frequencies start to show a localised increment. In this first phase, the second and third modes show a lower variation, if compared with that of the torsional mode. Over this part, when the settlement of materials caused a frequency increase, damping factors are almost constant: 8% for the second mode and 2% for the third one, while the first mode shows a slight but constant decrease.
A reduction in frequency values reflects damping factors which, in turn, are reduced. The most evident variation is that of the second mode, which presents a sudden drop to 0.50g, when also heavy damage was noted during the experiment.
The following values are ascending and descending but they vary around constant values of 2% and 3%. This phase corresponds to the formation of macro-elements on the models. The relative rigid rotation of the structural elements, instead of the formation of different mechanisms, caused these low damping factors and prevented a higher dissipation capacity. This observation is supported by the low damping factors over 0.55g X, when the structure was stiffened but macro-elements manifested. Therefore, the insertion of brace elements did not allow an increase in dissipation, confirming how this characteristic depends on the established mechanism of failure.

The analysis developed on the Time Domain validates the one carried out on the Frequency Domain. Figure 4.32 clearly shows that the trends are very similar even if, in a few cases, values present a slight difference.

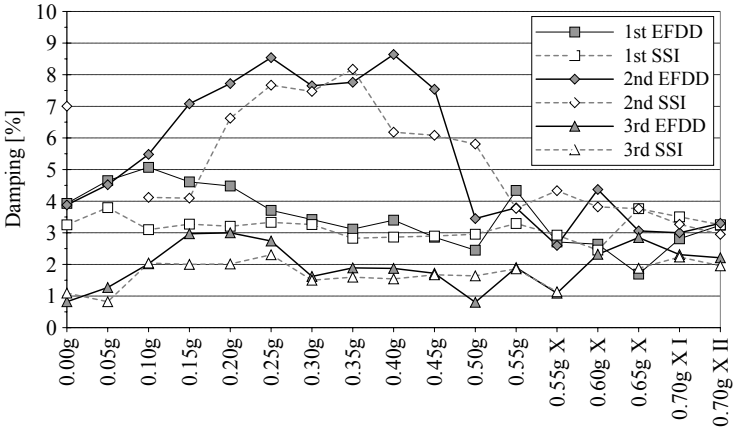

Figure 4.32: SM, Damping Factors.

4.4.3.4 Observations

The analysis of damping factors computed on the Frequency Domain is summarized in figure 4.33 and, as one can see, the obtained results reflect the previous analyses.
The main difference can be noted between the unstrengthened and the injected models.

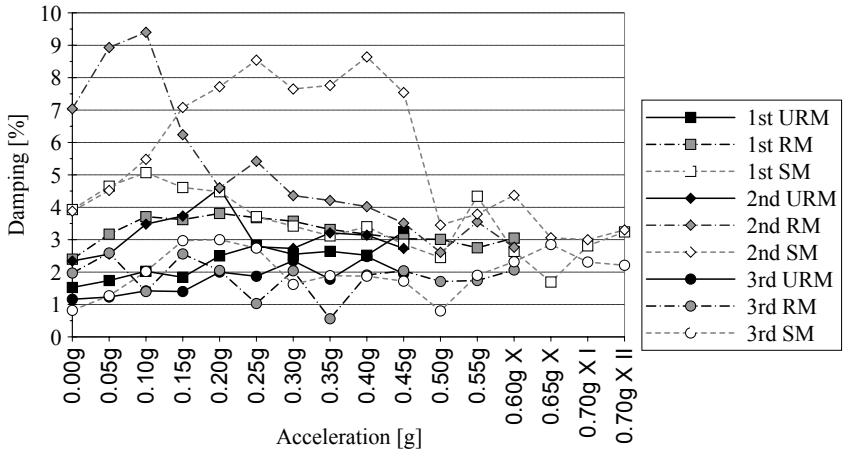

Figure 4.33: Comparison of the damping values of all building models.

Actually, the URM structure manifests very low values, ranging between 2% and 3%, and they remain almost constant during the whole experiment, with the only exception in the initial steps, where a slight increase takes place. Therefore, the original model is not able to develop considerable damping factors. Lastly, when a widespread damage arises in the structure, the dissipation capacity of the masonry is limited.
Instead, both injected models exhibited higher damping factors for all modes. Generally, they show an initial increase, followed by a phase with constant values. At higher seismic loads, damping ratios settle at about 3%. In both cases, highest ratios achieve more than 8%. Therefore, structural intervention using lime grout allows a greater dissipation capacity. However, one should note how injecting the URM model, leading to the RM one, enables high values of damping factors to eb obtained.
Finally, a considerable difference should be highlighted between the overall behaviours of the Strengthened and Repaired models, even if the peak values are almost similar. For instance, the RM structure develops the same modifications of damping values as the SM model but at lower seismic loads. Thus, the decrease, due to the initial damage, occurred between 0.10g and 0.25g on the RM model, instead of the interval between 0.15g and 0.40g for the SM model.
During the last part of each experiment, all structures manifest similar damping factors. This underlines how, when widespread heavy damage develops in models, the influence of lime grout injection is negligible. In any case, both injected models show a higher dissipation capacity, being able to sustain high damping factor at high seismic loads.

4.5 Analysis of Stiffness

The contemporary acquisition of both accelerations and displacements on relevant points of the structures allowed to perform the analysis of stiffness degradation at increased intensity of seismic inputs. While the analyses presented in section 4.4 employed accelerations acquired during both white-noise inputs at low intensity and ambient vibrations, the calculation of stiffness makes use of data obtained during the impressed seismic inputs. These acceleration records were related to the displacements and the consequent analysis provides further information about the dynamic behaviour

of the unstrengthened and injected structures.

4.5.1 Preliminary Oversimplifications and Data Processing

An in-depth processing was performed on acquired displacement data and further verifications were carried out to validate the reliability of the obtained results. These analyses were realized on both kinds of recorded data: accelerations and displacements.

4.5.1.1 Oversimplification of the structure

The same oversimplification of the structure was considered for all building models. This depends on the sensors of acceleration chosen to make this analysis and on further observations presented hereafter.

In order to obtain the best compatibility of the data acquired during the tests, two nearest sensors, one for displacements and one for accelerations, were chosen. Sensor fixed at each floor level were considered. Of these, displacement sensors placed on steel bolt anchors were selected. This choice allowed the use of accelerometers fixed to the corresponding internal timber beam. The rigid link between the external point, of displacement acquisition, and the internal one, of acceleration recording, is properly guaranteed by the steel anchors fixed to the timber beam and bolted to the end-plate.

This selection of sensors led to the consequent oversimplification of the structure. In first instance, the main value of the corresponding acquired data, in terms of both displacement and acceleration, was considered. Furthermore, the overall behaviour of each storey was considered equal to that represented by the obtained data at the corresponding floor level.
In addition, data presented in the following are also considered for the analysis of the capacity curve of each building model. The relationship between the shear force, sustained by walls parallel to the seismic action, and the corresponding displacements was computed starting from the same data employed for the stiffness analysis. In addition, the whole mass of each storey was considered as concentrated in the point where sensors were fixed. For these analyses, the data are presented in table 4.1.

4.5.1.2 Data Processing

An innovative measurement system was employed to monitor the displacement of more than a hundred relevant points of each structure. This technology is based on the optical monitoring of the position of all markers, namely small reflective spheres fixed on the masonry surface,using of eight optical cameras placed around the model. Starting from unprocessed data, some elaborations and analyses were performed to verify the reliability of measurements and the sensitivity of this monitoring system.

The first analysis was performed on original data in order to depurate these from the noise present due to two reasons: the acquisition system and low vibration induced by the shaking table at the lower seismic inputs. For these reasons, initial filtering was applied as a high-pass at a level of 2Hz. Further combinations of low-pass processing were performed at 20Hz and 25 Hz, without observing any substantial differences. The range of filtering was selected on the basis of the computed fundamental frequencies of the structures, to avoid loss of information in the considered interval.
Furthermore, data were processed to restore a fluctuation of measurements around a mean value equal to zero (linear-base correction).

These elaborations led to data less affected by uncontrollable causes. An initial comparison of the original data and results after both processing, filtering and linear correction, does not show any difference in the absolute measurements, meaning that lost information is out of the analysis range included between 5Hz and 20Hz.

Based on these data processing, the following elaborations were performed to verify the reliability of these measurements. A double differentiation of displacement data was computed. This operation allows a comparison of accelerations computed via this method and those recorded from accelerometers. As figure 4.34 shows, a good correlation between these data is found.
To give a further verification, the analysis of energy provided during the tests was considered. This was done computing the Arias Intensity, defined as:

$$I_A = \int_0^{\infty} E_A d\omega \tag{4.8}$$

where E_A is defined as the energy dissipated per unit of mass by a simple oscillator with ω as fundamental frequency and ν as damping factor. Figure 4.35 shows that the difference between the values of acquired accelerations and those computed starting from displacements are very close. This again confirms the reliability of the results.

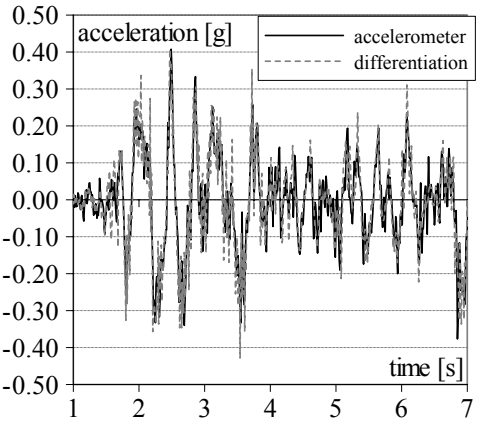

Figure 4.34: Comparison between recorded accelerations and those computed starting from displacements.

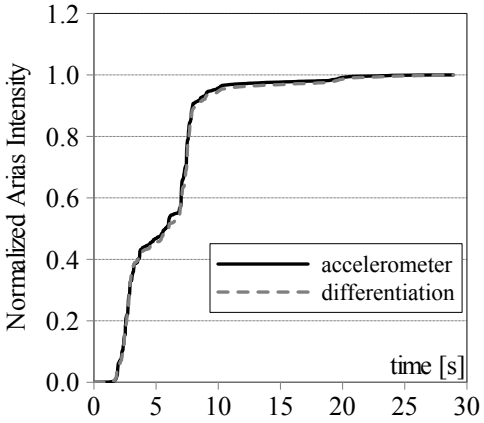

Figure 4.35: Comparison of Normalized Arias Intensity for recorded and computed accelerations.

Finally, a comparison of all acquired and computed data clarify how the sensibility of the optical system to measure displacement is about 0.1mm. For this reason, the results obtained during the first steps of each experiment are less reliable. However, the higher the input, the higher the reliability of data, since displacements are larger. Based on the preliminary analyses, one can conclude that values obtained for seismic accelerations higher than 0.10g are perfectly correct.

On the basis of above mentioned considerations, displacement data were employed to investigate the hysteretic relationship (figure 4.36) between shear force and displacements in both orthogonal directions.
Two different methods were employed to calculate the stiffness values:

- Linear regression;
- Maximum displacements.

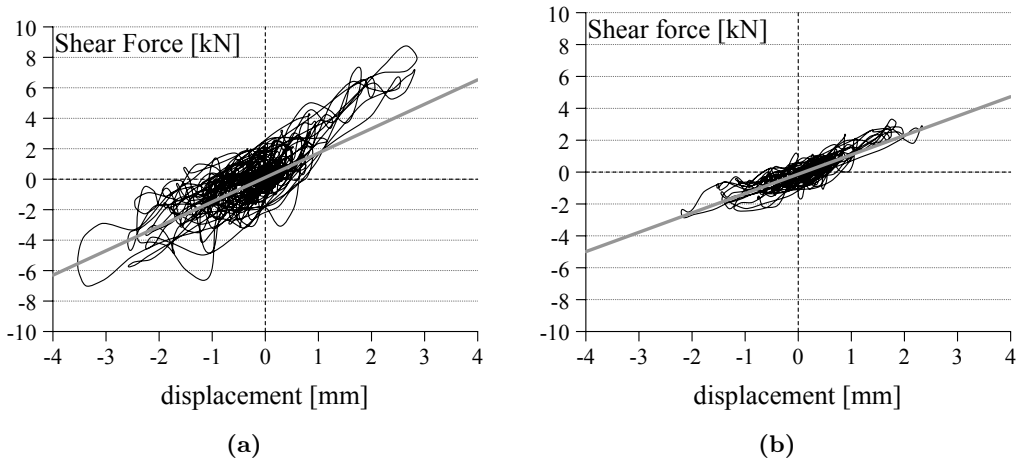

Figure 4.36: Example of hysteresis loops for SM model on the first (left) and second (right) storey in the X direction (0.40g).

The first method considers all data recorded during the test, while the second one makes use only of maximum displacements in a negative and positive direction. These analyses provided results with a not negligible difference. Furthermore, the first method supplied low values characterized by low coefficients of determination. For this reason and on the basis of considerations concerning the reliability of data, further analyses were performed.
The cause of this difference in the results, employing various processing methods, was identified in the wide parts of seismic input at low intensity, where acquired displacements are less accurate. As a consequence, instead of considering all data, two other methodologies were applied.
Firstly, the whole record of displacements, having a duration of about 30s (compare §4.1.3), was subdivided per seconds into 30 intervals and both previous methods, linear regression and maximum displacements, were applied in each one of these. The obtained results confirmed how the higher the seismic intensity, the more reliable are the results. Thus, the analyses were performed again considering the three different intervals, in which the input has accelerations with higher amplitude. Results obtained from both methods are in agreement and coefficients of determination are close to the unit, confirming the correctness of both previous considerations and analyses.
The results presented in the following paragraphs refer to the last analyses. For each building model and at each seismic step, four values of stiffness are computed: for both floors and in both horizontal directions.

4.5.2 URM Model

All computed stiffness values show an overall decreasing trend (figure 4.37a). During the first steps and for seismic intensities lower than 0.30g, the analyzed behaviours appear similar, manifesting an analogous reduction. Stiffness of the first storey in both directions is higher than that of the second one and this is mainly due to both a lower presence of openings and a higher vertical load acting on the considered wall section. Results at 0.15g could not be computed because of problems with the acquisition system, which made data unreliable.
Over 0.25g, a sudden drop is clearly evident and reflects both localised and overall

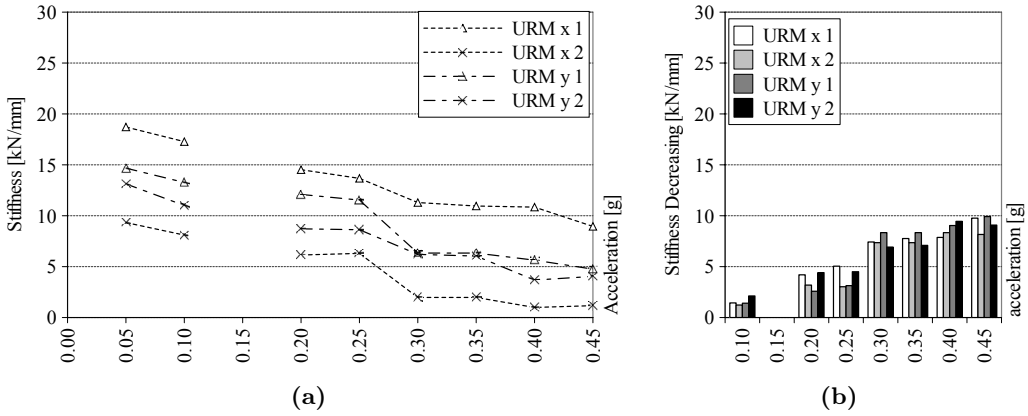

Figure 4.37: URM, Stiffness trend at increasing seismic intensity.

behaviour observed for the frequency trend. However, in this case the decrease is different depending on the floor and direction in question. Indeed, the highest stiffness reductions are concentrated on the first storey in the Y direction and on the second floor in the X direction, where the heaviest damage occurred. This differentiated decrease is confirmed and related to the computed mode shapes, presented in section §4.4.2. Actually, normalized modal deformations also manifest an increase at the first floor level (Y direction) in figure 4.27a, while they are reduced on the first storey in figure 4.27b, namely absolute modal displacements at the second floor level increased. For seismic accelerations higher than 0.30g, the stiffness reduction is limited up to end of the experiment. This confirms, as described in previous sections, how damage suddenly occurred and involved the whole structure, even if with evident differences among different parts. Furthermore, comparing the overall decrease both per level and direction, no substantial difference can be seen (figure 4.37b). In all cases, these reductions are higher than 50%, particularly they exhibit greater percentage values on the second storey.

4.5.3 RM Model

The overall behaviour of stiffness values for the repaired building model appears more complex than that of the URM model. A general reduction can be seen in figure 4.38a, even if few localised increases are present. The first rise manifests between 0.05g and 0.10g but this increase was also seen particularly for the first and second frequency values (figure 4.23a), thus it was expected.
Between 0.20g and 0.30g a general reduction of values takes place and, also in this case, a correlation with corresponding identified mode shapes is noticed (figure 4.28). Actually, the first storey along X and the second level in the orthogonal direction manifest a larger decrease. This behaviour is confirmed by increased normalized modal deformations in the X direction at the first floor level and, perpendicularly, their decrease at the same level. Confirmation of this behaviour is also provided by the analysis of frequencies (figure 4.23a), particularly the first and second one, in the same range of accelerations.
Over 0.35g, all computed stiffness values exhibit a monotonic decrease, which is greater for the first storey in both orthogonal directions. Also in this case, a certain relation can be found with computed frequencies. Actually, in the second part of the

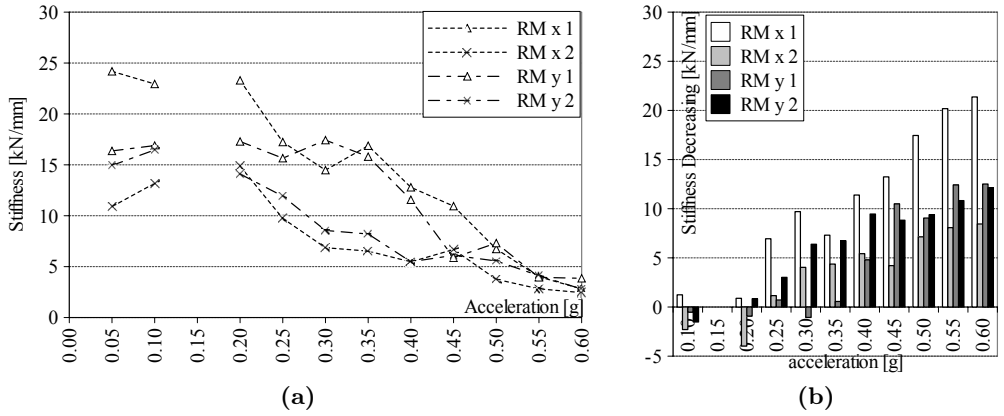

Figure 4.38: RM, Stiffness trend at increasing seismic intensity.

experiment, both quantities show an overall decrease higher than that manifested in the first part.

However, one should note how the overall reduction develops during the whole test and is not concentrated during a single step. This can be explained in the light of overall damage, which similarly occurred gradually.
Furthermore, figure 4.38b clarifies how a certain diversification in the damage position. Indeed, the first floor exhibits the highest stiffness degradation, particularly in the X direction, even if also that of the second storey is noticeable. All four cases show an overall decrease higher than 70%, compared to the initial condition.

4.5.4 SM Model

The Strengthened Masonry model shows high starting values of stiffness. The overall behaviour is decreasing even if several steps during the experiment manifest a large increase in this quantity (figure 4.39a). Furthermore, the initial values, for each floor, are similar, being higher on the first storey also in this case.
Stiffness values up to 0.20g exhibit a substantial invariance and this behaviour was also confirmed by the limited variation of frequency values presented in figure 4.24a. The first important considerations can be drawn on the basis of the effects manifested between 0.20g and 0.35g. A clear increase in values for stiffness at the first floor level should be noticed, while other parameters manifest a general decrease. This can be linked to the computed mode shapes (figure 4.29b), even if the most obvious relation should be drawn with identified frequencies. Actually, the first bending mode in the X direction (figure 4.24c) exhibits a localised increase in the same range of accelerations and this reflects also on the torsional mode, which behaves similarly.
Over a seismic acceleration of 0.35g and up to 0.55g, a large and overall reduction takes place for all computed stiffness, which settles at similar values. The analysis of both frequencies (figure 4.24a) and mode shapes (figure 4.29) validates the reliability of the obtained stiffness results, since their overall behaviour is very similar.

The insertion of brace elements on openings induced a noticeable variation on the overall behaviour of the SM model, as discussed in section §4.2.3, and the resulting system should be considered different from that of the first part. As a consequence, the stiffness was increased, as shown in figure 4.39a. However, the overall behaviour of the considered directions and storeys in question is similar and the total reduction in this

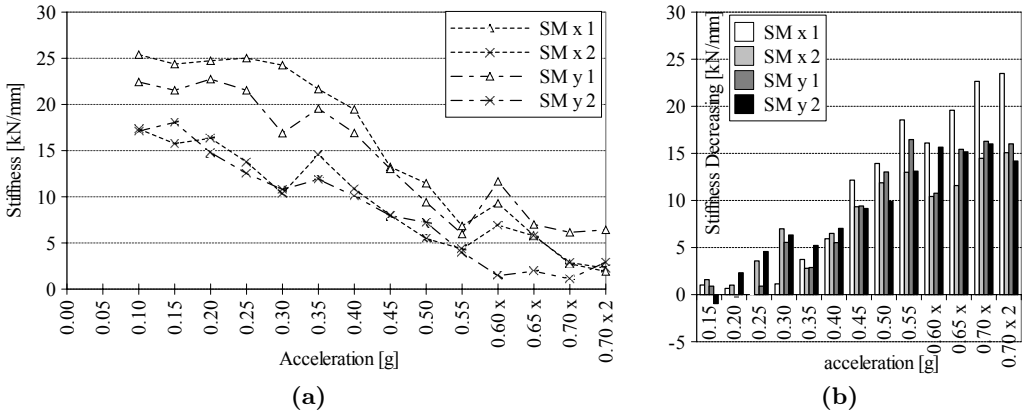

Figure 4.39: SM, Stiffness trend at increasing seismic intensity.

second part is very limited if compared with that up to 0.55g. These considerations were also drawn up for frequencies.

The analysis of the stiffness decreasing (figure 4.39b) indicates how, in the first phase, the decrease is concentrated in the second storey, while, at higher seismic intensities, the first floor level manifests the highest reduction, particularly in the X direction.

4.5.5 Observations

The results obtained from the analysis of stiffness degradation reflect those previously commented and show a high correlation with computed dynamic characteristics. Figure 4.40 compares, as the most important example, the stiffness values obtained on the first storey in both directions for the three building models.
Firstly, one should note how the stiffness in Y is lower than that computed in the orthogonal direction and this is in agreement with the analyzed frequencies, since the fundamental period in Y is higher than that in X. Furthermore, this relation between frequencies and stiffness is validated by the overall behaviour. Actually, the trend exhibited by stiffness values during the experiments is similar to that showed by frequencies and this is particularly evident for the SM model, where the wide localised increase between 0.15g and 0.40g can be seen in both analyses.

The comparison of the overall behaviours of the unstrengthened and injected models (figure 4.40) shows that the RM structure represents an intermediate situation between the URM and SM specimens. The effects of lime grout injection are clearly evident if one compares the final situation of the URM model and the initial values of the RM structure. In fact, the applied structural intervention is able to completely recover and increase on the RM model the initial stiffness of the URM one. This fact is also confirmed by the recovery of initial frequencies, as discussed in section §4.4.1. Moreover, the overall trend of the RM model is similar to that of the SM one, particularly in the Y direction (figure 4.40b).

Finally, as in the case of previous analyses, also the stiffness evaluation confirms how strengthening intervention leads to the best results. If compared to repairing, strengthening allows the degradation of structure to be limited more and induces a more regular overall behaviour. However, the RM model, in turn, manifests a better trend than that of the URM structure.

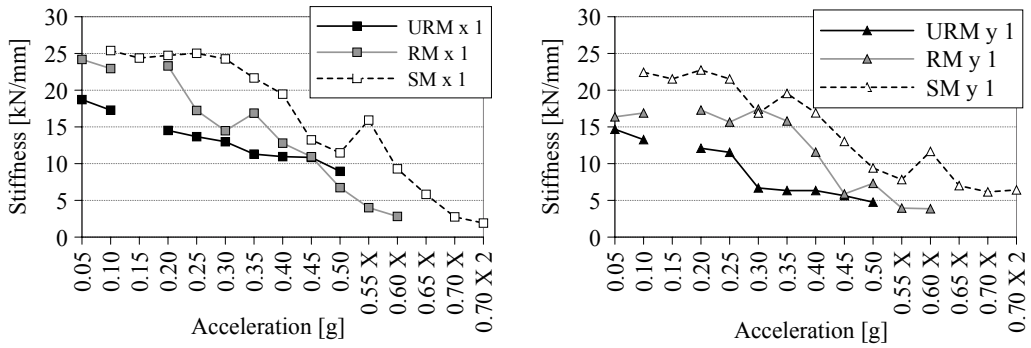

(a) First storey, X direction

(b) First storey, Y direction

Figure 4.40: Comparison of stiffness values of all models.

4.6 Seismic Resistance

On the basis of both acquired displacement data and recorded accelerations, the seismic resistance of models can be investigated. In particular, following the oversimplification proposed for the analysis of stiffness, an examination of acting shear forces for each storey and direction is presented in this section.

The recorded accelerations at each floor level were combined with the mass of the corresponding storey. This allowed, for each building model, an examination of its seismic resistance, which is defined by the lateral resistance and deformability of the investigated structure when forced by a horizontal seismic load. This led to calculating the Base Shear, namely the acting horizontal force, as:

$$BS = \sum_i m_i \cdot a_{i,max} \tag{4.9}$$

The combination of this parameter with the actual lateral displacement allows the so called $H - \delta$ charts to be created, presented in figure 4.41. These relationships represent the envelope of hysteretic loops also employed for the calculation of stiffness and presented, as an example, in figure 4.36.

Initial observation of figure 4.41 shows that both injected models could suffer higher seismic loads, with a maximum increase equal to 100% in the case of the Strengthened Model and to 75% for the Repaired structure. This confirms that using grout allows a noticeable increase in the strength of injected structures. Furthermore, figures 4.41b and 4.41c clarify that for a same lateral load, injected models manifest a limited floor displacement, if compared with values obtained from figure 4.41a. These observations can be applied to both floor levels and both investigated directions.

An analysis of attained displacements demonstrates how they are higher at increased strength. Injected models could suffer, on the first storey, about 20mm, instead of 5mm for the URM model. At the second level, the increase is evident only in the case of the Strengthened Model, which attained more than 35mm, while the URM an RM settled at about 25mm, even if the repaired structure also has larger values than the unreinforced one.

Lastly, in all cases the envelope can be oversimplified via a linear interpolation, where each changing slope corresponds to the beginning of further damage to the structure. In the light of this interpretation, the overall behaviour exhibited by the

models is very different.
The Unstrengthened Model (figure 4.41a) presents two different trends: an initial stiffer phase, corresponding to an undamaged situation, and a second phase, when heavy damage occurs and the inclination of the curve widely decreases. However, the model could not sustain higher lateral loads and the overall behaviour can be defined as that of a brittle material.
Instead, both injected models show a further phase beyond the first two exhibited by the URM model. This phase, considering the overall behaviour of the first storeys, manifests an increase in lateral displacements with almost constant seismic loads (figures 4.41b and 4.41c), providing a clear warning before the collapse of the injected structure.

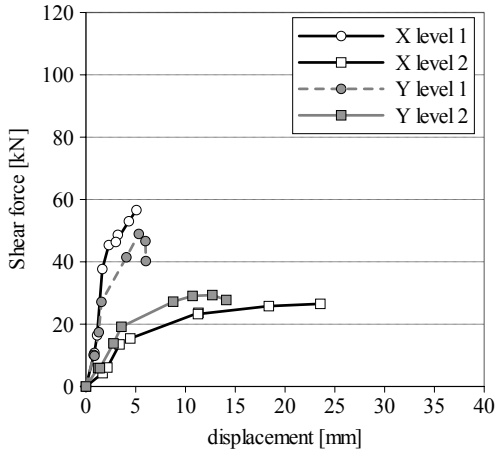

(a) URM model.

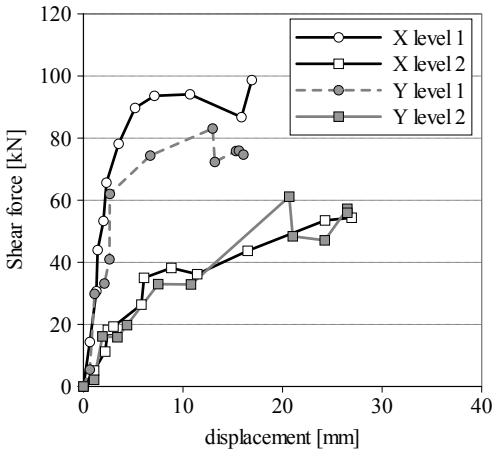

(b) RM model.

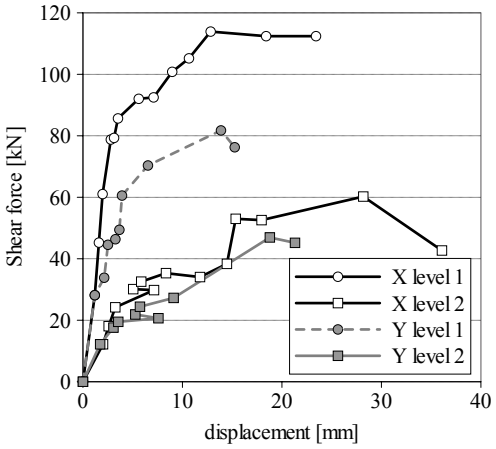

(c) SM model.

Figure 4.41: Relationships between Shear forces and corresponding storey drifts per each model.

However, one should consider how the acting shear forces are proportional to the involved masses and their spatial distribution on the models. In the case of the RM and SM models, the mass increase, due to the lime grout injection, was quantified to be equal at about 10% of the overall mass of the URM model; thus, this cannot be neglected. As a consequence, in order to make a better comparison of the behaviours

of models, the Base Shear values are normalized with reference to the weight of the considered structure. The new result, named Base Shear Coefficient, is thus presented in a non-dimensional form:

$$BSC = \sum_i \frac{H_i}{Q} \tag{4.10}$$

Figure 4.42 presents this analysis as a function of the first storey rotation angle, defined as the ratio between the actual maximum displacement and the height of the first level.
Results in both directions confirm the above discussed observations. Actually, figures 4.42a and 4.42b clarify how the injection of lime grout allows a substantial invariance of behaviour in the first linear phase. Furthermore, one should note that the initial overall behaviour of the RM model is very close to that of the URM one. Secondly, the trends of the BSC of both the RM and the SM models are overlapped in the first branch, meaning that in the linear phase their behaviours may be considered almost equal.
Moreover, damage, which induces the first slope change in the curves, occurs at higher seismic loads in the case of both injected models. For instance, the initial damage manifested at higher loads in the case of the Strengthened Model, while slightly lower values can be seen for the Repaired Model.
Finally, a higher ultimate drift, and thus also ultimate displacement, is allowed in both injected models, without any substantial difference, even if in the case of the SM model they are related to higher Base Shear Coefficients, namely lateral loads.

4.7 Prediction of Stiffness Increase

Results presented in the previous sections, particularly regarding the analysis of frequencies and stiffness degradation, manifest a deep relation. Furthermore, also results of the Repaired Model also seem to be related to those of the Unstrengthened Model, being the same physical model after injection. In all the performed analyses, the injection of lime grout (RM model) on the damaged structure (URM model) is able to recover and, in some cases, also improve the initial dynamic characteristics of the undamaged model.
For instance, the repairing intervention causes a slight increase in frequencies and, as a consequence, also an increase in stiffness, referred to the initial values of the URM model.

The above presented observations suggest how the overall behaviour of the Repaired Model can be predicted on the basis of the dynamic characteristics of the original and undamaged model (URM). In fact, the most evident relation obtained from the analyses, the one between frequency and stiffness, is the consequence of the basic and well-known relationship from the theory of the dynamic of structures:

$$f = \frac{1}{2\pi}\sqrt{\frac{k}{m}} \tag{4.11}$$

This relationship is obviously valid and applied to each single model separately. However, starting from the results of dynamic analyses, the frequency of the RM model seems to be correlated to that of the URM structure and, specifically, it is

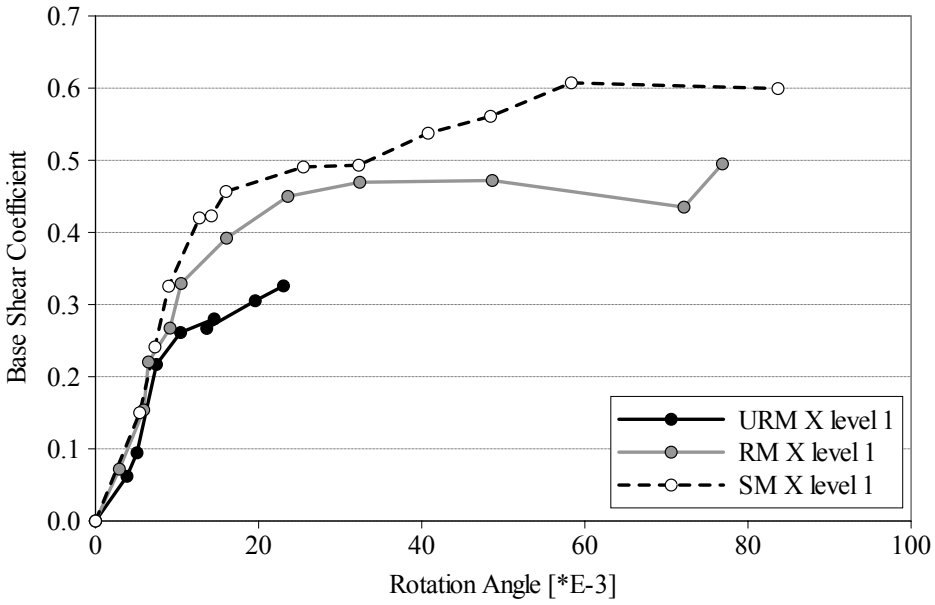

(a) X direction.

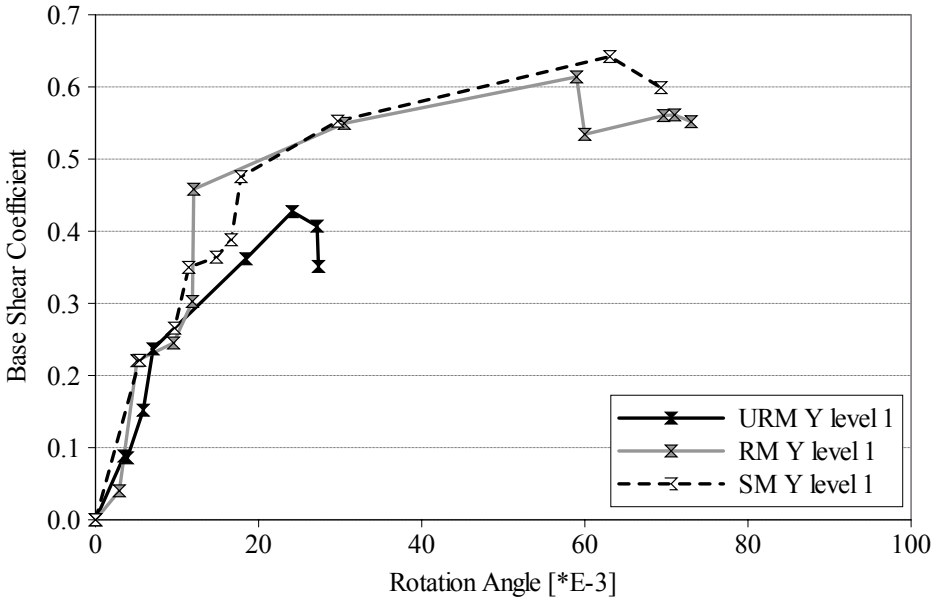

(b) Y direction.

Figure 4.42: Relationships between Base Shear Coefficients and the first storey rotation angle.

slightly higher. Therefore, the above presented relation for the Repaired model can be defined as proportional to that of the Unstrengthened structure (equation 4.12). Through few simple mathematical steps, this proportion defines a link between the

stiffness of the considered models on the basis of their masses.

$$f_{RM} = \frac{1}{2\pi}\sqrt{\frac{k_{RM}}{m_{RM}}} \propto \frac{1}{2\pi}\sqrt{\frac{k_{URM}}{m_{URM}}} = f_{URM} \tag{4.12}$$

$$k_{RM} \propto k_{URM} \cdot \frac{m_{RM}}{m_{URM}}$$

$$k_{RM} \propto k_{URM} \cdot \left(\frac{m_{URM} + m_{inj}}{m_{URM}}\right)$$

This leads to relate the stiffness values as a function only of the masses of both the URM model and the quantity of injected grout (equation 4.13). This was obtained since: $m_{RM} = m_{URM} + m_{inj}$.

$$k_{RM} \propto k_{URM} \cdot \left(1 + \frac{m_{inj}}{m_{URM}}\right) \tag{4.13}$$

This relationship can be easily applied in the case of the experimental campaign presented in this chapter, since the models were weighed during their movement on the shaking table and the amount of employed lime grout was monitored. However, in the case of a real intervention, the mass of the structure can be correctly predicted while the quantity of injected mixture is measurable.
The experimental data indicate an increase of the mass, due to the lime grout injection, approximately equal to 10% and this also induces a similar increase in stiffness, being about 2ton the weight of the grout and about 19ton that of the URM model. The results provided by equation 4.13 are in accordance with the experimental analyses, even if only a single comparison could be performed. In fact, the results relate the characteristics of the URM model, on original conditions, with the initial ones of the RM model. Thus, the relationship can be applied only at the beginning of experiments on both the structures in question, since their subsequent overall behaviour is different, as resulting from all the analyses.
Obviously, the above presented equation should be calibrated on the basis of a large number of experimental results. Furthermore, its application to simpler specimens will also allow the validity of equation 4.13 to be verified, which seems to be applicable to the present case.

As a final remark, one should note that this comparison can be made between the URM and RM models, since they are the same physical structure, before and after the repairing intervention. Instead, the characteristics of the SM and URM models cannot be compared, since they are two different structures.
However, the main aim of the proposed relationship (equation 4.13) between the stiffness of the Unstrengthened and Repaired models verifies the correctness of the obtained results and developed observations, starting from the theoretical equation 4.11.

4.8 Conclusive Remarks

The experimental campaign, carried out via several shaking table tests on three different masonry building models, allows important information to be obtained about the effectiveness of hydraulic lime-based grout injection as structural intervention suitable for historical multi-leaf stone masonries. Moreover, the main influences of

this intervention on the dynamic behaviour of building models, as well as further induced modifications, could be evaluated by means of several analyses presented in this chapter.
Moreover, further observations led to compare the effectiveness of the lime grout injection as *strengthening* or *repairing* technique. In fact, the obtained results highlighted similarities and differences of the overall behaviour of injected structures with or without a previous damage.

The first evident influence of the lime grout injection on the building models, is its capability to limit the development of the crack pattern. For instance, the injection allows the damage to be concentrated in a few cracks of extensive length and opening. This could be seen on both injected models, instead of the widespread crack pattern manifested by the Unstrengthened model. Furthermore, typical damage for this kind of masonry developed on the URM model, such as local separation of external layers and out-of-plane failure. Otherwise, the injection was able to prevent them on both injected models.
Furthermore, the survey of the damage development highlighted the positive effect of the admixture and no difference could be seen between repairing and strengthening interventions.

The second remark focuses on the increased strength induced by the use of lime grout. Both injected models could suffer higher seismic accelerations than the URM model. In fact, the RM and SM models sustained accelerations respectively increasing by about 30% and 50%, when referring to the unstrengthened case. The RM model could attain 0.60g, while the SM structure achieved more than 0.70g. Furthermore, the increase of sustained accelerations, obtained in the present research, resulted higher than the increase of 20% achieved by Benedetti [1980], which employed injection of a cement grout.

This result is directly connected, confirmed and extended by an analysis of the seismic resistance of masonry. In fact, the increase of weight, due to the injection of lime grout, induced higher forces on both the SM and RM models, at equal seismic accelerations, than that computed on the URM one. Nonetheless, the injected models are characterized by increased strength, which attains an overall increase of about 100% in the case of the Strengthened model and settles at 70% on the Repaired specimen. Also in this case, the obtained results performed better than those achieved by Benedetti [1980]. Actually, using cement grout, both repaired and strengthened models manifested a strength increasing limited to 20%.

Both injected models (RM and SM) exhibited a higher displacement capacity and a better overall behaviour since, after reaching the maximum lateral load, they were able to achieve larger displacements, sustaining the same seismic load. On the other hand, the URM model shows a very limited resistance beyond the initial linear phase and the displacement capacity is limited if compared with those of both injected models.

Finally, the analyses of induced accelerations and of Amplification Factors (AF) demonstrate how the injection allows monolithic behaviour to be maintained up to 0.45g, while the unstrengthened structure manifests the loss of this at 0.25g. Furthermore, the heaviest damage developed on the URM model, caused stability problems on the structure. Instead, these arose on both injected models only close to the end of the experiment because of the formation of macro-elements.

The further performed analyses highlight the wide and positive influence of lime grout injections on the dynamic behaviour of building models.

Firstly, one should consider how the repairing intervention allows the dynamic characteristics of the Unreinforced structure to be recovered, considered in an undamaged situation. In fact, this was verified in terms of frequencies, mode shapes, damping factors and stiffness.

Nevertheless, the trend of computed frequencies appears very different among all the models. The tendency of the URM model manifest monotonic decreasing and a sudden drop can be seen when heavy damage develops on the model. Differently, both the injected specimens exhibit a gradual reduction in frequencies and no unexpected decrease takes place. Comparing the results at the same load level, the URM manifested an overall decrease of about 20%, 25% and 30% for the 1^{st}, 2^{nd} and 3^{rd} frequency respectively, while the same quantities settle at 10%, 5% and 9% in the case of the SM model and 10%, 8% and 18% for the RM model. This confirms that strengthening induces better characteristics and lower decay than repairing.

These observations are also confirmed by the analysis of the mode shapes. Actually, in accordance with the trend of frequencies, the URM model shows a sudden drop at the arising of damage, while injection allows a gradual degradation of their vibrational modes to be induced. Furthermore, strengthening allows a wide range of normalized modal deformation, between 0.7 and 0.4, instead of 0.6 and 0.5 for repairing. Lastly, also in this case, injection allows the initial mode shape of the URM building to be recovered on the RM model.

The analysis of the damping factors underlines how this structural intervention allows an higher dissipation capacity. In fact, the Unreinforced structure manifested low and almost constant damping values, during the whole experiment, ranging between 2% and 4%. Instead, the injected models exhibited damping factors that reach values of about 10% and could sustain these up to 0.40g (SM model). Nonetheless, the RM building model manifested a premature degradation of these dynamic characteristics. This occurred due to a seismic acceleration ranging between 0.10g and 0.20g.

Further considerations can be made on the basis of the a stiffness analysis. The obtained results demonstrate a close relationship with the trends of frequencies, since the overall behaviour is very similar. Therefore, the most important stiffness degradation on the URM model occurs when the damage propagated on the structure, while injection allows a gradual reduction of stiffness to be induced throughout the whole experiment, without showing any sudden drop. Moreover, even if the overall stiffness reduction on injected models is very similar, the strengthening intervention can delay this degradation, when referring to the effects of the repairing intervention. Finally, once again, this analysis confirms that it is possible to recover and improve, on the RM model, the initial conditions of the URM structure via the use of lime grout injection.

The overall consideration of the analyzed dynamic parameters also highlights how the strengthening intervention, via injection of the hydraulic lime-based admixture, does not provide substantial modifications on the seismic behaviour of both strengthened and repaired models. Actually, the intervention with this material does not modify neither the initial frequencies nor the mode shapes nor the initial stiffness. On the other hand, the employment of different admixtures, particularly if cement-based (compare §1.2.2 for the static field and Benedetti [1980] for dynamic tests), seems to induce an increasing of the overall stiffness and this unavoidably modifies the original behaviour of the unstrengthened structure.
Finally, regarding all the above-mentioned observations, one should consider that the intervention using hydraulic lime-based grout can also involve only a part, instead

of the whole structure. In effect, the injection of this admixture does not induce significant differences from the remaining part of the structure in terms of stiffness, frequencies and vibrational modes, while it is able to improve the strength of the involved part.

All the analyses performed provide harmonious results. The developed considerations highlight how lime grout injection considerably increases the strength of structures. Furthermore, injection can preserve the dynamic characteristics of models, on which structural intervention is carried out, and can delay their degradation. The main considered characteristics are frequencies, mode shapes, damping factors and stiffness.
In the case of intervention on a structure that presents previous damage, namely the RM model, the injection allows a recovery of the initial conditions of the original model (URM) in the undamaged situation. The conditions in question are the above mentioned dynamic characteristics.
Finally, intervening on a structure with previous damage (RM model) or on an undamaged case (SM model) leads to different overall results. Strengthening intervention exhibits the best results in terms of dissipation capacity and overall degradation of dynamic characteristics, since they are preserved up to high seismic loads. Instead, repairing intervention manifests similar overall dynamic characteristics at low seismic intensities. However, frequencies, stiffness, damping values and mode shapes degrade earlier than the case of strengthening.
The accordance of the analyses performed led the development of a relationship, which links the stiffness of a repaired structure to that of the same structure, under unstrengthened and undamaged conditions, and to the mass of injected grout. This relationship, which needs to be verified and calibrated, clarifies how the structural intervention of injection inevitably induces change, even if limited, in the elements concerned. Furthermore, the relationship in question mainly confirms the connections between the analyses performed and validates their results.

Chapter 5

Compression Behaviour of Injected Stone Masonry Walls

Monotonic compression tests represent an important experimental phase, which permits the mechanical behaviour of multi-leaf stone masonry panels to be understood. As several authors have already discussed [Binda *et al.*, 2003b; Galasco *et al.*, 2009a; Oliveira *et al.*, 2006; Toumbakari, 2002; Valluzzi, 2000; Valluzzi *et al.*, 2004; Vintzileou, 2007; Vintzileou and Miltiadou-Fezans, 2008], deepening the knowledge of compression behaviour for this kind of stonework leads to significant considerations concerning the effectiveness of the investigated strengthening technique, namely the injection of hydraulic lime-based grout. The test procedure, the instrumentation and the results of compression tests will be presented in this chapter. The test set-up and a description of specimens can be found in section 2.2.1.

The aim of this experimental campaign is to investigate the variation in mechanical parameters, such as compressive strength, Young's modulus and the Poisson ratio. Furthermore, these tests will lead to an understanding of how the grout injection can influence the failure mode of multi-leaf masonries subjected to compression and, above all, if and how the mixture modifies the transversal deformations of piers.

Finally, one should consider that panels, presented in section 2.2.1 and described in the following, were recovered from two different building models subjected to several shaking table tests. Specimens distinguished by "S", obtained from the SM model, underwent 16 seismic tests, while masonry piers encoded with "R", obtained from the RM model, were subjected to 22 ground motions.
In conclusion, one should remember that "S" elements were strengthened, starting from undamaged conditions, whilst "R" piers were repaired by injection, being cracked and damaged. On this basis, further considerations can be made concerning the effectiveness of the intervention on both damaged and undamaged structures. For instance, it can be established whether this strengthening technique allows an improvement in the original mechanical properties, for "S" specimens, or the percentage required to restore the original mechanical properties, for "R" specimens.

5.1 Test procedure and instrumentation

Compression tests were carried out under displacement control with a Universal Amsler machine. This also allowed the post-peak branch of the load-displacement relationship to be investigated. EN 1052-1 [1998] was followed, applying an incremental loading rate of about 0.5kN/s.

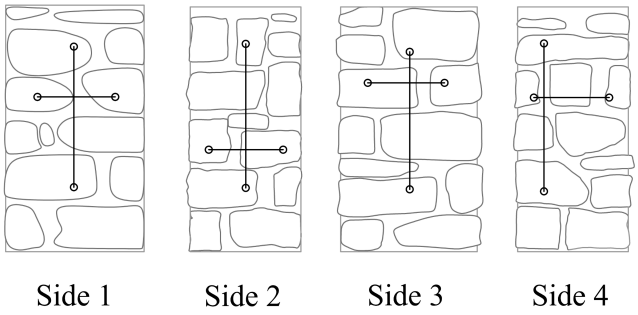

Figure 5.1: Example of instrumentation for slender specimens: type "A".

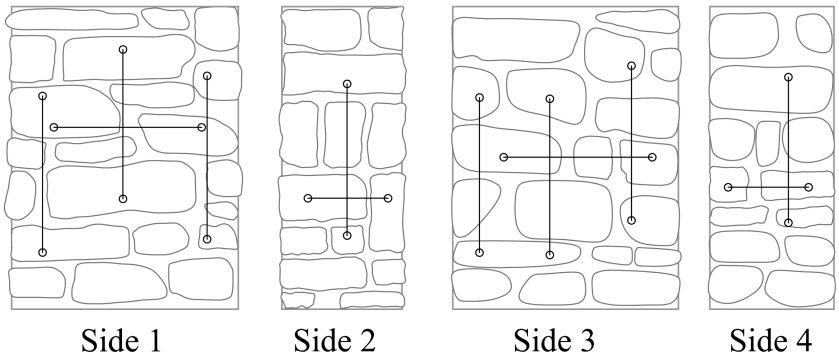

Figure 5.2: Example of instrumentation for squat specimens; type "B".

The specimens were instrumented with potentiometric displacement transducers, with two different ranges (±50mm and ±150mm), to estimate the vertical, horizontal and transversal deformations of panels. Instruments with lower extension and higher precision were placed horizontally, while the remaining transducers were fixed vertically. Two different configurations were adopted: type "A" in the case of slender elements (figure 5.1) and type "B" for squat specimens (figure 5.2), involving a different number of sensors.

5.2 Failure modes

The study of failure mechanisms for each specimen provides the first important observations on the overall behaviour of masonry samples. Furthermore, these remarks can enlighten both analyses and results presented in the following.
Different overall behaviours could be identified already during the tests. Furthermore, the damage progression on the specimens was quite different. For instance, the "R" elements seem to behave differently from the "S" samples. In fact, "R" specimens started to manifest cracks at a mean stress level lower than that of "S" elements, as figure 5.3 confirms. Figure 5.4 directly compares the stress level at which the first crack appears in the corresponding "R" ans "S" specimens, taken respectively from similar positions in RM and SM building models. As it can be clearly seen, the overall trend confirms previous observations excluding position 7. This can be justified considering that this element has a slenderness much lower than the remaining specimens (see table 2.7 on page 94). Moreover, pointing out the limited geometrical dimensions of samples R7 and S7, this deviation from the average trend becomes clearer.

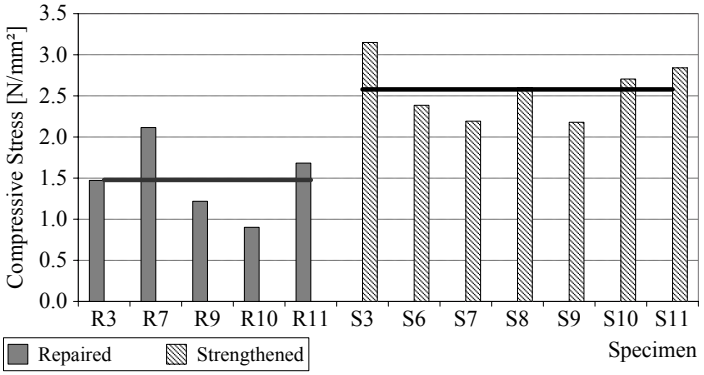

Figure 5.3: Stress levels for first crack appearance in each specimen.

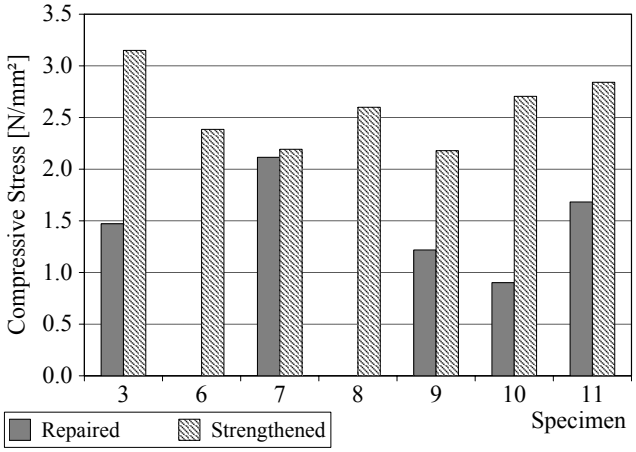

Figure 5.4: First crack appearance: comparison of compressive stress between specimens in the same position.

Further evidence, observed during the tests, regards the crack pattern. At the beginning, the first cracks were noticed on stones for both series (figure 5.5) and not on mortar joints, as expected [Valluzzi, 2000]. This may be due to the formation of localized cracks in stones, while a widespread damage and overall settlement of mortar joints could prevent cracks from being evident in bed joints at low vertical stress. Instead, at higher vertical loads, damage to mortar became evident.
Moreover, after the appearance of first openings in masonry specimens, the crack pattern developed gradually on the "R" series. On the other hand, "S" elements exhibited extensive damage just close to the failure point. In both cases a widespread crack pattern was seen, even if clearly on "S" specimens.

The explanation for this difference in their overall behaviour can be attributed, in part, to the effects induced by the admixture. In the case of strengthened specimens, grout injection was successful in creating a cohesive bond between the internal core and the external leaves. In the first part of the test and up to the occurrence of the first cracks, the masonry reacting similarly to homogeneous material. This being the case, grout injection created a slightly stiffer masonry pier. However, the repaired specimens, despite grout injection, did not behave as a monolithic matter, as in the case of strengthened panels.
The difference in the cohesive nature of the core for each specimen was clearly evident during demolition of samples, after the test. The internal core was more or less intact

Figure 5.5: Detail of cracks in stone at the beginning of the test.

in the case of the repaired specimens, whereas it was completely crushed on the strengthened samples. The reason for this can be found in the stronger cohesion, in the case of "S" specimens, between the external leaves and inner core, allowing a distribution of load among all the layers. As a consequence, this can also explain why heavy damage occurred on both the internal core and external leaves. On the other hand, in the case of "R" samples, the lack of cohesion at the interface, between the inner and outer layers, led to the majority of the load being taken by the stronger part, namely the external leaves, explaining why the internal core remained intact.
The final failure mode, exhibited by both specimen typologies, is that of an out-of-plane mechanism. What was observed during the tests was the separation of layers with the buckling of the external leaves. This type of failure is expected in this kind of masonry, since the connection between the leaves is the weak point. In fact, the monolithic behaviour of the masonry is only ensured by grout injection, since the material holds the leaves together.
Pictures from 5.6 to 5.9 clearly show the buckling of the external leaves and their consequent crushing, which caused the opening of large cracks leading to failure.
Figures 5.10 and 5.11 show the internal core during the demolition of both the repaired and strengthened specimens, where the previous observations are clearly evident.

5.3 Test results

Differences in the overall behaviour of the Strengthened and Repaired specimens, observed during the experiments, were confirmed from analyses of the stress-strain relationships (figures 5.12 and 5.13).
Both the vertical and horizontal strains are approximately linear up to 50% of the maximum attained vertical load on "R" samples (figure 5.12). Over this stress level, horizontal deformation widely increased, due to the opening of vertical cracks in the specimen. Vertical strains behave similarly. When the maximum strength is achieved, the sample is not able to sustain further stresses. As a consequence, the load quickly decreases and strains are limited, even if horizontal deformations are obviously larger than vertical ones.
Strengthened specimens (figure 5.13) manifest a vertical linear deformation almost up to the attainment of compressive strength. In fact, the change in vertical strain increase occurs at about 90% of the maximum achieved load. Instead, horizontal strains start to widely increase already at 30% of compressive strength. Beyond the attainment of maximum compressive strength, the samples of "S" series are able to sustain larger deformations. This reflect a gradual decrease in stress, followed by a noticeable increase in both vertical and horizontal deformations. Thus, differences between

Figure 5.6: Lateral view of specimen R7 after the test.

Figure 5.7: Lateral view of specimen S11 after the test.

Figure 5.8: Front view of specimen R7 after the test.

Figure 5.9: Front view of specimen S11 after the test.

Figure 5.10: Undamaged core of specimen R7 after the test.

Figure 5.11: Destroyed core of specimen S11 after the test.

Table 5.1: Compression strength of specimens and stress level corresponding to the first crack appearance.

Specimen	σ_{max} [N/mm^2] R	S	$\sigma_{I,cr}$ [N/mm^2] R	S	$\sigma_{I,cr}$ [%] R	S
3	7.05	7.31	1.47	3.15	20.9%	43.1%
6		7.87		2.39		30.3%
7	8.45	9.63	2.11	2.19	25.0%	22.8%
8		5.25		2.60		49.5%
9	5.58	7.59	1.22	2.18	21.8%	28.7%
10	7.29	8.14	0.90	2.71	12.4%	33.2%
11	6.01	8.24	1.68	2.84	28.0%	34.5%
average	6.88	7.72	1.48	2.21	21.6%	32.1%

strengthened and repaired elements are more evident in the post-peak behaviour, while during the first phase, up to the compressive strength, they are limited.
However, the overall behaviour of "R" and "S" specimens in both vertical and horizontal directions can be oversimplified with a piecewise linear function.

Further important results regard the compressive strength of tested specimens. As figure 5.14 shows, the variation range of compressive stress is notably larger, since values are included between about 5N/mm^2 and 10N/mm^2. A slight difference becomes clear from figure 5.15, displaying a comparison of compressive strength approaching specimens kept from the same position of different masonry buildings. In effect, "R" specimens highlight a slightly lower compressive strength than the corresponding "S". The characteristic values, divided according to typology, are reported in table 5.1. The difference in mean strength between the two series is lower than 1 N/mm^2. In fact, the maximum allowable stress on strengthened samples was 6.88N/mm^2, while repaired specimens settled at 7.72N/mm^2. However, as a general result also the mean value of 7.4N/mm^2 can be considered as representative of this kind of masonry.
An analysis of maximum achieved stress allows a in-depth study of the first crack appearance. As table 5.1 points out, the first cracks rise at about 20% of the compressive strength for "R" specimens, while "S" elements start to crack at stresses higher than 30% of the maximum achieved load. A typical development of the crack pattern for corresponding specimens (repaired and strengthened elements taken from the same position) is presented in figures 5.16 to 5.19. These images confirm the observations made concerning the previously discussed crack pattern development.

Of all of these, specimen S8 should be mentioned since it exhibited a strength considerably lower than the remaining "S" specimens. However, one should consider how the slenderness of this sample is about 2 times greater than other elements (see table 2.7 on page 94) and this can explain its overall behaviour. Actually, the buckling effect on the external layers was highly evident and earlier in S8 than in other cases, explaining its premature failure.

5.4 Analyses

Monotonic compression tests also permitted an evaluation of the deformability characteristics for this masonry typology.

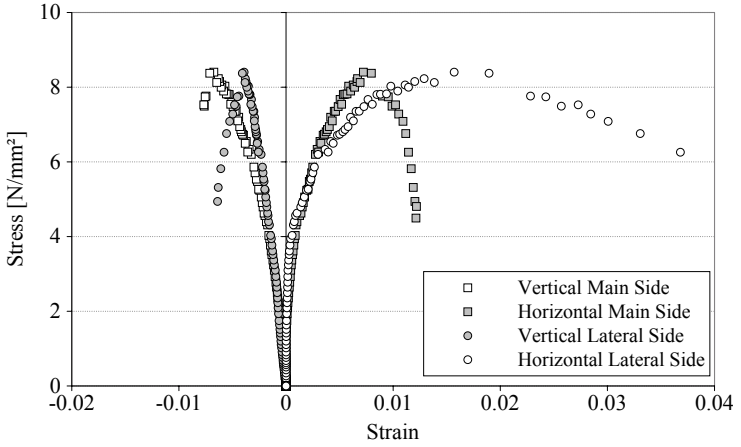

Figure 5.12: Stress-Strain behaviour on main and lateral sides of specimen R7.

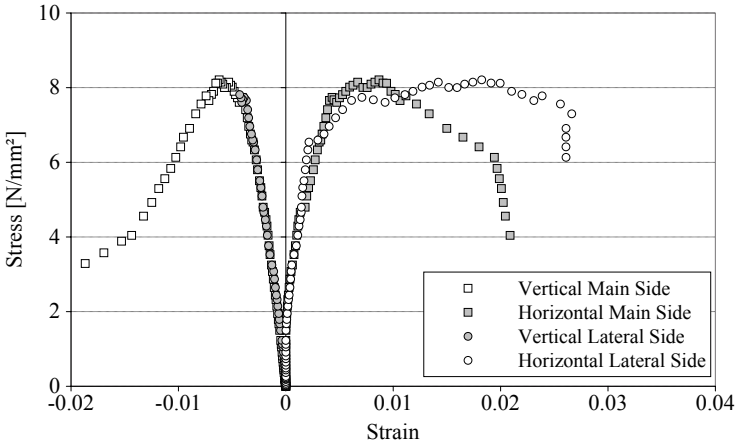

Figure 5.13: Stress-Strain behaviour on main and lateral sides of specimen S11.

The first elaboration regards the calculation of the Young's modulus. Unlike that reported on EN 1052-1 [1998], the elastic modulus was computed considering strains between 10% and 40% of the maximum load. This was done to neglect the first part of the tests, where a considerable arrangement of masonry took place, making the results unreliable. Moreover, a linear behaviour was obtained up to about 50% of compressive strength, confirming it was possible to calculate the Young's modulus in the previously mentioned range.
Figure 5.20 shows the Young's modulus calculated for all the specimens. The average value, considering all the samples, is 4000N/mm^2, with a coefficient of variation equal to 37%. However, the histogram presents quite a wide range of variation, particularly for "S" specimens. Sample S7, which exhibited the higher compression strength as previously observed, is characterized also by a higher Young's modulus, confirming overall behaviour slightly different from the remaining tested elements.
The calculation of the elastic modulus was also separated according to the series, sustaining the observations developed for compressive strength. "R" samples are characterized by an average value of 3471N/mm^2, while "S" elements resulted stiffer, with a main value of 4379N/mm^2. Naturally, both coefficients of variation are lower

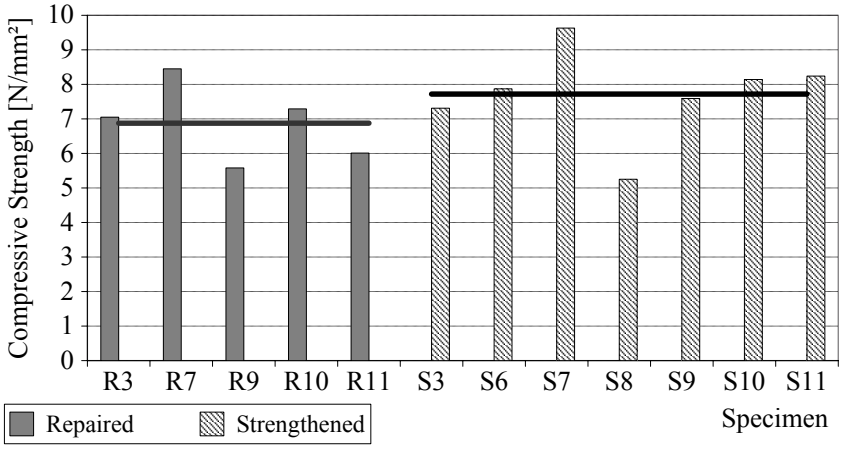

Figure 5.14: Compressive strength for the "R and "S" series.

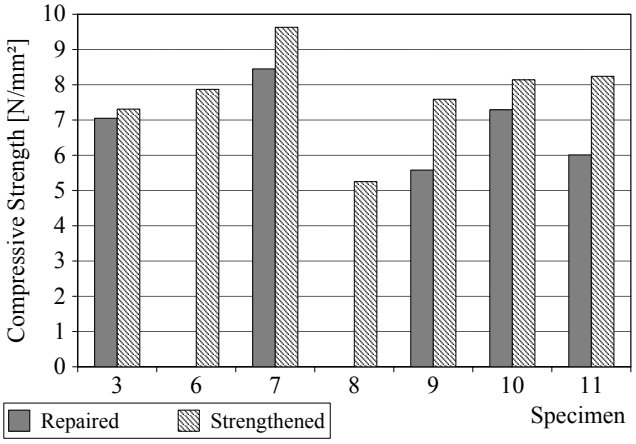

Figure 5.15: Comparison of compressive strength between specimens in the same positions.

than the total one. The values for each specimen are reported in table 5.2, with mean values divided per series.

Furthermore, the Poisson's ratio was computed at a stress level equal to 40% of compressive strength. Results are graphically reported in figure 5.21 and characteristic values are presented in table 5.2. As the histogram shows, values are quite scattered and some specimens exhibited ratios that seem to be too high and with a limited reliability. The average values, calculated separately for the two investigated series, are quite different, varying from 0.58, for the "R" series, to 0.78, for "S" specimens. Instead, a mean value calculated for all specimens amounts to 0.70. Therefore, the strengthened panels seem to deform more than the corresponding repaired ones. Nevertheless, one should consider that the value of stress at 40% of compressive strength for "S" elements is higher that that of 40% for "R" panels.
To further explore the Poisson's ratio, the horizontal and vertical strains of each specimen are plotted in figures 5.22 and 5.23. Comparing these two components, from which the Poisson's ratio is computed, the overall results appear to depend mainly on the horizontal strains than on vertical ones. In fact, while vertical deformations are comparable without showing noticeable differences between the "R" and "S" series, the horizontal strains of "S" specimens are larger than others.

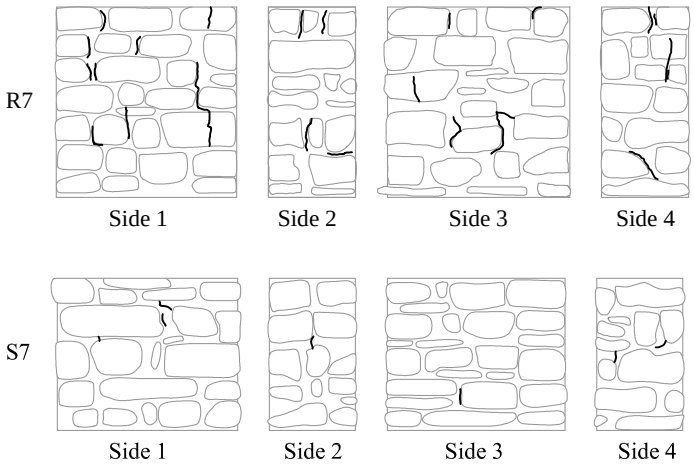

Figure 5.16: Crack pattern for R7 and S7 specimens at 4.20N/mm^2.

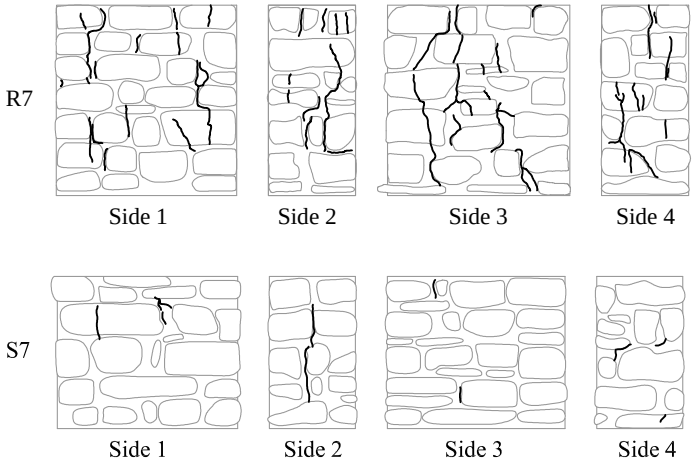

Figure 5.17: Crack pattern for R7 and S7 specimens at 7.00N/mm^2.

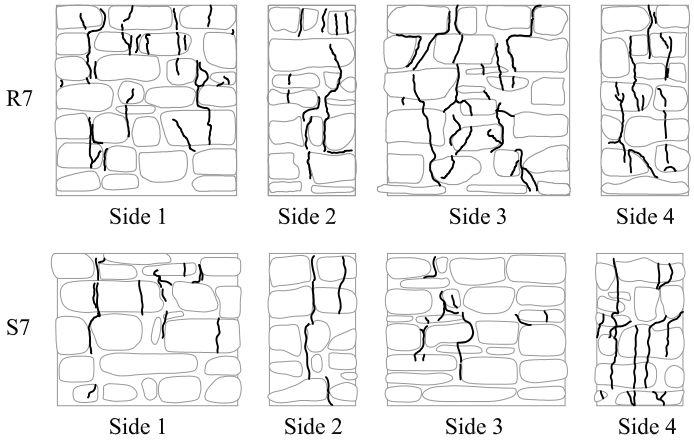

Figure 5.18: Crack pattern for R7 and S7 specimens at 8.40N/mm^2.

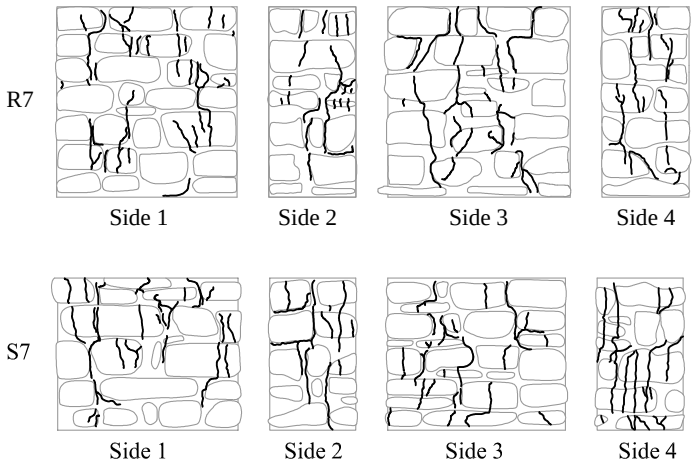

Figure 5.19: Crack pattern for R7 and S7 specimens at failure.

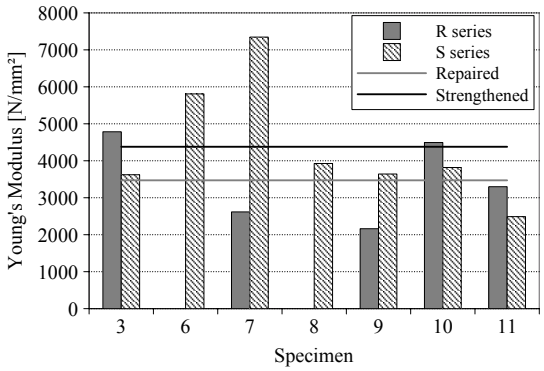

Figure 5.20: Elastic modulus for the "R and "S" series.

Table 5.2: Elastic modulus and Poisson's ratio of the "R" and "S" series.

Specimen	S Series			R Series	
	E [N/mm^2]	$\nu_{40\%\sigma_{max}}$ -		E [N/mm^2]	$\nu_{40\%\sigma_{max}}$ -
3	3622	0.98		4785	0.40
6	5809	0.73			
7	7346	1.61		2617	0.20
8	3927	0.24			
9	3642	0.91		2163	0.80
10	3818	0.14		4493	0.56
11	2489	0.84		3299	0.95
Average	4379	0.78		3471	0.58
Average of all specimens			E	[N/mm^2]	4001
Average of all specimens			$\nu_{40\%\sigma_{max}}$	-	0.70

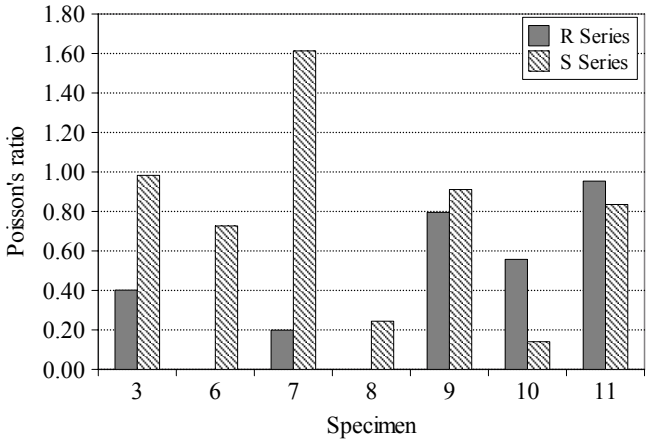

Figure 5.21: Poisson's ratio for the "R and "S" series.

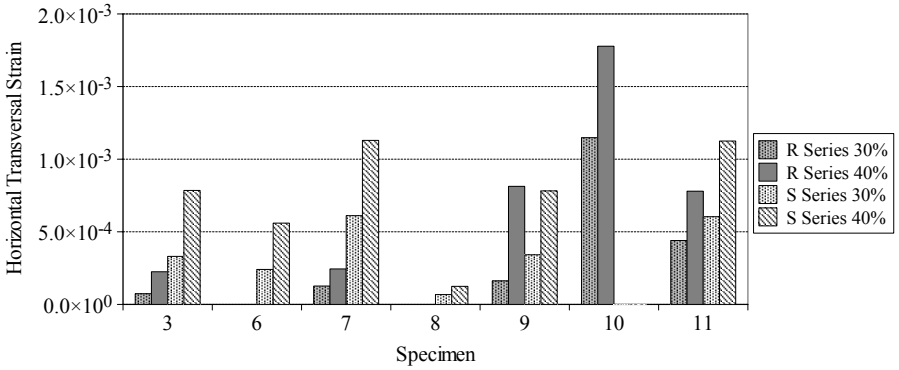

Figure 5.22: Horizontal deformations for the "R" and "S" series at 30% and 40% of compressive strength.

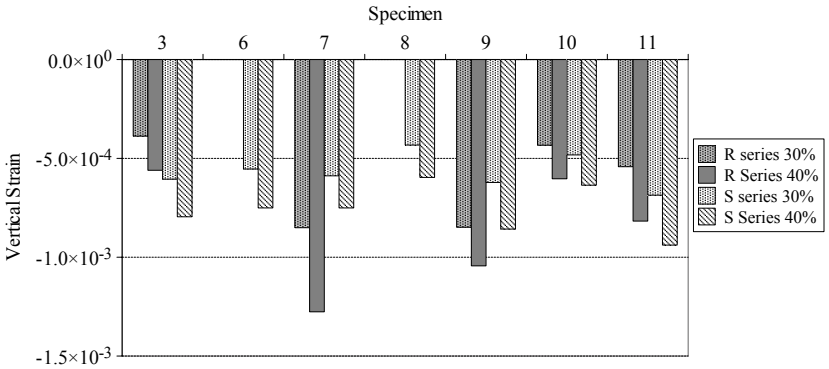

Figure 5.23: Vertical deformations for "R" and "S" series at 30% and 40% of compressive strength.

5.5 Oversimplification of compression behaviour

Observations and analyses performed on previous sections denote how specimens belonging to the same series, namely strengthened and repaired, exhibit similar behaviour in terms of compressive strength and both vertical and horizontal deformation. This constant overall behaviour allows oversimplification of the global trend manifested by specimens. Furthermore, as observed in section 5.3, the trend is linear up to cracks began to occur on masonry elements. Similarly, the following trends beyond this point behave linearly up to the achievement of failure. These considerations lead oversimplification of the behaviour of each specimen with a piecewise linear function, with four relevant points.
The first part of each test, characterized by an increase in vertical stress, starts from the beginning of the experiment up to the attainment of compressive strength. Instead, during the second phase, namely the post-peak behaviour, the vertical load decreases. In the oversimplification process, three different linear intervals, with different slopes, were considered in the first part, while a unique trend was employed to describe the second phase.

The first step of this analysis is presented in figure 5.24a, where the vertical strains are represented for all specimens. In this case, a wide variation in the overall behaviour of all the panels in question can be seen. These differences are more evident in terms of both maximum compressive strength and points at which the trend of each specimen changes.
In order to identifies a single representative trend, as a mean value of all samples, the stresses on each panel were normalized by the compressive strength of each specimen. Figure 5.24b, that represents this elaboration, exhibits a lower variation than in figure 5.24a, even if the trend of a few panels seems to deviate from the mean behaviour.

Considering separately strengthened and repaired samples (figures 5.25a and 5.25b) leads to a restricted range of variation even if, also in this case, differences can be seen among all oversimplifications. In fact, since the overall dimensions of specimens were limited, the position of the stones and the mechanical characteristics of both mortar joints and the stones widely influenced the overall behaviour and the characteristic mechanism of failure. Thus, starting from these considerations, the trends of a few samples can be neglected during the analysis if they deviate too much from the mean behaviour.

These analyses were also performed on data for the horizontal deformations in both directions, namely the main and transversal sides, and the results are presented in table 5.3. As the chart shows, the percentage of compressive strength at which the overall behaviour changes is very similar for strengthened and repaired specimens. In fact, vertical and horizontal strains on the main sides of all samples demonstrate an initial variation of about 55% of σ_{max}. The unique significant difference can be found on transversal deformation of lateral sides, where "S" samples manifested an earlier increase than "R" panels.
The second important variation can be identified at about 85% of σ_{max}. Beyond this point all deformations widely increased up to attain the compressive strength of masonry.
After the achievement of σ_{max}, specimens could sustain a further increase in strains corresponding to a mean decrease in stresses of about 15%.

For each of these identified phases, the slope of linear trends could be computed. The results are summarized in table 5.4. Positive values refer to the first part of

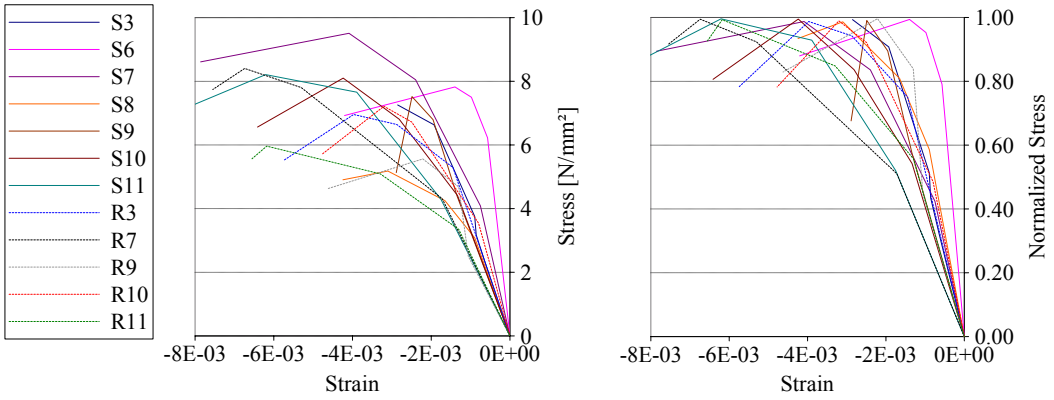

(a) Experimental behaviour **(b)** Normalized experimental behaviour

Figure 5.24: Oversimplification of compression behaviour of all tested specimens.

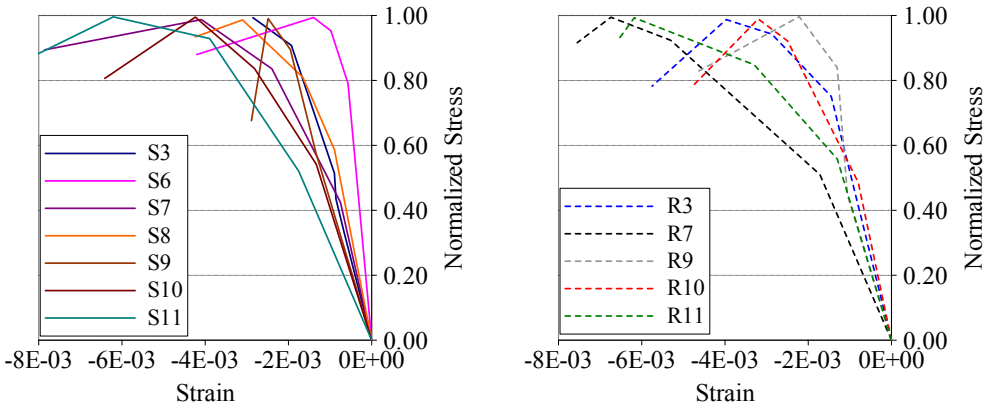

(a) S specimens **(b)** R specimens

Figure 5.25: Oversimplified normalized compression behaviour of all tested specimens.

the overall curve, when load increases, while negative slopes represent post-peak behaviour.
The computed data demonstrated a wide scattering. As a consequence, the standard deviations and the coefficients of variation were quite high. Nonetheless, the results obtained for both series in the vertical direction exhibit a limited difference, particularly during the first and second phases. Instead, slopes of horizontal strains manifested a larger difference, confirming previously observations developed, which highlight how the crack pattern developed differently on strengthened and repaired panels.

The obtained results confirm that a general rule can be identified to describe the overall behaviour of three-leaf stone masonry panels subjected to compression up to failure. Furthermore, data obtained from specimens after both strengthening and repairing interventions exhibit an overall limited variation that can be neglected in a more general description of compression behaviour for this kind of masonry.

Table 5.3: Identified phases and percentage of compressive strength at which changing in slope occurred.

	Vertical strains		Horizontal main strains		Horizontal transv. strains	
	S [%]	R [%]	S [%]	R [%]	S [%]	R [%]
1^{st} step	55	51	59	57	39	53
2^{nd} step	89	78	81	89	87	80
3^{rd} step	100	100	100	100	100	100
4^{th} step	85	86	89	77	86	82

Table 5.4: Computed mean slopes for each identified interval.

	Vertical direction		Horizontal main direction		Horizontal transv. direction	
	S [N/mm^2]	R [N/mm^2]	S [N/mm^2]	R [N/mm^2]	S [N/mm^2]	R [N/mm^2]
1^{st} step	3827	3107	31284	4169	6985	2168
2^{nd} step	2665	2720	2180	755	728	477
3^{rd} step	1310	534	378	295	186	200
4^{th} step	-1294	-806	-218	-261	-10	-71

5.6 Conclusive Remarks

Strengthened specimens exhibited a compressive strength slightly higher than that of repaired panels, as expected. This increase corresponds to about 10%. However, the main value can be considered equal to 7.4N/mm^2.
Furthermore, "S" specimens seem to deform more than "R" panels, particularly in the horizontal direction, while negligible differences could be recorded vertically. The average value of the elastic modulus can be considered 4000N/mm^2, while the Poisson ratio can be considered varying between 0.6 and 0.7.
Moreover, strengthened elements result slightly stiffer and manifest a different crack pattern, with reference to "R" samples. While repaired specimens developed gradual damage, starting from low stress levels, cracks in strengthened panels appeared at higher loads, manifesting a faster decay.

Results achieved in this experimental part underline how repaired elements exhibit slightly worse compression behaviour. However, one should note how these differences, particularly regarding mechanical characteristics, namely Young's modulus and Poisson's ratio, are limited. The reason for this limited difference may be due to two reasons.
Firstly, the repaired specimens may have internal cracks, occurred within the external leaves and the core. This may explain the development of visible cracks at a lower stress level than the strengthened specimens. These cracks would have developed during the shaking table test, which the RM model was subjected to twice.
The second reason may be ascribed to the lower cohesion between the external leaves and the internal core in the case of repaired specimens. In fact, if the inner part and outer leaves are not collaborating, this induces a greater part of the load to be carried

by the external leaves. Consequently, this can explain the premature appearance of cracks in the repaired elements.

Finally, the analysis of overall compression behaviour manifested some constants on all the specimens in question. In fact, the first modification of the deformation trend is manifested at about 50% of compressive strength, while the widest strains occurred between 80% and the maximum attained vertical stress.
These considerations allowed oversimplification of the global compression behaviour using a piecewise linear function, with four characteristic points. As a consequence, since the vertical stress was normalized during the analysis, a better calibration of these phases may be obtained using more data. This relationship could be applied in a more general case of masonry, for which the compressive strength is known, in order to provide an indication of the stress level at which the first linear phase and subsequent damage can occur.

Chapter 6

In-plane Cyclic Behaviour of Injected Stone Masonry Walls

In-plane cyclic tests provide important informations about mechanisms of failure, maximum displacement capacity, shear strength and other mechanical parameters, such as shear modulus and shear strain. Successive analyses supply further results about stiffness degradation, energy dissipation and viscous damping. The above mentioned parameters provide a basis for evaluating the effectiveness of this strengthening technique in the case of seismic actions. As expressed, the main aims are to examine mechanical strength and carry out energetic evaluations.

Cyclic shear compression tests will be discussed in this chapter. The adopted test set-up and a complete description of the specimens is reported in section 2.2.2. Previous similar experimental campaigns [Bernardini *et al.*, 1997; Galasco *et al.*, 2009b; Vasconcelos and Lourenço, 2009; Vasconcelos, 2005; Vintzileou and Miltiadou-Fezans, 2008], also carried out on specimens made with different materials [da Porto, 2005; Gouveia and Lourenço, 2007; Mosele, 2009; Tomaževič, 2000], constitute the basis of this experimental section. The results achieved during monotonic compression tests, presented in chapter 5, led to refining the test procedure and to determining experimental details. The testing method, instrumentation and results will be presented in the following sections.

6.1 Test procedure and instrumentation

The specimens were positioned in the test rig and a vertical pre-load was initially applied. After this preliminary phase, the horizontal displacement history was applied. The level of vertical stress, kept constant during the whole test, was chosen also on the basis of results achieved during compression tests, presented in chapter 5. On this basis and starting from the most typical mechanical strengths identified during the literature review (compare §1.2.2), the failure filed could be supposed. Furthermore, as suggested by some authors [Bosiljkov *et al.*, 2004; Tomaževič, 2000], the pre-compression levels may reasonably range between 15% and 30% of the compressive strength of specimens. A joined consideration of the above mentioned aspects led to employ these limits also in the present experimental investigation. As consequence, the applied stress levels were 1 N/mm^2 and 2 N/mm^2 and the resulting test matrix is as summarized in table 6.1. A more diffuse discussion on this will be presented in section 6.5, where the designed failure field will be verified on the basis of both experimental observations and results. Nevertheless, these rather high loads are mainly justified by:

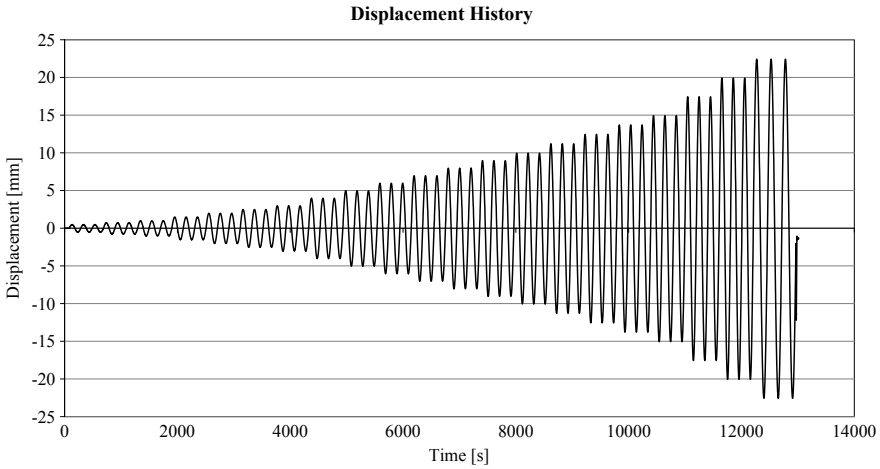

Figure 6.1: Example of applied displacement history.

Table 6.1: Pre-compression levels applied during shear compression tests, geometric properties and computed elastic modulus.

Specimen	σ'_0 N/mm^2	Thickness [mm]	Width [mm]	Height [mm]	Slenderness -	E [N/mm^2]
R2	1.0	320	1463	1221	0.8	4057
S2	2.0	325	1453	1370	0.9	2738
Specimen	σ'_0 N/mm^2	Thickness [mm]	Width [mm]	Height [mm]	Slenderness -	E [N/mm^2]
R4	1.0	320	913	1236	1.4	5513
S4	1.0	331	923	1275	1.4	6708
R5	2.0	321	930	1381	1.5	4640
S5	2.0	328	929	1381	1.5	4323

- Firstly, one of the principal aims of this experimental research is to investigate the influence of grout injection on the shear strength of multi-leaf masonries. Therefore, applying a higher stress level will force the shear failure mechanism also on slender specimens, in which the rocking or flexural behaviour is more probable if the vertical stress is low. This will lead to a deeper understanding of the overall behaviour of this kind of strengthened masonry structure.

- Secondly, one should remember that the tested specimens are representative of reduced scale elements, as discussed in section 2.1.1. On this basis, and as a consequence of the scale factor chosen to realize the model (see table 2.3), the stress level of the reduced specimen and that of the full scale element shall be equal. Hence, this stress level should be considered applied to a section with a mean overall depth of 50cm. However, in this case the stress results higher than that verifiable in real situations on historical stone masonry buildings [Binda *et al.*, 1999, 2007; Gardin, 2007]. In any case, the first reason prevails and warrants the choice.

Specimens, obtained from both repaired and strengthened specimens (figure 2.19), are characterized by two different slenderness ratios, approximately equal to 1.0 and

Table 6.2: Mean values of elastic modulus.

Considered Specimens	E [N/mm^2]
all	4663
R series	4736
S series	4590

1.5. Since these elements were recovered, even if they were taken from the same positions, their height was not perfectly equal and this caused a slight difference in slenderness factors.

Furthermore, during the preliminary phase of shear compression tests, consisting of the application of a vertical load to achieve the chosen precompression level, it was possible to evaluate the elastic properties of each panel. The results are summarized in table 6.1. As this table shows, elastic properties are characterized by a certain variation which seems to be dependent more on the applied vertical stress than on the masonry series. Table 6.2 confirms this observation and shows a very limited variation between the two series in question.

Shear compression tests were performed under displacement control, imposing increasing amplitudes at a frequency of 0.004Hz [Tomaževič and Velechovsky, 1992]. Each peak of displacement was repeated three times (figure 6.1). All tests were carried out up to the failure of specimens and the displacement testing control also allowed the examination of the softening phase.

The samples were instrumented with 20 potentiometric displacement transducers, with three different ranges (±50mm, ±150mm and ±200mm), and 10 LVDTs, with two lengths (±50mm and ±100mm). The instruments monitored the deformation of masonry panels and the relative horizontal displacement between the floor of the laboratory and the concrete base of the specimen but also between the masonry panel and both top and bottom bond beams. Two LVDTs, vertically fixed at the opposite edges of the concrete base, measured displacements due to the rotation of the bottom beam (figure 6.2). This monitoring allowed to detract the horizontal fictitious movements, due to the small rotation of specimens caused by the application of horizontal force, from the horizontal measured displacements. The effects of this elaboration on the measured displacements were generally limited (figure 6.3a) even if they could not be considered negligible, particularly in the case of squat specimens. This was due to a combination of effects caused by a thin vertical rubber layer, employed to allow perfect contact between the concrete base and the fixing system, with the higher acting horizontal forces (figure 6.3b). Further instruments, fixed to the upper part of each specimen, permitted the study the overall displacement capacity.

6.2 Failure modes

The specimens exhibited different overall behaviours during the execution of tests even if, on the other hand, similarities linked all the experiments. For instance, specimens with the same slenderness ratio and stress level showed comparable overall behaviours. Four different phases could be identified for each panel, depending on the ratio between the height and the width of sample and the applied vertical load:

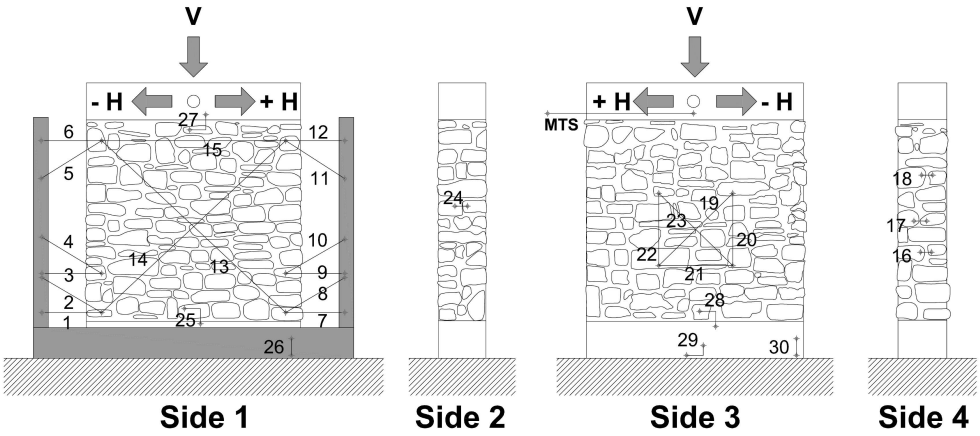

Figure 6.2: Instrumentation of a specimen and load application.

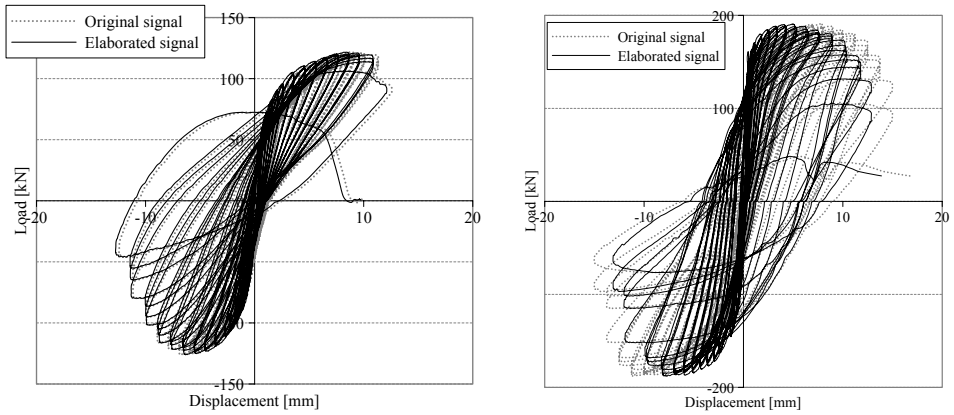

(a) Specimen R5: minimal effect due to the processing of the original signal.

(b) Specimen R2: large effect due to the processing of the original signal.

Figure 6.3: Comparison between the effects of depuration in two samples.

(i) The first identified phase is related to the opening of the first cracks. This phenomenon occurred on all specimens at a displacement level ranging between 1mm and 2mm, independently of both the pre-load applied and the slenderness of the element. These cracks appeared horizontally on the first or second mortar bed joint at about 10cm or 15cm from the bottom of the specimen.

(ii) After the opening of these cracks, the overall behaviour was different, according to the different typology of specimen. Both slender specimens with higher vertical stress, namely specimens S5 and R5, exhibited the beginning of diagonal oriented cracks due to shear mechanisms. Instead, slender specimens with a lower axial load, S4 and R4 samples, showed a crack pattern due to a rocking mechanism, highlighting sub-vertical cracks in the compressed toe because of bending. In all cases, these effects could be identified on panels in a displacement range varying between about 2mm and 4mm.

(iii) The previously described mechanisms developed on specimens up to the attainment of maximum lateral resistance, when an overall degradation could be identified and this represents the third phase of the observed experimental behaviour.

(iv) The final phase was characterized by the achievement of maximum horizontal displacement at which masonry panels completely failed. The majority of specimens exhibited a brittle collapse, anticipated by the pulling out of central parts of lateral edges (figure 6.4a).

In all cases, the first cracks occurred at the interface between mortar and stones in the lower part of specimen. However, as above described, the development of a crack pattern was different depending on the slenderness and the applied precompression level. Cracks in stones (figure 6.4a) occurred earlier on slender specimens with a higher vertical load than on other samples, even if on all panels this damage was clearly evident (figure 6.5).
Moreover, both slender specimens tested under low vertical stress exhibited the same overall behaviour before failure. Firstly, as above described, a rocking mechanism cracked the wall horizontally at about 15cm from the bottom of the panel. When this crack involved the whole width of samples and beyond the attainment of lateral resistance, the part above the breaking line became squat. Immediately after this, due to a shear mechanism, a deep diagonal crack suddenly apperared and, shortly afterwards, led to its collapse.
Furthermore, each specimen exhibited the beginning and the development of its characteristic failure mode but, when the damage was widely diffused and the panel was close to failure, sub-vertical cracks appeared (figure 6.4b). Therefore, over the attainment of lateral resistance, the effects of compression became noticeable. This caused the opening of cracks in transversal sides, due to the buckling of external layers of masonry, as already observed during compression tests (section 5.2).

The final remarkable observation focuses on the status of grout injection at the end of the test. In all cases, when the specimen failed, the separation of the outer layers was evident and the main damage was concentrated at the interface between the external leaves and the internal core, constituted by injected grout (figures 6.5 and 6.6). In several cases, after the collapse of the external stones, the core could be seen and it appeared almost undamaged, confirming its separation and independent behaviour from the stones. This was particularly evident at the bottom and at the top of panels, while the central part was destroyed. This explanation confirms failure based on the buckling of external leaves, being the easiest verifiable mechanism in

(a) **(b)**

Figure 6.4: Cracks occurring in stones (left) and the formation of sub-vertical cracks (right) on specimen R5.

(a) **(b)**

Figure 6.5: Examples of lateral cracks for specimens S5 (left) and R5 (right).

(a) **(b)**

Figure 6.6: Separation of outer layers on specimens R2 (left) and S2 (right).

the middle part of the specimen. Finally, even if the opening of cracks on transversal sides is influenced by stone interlocking, the panels of the "S" series seem to manifest this mechanism when the overall crack pattern is widely diffused, while "R" samples had earlier manifested this behaviour.

6.3 Test results and analyses

In this section, an overview of the main results obtained during the combined shear and compression tests are presented. Several elaborations are presented separately, for a clearer exposition, while overall observations, based on all processing, will be given in the conclusion.

On the basis of the exhibited failure mechanisms, presented in the previous section, four different limit states were identified to allow a more significant comparison of results at different identified phases. The limit states [Bosiljkov *et al.*, 2004] are defined in the following points:

- Flexural cracking (H_f,δ_f), characterized by the occurrence of horizontal cracks in the first or second mortar bed joint;
- Cracking limit state (H_{cr},δ_{cr}), defined by the occurrence of cracks typical of the established mechanism, characterizing the failure of the specimen. The shear or rocking mechanism depends on the slenderness of the panel and vertical applied precompression;
- Maximum resistance (H_{max},$\delta_{H,max}$), attainment of resisting lateral force;
- Ultimate limit ($H_{\delta,max}$,δ_{max}) achievement of maximum displacement of the wall before its collapse.

Since the first identified mechanism occurred between 1mm and 2mm for all specimens, independently of the slenderness ratio and applied vertical stress, it appeared as less important and the following analyses are based on a comparison of the last three Limit States.

6.3.1 Lateral load and displacement

The analyses presented in this section are based on elaborations obtained starting with the hysteretic behaviour exhibited by different specimens. The first considerations are focused on the lateral load versus the horizontal displacement relationship. Further observations are developed concerning the computed secant stiffness for each specimen, calculated as the ratio between the actual horizontal load and the corresponding horizontal displacement. These values are related to the effective stiffness of the wall, considered as the secant stiffness at the attained cracking limit ($K_e = H_{cr}/d_{cr}$). Moreover, the envelope of hysteresis loops completes the first elaborations of this experimental campaign.

Slender specimens subjected to lower vertical stress (σ'_0=1N/mm^2), namely S4 and R4, were characterized by a diffuse crack pattern in the bottom part of the panel. This damage, due to a rocking type of mechanism, started to occur at about 4mm, with a drift slightly lower than 0.30%. The remaining slender panels, S5 and R5, prestressed with a higher vertical load (σ'_0=2N/mm^2), showed the above described shear failure mechanism at a mean horizontal displacement and a mean drift respectively of 3.6mm and 0.27%, values slightly lower than that of 4 series. Therefore, independently of the level of the vertical load, both failure mechanisms occurred at similar values of force and displacement.
Squat specimens exhibited a different behaviour, since the initiation of cracks took place at displacement appreciably lower than that of previous ones. While at 1N/mm^2 (specimen R2) the shear mechanism can be clearly defined starting at 1.23mm, corresponding to 0.10% of drift, sample S2 manifested initial damage due to the mechanism at 2.19mm, corresponding to 0.16% of drift. This seems to indicate a relative influence of precompression in the case of squat specimens, even if panel S2 showed an anomalous behaviour due to the appearence of vertical cracks, mainly caused by a worse interlocking of stones.

Generally, the development of the crack pattern, occurring on each main side of the specimens, was different. Firstly, damage, as diagonal shear cracks for samples S5, R5 and R2, started in the weakest face, appearing on both mortar bed joints and stones, right from the beginning. Subsequently, at higher displacements, a similar overall behaviour occurred also on the opposite side. However, while cracks on

Table 6.3: Characteristic values of horizontal force, displacement and rotation angle at identified Limit States.

	Cracking limit			Maximum resistance			Maximum displacement		
Sp	H_{cr} kN	δ_{cr} mm	ϑ_{cr} %	H_{max} kN	δ_{Hmax} mm	ϑ_{Hmax} %	$H_{\delta max}$ kN	δ_{max} mm	$\vartheta_{\delta max}$ %
R2	151	1.23	0.10%	187	5.09	0.42%	147	11.76	0.96%
S2	221	2.19	0.16%	256	5.08	0.37%	225	9.60	0.70%
R4	71	3.73	0.30%	80	14.59	1.18%	75	24.67	2.00%
S4	75	3.55	0.28%	88	11.33	0.89%	71	22.01	1.73%
R5	108	3.59	0.26%	124	7.36	0.53%	97	11.09	0.80%
S5	110	3.86	0.28%	122	7.13	0.52%	108	9.81	0.71%

mortar appeared because of tension stresses, the stone crushed due to the action of a compression strut.

The attainment of maximum lateral resistance emphasized the effects of the previously established mechanism. Specimens S5 and R5, developed a well defined diagonal crack passing through the outer layers of multi-leaf masonry panels and they achieved a force of about 120kN at approximately 7mm and 0.50% drift. Slender specimens at a lower vertical stress of $1N/mm^2$ (S4 and R4) were clearly characterized by a rocking mechanism. This caused the formation of a horizontal crack, involving the whole specimen at about 15cm from the bottom, while the upper part rigidly rotated. The lower vertical stress allowed an overall displacement about two times greater than that of slender specimens at double precompression level. The maximum force was achieved respectively at about 11mm and 14mm. As a consequence, the mean drift proved to be doubled and equal to 1%.
Squat specimens achieved the maximum lateral force at a similar displacement of about 5mm and drift of 0.40%. Also in these cases, the attainment of maximum resistance Limit State was attended by the opening of wide diagonal cracks. In all cases, at maximum resistance Limit State, the crack pattern was widely diffused on the whole surface of each specimen, involving the main faces but also the vertical openings in the transversal sides. This behaviour was more evident in samples tested at $2N/mm^2$, namely S5, R5 and S2.

During the final part of the experiments, leading to the failure of specimens, a similar behaviour was observed for all panels. In the decreasing branch of the load-displacement curve, the mechanical characteristics of samples deteriorated and wide cracks appeared on transversal sides. Therefore, the failure mechanism established during the first part of the tests was affected by the compression mechanism of failure, particularly for the highest precompression level.
The above described results are summarized in table 6.3. Figures from 6.7 to 6.24 show the overall behaviour of each panel, presenting their typical failure mode, their hysteresis loops and both envelopes, as well as the positive and negative branch of hysteretic behaviour.

6.3.2 Hysteresis envelopes and ductility ratios

Figure 6.25 compares the afore-mentioned envelopes of hysteretic loops and clarifies the differences in the overall behaviours of different series.

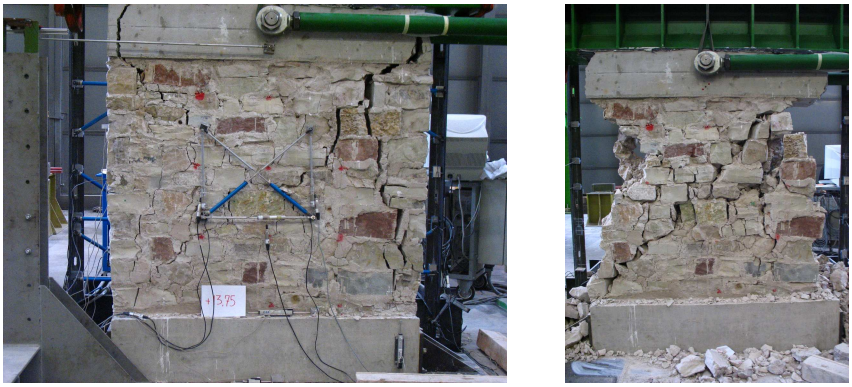

Figure 6.7: Specimen R2 at failure.

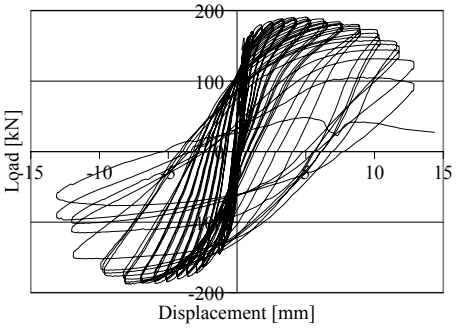

Figure 6.8: R2: hysteresis loops.

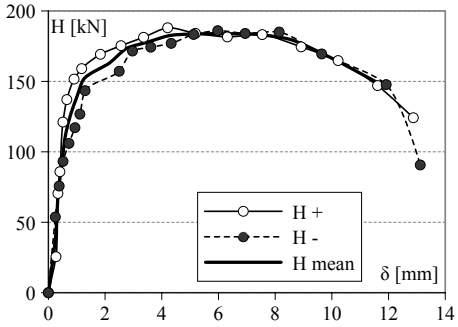

Figure 6.9: R2: hysteresis envelopes.

Figure 6.10: Specimen R4 at failure.

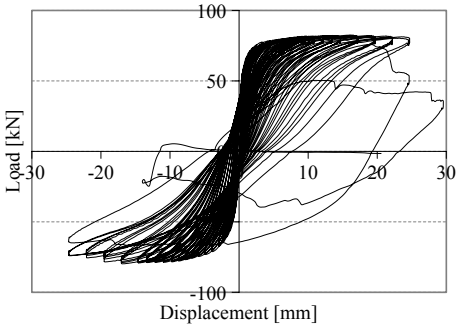

Figure 6.11: R4: hysteresis loops.

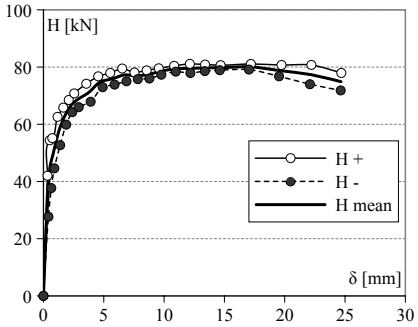

Figure 6.12: R4: hysteresis envelopes.

Figure 6.13: Specimen R5 at failure.

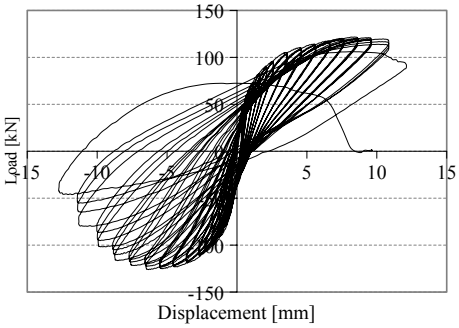

Figure 6.14: R5: hysteresis loops.

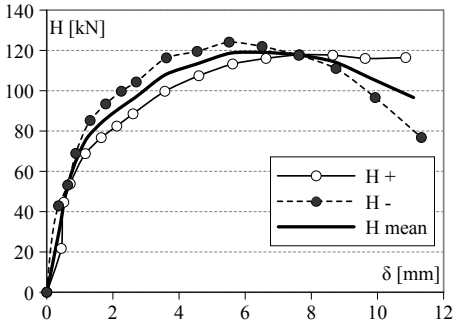

Figure 6.15: R5: hysteresis envelopes.

Figure 6.16: Specimen S2 at failure.

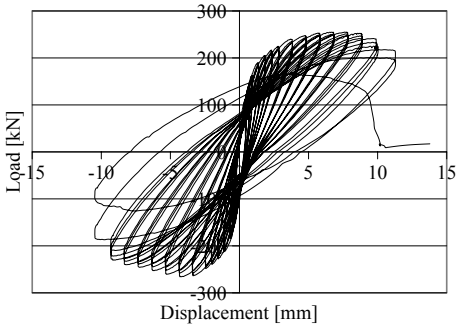

Figure 6.17: S2: hysteresis loops.

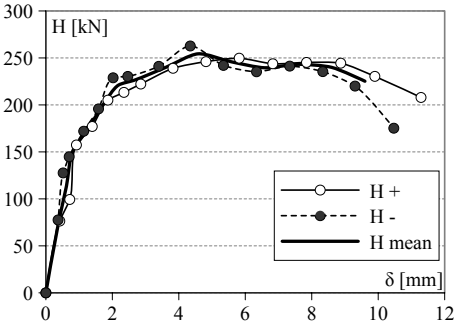

Figure 6.18: S2: hysteresis envelopes.

Figure 6.19: Specimen S4 at failure.

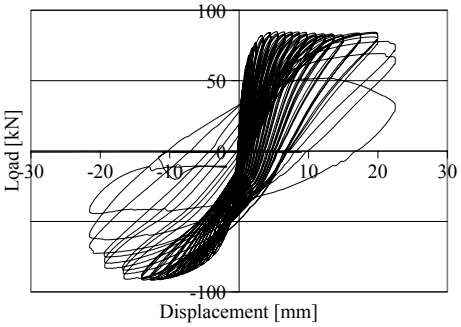

Figure 6.20: S4: hysteresis loops.

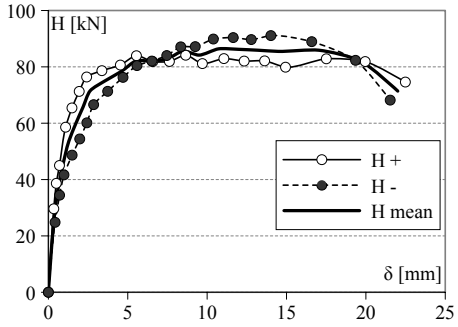

Figure 6.21: S4: hysteresis envelopes.

Figure 6.22: Specimen S5 at failure.

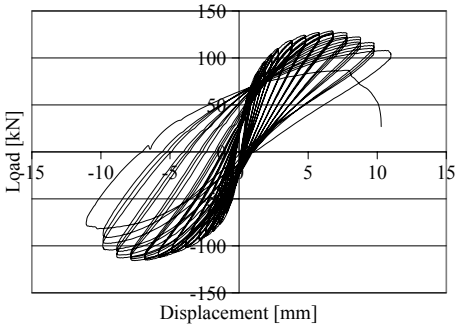

Figure 6.23: S5: hysteresis loops.

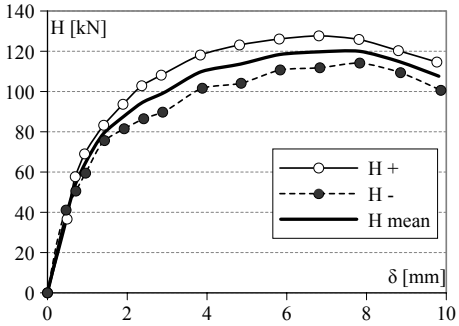

Figure 6.24: S5: hysteresis envelopes.

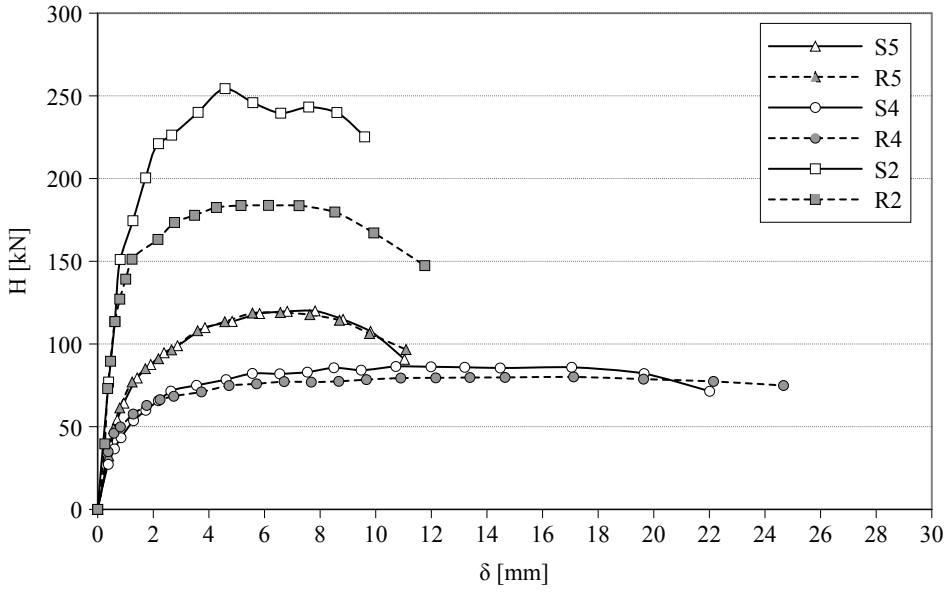

Figure 6.25: Envelopes of hysteresis loops for all the tested specimens.

As a rule, slender elements with a low vertical load, namely series "4", in which the rocking mechanism prevails, are characterized by low horizontal forces and higher horizontal displacements. Moreover, in the load-displacement curve, two widely different phases can be found: a first part with high stiffness, followed by a sudden increase of lateral displacement at an almost constant load.
Slender specimens of series "5" exhibited an initial stiffness slightly higher than that of series "4". Instead, both squat elements behave similarly in the linear phase of the experiment while, with higher vertical stress, S2 attained about 250kN instead of 190kN of R2 in the second part. Series "5" showed a second part of the curve and ultimate displacements similar to those of squat elements, even if with a lower lateral resistance.
Finally, one should consider that the behaviours of "R" and "S" specimens, referred to the same position, i.e. 2, 4 and 5, are very close to each other, highlighting any substantial difference in the overall curve and, particularly, in terms of initial stiffness, maximum achieved lateral resistance and maximum displacement.

The lateral resistance degradation and the displacement capacity provide important coefficients to evaluate the change in the overall behaviour of specimens. For this reason, resistance indicators and displacement capacity indicators are calculated as the ratio of the considered magnitude at two different Limit States. The most common ratios, reported in table 6.4, are respectively: H_{cr}/H_{max}, $H_{\delta max}/H_{max}$, $H_{\delta max}/H_{cr}$, with regard to the acting horizontal force, and $\delta_{cr}/\delta_{Hmax}$, $\delta_{max}/\delta_{Hmax}$ and δ_{max}/δ_{cr}, concerning deformation capacity. Figures 6.26 and 6.27 give a graphical representation of these ductility ratios. Some observations can be drawn on the basis of these results and are presented in the following.

Firstly, the corresponding resistance ratios of specimens tested at lower and higher vertical stress are very close. This means that, even if the failure mode can change between the two mentioned groups, the ratio almost crucial points of envelopes becomes about constant. The cracking limit state always occurred between 80% and 90% of the resistance force (H_{cr}/H_{max}). This means that, when the mechanism

Table 6.4: Resistance indicators and displacement capacity indicators for all the tested specimens.

specimen	$\frac{H_{cr}}{H_{max}}$	$\frac{H_{\delta max}}{H_{max}}$	$\frac{H_{\delta max}}{H_{cr}}$	$\frac{\delta_{cr}}{\delta_{Hmax}}$	$\frac{\delta_{max}}{\delta_{Hmax}}$	$\frac{\delta_{max}}{\delta_{cr}}$
σ'_0=1N/mm^2						
R2	0.81	0.79	0.97	0.24	2.31	9.53
R4	0.89	0.93	1.05	0.26	1.69	6.61
S4	0.86	0.81	0.95	0.31	1.94	6.19
average	0.85	0.85	0.99	0.27	1.98	7.45
σ'_0=2N/mm^2						
S2	0.86	0.88	1.02	0.43	1.89	4.39
R5	0.87	0.78	0.89	0.49	1.51	3.09
S5	0.90	0.88	0.98	0.54	1.38	2.54
average	0.88	0.85	0.96	0.49	1.59	3.34

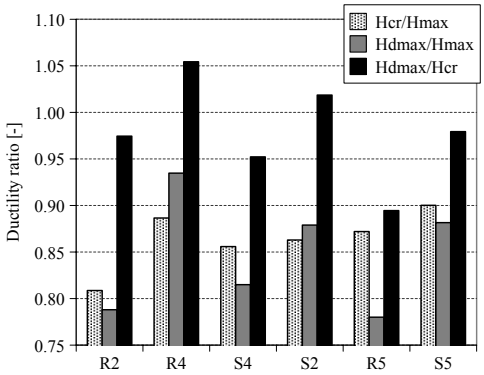

Figure 6.26: Histogram of resistance indicators.

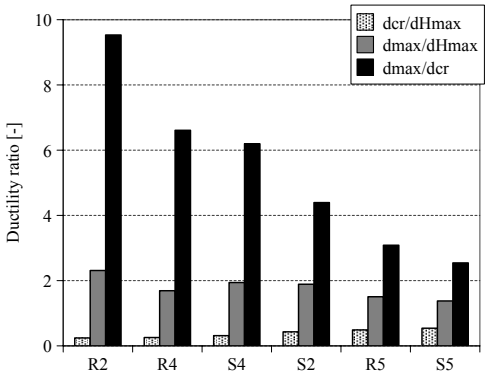

Figure 6.27: Histogram of displacement capacity indicators.

typical of each specimen is manifested, the lateral resistance of the wall is not achieved, even if the residual resistance is quite low.
Furthermore, all specimens exhibited a similar decrease after the attainment of the maximum horizontal force. The second resistance indicator ($H_{\delta max}/H_{max}$) underlines a mean reduction equal to 15% of the force measured when the specimens fail. This evidence underlines the relative resistance degradation of both kinds of specimen.
Finally, the third resistance indicator ($H_{\delta max}/H_{cr}$) is close to the unit, confirming the capacity of specimens to sustain a load decrease of about 15%.

The displacement capacity indicators exhibited an overall behaviour different from that of the resistance indicators. In some cases, the values obtained from samples subjected to dissimilar vertical stresses are widely different.
The first displacement indicator ($\delta_{cr}/\delta_{Hmax}$) for panels loaded with a vertical stress of 1N/mm^2 is about half that calculated for samples subjected to higher axial stress, respectively 27% and 49%. This fact underlines how, even if the difference between load at the cracking limit and at maximum resistance is restricted, great displacements are necessary to attain the maximum resistance Limit State.
Further significant information is provided by the $\delta_{max}/\delta_{Hmax}$ ratio. Both precom-

pression levels showed similar mean results: 1.59, for samples subjected to $2N/mm^2$, and 1.98, for specimens with $1N/mm^2$ of vertical stress. As expected, a lower precompression level allows a large displacement before the collapse of the wall. One should also note that this ratio is higher for squat panels than for slender ones, independently of the applied vertical load. This seems to indicate that squat specimens are able to sustain greater deformations before collapse, even if figure 6.25 showed how slender specimens permit higher absolute displacements.
Additional information, related to the risen failure mechanism, is provided by the last capacity indicator (δ_{max}/δ_{cr}). As expected, specimens subjected to a lower vertical stress exhibited a greater ratio, since σ'_0=$1N/mm^2$ allowed the rocking mechanism. Actually, these elements (R2, S4 and R4) indicated a quite large resistance after the beginning of cracks, related to the main failure mechanism.
This was not the case for walls with higher precompression: samples S2, R5 and S5, dominated by a shear mechanism, presented a more brittle failure. In both the afore-mentioned groups, squat specimens showed values over the computed average, confirming that they are able to sustain both higher loads and deformations.

Further observations can be obtained from the analysis of other transducers, providing more information on the overall behaviour of specimens and local problems of injected multi-leaf stone masonry.
Displacement sensors, fixed on transversal sides of specimens, allowed the lateral crack opening to be controlled. Figure 6.28 shows the opening of cracks on the two opposite heads of each specimen.
As described above, the charts clarify how the overall behaviour is widely influenced by the localised position of stones and localised mechanical characteristics. In fact, graphs show a very different behaviour of the left and right sides of each wall.
However, when heavier damage is induced on the panels, specimens subjected to higher vertical stresses manifest a faster degradation and opening of cracks.
Moreover, most specimens exhibit a large opening of cracks also before the attainment of maximum lateral resistance, particularly on the left side. Furthermore, over the achievement of $\delta_{H,max}$, several specimens manifest a wide increase in damage.
These measurements and observations confirm the remarks concluded during the experiments and emphasize the overall behaviour of this masonry typology. In fact, grout injection allows a monolithic behaviour in the first part of the tests, while at increased lateral displacements external layers start to behave independently.

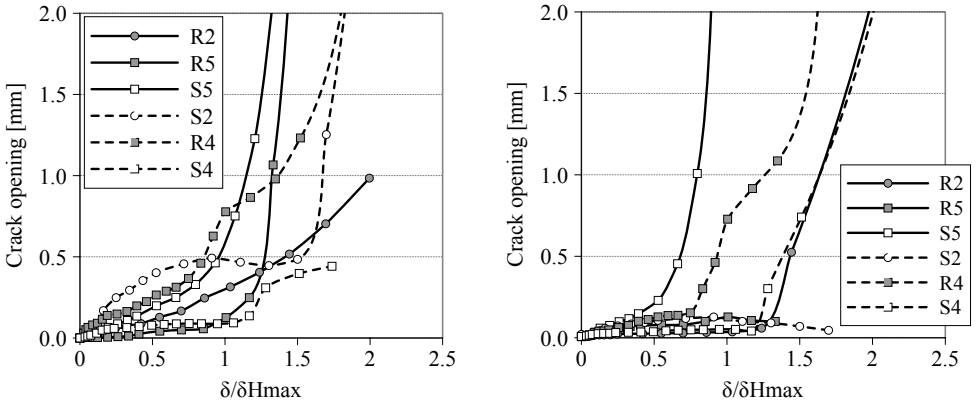

Figure 6.28: Lateral crack opening as a function of $\delta/\delta_{H,max}$ of both sides.

6.3.3 Stiffness degradation and Limit States

Different behaviours of specimens are also evaluated in terms of both stiffness degradation and, starting also from these results, identification of fundamental Limit States for each panel. The stiffness is computed as the secant value, calculated as the ratio between the actual horizontal force (H) and its related displacement (δ). The positive and negative parts of load-displacement curves were considered separately and a final mean value was considered for comparisons. Charts presented in this section are normalized as a function of ratios between the actual and the effective stiffness (K/K_{cr}) in the y-axis and the ratio between the actual displacements and that attained at maximum resistance (δ/δ_{Hmax}) in the abscissae.

The observation of all charts regarding stiffness degradation clearly underlines how the right and left parts of each specimen behave in a slightly different manner. Actually, the stiffness, computed in the positive and negative branches of envelope curves, shows a different limit in the displacement ratio, attaining values that, in some cases, present substantial differences. This confirms the observations carried out for positive and negative parts of envelop curves (figures 6.9, 6.12, 6.15, 6.18, 6.21, 6.24), where differences were also noted. On the other hand, both curves regarding the stiffness manifest a similar decreasing trend.
All these phenomena can be explained with in-depth experimental observation. A simple examination of the panels before the tests highlights their strong asymmetry, regarding the masonry texture, and this caused the previously described behaviour. During experiments, essential differences were also noted in the formation of the crack pattern (section 6.2). For instance, the first cracks occurred at different displacement levels on the left and right parts of samples. This means that the cracking point, due to a shear or rocking mechanism, depending on the precompression level and slenderness of specimens, was fixed at two different displacement steps and this behaviour amplifies the difference of the δ/δ_{Hmax} ratio.
The manifest heterogeneity of the masonry in question is reflected in two main consequences noticeable from the above mentioned charts. For all specimens, the stiffness computed during the first hysteresis cycles of small amplitude, often with the same displacement peak, shows a high variation (e.g. figures 6.35 and 6.39). This may be due to the settlement of masonry, which needs some cycles before achieving a stable behaviour. Furthermore, in the case of panels R2 and R5 (figures 6.35 and 6.39) the settling of materials caused a noticeable increase in stiffness between the first and second step of displacement history. Over this value, the behaviour was completely similar to that observed for other specimens. One should also notes that the previously explained aspects are more evident for the "R" series.

Further observations can be drawn also on the basis of different slenderness ratios and vertical stress applied to the tested specimens.
Both squat specimens highlighted a staring stiffness ratio K/K_{cr} lower than that exhibited by slender specimens. However, the absolute values of stiffness are clearly higher on squat specimens than on slender ones. The combination of these leads to observe that cracking limit is before achieved by squat elements, as confirmed by experimental remarks and figure 6.42. Moreover, vertical axial stress influenced S2 and R2 samples differently. The panel with lower precompression (R2) seems to degrade more rapidly than the other one but it succeeds in sustaining a higher overall decrease (figure 6.42) even if these differences are limited.

The overall behaviour exhibited by slender specimens reflects the behaviour described for squat samples. In addition, the parallelism regarding observations on

precompression effects is respected. In this case, the faster degradation of stiffness for panels with a lower vertical stress, namely S4 and R4, can be justified by the development of the rocking mechanism. This causes an expected attainment of the cracking point but a great displacement at failure, as confirmed by the ductility capacity indicator δ_{max}/δ_{cr}.
On the contrary, slender specimens with a higher vertical load do not manifest a substantial difference in their overall behaviour before and after the achievement of the cracking point and they fail in a more sudden way.

Figure 6.41 clearly indicates how the applied vertical load induces a different behaviour on samples with the same slenderness ratio. Actually, one can observe as the higher the precompression level, the faster the stiffness degradation. Furthermore, this figure also underlines any substantial difference in the results of this analysis for strengthened and repaired specimens.

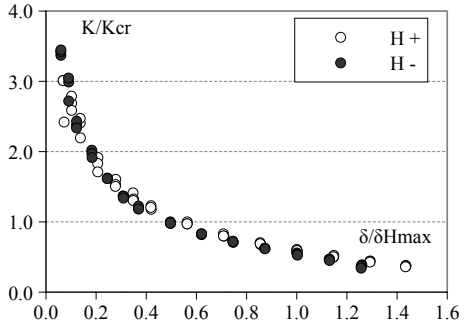

Figure 6.29: S5: Stiffness degradation.

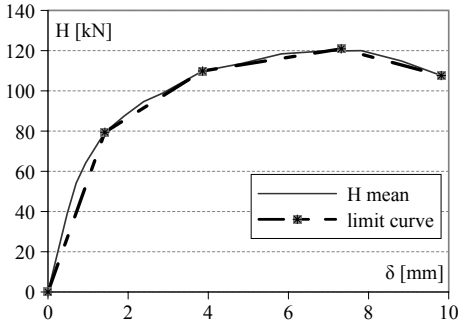

Figure 6.30: S5: Limit States.

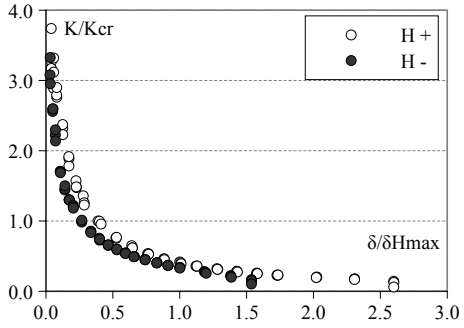

Figure 6.31: S4: Stiffness degradation.

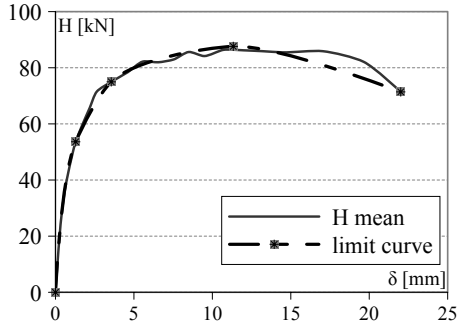

Figure 6.32: S4: Limit States.

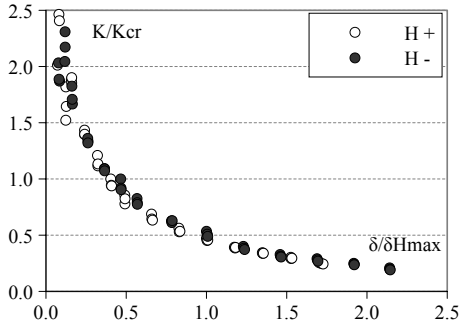

Figure 6.33: S2: Stiffness degradation.

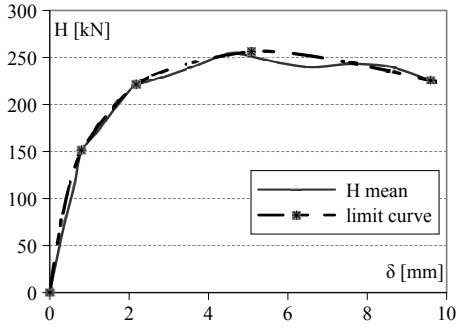

Figure 6.34: S2: Limit States.

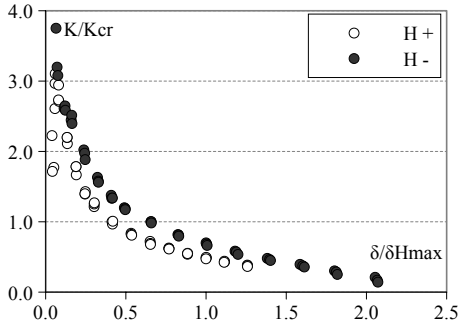

Figure 6.35: R5: Stiffness degradation.

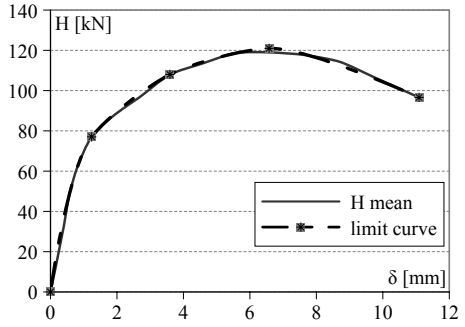

Figure 6.36: R5: Limit States.

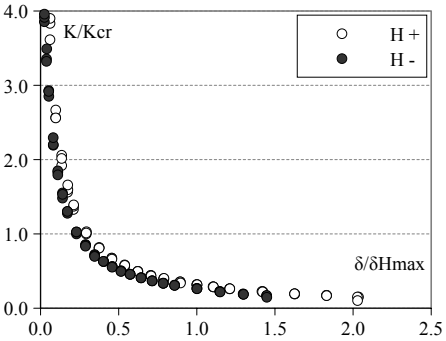

Figure 6.37: R4: Stiffness degradation.

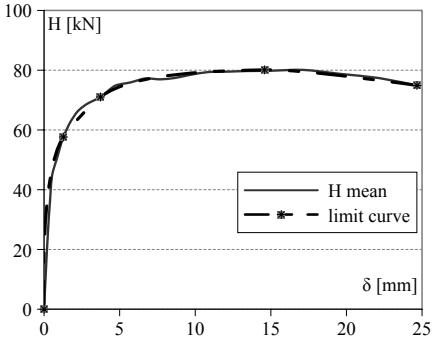

Figure 6.38: R4: Limit States.

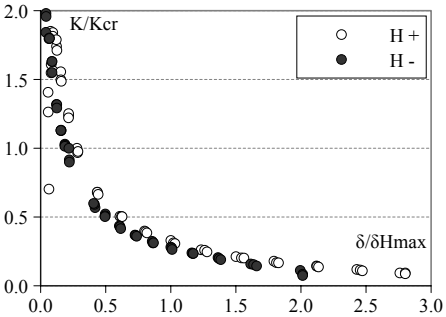

Figure 6.39: R2: Stiffness degradation.

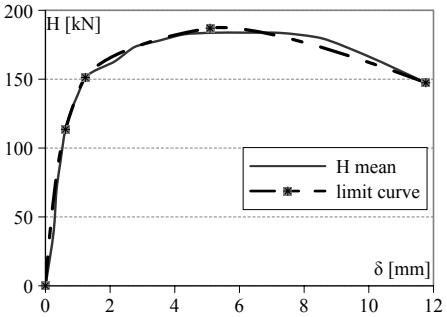

Figure 6.40: R2: Limit States.

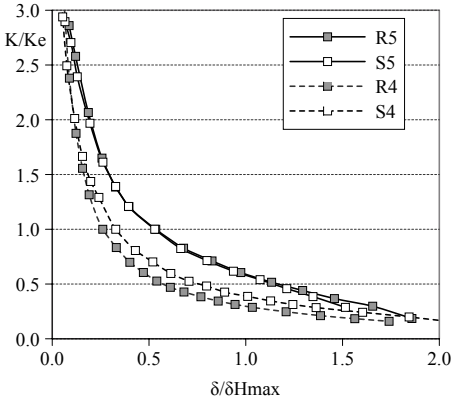

Figure 6.41: Trend of stiffness degradation for slender specimens.

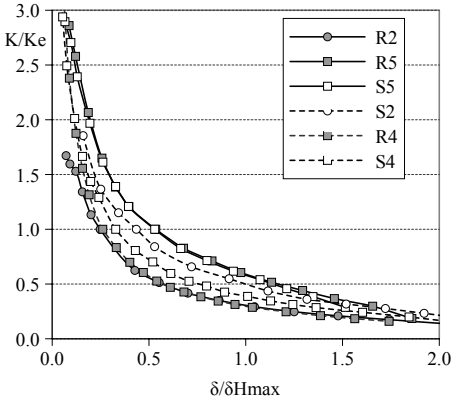

Figure 6.42: Comparison of the stiffness degradation of all specimens.

On the contrary, figure 6.42 shows that the slenderness ratio has less influence than the applied vertical load. In fact, the squat specimen at lower precompression, namely R2, manifests a trend in decreasing stiffness very close to that of slender samples subjected to low vertical stress. Moreover, the squat panel (S2) and slender specimens, tested at a higher vertical load, behave similarly.

In all cases, the Limit State curves [Bosiljkov *et al.*, 2004] are able to provide a good oversimplification of the overall behaviour of masonry specimens (figures 6.30, 6.32, 6.34, 6.36, 6.38, 6.40).

6.3.4 Energy dissipation and viscous damping

Important information is provided by the analysis of energies within the studied system and the related viscous damping. A brief summary is presented as follows. The parameters considered for this analysis are input energy (E_{inp}) and dissipated energy (E_{hys}). E_{inp} represents the work done to deform the wall and depends on the input displacement history, employed during the tests. This quantity is represented by the area within the hysteresis loop A_{hys} between two consecutive displacement peaks. The general expression for the determination of this energy is given by:

$$\Delta E_i = \int_{(H=0)_i}^{(H=0)_{i+1}} dE \tag{6.1}$$

The values of the input and the dissipated energy can be found by substituting, in the second part of equation 6.1, respectively the expression given by formulations 6.2 and 6.3:

$$dE_{inp} = \begin{cases} 0, & \text{if } Hdu \leq 0 \\ Hdu, & \text{if } Hdu > 0 \end{cases} \tag{6.2}$$

$$dE_{hys} = Hdu \tag{6.3}$$

Considering the input and dissipated energy, from the beginning of the test until a certain hysteretic cycle with the amplitude of displacement in question, means integrating previous quantities:

$$E_{inp\,/\,hys} = \sum_{i=1}^{k} \int_{(H=0)_i}^{(H=0)_{i+1}} dE_{inp\,/\,hys} \tag{6.4}$$

The ratio between the input and dissipated energy, E_{inp}/E_{hys}, as well as the coefficient of equivalent viscous damping ξ, is an indicator of the energy dissipation capacity of the specimens. This coefficient is defined, per each loading cycle, as the ratio between the energy dissipated in that cycle, which is again the area of the hysteresis loop (A_{hys}) and the input potential energy E_p. The general expression is presented by the following equation:

$$\xi = \frac{A_{hys}}{2\,\pi E_p} \tag{6.5}$$

where the potential energy E_p is calculated on the basis of the displacement amplitude and horizontal force H at any cycle:

$$E_p = \frac{1}{4}\,(H_+ - H_-)\,(d_+ - d_-) \tag{6.6}$$

Table 6.5 summarizes the input and dissipated energy at the identified Limit States. Similarly, table 6.6 provides the values of equivalent viscous damping calculated using the previously described method. Figures 6.43 and 6.44 report the same parameters in a graphical form.

The values of the ratio between input and dissipated energy are generally high but they are also characterized by a wide variation. These ratios range between an initial maximum value up to 80% and attain minimum ratios of about 30%. Despite the limited reliability of values obtained from first hysteresis cycles, due to their great variability caused by the settlement of materials, the energy ratios can be considered effectively in a range between 60% and 30%.
Usually, specimens of the "S" series exhibited an initial energy ratio slightly higher than that computed for "R" samples; while strengthened panels achieve about 80%, repaired ones settle between 60% and 70%. Furthermore, the range of variation for "S" panels is wider. A further characteristic, that links the overall behaviour of most analyzed cases, is a general decrease of the ratio during the first part of the test, up to the minimum values, corresponding to the attainments of lateral resistance. Beyond this phase, the energy ratio shows a limited increase up to failure.
The trend of results achieved with this analysis can be read in the light of comments drawn in previous sections. In fact, the energy trend behaves similarly to stiffness degradation. Corresponding panels, obtained from the same position but in a different series, show alike curves with slight differences.

Squat specimens demonstrate a limited interval of energy variation (figure 6.57). However, while the R2 specimen is able to increase the ratio over the achievement of lateral resistance, S2 shows a plateau. This may be due to the high vertical stress level applied, which caused the masonry failure when a wide crack pattern appeared in the specimen.

The trend of the slender specimen seems to depend on the precompression level (figure 6.58). If a low vertical stress is applied, the ratio between the dissipated and input energy shows a fast decreasing during the first millimetres of displacement. Beyond this interval, the ratio becomes almost constant, without any final increase. Furthermore, the main decrease is concentrated between the beginning of the test and the achievement of cracking point, i.e. the rocking mechanism for the elements in question.

Table 6.5: Cumulative input and dissipated energy at shear cracking, maximum resistance and at collapse.

Sp	Cracking limit			Maximum resistance			Maximum displacement		
	E_{hys} kNmm	E_{inp} kNmm	$\frac{E_{hys}}{E_{inp}}$ %	E_{hys} kNmm	E_{inp} kNmm	$\frac{E_{hys}}{E_{inp}}$ &	E_{hys} kNmm	E_{inp} kNmm	$\frac{E_{hys}}{E_{inp}}$ %
R2	1349	2852	47.3%	6720	14768	45.5%	32959	56379	58.5%
S2	3090	5044	61.3%	9586	17757	54.0%	28680	51386	55.8%
R4	1412	3458	40.8%	11193	34883	32.1%	21855	65094	33.6%
S4	1157	2883	40.1%	7482	22326	33.5%	22808	55604	41.0%
R5	2164	4488	48.2%	5988	13178	45.4%	15191	29616	51.3%
S5	2070	4537	45.6%	6392	14677	43.6%	12564	25858	48.6%

Table 6.6: Values of equivalent viscous damping at shear cracking, maximum resistance and at collapse.

	Cracking limit	Maximum resistance	Maximim displacement
specimen	ξ_{cr} %	ξ_{Hmax} %	$\xi_{\delta max}$ %
R2	12.42%	12.27%	30.39%
S2	13.04%	11.58%	16.02%
R4	9.56%	7.73%	10.22%
S4	8.10%	7.43%	21.36%
R5	11.14%	11.13%	17.64%
S5	9.63%	11.12%	16.62%

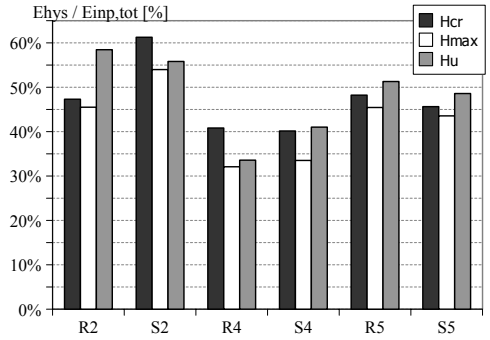

Figure 6.43: Energy ratio for all specimens at different limit states.

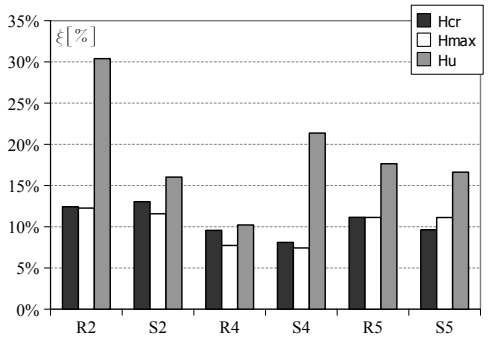

Figure 6.44: Viscous damping for all specimens at different limit states.

Instead, in the case of a higher vertical load, the main initial decrease develops during a longer phase until lateral resistance is attained. This is reflected in the fact that no plateau can be seen on the curve. Over the attainment of minimum of energy ratio, a slight increasing of about 10% is computed. However, one should remember that this experimental configuration, depending on the chosen the slenderness ratio and applied vertical stress, leads to a brittle failure.
Moreover, figure 6.58 once again confirms as the results provided by the strengthened and repaired specimens are very similar and no substantial difference can be seen.
The overall behaviour manifested by the energy trend seems to be clearly dependent on the applied vertical precompression level (figure 6.58), as in the case of stiffness analysis. However, the obtained results highlight that the slenderness ratio also has a certain influence. For instance, the lower the slenderness ratio, the higher the energy dissipation capacity, with the same vertical stress. In fact, R2 behaves similarly to the corresponding slender specimens under lower precompression up to the cracking point, while over this lateral displacement the overall behaviour is similar to slender specimens under a higher vertical load. Finally, S2 manifests a further different trend, unlike the other samples.

The trend of equivalent viscous damping is similar to that reported for the energy ratio. Initial values, instantly very high because of the settlement of materials, are characterized by a limited reliability, due to the previously mentioned causes, and they are higher than 20%. Viscous damping can be considered lower than 20%, which means considering results over the first displacement step.

Squat specimens exhibited the highest values and both samples manifested a similar behaviour (figure 6.59). The initial damping is about 20%, while a subsequent decreasing up 10%, corresponding to the attainment of lateral resistance, can be seen. Finally, the damping values settle approximately at 20%. In this case, as described for the energy trend, the specimen with lower precompression, namely R2, manifests an initial fast decrease followed by a plateau, with the critical point when the cracking limit is identified. Instead, the S2 sample, with higher vertical stress, presented a minimum corresponding to the point of lateral resistance. Both specimens exhibit a final increase in damping values, even if this rise occurs just close to the failure, when the specimen is completely crushed and a greater load or displacement can be sustained.

Slender specimens behave similarly (figure 6.60), since they show a different trend depending on the applied vertical load and, therefore, on the characteristic failure mode. As alredy showed in previous analyses, equivalent viscous damping also depends on the applied vertical stress (figure 6.60), even if the difference in values in the main part of each test is very limited. Differences varying the vertical load can be seen in the first and last part of curves. During the initial phase, a lower precompression induces a faster decrease in damping values. On the other hand, at the end of experiments, lower precompression allows a higher capacity displacement, while R5 and S5 show a brittle and premature failure. Lastly, a few samples also presented scattered results in the final part of the experiment, probably due to the incipient failure of the panel.

In conclusion, table 6.7 presents the energy dissipation indicators ($I_{E,dis} = E_{hys}/Einp$) for slender specimens at the identified limit states, considering different applied vertical stresses. Series "5" manifests higher values than series "4" on both dissipation indicators and equivalent viscous damping, confirming the above described observations. Instead, if strengthened and repaired panels are considered separately (table 6.8), any consistent difference can be underlined. On the contrary, the computed damping ratio seems to be independent from the vertical stress applied to samples (table 6.7), while a noticeable variation can be seen between the strengthened and repaired panels (table 6.8).

Table 6.7: Dissipation indicators and equivalent viscous damping at different limit states divided per vertical stress level.

Vertical stress	Cracking limit		Maximum resistance		Maximum displacement		$\frac{(I_{E,dis})_{du}}{(I_{E,dis})_{cr}}$	$\frac{\xi_{du}}{\xi_{cr}}$
N/mm^2	$(I_{E,dis})$	ξ	$(I_{E,dis})$	ξ	$(I_{E,dis})$	ξ		
1	0.40	8.8%	0.33	7.6%	0.37	15.8%	0.92	1.79
2	0.47	10.4%	0.44	11.1%	0.50	17.1%	1.06	1.65

Table 6.8: Dissipation indicators and equivalent viscous damping at different limit states for slender elements divided per series.

	Cracking limit		Maximum resistance		Maximum displacement		$\frac{(I_{E,dis})_{du}}{(I_{E,dis})_{cr}}$	$\frac{\xi_{du}}{\xi_{cr}}$
series	$(I_{E,dis})$	ξ	$(I_{E,dis})$	ξ	$(I_{E,dis})$	ξ		
R	0.45	10.4%	8590.36	9.4%	0.42	13.9%	0.95	1.35
S	0.43	8.9%	18501.47	9.3%	0.45	19.0%	1.04	2.14

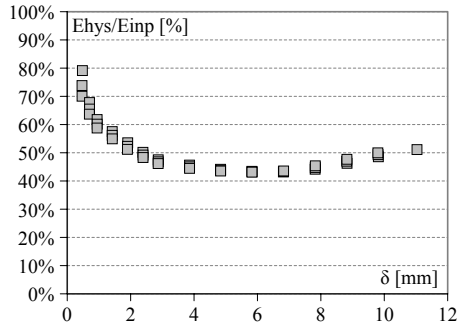

Figure 6.45: S5: Dissipated/Input Energy ratio vs displacement.

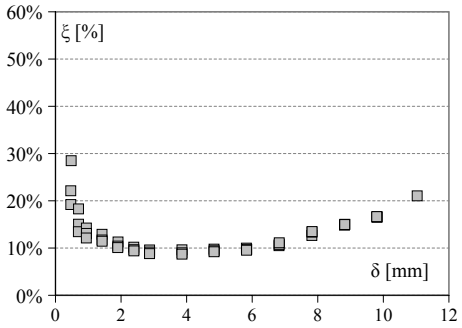

Figure 6.46: S5: Viscous damping vs displacement.

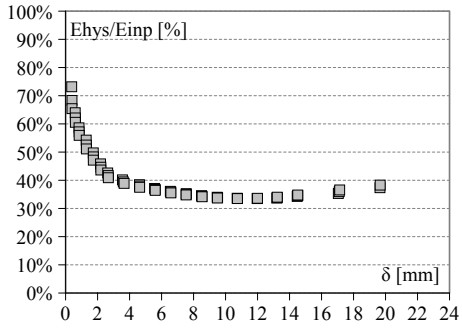

Figure 6.47: S4: Dissipated/Input Energy ratio vs displacement.

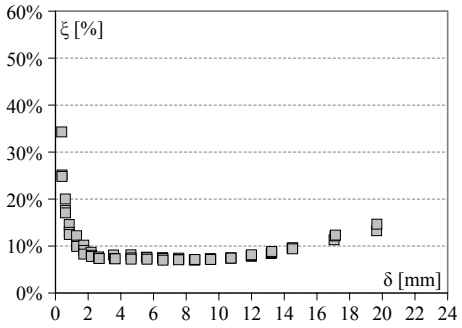

Figure 6.48: S4: Viscous damping vs displacement.

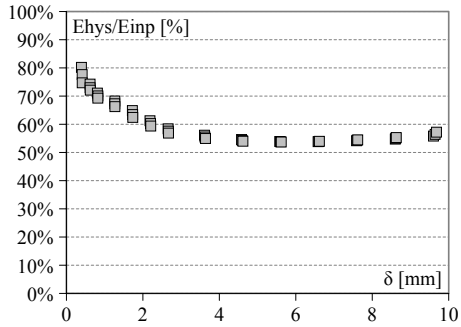

Figure 6.49: S2: Dissipated/Input Energy ratio vs displacement.

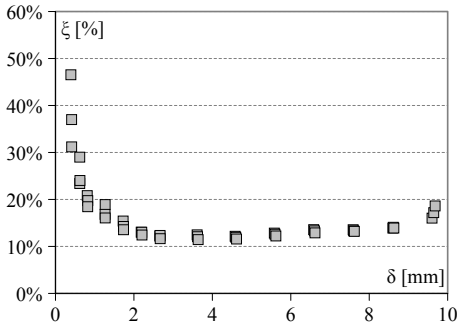

Figure 6.50: S2: Viscous damping vs displacement.

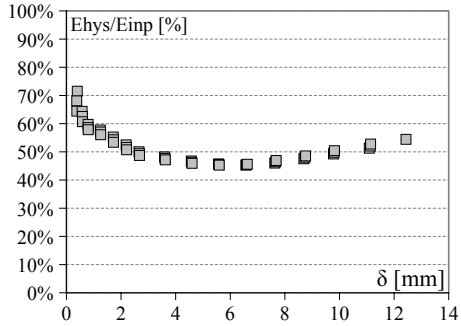

Figure 6.51: R5: Dissipated/Input Energy ratio vs displacement.

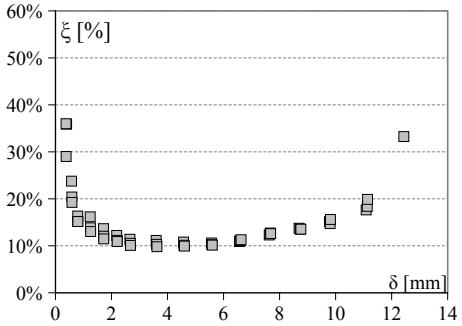

Figure 6.52: R5: Viscous damping vs displacement.

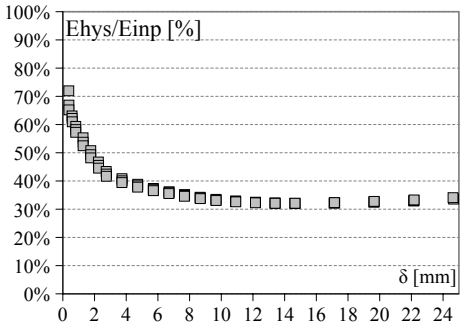

Figure 6.53: R4: Dissipated/Input Energy ratio vs displacement.

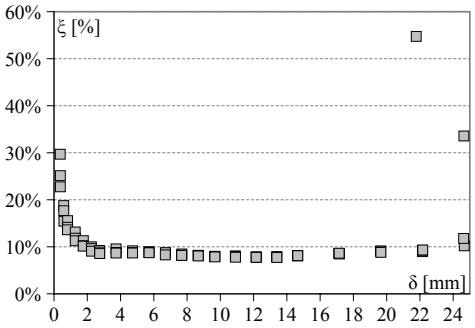

Figure 6.54: R4: Viscous damping vs displacement.

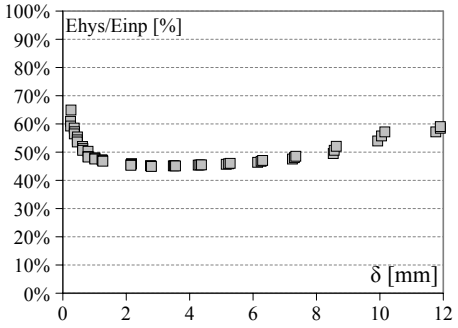

Figure 6.55: R2: Dissipated/Input Energy ratio vs displacement.

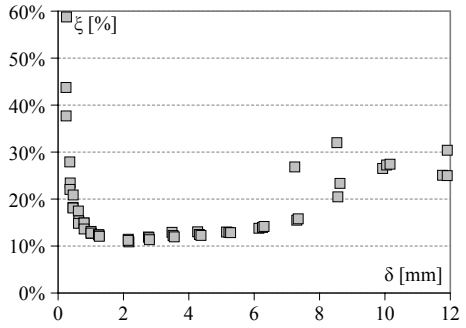

Figure 6.56: R2: Viscous damping vs displacement.

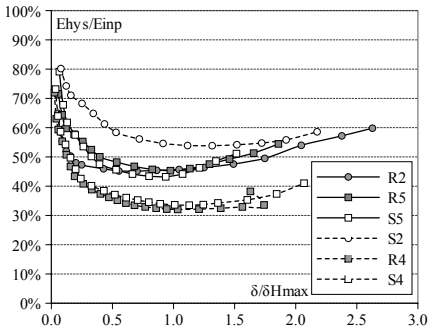

Figure 6.57: Comparison of Energy dissipation of all specimens.

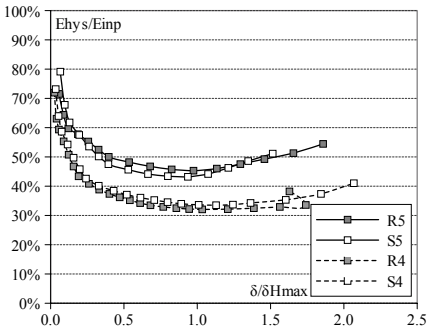

Figure 6.58: Trend of Energy dissipation for slender specimens.

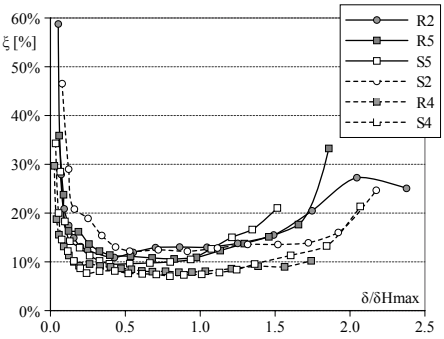

Figure 6.59: Comparison of Energy dissipation of all specimens.

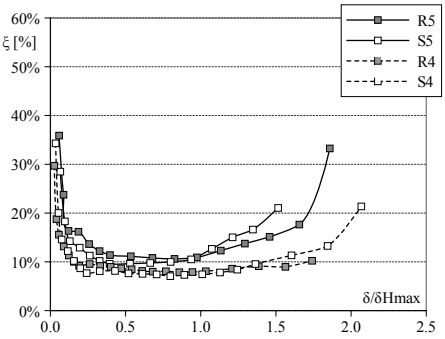

Figure 6.60: Trend of Energy dissipation for slender specimens.

6.4 Evaluation of Mechanical Parameters

Shear compression tests allowed mechanical parameters to be estimated, characterizing the investigated masonry typology. The preparatory phase, namely the application of vertical precompression up to the selected stress level on each panel, permitted the elastic modulus of masonry to be estimated. On the other hand, data collected during the experiments provided in-depth knowledge about shear characteristics, namely the maximum allowable shear stress and shear modulus, and further mechanical parameters.

Elastic modulus of masonry was evaluated using the methodology presented in chapter 5, where this mechanical property was computed between 10% and 40% of compressive strength. However, since the higher stress level was not achieved in the pre-load phase, the Young's modulus was computed between the unload state and the maximum attained vertical stress, before the application of lateral displacement. The results are presented in table 6.9. The average of all data is equal to 4663N/mm^2, even if different trends should be distinguished. In fact, one should note as the lower the applied vertical tress, the higher the computed elastic modulus. More reliable results seem to be obtained from the higher precompression, since the stress interval is wider and more similar to that presented in chapter 5. The average of these values settles at about 4600N/mm^2 and this can be considered as representative of all specimens.

The first important result provided by the analysis of data recorded during the tests is the maximum allowable shear stress. As for other elaborations, the value of the vertical load widely influences the overall behaviour. As a consequence, the higher the precompression, the higher the attained τ_{max}, and values range between 0.30N/mm^2 and 0.50N/mm^2 (table 6.9), with a mean value of 0.38N/mm^2. Furthermore, one should remember that lower values are related to a rocking failure, while higher ones to a shear mechanism.

Lastly, on the basis of the observed mechanism of failure for each specimen, the tensile strength could be evaluated. Starting from equations 6.9, 6.10 and 6.11 and knowing all the input data, the results presented in table 6.9 were obtained. Once again, also f_t values appear to depend on the applied vertical load, the higher the precompression level, the higher the tensile strength. Values range between 0.10N/mm^2 and 0.17N/mm^2, with an average of 0.14N/mm^2.

One should note that the values of previously commented quantities, particularly maximum shear stress and tensile strength, are widely dependent on the vertical load than on the structural intervention, namely strengthening or repairing. Actually, differences of the results of the "S" and "R" series are very limited and they can be imputed to a normal scattering, characterizing the experimental analyses.

Table 6.9: Mechanical characteristics obtained during shear compression tests.

Sp.	σ'_0 [N/mm^2]	τ_{max} [N/mm^2]	f_t [N/mm^2]	E [N/mm^2]
R2	1.0	0.40	0.10	4057
S2	2.0	0.53	0.13	2738
R4	1.0	0.28	0.12	5513
S4	1.0	0.28	0.14	6708
R5	2.0	0.40	0.17	4640
S5	2.0	0.42	0.17	4323

A further analysis was performed inorder to calculate the characteristic shear modulus for the multi-leaf stone masonry. Since the results are indirectly obtained, namely they are the result of further analyses, three different methods were applied and the results are compared in table 6.10.
In the first methodology, the shear modulus G_k was evaluated starting with the computed effective stiffness of each wall. On this basis, the equation employed for the analysis is presented as follows:

$$K_e = \frac{G_k \cdot A}{1.2 \cdot \left[1 + \alpha \cdot \frac{G_k}{E} \left(\frac{h}{l}\right)^2\right]} \tag{6.7}$$

where α is a coefficient depending on the applied boundary conditions. α varies between 0.83, in the case of a fixed-ended wall, and 3.33, in the case of a cantilever wall. The analysis was implemented considering the upper limit of G_k, namely α=3.33, since the experimental set-up was designed to test specimens under cantilever conditions. However, one should remember that the real situation diverges from the theoretical condition.
The second method makes use of experimental data. The horizontal displacements of the upper part of the wall were considered and shear rotations (γ) were computed. The following relation was employed:

$$G_{exp} = \frac{\tau_\nu}{\frac{1}{2} \cdot \sum_i^2 \gamma_i} \tag{6.8}$$

The values of shear stress and rotation were considered at cracking point. Furthermore, these results were verified to be in the range between 30% and 60% of maximum shear resistance [Bosiljkov, 2000; Bosiljkov *et al.*, 2005].
Finally, the average value of shear moduli experimentally obtained and ranging between 30% and 60% of shear strength was considered (G_{30-60}).

As the comparison presented in table 6.10 shows, slender specimens tested under lower vertical stress exhibit low values of shear modulus in all the considered methods. In fact, their results cannot be considered perfectly reliable, since the failure was widely affected by the rocking mechanism. On the contrary, the remaining samples provide similar results with a lower scattering, also considering the different analysis methods. However, since first method (G_k) arises from computed stiffness, the values seem to be influenced by the applied vertical load.

Table 6.10: Comparison of Shear Modulus obtained from different analyses (all quantities are expressed in [N/mm^2]).

Sp.	σ_0'	G_k	G_{exp}	G_{30-60}	E/G_k	E/G_{exp}	E/G_{30-60}
R2	1.0	494	337	317	0.12	0.08	0.08
S2	2.0	576	285	486	0.21	0.10	0.18
R4	1.0	109	85	317	0.02	0.02	0.06
S4	1.0	118	93	210	0.02	0.01	0.03
R5	2.0	227	263	256	0.05	0.06	0.06
S5	2.0	210	266	367	0.05	0.06	0.08

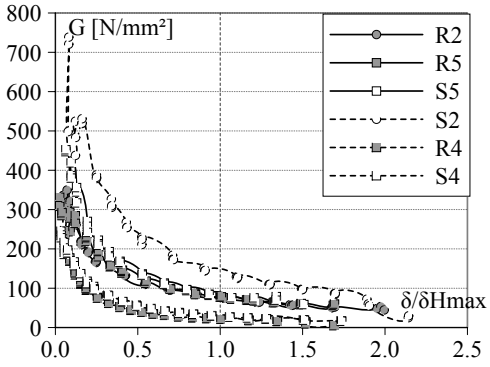

Figure 6.61: Comparison of G_{exp} values of all specimens.

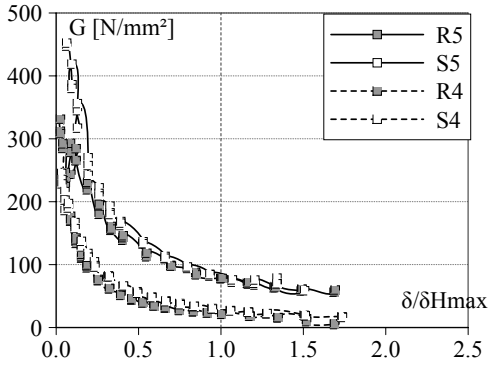

Figure 6.62: Comparison of G_{exp} values of slender specimens.

Furthermore, figures 6.61 and 6.62 provide a graphical representation of the shear modulus trend obtained from experimental data (G_{exp}). Both charts confirm that the applied vertical stress influences the results. In fact, the lower the precompression, the faster the overall decrease, due to the established mechanism. Moreover, squat specimens manifest a further and different behaviour.
The obtained results widely vary depending on both the experimental conditions and the analysis method employed. However, on the basis also of previous similar campaigns (compare §1.2.2), more reliable results seem to be those which refer to the first method of calculation.

6.5 Verification of Failure Field

Theoretical analysis of the calculation of failure mechanisms for the samples in question, subjected to both compression and in-plane horizontal loads, allows to compute the failure filed for these structural elements. Preliminary research into the state-of-art, regarding shear compression tests on stone masonry panels, led to a mean tensile strength ranging between 0.12N/mm^2 and 0.17N/mm^2. This characteristic strength, combined with information obtained from compression experiments presented in chapter 5, permitted to calculate the failure filed that led to the choice of the vertical stress to be applied during shear compression tests presented in this chapter, namely 1.00N/mm^2 and 2.00N/mm^2.

The main studied mechanisms to predict the failure of elements are shear, compression and flexure, respectively. As expressed, the experimental program aims at studying the typical failures, depending on the slenderness ratio of elements and on the applied vertical stress. Furthermore, the tests allow an examination of the shear failure, which constitutes a brittle collapse for these elements and which should be well predicted in order to be correctly designed and verified to avoid this.

The following equations were employed during both the design and verification phases. Normally applied for the strength prediction of masonry typology mainly made of bricks, any further formula was previously calibrated for three-leaf stone masonry. As a consequence these were also applied in this research. The theoretical

equations [Tassios, 1988] are:

$$\tau = \frac{f_t}{b}\sqrt{1+\frac{\sigma_0'}{b}} \qquad \text{Shear Mechanism} \qquad (6.9)$$

$$\tau = \left(1-\frac{\sigma_0'}{\sigma_{max}}\right)\cdot\frac{\sigma_{max}}{6\cdot h/l} \qquad \text{Compression Mechanism} \qquad (6.10)$$

$$\tau = \left[\frac{\sigma_0'}{\sigma_{max}}-\left(\frac{\sigma_0'}{\sigma_{max}}\right)^2\right]\cdot\frac{\sigma_{max}}{2\cdot h/l} \qquad \text{Flexural Mechanism} \qquad (6.11)$$

For instance, the first method of prediction for the shear mechanism was proposed by Turnšek and Čačovič [1971] and subsequently refined [Turnšek and Sheppard, 1980].

The employment of computed mechanical characteristics on the above mentioned equations led to design the typical failure fields presented in figures 6.63 and 6.64.

As designed and expected, the failure of all specimens, squat and slender, occurred in the changing phase between two subsequent failure mechanisms, namely between flexure and shear, as well as between shear and compression. This was included in the initial aims, since this allows the effectiveness of the failure prediction to be verified using the presented equations. Furthermore, testing specimens at two different precompression levels, obtaining a shear failure, permits the calibration of the fit line that oversimplifies this mechanism.

The results, presented in figures 6.63 and 6.64, confirm the good capability of equations 6.9, 6.10 and 6.11 to predict the overall behaviour also for this particular kind of masonry. This is mainly possible thanks to the employment of lime grout injection, which conferred a monolithic behaviour instead of failure because of the buckling of external leaves.

The squat specimen tested under lower precompression, namely R2, manifested an initial flexural behaviour, causing both vertical cracks on the compressed toe and horizontal damage on the lower part of the sample. However, at increased later displacement, diagonal cracks gradually developed and a shear mechanism was established. This is correctly confirmed in figure 6.63.

Higher vertical stress induced on S2 the development of typical diagonal shear cracks. Nevertheless, when damage widely developed, sub-vertical cracks, due to compression, occurred and caused the failure of the specimen. This situation is well represented by the position in chart 6.63, confirming the reliability of the predictions made.

The slender specimens allowed a more definite verification, since four panels were tested and positioned on the created failure field (figure 6.64). As this chart shows, “S” and “R” specimens exhibited similar overall behaviours and any substantial difference in the shear compression strength could be seen between the repaired and strengthened specimens.

Both slender specimens tested under lower vertical stress manifested a behaviour mainly governed by flexure and, after the development of the first cracks, a clear rocking mechanism occurred. This is in accordance with the position of points in chart 6.64, indeed they are placed in the first branch of the failure field. However, as described in section 6.2, these mechanisms caused the formation of a horizontal crack at 15cm from the bottom, which separated the specimens in two parts. The upper one became a squat specimen and this failed in shear. In effect, it can be joined with

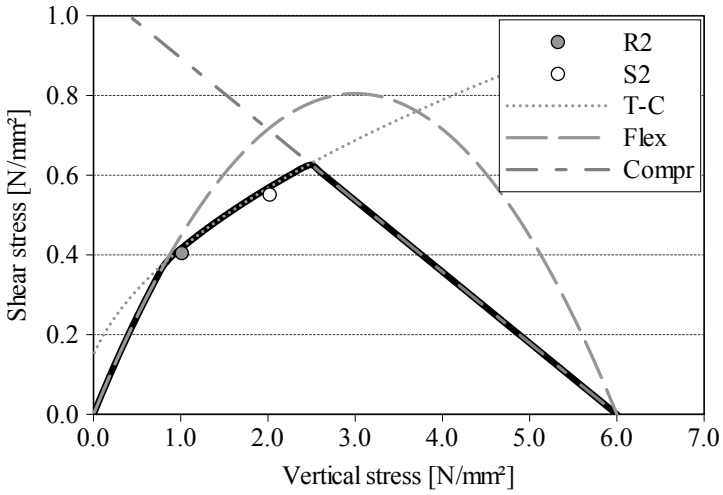

Figure 6.63: Failure field of tested squat specimens.

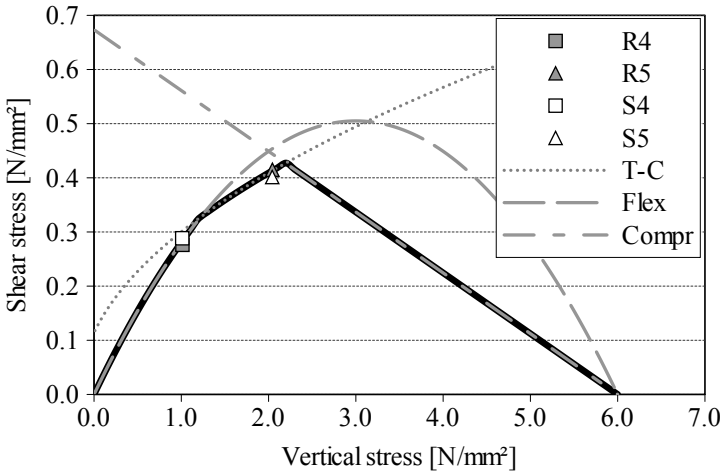

Figure 6.64: Failure field of tested slender specimens.

the sample R2, as it has the same precompression and presented in figure 6.63, which manifested a shear failure.
Slender samples under a higher precompression level are also easily predicted. They exhibited an initial and evident crack pattern due to a shear mechanism even if, with widespread damage present, sub-vertical cracks due to the high vertical stress occurred. As a consequence, the failure was governed by the compression behaviour.

6.6 Conclusive Remarks

Shear compression tests were performed on a series of six panels, with different slenderness ratios and precompression levels. This experimental part leads to an evaluation of the effects of grout injection on the behaviour of multi-leaf stone masonry, subjected to an in-plane seismic action. The main results and observations are discussed as follows. First remarks focus on the analysis of the crack pattern and on failure mechanisms:

- The failure mechanism was mainly governed by the applied vertical load, considering results obtained from specimens with an equal slenderness ratio. A shear mechanism arose with a vertical stress of $2N/mm^2$, while a mixed rocking and flexural mechanism occurred at a vertical stress level of $1N/mm^2$.
- No substantial difference could be seen in the failure mechanism between specimens of the "R" and "S" series, with the same slenderness and tested under equal conditions.
- Both the main sides of each specimen behave similarly, even if one was damaged earlier and the other repeated the failure mechanism at a higher lateral displacement.
- Specimens exhibited their in-plane failure mechanism depending on the slenderness ratio and precompression level up to the maximum lateral resistance. Beyond this point, damage due to compression effects became evident.
- Both strengthened and repaired specimens manifested large cracks on their transversal sides. However, the "S" samples opened these cracks close to the failure, while the "R" panels showed this behaviour earlier.
- The bucking effect on the external layers of masonry widely influenced the collapse of all the specimens.

Further conclusions can be drawn on the basis of developed analyses regarding the overall behaviour during experiments. Calculation of ductility ratios, stiffness degradation, identification of limit states and evaluations of energy dissipation and damping factors are the parameters in question:

- An increase in vertical stress allowed the attainment of higher lateral resistance for both squat and slender specimens.
- The first cracks are independent of both the slenderness ratio and the precompression level, and they appear between 1mm and 2mm. Also the initial cracks, due to the failure mechanism, start to occur at similar displacement for all specimens, ranging between 2mm and 4mm.
- Analysis of the lateral crack opening confirms that grout injection allows a monolithic behaviour in the first range of the experiments. However, the attainment of lateral resistance induces heavy damage, which leads to the independent behaviour of external layers.
- The higher the slenderness ratio, the higher the displacement capacity indicator between the lateral resistance limit and ultimate displacement.
- The lower the vertical stress level, the higher the ratio between displacement at failure and at the beginning of the failure mechanism. This was observed for both slender and squat specimens.
- All specimens could sustain, on average, an overall decrease of about 15% beyond the resistance limit state.
- Beyond the beginning of the failure mechanism, specimens with high vertical stress attain the later resistance faster.

- Samples with a lower vertical load degrade more rapidly than others but they succeed in sustaining a higher overall ultimate force in the decreasing branch of the load-displacement curve.
- The decreasing trend of stiffness is almost equal for corresponding strengthened and repaired specimens tested under the same conditions.
- Envelopes of hysteresis cycles can be properly oversimplified with a quadri-linear curve.
- The energy dissipation is quite high in all cases and for all identified Limit States.
- The initial energy dissipation is higher for strengthened specimens, even if the overall trend is almost similar and any further considerable difference was noted after the appearance of the first cracks.
- A slight influence of the precompression level on dissipated energy was observed. The higher the vertical stress, the slightly higher the dissipated energy, even if a more brittle failure was observed in the latter case.
- On the contrary, strengthened specimens exhibited higher damping values than repaired samples, even if, also in this case, this difference is limited.
- The computed elastic modulus settles at about 4600N/mm^2 and it is in agreement with the one obtained during monotonic compression tests presented in the previous chapter.
- Further mechanical parameters, as in previous analyses, are dependent on the applied vertical stress. In fact, the maximum allowable shear stress and tensile strength range respectively between 0.3N/mm^2 and 0.5N/mm^2, for τ_{max}, and 0.10N/mm^2 and 0.17N/mm^2, for f_t.
- An analysis of the shear modulus provided quite scattered results, depending on the implementation method and on the applied vertical load. A reasonable and reliable range of variation can be considered between 250N/mm^2 and 350N/mm^2.
- Theoretical equations can correctly predict the first mechanism established on the masonry element in question, namely shear, flexure or compression. However, after the development of the actual mechanism, further damage arise, due to localised separation of the external layers. This induces a fast overall degradation and the failure is mainly due to these problems.

These observations lead to a few overall conclusions regarding the main aim of this experimental section.

- Injection allows the development of typical failure mechanisms (shear, flexure, rocking) instead of out-of-plane failure and the separation of outer layers, characteristic of multi-leaf stone masonries.
- Injection cannot completely prevent the buckling of external leaves. However, this mechanism occurs close to the failure, causing the collapse of the specimen, but it takes place after the mechanisms presented in point one.

- Strengthened and Repaired samples behave similarly, all performed analyses provide results differentiated by a normal scattering due to experimental problems. The unique limited difference regards the slightly higher dissipation capacity manifested by the "S" specimens.
- The traditional theoretical equations presented in this chapter can correctly predict the first established mechanism and these seem to be employed also for design and verification analyses.

Chapter 7

Finite Element Analysis

This chapter provides a brief overview on the analyses of two different FE models in order to realize a numerical simulation of the laboratory compression tests carried out within this research.
The results presented hereafter constitute a preliminary phase for a subsequent development of further FE models aiming at modelling more complex mechanical behaviours, as those obtained during shear compression tests, on simple panels, and shaking table experiments, on whole building models.

7.1 Introduction

The numerical modelling of the masonry behaviour is a difficult topic for several reasons. In fact, the overall behaviour is the result of the interaction of its constituents: resisting elements, namely the bricks or stones, and binding materials, normally constitute by mortar. Their mechanical characteristics, such as strong anisotropy and complex stress-strain relationships, and further features, like the thickness of the mortar bed joints and the quality of the masonry execution, as well as their interaction, influence the overall behaviour of the masonry. Further aspects may modify its overall behaviour, such as the texture of the resisting elements, the conditions of conservation and the relative decay as well as the environmental influences. Moreover, also the stress state, due as example to the precompression level or the lateral confinement, has a wide influence on the resulting overall characteristics.

The researches on this field normally consider two different approaches with their consequent advantages and disadvantages: micro-modelling and macro-modelling. The first approach separately consider each constituent material, mainly resisting elements, mortar and their mutual interaction, while the second idea provides an homogenization, at different levels, of the masonry. In the latter way, the masonry can be considered as a unique and homogeneous solid.
In both cases several aspects and opened issues should be still deepened, such as the post-peak phase, the interaction among materials and the overall tensile strength.

7.1.1 FE Analysis of Stone Masonry Structures

The employment of the numerical analyses to deepen the knowledge of the masonry structures is a methodology currently applied and under great development, in spite of the wide difficulties previously listed.
The great diffusion and enhancement of computational possibilities during last decades

have allowed the development of these numerical simulations to be substantially incremented. The Finite Element Method (FEM) represents a powerful and reliable methodology to provide an analysis of the stress-strain relationship as well as of both overall behaviour and failure mechanisms of the considered structures. Nevertheless, a mathematical description of the mechanical laws of constitutive materials, namely a stress-strain relationship up to failure, should be known [Bosiljkov, 2004b].
However, considering mathematical models in order to describe all the interactions and to reproduce all the observed phenomena will lead to a very complex analysis, which would result inapplicable in the case of large structures. For this reason, simplified constitutive models, able to incorporate all the interacting mechanisms, should be developed and verified through the comparison with experimental results and in-situ investigations [Lourenço, 2001; Lourenço *et al.*, 1998].

The hypotheses of homogeneity, isotropy and linear elastic properties cannot be generally considered as satisfactory in the case of the masonry structures [Hendry, 1998; Lourenço, 2001; Tassios, 1988]. For these reasons, several and different criteria were developed to account these aspects and to correctly model the overall compressive and tensile behaviour of the masonry.
The compressive behaviour may be oversimplified by a linear elastic law only at low stress levels while, at higher loads, the non-linear range occurs widely before the appearance of the first visible crack. A common criterion applied in FE analyses of masonry elements is a plasticity model for continua, related to the macro-modelling idea. On this basis, different elasto-plastic constitutive laws and other plasticity models, such as Drucker-Prager and Mohr-Coulomb criteria, have been applied to model the compressive behaviour of the masonry [Heyman, 1997; Rots, 2002].
Similarly, the tensile behaviour may be considered as a linear function only up to very low stress values. Nevertheless, the occurrence of a damage leads to the most problematic phase to be modelled, namely the cracked state. In order to account the occurrence of damage, different approaches were developed, such as the discrete or smeared crack analysis. In particular, the latter model considers a decomposition of the total strain (ε) into an elastic (ε^e) and a crack (ε^{cr}) component. Furthermore, the effect of damage is spread on the whole area pertinent to an integration point [Rots, 1997].
Nevertheless, one should note that the choice of the best method of analysis to be used depends on several factors and, among these, the knowledge level of the structure to be modelled is one of the most important points [Lourenço, 2002], since different methods may lead to unlike results.
In the light of the main aims of the FE models developed in the following sections, a combination of the plasticity-based Drucker-Prager criterion with the smeared cracking Rankine method, respectively for the compressive and tensile behaviours, could provide reliable results with a limited computational cost, instead of more complex and detailed but also high costly criteria.

The studies and the numerical simulations developed on similar masonry structures, namely multi-leaf stone masonry or more generic stone elements, are very limited, particularly in the case of combined experimental and numerical analyses. Some studies, which provide relevant information in order to develop the FE analysis presented in this research, are resumed as follows.

Pina-Henriques and Lourenço [2003] developed FE models suitable for the numerical analysis of multi-leaf masonries but also applicable to more generic masonry elements. Particularly, the study aimed at investigating the short and long term

effects on the multi-leaf masonry elements. On this purpose, three different methods were employed, namely a Plane Stress (PS), a Plain Strain (PE) and an Enhanced Plain Strain (EPE). In particular, the EPE analysis allows masonry layer to be modelled using 3D elements. Moreover, imposing an equal displacement to all the leaves, the out-of-plane behaviour may also be considered. A comparison with the experimental results confirms the possibility of EPE model to correctly predict the established mechanism, mainly due to the early failure of the weaker materials on the out-of-plane direction, if any confining effect is provided.

Binda *et al.* [2006] developed an experimental campaign and a numerical simulation in order to investigate and predict the overall behaviour of the multiple-leaf masonry walls. Both analyses prove that several factors influence the results and the failure mechanisms, such as the mechanical properties of the leaves, their geometrical dimensions and their mutual connection. The numerical analyses employed plane stress continuum elements. Furthermore, the materials, as units and mortar, were smeared out in a continuum material. This was modelled considering a composite plasticity method, combining a Drucker-Prager yield criterion with a Rankine yield criterion, respectively in compression and in tension. Finally, unlike discretizations of the specimen geometry were considered as well as different methodologies of interaction of the leaves.
The numerical analyses provide a good correlation with the experimental results, obtained from both the compression and shear compression tests.

Senthivel and Lourenço [2009] performed a two dimensional non-linear finite element analysis in order to investigate the load-displacement capacity and the failure mechanisms of the stone masonry shear walls. The numerical simulation was compared with the results of an experimental campaign performed on elements subjected to a combination of the vertical compression and horizontal in-plane loading. These experiments and analyses involved three different masonry typologies: a dry-stone masonry, an irregular stone masonry (with bonding mortar) and a rubble masonry (with irregular mortar joints). A micro model, based on the plasticity theory, has been used to carry out the analysis. Furthermore, simplified relationships to calculate the mechanical properties of masonry elements are proposed, starting from the mechanical parameters of constituents.
The results show as the numerical simulations may provide results with a strong concordance with the experimental observations, in particular in terms of stress distribution. Furthermore, the load-displacement curves of the experimental tests could be correctly predicted by the FE models up to the maximum attained displacement. Furthermore, also the failure mechanisms could be well predicted.

7.1.2 Development of FE models

On the basis of the previous similar numerical studies, the choice of the modelling methodology was induced by the observations preformed during the execution of the compression tests (compare §5). Actually, the widespread identified crack pattern involved damage on mortar bed joints as well as on stone elements. Furthermore, one should note that the cracks early occurred to both constituents. These observed effects induced to lean for the homogenization of materials, considering a macro-model of the whole tested element.

However, the overall behaviour of the injected panels appeared strongly dependent on the applied strengthening technique, as demonstrated by previous researches (compare §1.2.1). Particularly, this led to consider the effects of grout injection on the

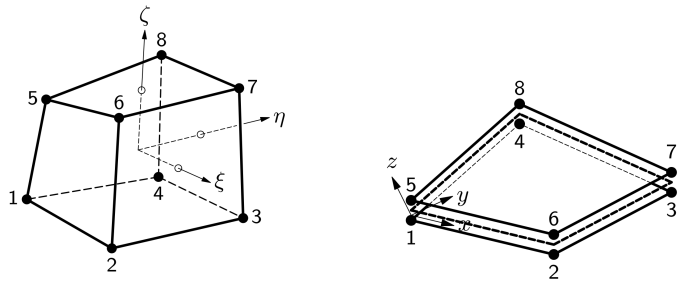

Figure 7.1: Scheme of the employed elements [DIANA ^{TM}, 2005].

inner core of masonry panels. In fact, this intervention induced the two main effects already underlined on the conclusive remarks of chapter 5: providing a connection between external layers and delaying the buckling problems of these leaves.
As a consequence, the first proposed FE model will be based on this consideration and it will be realized considering two different materials. Being the will to attain the as easy as possible model, the second numerical simulation attempt a further oversimplification, employing a single material in order to model the whole masonry panel.

The experimentally observed damage, due to the tensile stresses and characterized by sub-vertical cracks, and the occurred failure mechanism, mainly caused by the buckling of external leaves, led to consider a three-dimensional modelling, differently from more similar studies that considered only a planar analysis [Binda *et al.*, 2006; Pina-Henriques and Lourenço, 2003]. Actually, the cracks initially arise and propagate on the main sides and this has important consequences on the overall behaviour of specimen, since the horizontal deformations on this principal direction (X) widely increase.
Nevertheless, after this first phase, vertical cracks occurred also on the transversal sides (Y), to the interface between external layers and internal core. As a consequence, a wide increase of the horizontal deformations also on the transversal direction occurred and their subsequent growth led to the failure. These phenomena, observed during the tests, appeared as inseparable to describe the development of the overall behaviour of the three-leaf stone masonry and, for this reason, a three-dimensional modelling was considered.

A subsequent and further simplification of this numerical simulation led to create a second model, in which the whole masonry specimen is modelled as an unique and homogeneous material. Also in this case a three dimensional development is maintained for the same reasons above mentioned.

The development of these models, as expressed above, constitutes the base for further enhancements and for the modelling of more complex tests on this masonry typology.

The numerical modelling was performed through the program TNO DIANA^{TM}. The homogeneous materials, namely internal and external layers as well as the steel plate, are modelled considering a eight-node solid brick element (element type: HX24L), while for both interface typologies, namely "A" and "B", an interface element between two planes in a three-dimensional configuration is applied (element type: Q24IF). The elements are presented in figure 7.1.

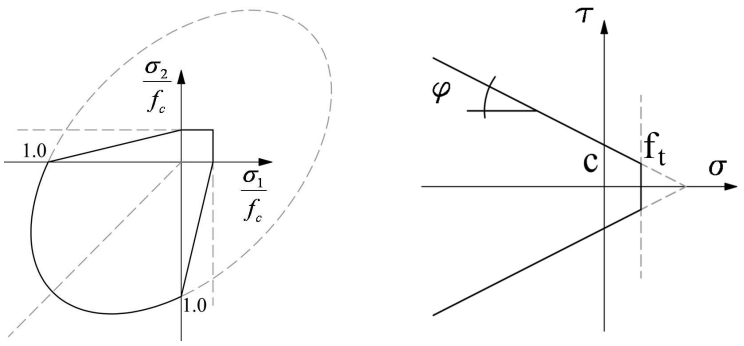

Figure 7.2: Failure criteria for solid elements (left) and interface elements (right).

The Drucker-Prager model is considered as plasticity criterion to model the compression behaviour of the brick elements, in order to account the biaxial stresses, and this is coupled with a smeared-cracking criterion in tension, in this case the Rankine method (figure 7.2).
Differently, a Mohr-Coulomb criterion, together with a brittle failure criterion in tension and a constant shear retention factor, is used to describe the frictional behaviour of the interface elements (figure 7.2).
The same failure criteria are employed in the case of the corresponding elements of both developed models.

7.2 Multi-material model

The first developed numerical model involves two different materials and an interface to simulate the overall behaviour of the three-leaf stone masonry specimens. As presented in the introduction, an homogeneous material was considered for the external layer and a second homogeneous material was employed to model the internal core, constituted by stone fragments bound together by the injected hydraulic lime-based grout. The model is completed by an interface element, that links these materials (figure 7.3).
The numerical model take into account also the testing system, that is simplified by a thick steel plate, in order to correctly apply the load. Furthermore, an interface element is also provided between this element and the specimen in order to simulate the real testing condition.
Lastly, the symmetry of the samples allowed to consider only a eighth of the whole masonry element subjected to the monotonic compression test.

7.2.1 Mechanical Properties of Materials

The mechanical characteristics of the employed materials were gathered from the experimental tests performed on the single constituents as well as on composite specimens, namely injected cylinders and masonry panels. However, further considerations should be developed to obtain the input values for the FE model. THe considerations and the mechanical parameters of each element will be presented as follows.

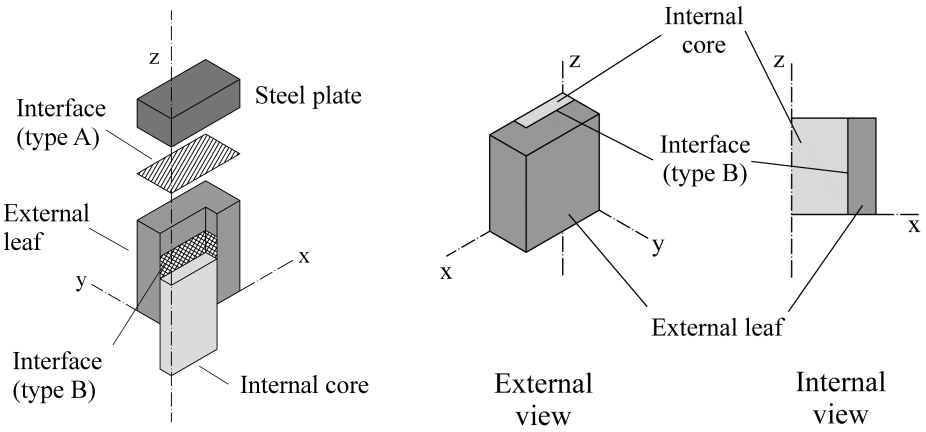

Figure 7.3: Outline of the multi-material model (left); external and internal view of the specimen (right).

7.2.1.1 External leaf

Any experimental test was performed on the single external layer. Actually, the compression tests presented in chapter 5 are referred to the whole specimens, whose strength is due to the contribution of both the external leaf and internal core.
Nevertheless, Vintzileou and Tassios [1995] proposed two formulations, subsequently refined by Valluzzi *et al.* [2004], to calculate the compressive strength of the injected masonry elements:

$$f_{wc,0} = (V_{ex}/V) \cdot f_{ex,c} \tag{7.1}$$

$$f_{wc,s} = f_{wc,0} + (V_{inf}/V) \cdot f_{inf,s} \tag{7.2}$$

The final compressive strength of the injected wall ($f_{wc,s}$) depends on: (i) the compressive strength of the unstrengthened wall ($f_{wc,0}$), due only the the contribution of external leaf (equation 7.1), (ii) the volume of the internal core (V_{inf}) and (iii) its compressive strength ($f_{inf,s}$). Starting from the proposed formulation (equation 7.2) and knowing the final masonry compressive strength ($f_{wc,s}$), the contribution of external leaf could be computed (f_{gr}).
All mechanical properties of the modelled external layer are summarized in table 7.1. Furthermore, the whole stress-strain relationship was taken into account through a piece-wise linear function, obtained applying the equation 7.2. Even if this equation is proposed for the computation of the compression strength, it was employed also to calculate the remaining relevant points. The starting values for this analysis are those previously presented in the section 5.5.

Table 7.1: Multi-material: Mechanical properties of the External leaf.

E N/mm^2	ν -	f_t N/mm^2	ε_u -	f_c N/mm^2	c N/mm^2	$sin\varphi$ -	φ -
4188	0.315	0.14	0.03	9.80	3.999	0.20	11.54

7.2.1.2 Internal core

The mechanical values of the internal core are mainly calibrated considering the experimental compression tests performed on the injected cylinders (compare §3.1.4). Some experiments on these elements were realised monotonically, in order to study both the elastic properties, at a lower vertical stress level, and the mechanical properties in the post-peak phase, up to the failure. Nevertheless, these results were slightly incremented to account the three-axial stress states that arise in the upper part of the specimen, due to the friction with the steel plate.
Main values are reported in table 7.2. Finally, the whole stress-strain experimental relationship was taken into account with a piece-wise linear function.

Table 7.2: Multi-material: Mechanical properties of the Internal core.

E	ν	$f_{t,i}$	ε_u	f_c	c	$sin\varphi$	φ
N/mm^2	-	N/mm^2	-	N/mm^2	N/mm^2	-	-
1850	0.200	0.13	0.03	2.73	1.114	0.20	11.54

7.2.1.3 Interface

Any experimental tests was performed to study the mechanical properties of the interaction between internal core and external layer, represented by the interface element. However, an early damage could be seen in this zone during the compression tests on the masonry panels. Actually, the occurrence of vertical cracks on the lateral sides may be the consequence of a damage previously arose at the interface between the core and the external leaf. This early behaviour was taken into account considering a tensile strength of the interface (type B) lower than that of other materials.
Main values are reported in table 7.3. Dilatancy was considered as null [Rots, 1997].

Table 7.3: Multi-material: Mechanical properties of the interface (type B).

K_n	K_{tg}	f_t	c	$tan\varphi$	φ
N/mm^2	N/mm^2	N/mm^2	N/mm^2	-	-
1.0E+07	1.0E+05	0.12	0.100	0.20	11.31

7.2.2 Results

The mechanical properties of each material presented in the previous sections provide the best combination of results in terms of both stress-strain relationships and stress distribution. Actually, the output values are represented by the curve "R2" in figures 7.4 and 7.5.
Firstly, one should note that the relationships employed as input, namely "External leaf" and "Internal core", provide optimal results in terms of vertical strains. In fact, these input data allow a mechanical interaction, that yields to a very good correlation between the FEM analysis and the average of the experimental results (figure 7.4).
Nevertheless, model "R2" is not able to reach the stress peak of the experimental curve, due to the attainment of the tensile strength in some parts of the specimen. This fact leads to a premature failure of the specimen in the FE model (figure 7.7). Moreover,

this stress distribution shows as the damage earlier occurs in the transversal side (figure 7.7a) and only later in the main one. Figure 7.7b shows how the attainment of the tensile strength initially interests only the external part of the outer layer of the model. Furthermore, the internal core and the external layer present different stress distributions, since they behave independently.
Moreover, the horizontal strains could be well predicted only up to about $3N/mm^2$, when the specimens were in undamaged conditions during the experiment. Over this vertical load level, the strain-strain relationship loses the linear trend but the strain increase is very low and limited if compared to the experimental curve. This is clearly evident in the case of horizontal strains along the "Y" direction (figure 7.5), namely on the transversal side.
This numerical simulation may predict the results up to about $7N/mm^2$. At this load level, the damage involves the whole specimen (figure 7.8a), even if particularly in the transversal direction, as experimentally observed. The internal core is completely cracked and any stress may be still sustained (figure 7.8b), while a heavy damage involves the external layer. Furthermore, the figure 7.8b clearly highlights that the two considered materials behave independently.

A slight decreasing of the tangential stiffness of interface (type A) between the steel plate and specimen, corresponding to a lower horizontal retention in the upper part of the model, induced lower stresses (model "R1"), being the same vertical load of "R2". This allowed to delay the attainment of the tensile strength onto the external layer and, consequently, this permits to reach higher vertical loads, up to about $8N/mm^2$ (figure 7.4). Nevertheless, also in this case, the load peak is not attained.
Furthermore, the figure 7.5 clearly indicates that, even if the failure is delayed, any noticeable change is induced on the horizontal behaviour.
Finally, the stress distribution on model "R1" is very close to that of model "R2", without no substantial difference.

Nevertheless, these models manifested the beginning of first vertical cracks slightly later than that observed during the experiments. For this reason, a further important change was introduced starting again from the mechanical parameters of model "R2" and leading to the model "R3". In order to correct the problem just mentioned, the tensile strength of the external leaf was reduced to $0.09N/mm^2$.
This induced a stress distribution, not reported here for briefness, equal to those of both previous models. Nevertheless, this model could better predict the load level at which the vertical cracks start to occur. However, if on one hand this shrewdness allowed a better correlation between the FE model and experimental observations during the first phase, this also induces a premature failure of the model, that attains only $6N/mm^2$ in compression.

The last change has been introduced to attain the load peak on a FE model. This could be possible only reducing the tangential stiffness of the horizontal interface (type A) and maintaining the remaining mechanical characteristics equal to those of the model "R2". Also in this case, as for previous models, any substantial difference could be noticed on the stress-strain relationships. Actually, the strains on both the vertical and horizontal directions (figures 7.4 and 7.5) trace those previously computed and only an higher load is reached.
Nevertheless, one should note as this was possible only to detriment of a correct stress distribution. In effect, the attainment of the tensile strength on the external leaf, that is the cause of the failure, is delayed, since the horizontal retention at

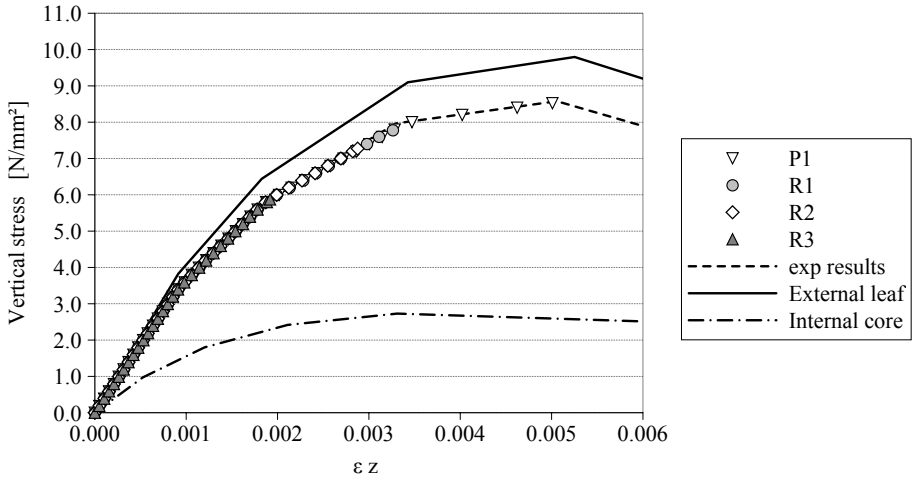

Figure 7.4: Stress-strain relationships on the vertical direction.

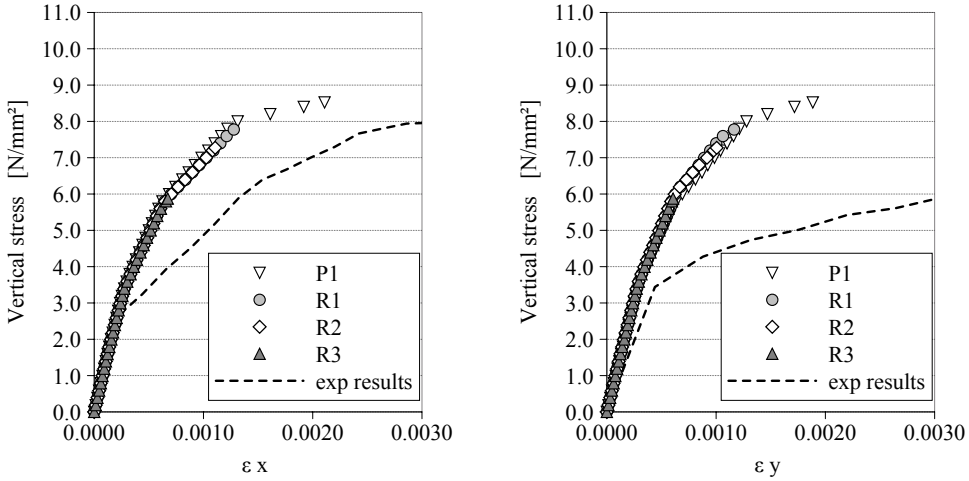

Figure 7.5: Stress-strain relationships on the horizontal directions.

the top of the specimen is decreased. The beginning of damage occurs close to the failure, at about 8N/mm^2, and, as figure 7.9a shows, the tensile strength is attained almost contemporary on both transversal and main sides. This is different from the experimental observations, since the tensile strength is attained at a too high stress level. Figure 7.10b confirms as the internal and the external parts behave independently and the damages initially involve the outer part of the external leaf. Finally, the stress distribution at failure 7.10 is very similar to that presented in the case of model "R2".

In all above presented models, the mechanical characteristics of the vertical interface (type B), namely that between the internal core and the external leaf, are considered as constant. All cases manifest the opening of the interface elements at a stress level of about 2N/mm^2 (figure 7.6). Furthermore, this always occurred before the loss of the first linearity on the stress-strain relationships (figures 7.4 and 7.5). The width of the openings attains similar values (figure 7.6), independently from the model, and this is reached at about 4N/mm^2. Nevertheless, over this load level, the cracks gradually closed, since the horizontal strains of the internal core increased

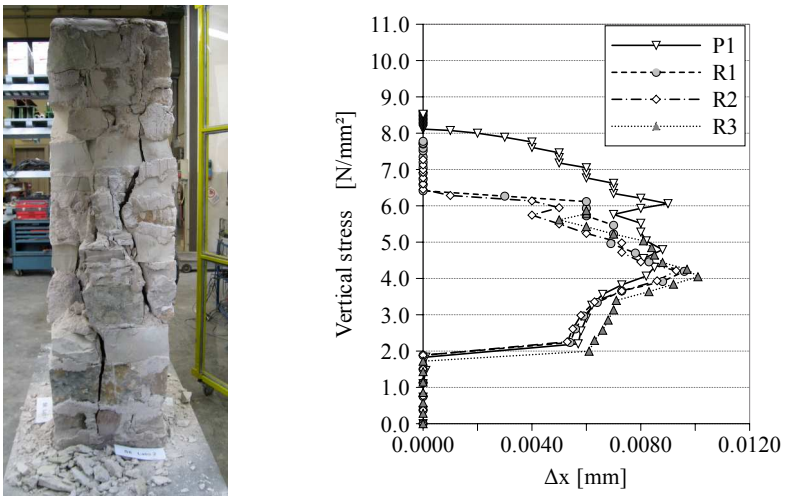

Figure 7.6: Gap between External leaf and Internal core: experiment (left) and FE model (right).

more than those occurred on the external leaf. However, being this is an internal behaviour, a direct observation and confirmation of this phenomenon during the experiments was not possible.

7.2.3 Observations

The results provided by the four presented models, in terms of stress-strain relationship, appear very close, without any noticeable difference. The unique consideration can be done about the maximum attained vertical stress, which is different among the models. Furthermore, one should note the wide influence of the horizontal interface (type A) on the overall behaviour of the model. Actually, the variation if this parameter is able to delay or to anticipate the failure of the model. Nevertheless, any investigated parameter could modify the stress distribution on the model. In all cases the failure occurred because of the attainment of tensile strength on the external leaf. The influence of the tangential stiffness previously mentioned (type A) could only modify the stress level at which the cracks appeared and, consequently, the vertical stress level at which the failure occurred.
Finally, the change of mechanical properties does not induce any substantial difference on the behaviour of the interface (type B). Only the model "P1" manifested a closing of the cracks at a higher level, due to the delayed tensile failure on the external leaf, while its opening occurs at the same stress level for all the models.

Furthermore, one should note as the models of the "R" series show a similar stress distribution, that is representative of the real situation. In fact, in this case, the beginning of damage presents a correct sequence, starting from the transversal side and, only subsequently, reaching the main side. Furthermore, the first damage on model "R2" occurs at a correct load level and not close to the failure, as in the case of the model "P1".

Finally, a model composed by two different materials linked by an interface element is able to correctly predict the stress-strain distribution. The maximum attained load level depends on the tensile strength of the outer material and on the properties of the upper interface, that controls the horizontal retention and, consequently, the induced stresses.

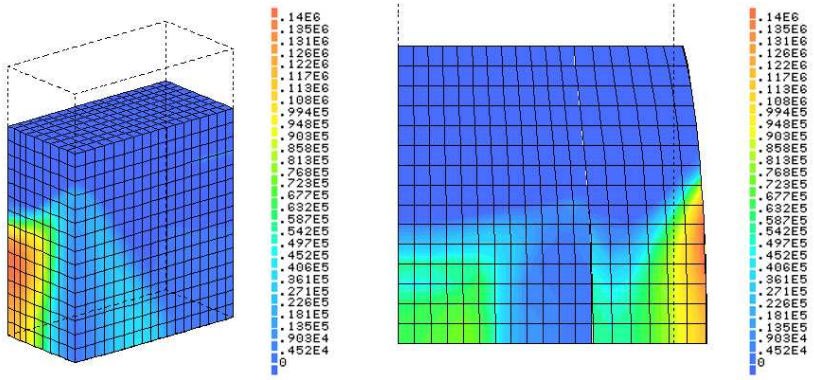

(a) External view **(b)** Internal view

Figure 7.7: Tensile stresses in the horizontal X direction at 4.72N/mm^2, model R2.

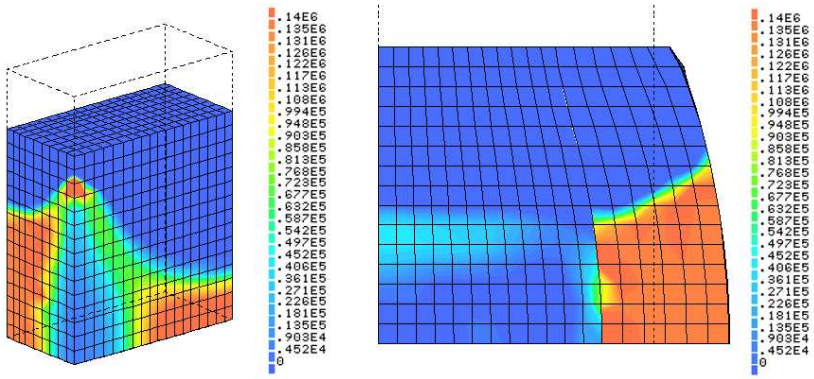

(a) External view **(b)** Internal view

Figure 7.8: Tensile stresses in the horizontal X direction at failure, model R2.

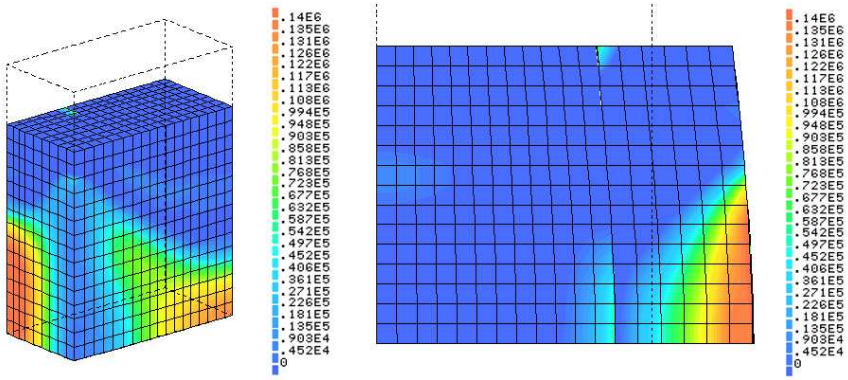

(a) External view **(b)** Internal view

Figure 7.9: Tensile stresses in the horizontal X direction at 8.07N/mm^2, model P1.

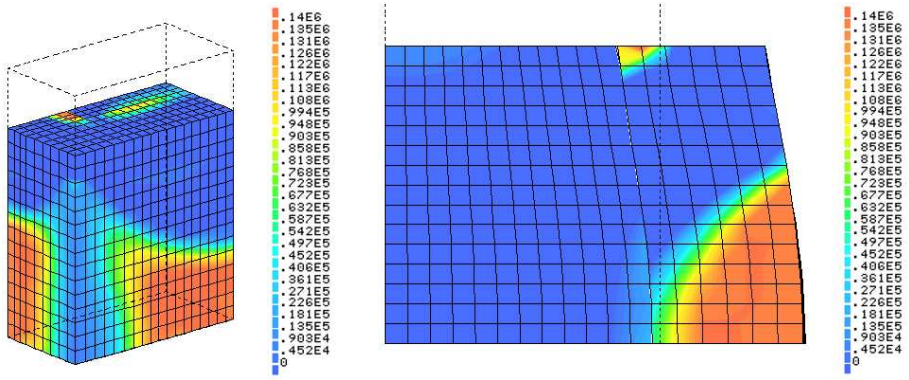

(a) External view **(b)** Internal view

Figure 7.10: Tensile stresses in the horizontal X direction at failure, model P1.

However, the higher the maximum attained stress level, the higher is the load that induces vertical cracks and, furthermore, the less representative of the real experimental condition is the model. Nevertheless, in all the cases, the modelled horizontal strains are very limited if compared with the experimental results.
The stress distribution and the consequent induced damage obtained from the FE models are similar to those experimentally observed. The unique difference of the presented models is the load level at which these damages occur, while the position and the type of fractures are very similar.
Finally, any combination of the mechanical parameters allowed to model the post-peak phase.

7.3 Single-material model

A second FE model is developed with the aim to simplify the analysis presented in the previous section. For this reason, a masonry specimen is modelled as an homogeneous material (figure 7.11), without distinguishing the external leaf and the internal core. The observations, which led to this choice, are the same drawn for the multi-material model, taking into account the will to simplify the model presented in the introduction.

7.3.1 Homogeneous Material

The mechanical properties of the single-material model are computed from a combined comparison of the oversimplification of the compressive behaviour, obtained via the experimental tests (compare §5.5), and the results computed with the multi-material models. Actually, in this case, an average material is considered to describe the overall behaviour of the specimen. The resulting stress-strain relationship is a piece-wise linear function also in this case.
Main characteristics are summarized in table 7.4.

7.3.2 Results

The mechanical parameters presented in the previous section are employed as input of both FE models hereafter presented.

Table 7.4: Single-material: Mechanical properties of the homogeneous material.

E N/mm^2	ν -	f_t N/mm^2	ε_u -	f_c N/mm^2	c N/mm^2	$sin\varphi$ -	φ -
3808	0.315	0.14	0.03	8.58	3.502	0.20	11.54

The first model, named "H-R1", may correctly predict the experimental results up to 8N/mm^2. The vertical strains (figure 7.12), computed through the FE model, are in accordance with those obtained during the experiments and the change in the slopes of the stress-strain relationship can be effectively predicted.
Nevertheless, the results in both horizontal directions widely underestimate the real behaviour (figure 7.13) and this is clearly evident in the case of strains in the transversal direction ("Y"). In fact, after the occurrence of vertical cracks in the real specimen, both the displacements and deformations suddenly increase. Differently, the FE model shows a very limited variation and the occurrence of damage can not well predicted, even if the numerical analysis correctly highlights an accumulation of tensile stresses in the transversal section. A similar behaviour can be seen also in the main side of the specimen, even if in a limited way.

The stress distribution appears in accordance with the experimental observations. Actually, the first visible damage can be detected in the transversal side of the specimen and, only subsequently, on the main one. This is confirmed by the figure 7.14a, where it is clear that the tensile strength is attained earlier in the lateral side, at a vertical stress of about 5N/mm^2. Differently, when last step of the modelling is reached (7.14b), a damage can be seen also on the main side, due to the attainment of the tensile strength of the material. Furthermore, as in the real case, most heavy damages are in the lateral part.

The second model, proposed in figures 7.12 and 7.13, named "H-P1", makes use of the same input data and only the tangential stiffness of the horizontal interface (type A) is decreased. As in the case of the multi-material model, this implies a lower horizontal retention, that induces lower horizontal tensile stresses in the material. As a consequence, this model provides results similar to those of the previous one but this is able to attain a higher compressive stress, up to the peak of the experimental data.

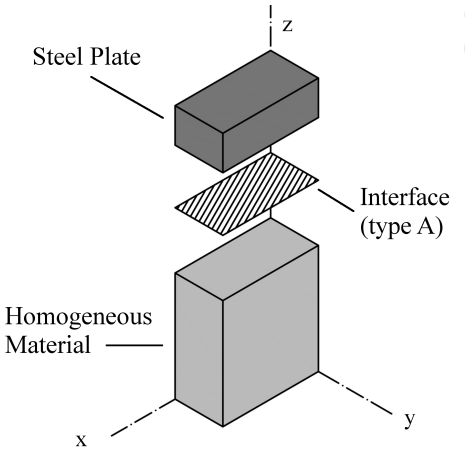

Figure 7.11: Outline of the single-material model.

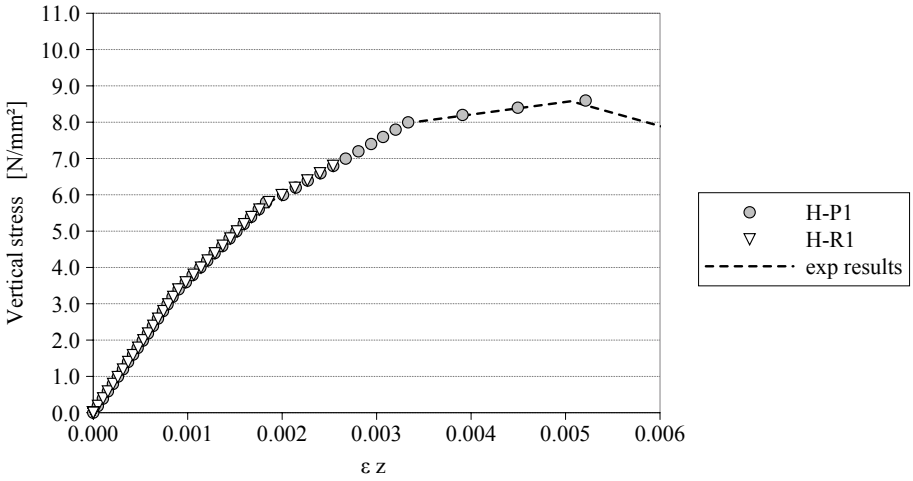

Figure 7.12: Stress-strain relationships on the vertical direction.

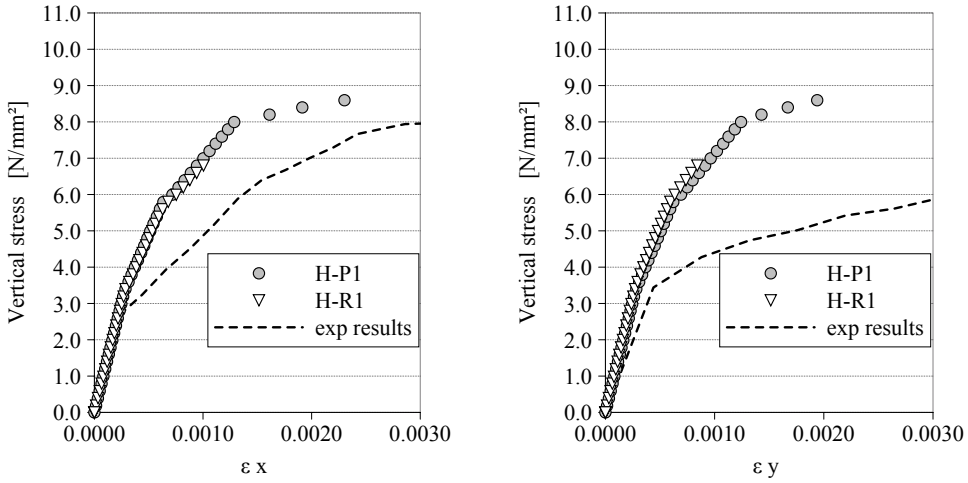

Figure 7.13: Stress-strain relationships on the horizontal directions.

Nevertheless, some problems remain in the calculation of the horizontal deformations (figure 7.13). Actually, results are very similar to those of the first model ("H-R1"). Furthermore, even if the strains widely increase in the last part of the modelled curve, they are very limited if compared to the real situation.

The stress distribution in this model (figure 7.15) appears different from that modelled in the first numerical simulation ("H-R1"). In fact, the attainment of the tensile strength on the material, corresponding to the occurrence of a damage on the model, is achieved at a compressive stress of about $8 N/mm^2$. Furthermore, in this models the damage occurs almost contemporary in both the main and transversal sides (figure 7.15a). The final stress distribution (figure 7.15b) involves a widespread part of the specimen and the tensile stresses are widely diffused also on the main direction ("X").

7.3.3 Observations

Both models provided very similar results in terms of stress-strain relationships, since the vertical and horizontal deformations are very close and similar to those

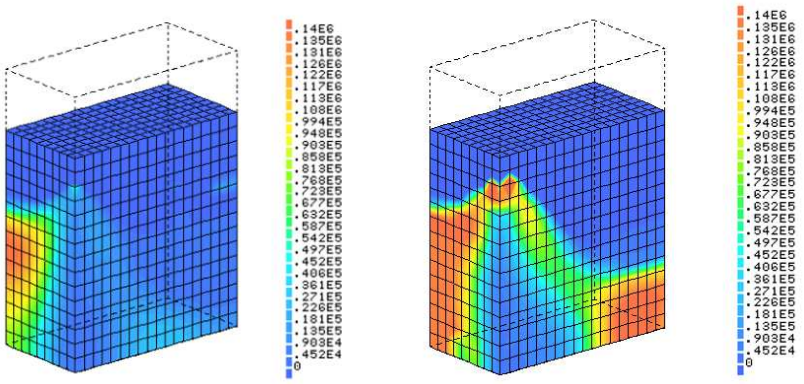

(a) Vertical stress level of 5N/mm^2 **(b)** At failure, 7.87N/mm^2

Figure 7.14: Distribution of tensile stress in the horizontal X direction, model H-R1.

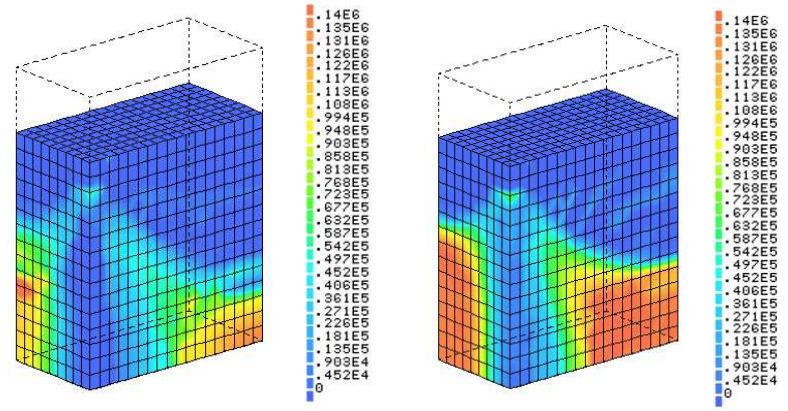

(a) Vertical stress level of 8N/mm^2 **(b)** At failure, 8.60N/mm^2

Figure 7.15: Distribution of tensile stress in the horizontal X direction, model H-P1.

experimentally obtained in the "Z" direction. The difference is mainly due to the tangential stiffness of the interface element, that controls the failure of the model.

Nevertheless, the stress distribution differently evolved in the presented numerical simulations. Actually, the model "H-R1" early attained the tensile strength of the material. Moreover, the damage occurred firstly in the transversal direction and only later in the main side, as experimentally observed. Differently, the second model showed an almost contemporary occurrence of damage on both the transversal and main side. Furthermore, this occurred at a too much high vertical load, since it is very close to the failure and no correspondence with the experimental behaviour could be found.

Finally, the first model seems to provide more reliable results, since the stress distribution is close to that experimentally observed. However, this FE simulation cannot attain the maximum experimental load, due to a premature failure. This is due to a widespread damage, diffused in the whole specimen, as a consequence of the tensile strength. In both cases, since a unique material was employed, any drop nor difference could be seen in the stresses between the internal and external parts of the models.

7.4 Comparison among FEM and experimental results

The first important consideration can be drawn on the basis of the comparison between the more reliable models, in the case of the multi- (model "R2") and single-material (model "H-R1").
The corresponding homogeneous and multi-material models provide almost equal results in terms of stress-strain relationships. In fact, the vertical deformations (figure 7.16) of model "H-R1" perfectly trace that of model "R2". Furthermore, also the results of horizontal strains shows a good accordance, as clearly indicated in figure 7.17.
Nevertheless, in both cases the load peak cannot be attained, since the premature failure of models. Moreover, both the multi- and single-material models are unable to predict the large horizontal strains, after the occurrence of the first vertical cracks.

The comparison between the stress distribution obtained from these numerical simulations shows a good accordance as well.
The multi-material and the homogeneous models behave similarly. In fact, the figure 7.7a and the figure 7.14a exhibit a very similar position of the stress accumulation and also of damage level. In both cases, cracks occurred firstly in the transversal side. Obviously, the model "R2" results more detailed, due to the employment of two different materials. Moreover, the use of an interface allows the internal behaviour of the core to be investigated. Nevertheless, at a low vertical stress level, namely about $5N/mm^2$, the internal part of both models behave similarly (figures 7.7b and 7.18a). Differently, differences can be noted at failure. The external stress distribution is very similar between the models (figures 7.8a and 7.14b). Only in the case of the multi-material model, the area interested by the attainment of the tensile strength appeared slightly larger. Nevertheless, any substantial difference can be externally seen.
However, the internal behaviour manifested slight differences, since the model "R2" is more detailed. Actually, the area interested by the attainment of the tensile strength in the model "H-R1" (figure 7.18b) is almost half of the whole section, while the damage on the internal part of the model "R2" (figure 7.8b) involve only the external layer, since the internal core fails at a very lower load level.

Finally, both models failed because of similar problems, mainly due to the attainment of the tensile strength on the load bearing material. The differences, even if existing, appear as not substantial and the loss of details leads to the advantage of a lower computational load, in the case of the homogeneous model.

With the aim to validate the results obtained through the FE model, a comparison among the numerical simulation and the experimental observations is performed as follows. Results provided by the model "R2" are considered, since the employment of two materials and an interface allow an easier and more detailed comparison. The extension of validity to the homogeneous model can be accepted on the basis of the above mentioned remarks, considering a slight relaxation of the correspondences with the experimental case, as a consequence of the adopted simplification.

The first noticeable consideration concerning the monotonic compression tests is the unavoidable detachment between the internal core and the external layer. In fact, this leads to a separation of the leaves and induces vertical cracks. The numerical model allows to simulate this behaviour, as shown in figure 7.19a. Since the tensile strength of the interface is lower than that of other materials, a first damage occurs in this position of the FE model. Moreover, after this evidence, the internal and external

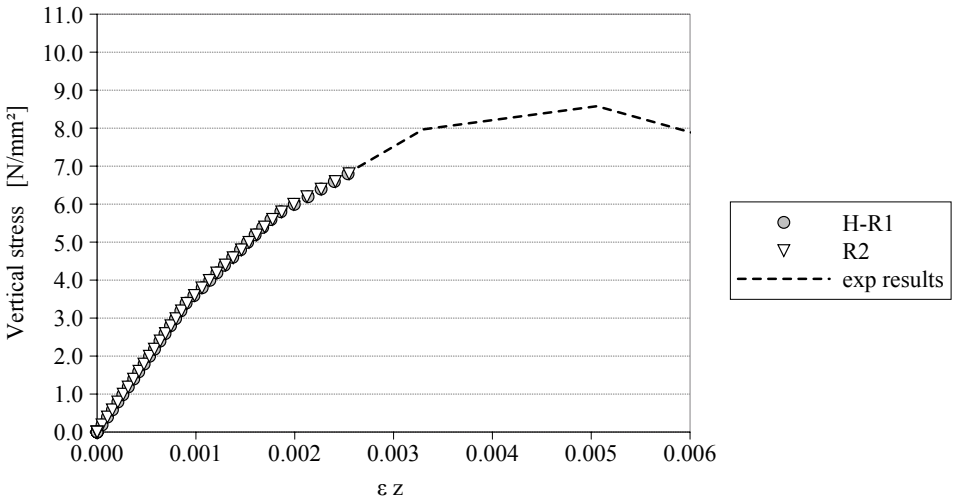

Figure 7.16: Stress-strain relationships on the vertical direction.

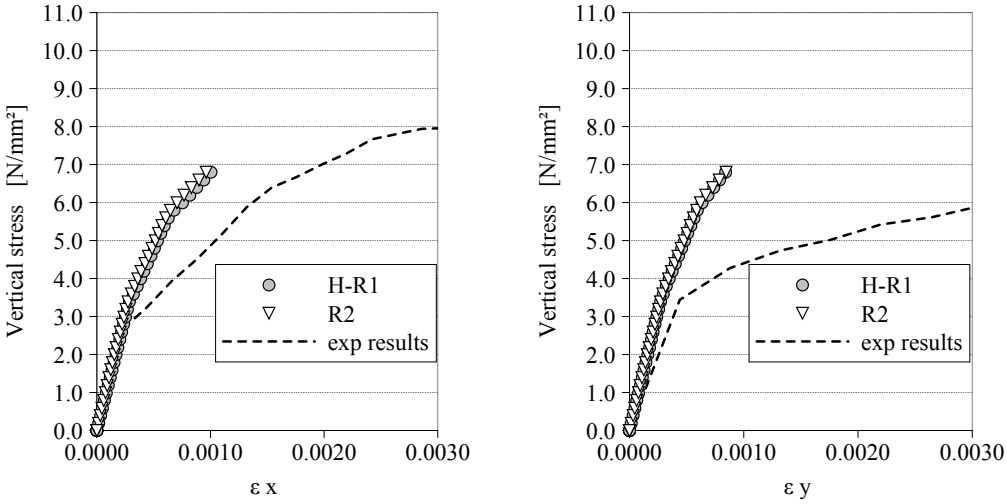

Figure 7.17: Stress-strain relationships on the horizontal directions.

parts behave independently. The internal core attains its strength before that of the external layer. this confirms that the grout injections provides its contribution only during the first part of the tests, when the admixture allows to delay the wide out-of-plane deformation of the external layers.

Over this point, cracks occur early on the lateral direction (figure 7.20b) and, subsequently, also on the main sides (figure 7.22b). Furthermore, the damage arises in the middle and develops through the surfaces. As presented also in the previous section, this order of damage appearance is notable also on the numerical models (figures 7.20a and 7.22a). One should note as, due to the chosen failure criterion in tension, the model concentrate the tensile failure in a limited zone, while a discrete cracking obviously appears on the surface of specimen.

Nevertheless, after the appearance of cracks on the lateral and main sides, only the external leaf can be considered as load bearing, due to damage at the interface. As a consequence, the stress level widely increases only in the outer part (figure 7.21a), inducing a damage on stones (figure 7.21b).

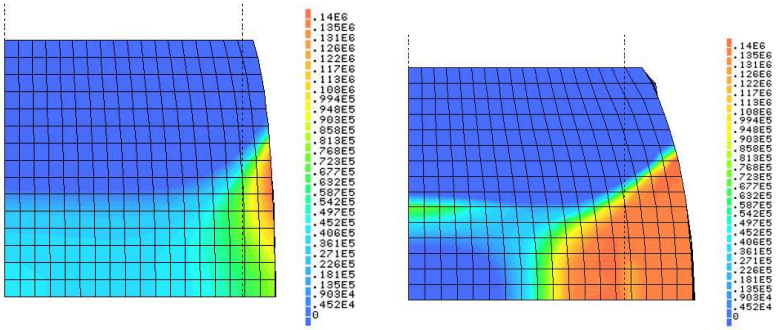

(a) Internal view at 5N/mm^2 **(b)** Internal view at failure

Figure 7.18: Distribution of tensile stress in the horizontal X direction, model H-R1.

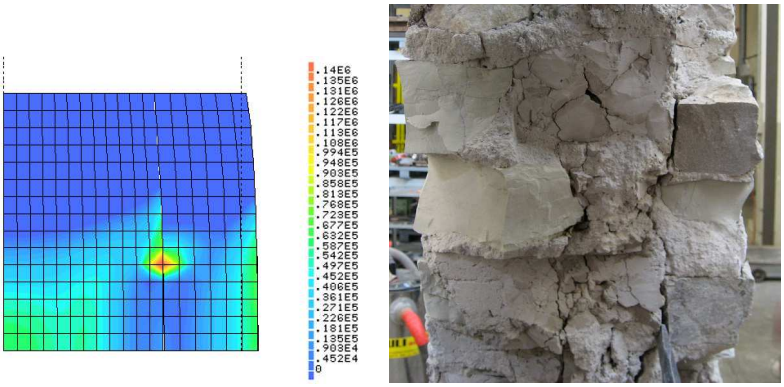

(a) Tensile stress along X, model R2 **(b)** Experimental behaviour

Figure 7.19: Comparison at about 3.36N/mm^2.

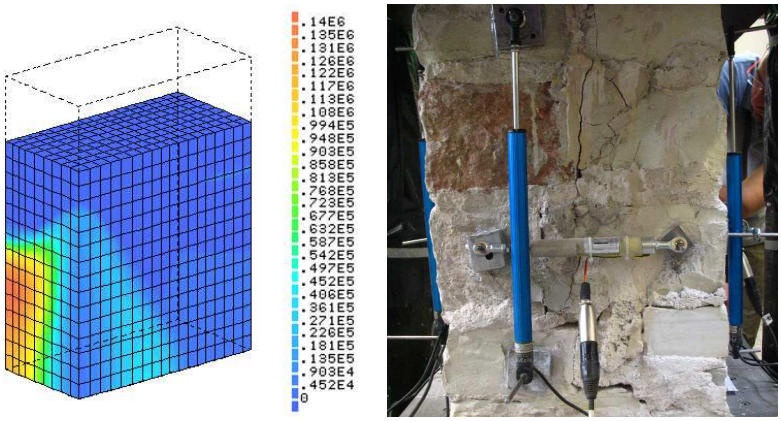

(a) Tensile stress along X, model R2 **(b)** Experimental behaviour

Figure 7.20: Comparison at about 4.72N/mm^2.

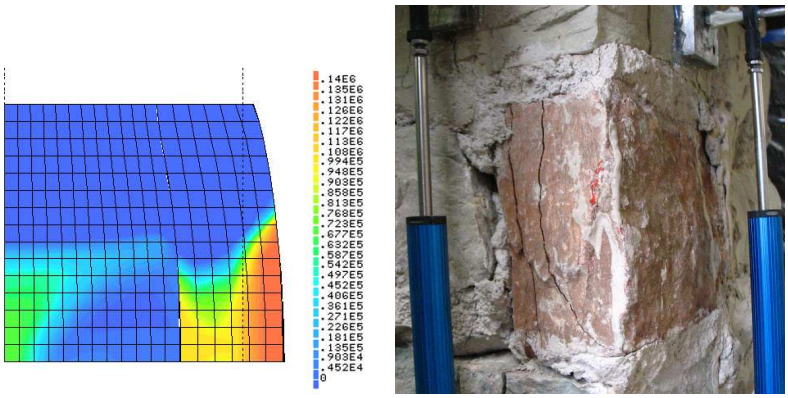

(a) Tensile stress along X, model R2 **(b)** Experimental behaviour

Figure 7.21: Comparison at about 5.95N/mm^2.

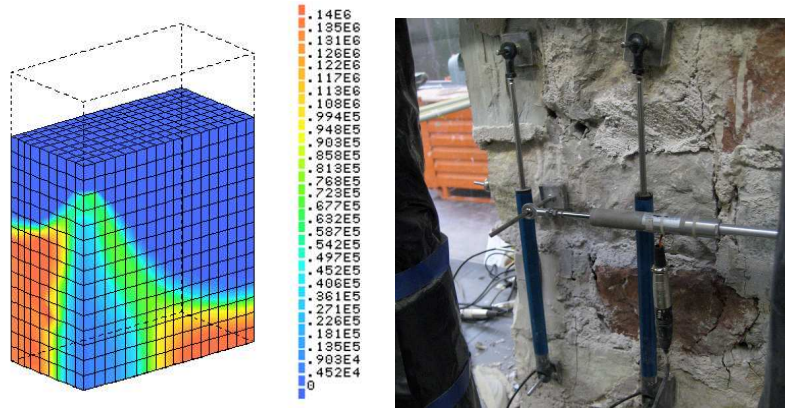

(a) Tensile stress along X, model R2 **(b)** Experimental behaviour

Figure 7.22: Comparison at about 6.92N/mm^2.

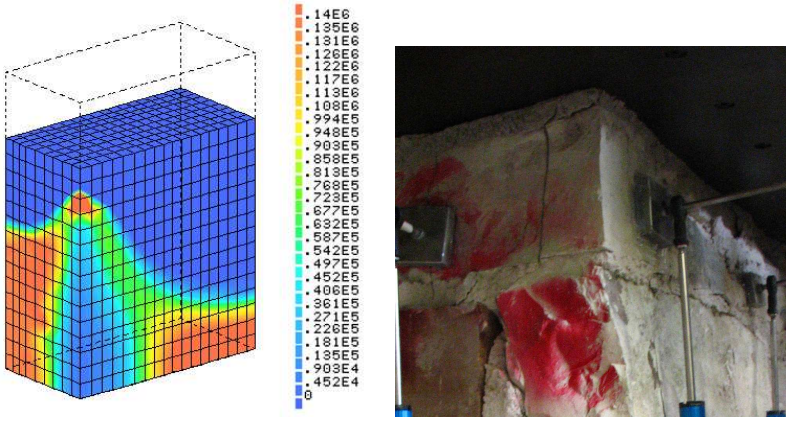

(a) Tensile stress along X, model R2 **(b)** Experimental behaviour

Figure 7.23: Comparison at about 7.27N/mm^2.

Finally, before the failure of the numerical model, a stress concentration can be found on the top of the sample, just below the corner (figure 7.23a). This accumulation could be seen also during the experiment, since stones in these position crushed (figure 7.23b).

Over this load level the numerical simulation failed, due the attainment of the tensile strength in a wide part of the external leaf. In fact, a further increase of the vertical load can be no way redistributed. The experimental test exhibits a similar behaviour, since the crack pattern widely develops, involving the whole surface of the specimen. This inability to redistribute the stresses prevents also the numerical models to simulate the post-peak phase.

7.5 Conclusive Remarks

The numerical analyses presented in this chapter allow to drawn few conclusions reported as follows.

Both model typologies, namely multi- and single-material FE models, show similar results as well as analyses within each category.

The stress-strain relationships are almost equal and similar problems arise in both models, leading to a premature failure. The vertical experimental strains are well predicted up to the non-convergence of the models. Nevertheless, all numerical simulations show a wide underestimation of the horizontal strains, particularly in the transversal sides. This divergence begins when a damage occurs on the specimen, while the FE models are not able to attain these large deformations.

Moreover, the stress distribution shows a good correlation with the experimental observations. The multi-material models are able to predict more in detail the real condition, since the interaction among different materials induces a more correct stress distribution.

In both cases a wide influence of the interface elements, that separate the specimen from the testing system, should be underlined. This was one of the main parameters that controlled the failure mechanism of each model. Actually, the lower the tangential stiffness, the lower is the horizontal retention at the top of the specimen and, consequently, the lower the induced tensile stress.

These problems can be overcome with some shrewdness in the case of both multi-material and homogeneous models. If the tangential stiffness of the interface (type A) is decreased, the load peak of the experimental curve can be attained in both model typologies. Nevertheless, this can be done only to detriment of a correct stress distribution. Actually, this change delays the beginning of damage, that occurs only close to the failure and at a too high load level.

The multi-material model, as discussed, provides more detailed results, even if the overall behaviour provided by the single-material model is very similar. Slight differences occur in the internal core, even if any experimental verification could be done. On the other hand, the employment of an easier model allows a lower computational cost.

In the light of the final aim of this numerical modelling, one can conclude as the results obtained from the single-material model are reliable, since this is proved by the analogy with those, more detailed, achieved by the multi-material model.

As a consequence, a possible development of these analyses, here presented, should be identified in a further simplification of the model. In fact, the presented results seem to indicate as a planar model can similarly predict the overall behaviour, considering

that the transversal strains will not be modelled. Nevertheless, as commented, these deformations can not be correctly predicted with the proposed three dimensional models. This would result in the possibility to model more complex mechanical behaviours, such as a planar stress state, on the base of the results obtained from shear compression tests.

Finally, the calibration of this model would provide a simple constitutive law, employable on the modelling of a whole structure subjected to a dynamic loading and the results would be comparable with those achieved during the shaking table tests.

Chapter 8

Conclusions

In this chapter some general remarks and final observations arising from the experimental work and the performed analyses are drawn.

The research aims at deepening the knowledge of the effects induced by the injection of hydraulic lime-based grout on multi-leaf stone masonry structures. The conclusions, following the thesis layout, are divided into the two main investigated fields: the overall dynamic behaviour of injected masonry buildings and the influence of injection on the quasi-static behaviour of structural elements, namely compression and in-plane solicitations. Moreover, a further section is added to present the most relevant conclusions obtained from the FE analysis.

These final remarks, starting with the experimental observations and the subsequently performed analyses, aim at defining the reliability and the effectiveness of the employment of structural injections of an expressly designed material.

Finally, further interesting issues have arisen from the experimental tests, the performed analyses and the achieved results. Moreover, open questions and possible future investigation fields are presented, for which further experimental research and numerical studies are needed.

8.1 Dynamic behaviour of injected multi-leaf stone masonry buildings

Shaking table tests on multi-leaf stone masonry buildings were performed with the aim of studying the influence of injections on the dynamic behaviour of historical structures. This technique, like other strengthening methodologies, is already widely employed by professional engineers and companies even if few studies, focusing on the dynamic effects of its use, have already been carried out. Moreover, the research also investigated the possible differences in intervening on a damaged (repair) or undamaged (strengthening) structure. This allowed the examination of the most effective application of the injection technique but also led to identify its limits and consequences.

Preliminary sonic investigations, performed before and after injection operations on the building models and on the panels, allowed to confirm their important role in the design of the strengthening intervention and on its verification.

- Both direct and the tomographic sonic investigations, demonstrated that they are able to identify the void presence and further internal characteristics of the analyzed masonry.

- A comparative evaluation of the achieved results can provide information on the masonry quality, with an adequate and wide reference database.
- The most effective result provided by sonic investigations regards their capability to evaluate grout penetration, through the comparison of the analyses performed before and after the grout injection.
- Sonic analyses also represent an important verification phase of the grout injection. They allow the good quality of injection operations to be evaluate, mainly analysing the homogeneity of distribution of the sonic velocities. In fact, strengthening intervention should be realized obtaining a uniform distribution of the grout to avoid undesirable effects due to different behaviours of the single parts of the same structure.

The actual execution of the shaking table experiments led to evaluate in detail the influence on the overall dynamic behaviour of the injected structure. As a consequence, vantages and disadvantages of the considered intervention technique could be identified.

- The employment of the lime grout injection is able to significantly reduce local failure problems. Actually, most relevant failure mechanisms, i.e. brittle collapse due to the separation of external masonry layers and the out-of-plane mechanism, could be avoided. This was proved in the case of both strengthening and repairing interventions.
- Injections are able to limit the crack pattern on building models. While on the unreinforced model a widespread crack pattern occurred, the Strengthened model exhibited limited and concentrated damage. The Repaired specimen manifested restricted damage, even if more extensive than that of the SM model and even if the most important cracks occurred in the unreinforced structure opened again.
- Both injected building models could suffer higher seismic accelerations than the unreinforced reference specimen, confirming the effectiveness of the intervention technique in increasing the strength of the injected structures. The repairing intervention allowed to sustain an increase of about 30% of the seismic acceleration. In the case of strengthening, this increase attained about 50%.
- The intervention operations led to an increase of the mass of the specimen, depending on the quantity of the injected grout. This increasing was about 10% in the case of both injected models. This additional mass, when subjected to seismic excitation, induces higher loads on the structure.
- The analyses based on the calculation of the Base Shear Coefficient allow the strength increase to be quantified. Despite the observation at the previous point, the strengthened model could suffer a lateral seismic load two-fold that of the unreinforced one. Instead, the repaired building demonstrated an overall increase of lateral load of about 50%.
- The hydraulic lime-based grout injection is able to re-establish, on the repaired model ("RM"), the original frequencies of the unreinforced one ("URM") in undamaged conditions, with a limited increase. Furthermore, also the initial

vibrational modes of an undamaged structure ("URM") may be recovered through the lime grout injection of a damaged masonry model ("RM").

- The grout injection allows the damping factors to be increased. Nevertheless, when heavy damage occurs to an injected structure, the dissipation capacity is almost similar to that of an unstrengthened structure.

However, the dynamic experiments also underlined a different structural behaviour between repaired and strengthened building models.

- The repaired model manifested the reopening of cracks previously appeared on the unreinforced structure. Moreover, also further damage and mechanisms already developed on the URM specimen could be seen on the RM model. Instead, the strengthened building showed a similar crack pattern but it arose at higher seismic loads.

- Both injected models manifested that this strengthening technique is able to substantially limit the frequency decrease, providing limited damage to both structures. However, the strengthened model ("SM" specimen) exhibited a better behaviour, since it was able to limit the frequency decrease up to higher seismic loads. On the other hand, the repaired model ("RM" specimen) demonstrated an initial behaviour similar to that of the SM sample but, at increasing dynamic inputs, the frequency decrease was faster and the overall reduction was higher. This difference becomes even more evident if, instead of the overall decrease, frequencies at same load level are compared.

- The strengthened structure manifested a monolithic behaviour up to higher seismic loads than the repaired model, that was in turn higher than the unreinforced one. This was confirmed by a comparison among the load level at which the three models had a significant changing on mode shapes.

- The injection allowed a higher dissipation capacity and this is most effective in the case of strengthening. The analysis of the damping factors demonstrated that these manifested a limited overall decrease on the SM model, if compared with those of the RM specimen.

- The analysis of stiffness degradation confirms the results summarized above for all the tested building models. The unreinforced specimen had the highest decrease, while the strengthened and repaired samples could sustain higher loads with a lower stiffness reduction, corresponding to a lower damage level when subjected to the same seismic load. Nevertheless, the SM model showed the lowest decrease, while the RM structure can be considered an intermediate condition between the strengthening and unreinforced cases.

Finally, a relation, mainly depending on the mass of both injected grout and structure, is proposed with the aim to provide an indication of the stiffness increasing, in the case of repairing intervention of a damaged structure. Nevertheless, a higher number of data should be collected to verify this relationship, due to the limited number of available measurements.

The employment of hydraulic lime-based grout injection as a strengthening technique undoubtedly causes a partial modification of the dynamic behaviour with reference to the unreinforced case.

The simple execution of the injection operations resulted in a limited alteration of some basic quantities, listed below, that characterize the overall dynamic behaviour of the structure. Furthermore, no difference could be seen between the repaired and strengthened models concerning these quantities:

- Limited frequency and stiffness increase after grout injection;
- Substantial invariance of the mode shapes;

However, the experimental campaign also highlighted the substantial modifications induced by the injection employment on further quantities:

- Higher strength;
- Limitation of crack pattern;
- Increase of damping factors;
- Limited degradation of frequencies, stiffness and mode shapes;

The dynamic experimental campaign establishes the feasibility and the effectiveness of hydraulic lime-based grout injection. This operation allows greater safety of multi-leaf stone masonry buildings in the event of an earthquake.
Both interventions, strengthening and repairing, demonstrated positive consequences. However, the injection of an undamaged structure is more effective than intervening in previously damaged buildings.
The above mentioned remarks allow to observe that the intervention may be performed also in a localised part of a structure, without involving the whole building. In fact, any substantial variation of frequencies, mode shapes and stiffness is induced in the injected portion of masonry, with reference to the unstrengthened part. Instead, the failure mechanisms and further mechanical properties, such as compressive and shear strength, will be improved.
Finally, one should consider as, when heavy damage occurs in an unstrengthened structure, the repairing through injection is not able to always provide an adequate safety level. This implies that further and different interventions should be evaluated and possibly combined with that of grout injection.

8.2 Mechanical behaviour of injected structural elements

The shear compression experimental campaign, preceded by a series of compression tests, completed the knowledge of the effects of the hydraulic lime-based grout injection on multi-leaf stone masonry walls. While shaking table tests expressly studied the dynamic behaviour of whole structures, this experimental part focused on both the compression and in-plane behaviour of single structural elements, made of the same masonry typology.

Preliminary compression tests provided the basic mechanical characterization of injected elements and these also allowed an examination of their typical failure modes. Furthermore, the monotonic compression experiments proved only slight and negligible differences between strengthened ("S" specimens) and repaired ("R" specimens) panels.

- The final observed crack pattern was quite similar, even if it developed differently up to the attainment of failure. While repaired samples damage almost uniformly along the experiment, the "S" series manifested fewer cracks up to more than 60% of their compressive strength and, only over this point, widespread damaged.
- The mean compressive strength of the "S" series results very similar to that of the "R" series, with a slight increase lower than 10%.
- The elastic modulus of the two typologies differed by about 20%, even if one should note that the values are low, approximately 4400N/mm^2 for the "S" series and 3600N/mm^2 for the "R" samples. A mean value of 4000N/mm^2 seems to be representative of all the specimens, since the scattering among all results is limited.
- The injection seems only to delay and not avoid the failure mode typical for this masonry typology. In fact, the collapse occurred as normally described in literature: vertical cracks opened on the masonry thickness and the collapse occurred because of the out-of-plane failure of the external layers.

In conclusion the differences between the strengthened and repaired elements appeared as limited and restricted to a few aspects, namely the mean strength and deformation capability. As a consequence, their mechanical behaviour when subjected to vertical loads can be equated.

Shear compression tests allowed an evaluation of the influence of some parameters, namely different level of vertical stress and slenderness ratio, on the overall behaviour of injected multi-leaf stone masonry.

- The injection intervention allowed a more monolithic behaviour of the samples, in case of both strengthening and repairing. As a consequence, the classical failure mechanisms, in particular the shear and the flexure, can develop on the panels.
- The typical formulations for the prediction of the different failure modes can be satisfactory applied. Particularly, the relation proposed by Turnšek and Sheppard can correctly predict the shear mechanism.
- The initial behaviour and first cracks appeared independent of both the aspect ratio and the precompression level. In fact, the initial damage always occurred between 1mm and 2mm of lateral displacement.
- The overall behaviour of the slender samples was mainly governed by the imposed precompression level. A lower vertical stress induced a rocking mechanism on the specimens, which presented higher displacement capacity indicators.
  On the other hand, the specimens subjected to a higher axial load exhibited a brittle failure mode because of a shear mechanism.
- Squat specimens exhibited a widely different overall behaviour, mainly dependent on the applied vertical load. A low precompression level led the sample to fail because of the shear mechanism. This specimen manifested overall characteristics only slightly different from the slender specimens with a high vertical load, especially in terms of capacity indicators.
  On the other hand, a higher vertical load induced an initial shear mechanism, while a subsequent compressive behaviour led to the failure of the specimen.

- The stiffness degradation appeared mainly dependent on the applied vertical load. Actually, the higher the precompression level, the faster was the overall decay, even if the final values are almost similar.

- The higher the vertical stress on slender specimens, the higher was the energy dissipation and damping factors. In fact, the higher precompression level led to an energy dissipation that hovered around 45% and to resistance indicators similar to those occurred at lower vertical stress. Nevertheless, this conditions induced also a lower capacity indicator and a brittle failure mode, due to a shear mechanism.

- The squat specimens showed a limited increase of the dissipation capacity, when the applied vertical load is increased. The energy dissipation was sightly increased but the damping factors at both cracking and lateral resistance limits are almost equal. Furthermore, the energy dissipation on squat samples with lower precompression was similar to that of slender specimens with higher vertical stress, even if the overall degradation of the squat specimens occurred earlier.

- In all cases, over the attainment of the maximum later capacity and after the complete development of its typical mechanism, depending on both the slenderness and applied vertical load, the crack pattern was influenced by the effect of the compression load. This caused the beginning of sub-vertical cracks on the main sides. Furthermore, an evident damage also occurred on the lateral sides, due to the out-of-plane failure mechanism of the external layers.

On the basis of these considerations, no substantial difference in the overall behaviour could be seen between the repaired and strengthened panels. Furthermore, the injection of hydraulic lime-based grout allowed the development of typical failure mechanisms and was able to delay the beginning of separation of the external layers. This collapse mechanism was not prevented, but manifested only close to the failure. Energy dissipation seems to be the only analysis which presented a slight difference, with higher values for the "S" series than for the "R" one.

Finally, all the remarks and observations drawn on the basis of the results obtained from both the dynamic tests, presented in the previous section, and those achieved by quasi-static experiments, above summarized, lead to two further conclusions.
The shaking table tests allowed to propose a modification, concerning the part where the intervention by grout injection is considered, of the annex 11.E of the OPCM 3274 [2003] and following modifications [OPCM 3431, 2005].
Furthermore, the observations performed during the whole injection process, the preliminary and subsequent non-destructive investigations and the results obtained from the whole experimental campaign allowed to draw up a detailed Technical Report. This document (compare Appendix B) would be an important result in order to provide future guidelines for the execution and the verification of the strengthening intervention by injections.
Both these documents are drawn up within the ReLUIS National Project (Progetto esecutivo 2005-2008, Attuazione Accordo di Programma Quadro DPC-Reluis del 15 Marzo 2005).

8.3 FE modelling of injected elements

The numerical simulation performed within this research was limited to FE model for the analysis of compression tests on injected elements. Two different analyses were developed: (i) complete models investigated the behaviour of both the internal and external layers and their interaction, (ii) simplified models considered a unique and homogeneous material. Some conclusions can be drawn on the obtained results:

- Both series of models can satisfactory predict the vertical strains as well as the stress distribution in the whole specimen, providing a correct simulation of its overall behaviour.
- The considered models cannot correctly predict the experimental horizontal deformations. These values are underestimated, due to a large increase of the horizontal strains when a widespread crack pattern occurs on the sample.
- Both models can correctly predict the failure mechanism and the stress distribution of the injected specimens. This can be obtained to the detriment of a correct prediction of the failure load, which is underestimated if compared with the experimental result.
- The subsequent simplification of the models, employing an homogeneous material, provides results similar to those achieved by the multi-material models, allowing a lower computational cost. This represents a fundamental aspect for a next development of more complex analyses.

8.4 Further developments of the research

The overall research program included a wide experimental program on both structures and substructures as well as on numerical investigations. The results obtained in these mentioned fields can be deepened and further studies and analyses can increase the knowledge about static and dynamic behaviour of injected multi-leaf masonries. On the light of the presented outcomes, some possible developments are listed hereafter:

- Performing dynamic tests on sub-structural elements, namely simple panels, in unstrengthened and strengthened conditions will allow to deepen the study about the influence of lime grout injection on their out-of-plane behaviour.
- Performing further quasi-static experiments would allow a better comprehension of lime grout injection on both compression behaviour and shear compression capacities. Actually, specimens on unreinforced conditions, not comprehended within this thesis, and a greater number of repaired and strengthened samples would lead to estimate the effectiveness of the lime grout on improving the masonry behaviour.
- Carrying out quasi-static tests on the above mentioned samples, considering both reduced and full scale elements, would permit to relate the presented results with a real condition. Furthermore, this would allow to study the influence of the scale factor on experimental tests and analyses.

- The obtained results and further shear compression tests would permit to provide an analytical model for the prediction of shear strength in case of unstrengthened, repaired and strengthened elements.
- A simplified planar FE model could be developed to provide a numerical simulation of the performed shear compression tests. This would constitute the preliminary phase for subsequent dynamic analyses of the whole building models, tested on the shaking table.
- A forthcoming campaign of in-situ investigations on historical stone masonry building damaged by the recent earthquake occurred on Abruzzo (Abruzzo earthquake, April 6^{th}, 2009) has been designed by the University of Padua and this will be performed in a short-time. This campaign will involve diagonal tests on unstrengthened and injected panels. This will provide further information concerning the effectiveness of the grout injection and will constitute a verification of the results obtained in the present research.

References

AA. VV. (2006a). Scheda per il rilievo del danno ai beni culturali - chiese. Technical report, GNDT (Gruppo Nazionale per la Difesa dai Terremoti).

AA. VV. (2006b). Scheda per il rilievo del danno ai beni culturali - palazzi. Technical report, GNDT (Gruppo Nazionale per la Difesa dai Terremoti).

AA. VV. (2008). Manuale per la compilazione della scheda di primo livello di rilevamento danno, pronto intervento e agibilità per edifici ordinari nell'emergenza post-sismica (aedes). Technical report, GNDT (Gruppo Nazionale per la Difesa dai Terremoti).

Abbaneo, S., Anzani, A., and Binda, L. (1996a). *Il rilievo delle sezioni e il comportamento meccanico delle murature*, pages 127–144. Storia delle Tecniche Murarie e Tutela del Patrimonio, Esperienze e Questioni di Metodo. (in italian).

Abbaneo, S., Berra, M., and Binda, L. (1996b). Pulse velocity test to qualify existing masonry walls: usefulness of waveform analyses. In *Proc. 3rd Conference: Nondestructive evaluation of civil structures and materials; Boulder, Colorado*, pages 81–95.

ABK (1981). Methodology for mitigation of seismic hazards in existing unreinforced masonry buildings: Wall testing, out-of-plane. abk topical report 04. Technical report, ABK.

Adami, C.-E. and Vintzileou, E. (2008). Interventions to historic masonries: Investigation of the bond mechanism between stones or bricks and grouts. *Materials and Structures*, **41**(2), 255–267.

Allemang, R. J. (1984). Experimental modal analysis bibliography. In *Proceedings of 2nd International Modal Analysis Conference (IMAC II), Orlando, FL*, page 1085Ũ1097.

ARTeMIS Extractor (SVS). Version 4.1. Structural Vibration Solutions A/S. Aalborg East, Denmark (`http://www.svibs.com/`).

BAM (2004). Report on the evaluation at pilot sites (report for owners of historic buildings). pilot site: Altes museum in berlin/germany. on-site investigation techniques for the structural evaluation of historic masonry buildings. Technical report, BAM (Bundesanstalt für material forschung und prüfung), SLG (Stiftung Luther Gedenkstätten in Sachsen-Anhalt) and partners (laFb, IDK). Deliverable D10.2 & D.10.4 ONSITEFORMASONRY, `http://www.onsiteformasonry.bam.de/`.

Bariola, J., Ginocchio, J. F., and Quinn, D. (1990). Out-of-plane seismic response of brick walls. In *Proceedings of 5th North American Masonry Conference, Champaign.*

Baronio, G., Binda, L., Tedeschi, C., and Tiraboschi, C. (2003). Characterisation of the materials used in the construction of the noto cathedral. *Construction and Building Materials*, **17**(8), 557 – 571. The reconstruction of Noto and Dresden Cathedrals.

Benedetti, D. (1980). Repairing and strengthening stone masonry buildings. In *Proceedings of the International Research Conference on Earthquake Engineering, Skopje*, pages 503–515.

Benedetti, D. and Castellani, A. (1980). Dynamic versus static behaviour of a masonry structure under lateral loads. *Engineering Structures*, **2**(3), 163–170.

Benedetti, D. and Pezzoli, P. (1996). Shaking table tests on masonry buildings. Technical report, Polytechnic of Milan & ISMES Research Centre.

Benedetti, D., Carydis, P., and Pezzoli, P. (1998). Shaking table tests on 24 simple masonry buildings. *Earthquake Engineering & Structural Dynamics*, **27**(1), 67–90.

Beolchini, G. C., Grillo, F., Ricciardulli, G., and Valente, G. (1997a). Comportamento di una parete in muratura di pietrame rinforzata con iniezioni diffuse di malta di cemento soggetta a forze cicliche nel piano. In *Atti 8ř Convegno Nazionale ANIDIS, L'ingegneria sismica in Italia, Taormina.*

Beolchini, G. C., Grillo, F., and Ricciardulli, G. (1997b). Prove cicliche a compressione diagonale su pannelli in muratura di pietrame rinforzati con diverse tecniche: confronto dei risultati. In *Atti 8ř Convegno Nazionale ANIDIS, L'ingegneria sismica in Italia, Taormina.*

Bernardini, A., Modena, C., Lazzaro, G., and Valluzzi, M. R. (1997). Cyclic behaviour and modelling of reinforced masonry panels. In *Proc. 11th Int. Brick/Block Masonry Conf., Shangai, China.*

Berra, M., Binda, L., Baronio, G., and Fatticcioni, A. (1988). Ultrasonic pulse transmission: a proposal to evaluate the efficiency of masonry strengthening by grouting. In *2nd International Conference on Non-Destructive Testing, Micro-analytical Methods and Environment Evaluation for Study and Conservation of Works of Art*, volume I, pages I/10.1–I/10.19.

Berra, M., Binda, L., Anti, L., and Fatticcioni, A. (1992). Non destructive evaluation of the efficacy of masonry strengthening by grouting techniques. In *Proceedings of International workshop: Effectiveness of injection techniques for retrofitting of stone and brick masonry walls in seismic areas*, pages 63–70. Polytechnic of Milan, Italy.

Bettio, C., Gelmi, A., Modena, C., and Rossi, P. P. (1993). Caratterizzazione meccanica e consolidamento statico delle murature dei centri abitati di antica origine della provincia di trento. In *Murature, Sicurezza e Recupero, Trento.* in Italian.

Binda, L. (1999). Caratterizzazione delle murature in pietra e mattoni ai fini dell'individuazione di opportune tecniche di riparazione. Technical report, Politecnico di Milano. relazione finale, contratto CNR/GNDT.

Binda, L. and Penazzi, D. (2000). Classification of masonry cross sections and of typologies of historic buildings. Technical report, Book of Commission RILEM MMM.

Binda, L. and Saisi, A. (2001). State of the art of research on historic structures in italy. Department of Structural Engineering, Politecnico of Milan, Italy.

Binda, L. and Saisi, A. (2005). Research on historic structures in seismic areas in Italy. *Progress in Structural Engineering and Materials*, **7**(2), 71–85.

Binda, L. and Tiraboschi, C. (1999). Flat-jack test as a slightly destructive technique for the diagnosis of brick and stone masonry structures. *International Journal for Restoration of Buildings and Monuments*, pages 449–472.

Binda, L., Modena, C., Baronio, G., and Abbaneo, S. (1997a). Repair and investigation techniques for stone masonry walls. *Construction and Building Materials*, **11**(3), 133 – 142.

Binda, L., Modena, C., Baronio, G., and Abbaneo, S. (1997b). Repair and investigation techniques for stone masonry walls. *Construction and Building Materials*, **II**(3), 133–142.

Binda, L., Baronio, G., Penazzi, D., Palma, M., and Tiraboschi, C. (1999). Caratterizzazione di murature in pietra in zona sismica: Data-base sulle sezioni murarie e indagini sui materiali. In *9º Convegno Nazionale di Ingegneria Sismica, Torino*. (in italian).

Binda, L., Saisi, A., and Tiraboschi, C. (2000a). Application of sonic tests to the diagnosis of damage and repaired structures. *International Journal Non-Destructive Testing and Evaluation*.

Binda, L., Lagomarsino, S., Modena, C., Penazzi, D., and Valluzzi, M. R. (2000b). Indagine su materiali e strutture di edifici dei centri storici colpiti da sisma del 1997: Montesanto e Roccanolfi. In *Il Patrimonio Storico Architettonico e il Terremoto: la Diagnosi e gli Interventi di Recupero, L'Aquila*, pages 85–104.

Binda, L., Saisi, A., and Tiraboschi, C. (2000c). Investigation procedures for the diagnosis of historic masonries. *Construction and Building Materials*, **14**(4), 199 – 233.

Binda, L., Baronio, G., Palma, M., and Penazzi, D. (2000d). Località di Roccanolfi di Preci e Montesanto di Sellano: Redazione di Schede per il Rilievo Tipologico e dei Danni Sismici agli Edifici. In *Il Patrimonio Storico Architettonico e il Terremoto: la Diagnosi e gli Interventi di Recupero, L'Aquila*, pages 85–104.

Binda, L., Baronio, G., Cardani, G., Penazzi, D., Tedeschi, C., and Tongini, F. R. (2001). *Il Progetto di Conservazione*, pages 174–197. S. Pesenti, Alinea.

Binda, L., Penazzi, D., and Saisi, A. (2003a). Historic masonry buildings: Necessity of a classification of structures and masonries for the adequate choice of analytical models. In *6th International Symposium: Computer Methods in Structural Masonry (STRUMAS VI), Roma*, pages 168–173. T.G.Hughes & G.N. Pande, Computers & Geotechnics, Ltd.

Binda, L., Anzani, A., and Fontana, A. (2003b). Mechanical behaviour of multiple-leaf stone masonry: experimental research. In *International Conference Structural Faults & Repair, London*. Keynote Lecture.

Binda, L., Saisi, A., and Zanzi, L. (2003c). Sonic tomography and flat-jack tests as complementary investigation procedures for the stone pillars of the temple of s. nicolò l'arena (italy). *NDT & E International*, **36**(4), 215 – 227. Structural Faults and Repair.

Binda, L., Saisi, A., and Zanzi, L. (2004). Report on calibration and testing results. Technical report, Polytechnic of Milan. On-site investigation techniques for the structural evaluation of historic masonry buildings, `http://www.onsiteformasonry.bam.de/`.

Binda, L., Pina-Henriques, J., Anzani, A., Fontana, A., and Lourenço, P. (2006). A contribution for the understanding of load-transfer mechanisms in multi-leaf masonry walls: Testing and modelling. *Engineering Structures*, **28**(8), 1132 – 1148.

Binda, L., Cantini, L., Cardani, G., Saisi, A., and Tiraboschi, C. (2007). Use of flat-jack and sonic tests for the qualification of historic masonry. In *10th Tenth North American Masonry Conference (10NAMC), St. Louis, Missouri*, pages 791–803.

Borri, A., De Maria, A., and Cangi, G. (1999). *Regione dell'Umbria - Manuale per la riabilitazione e la ricostruzione post-sismica degli edifici*, chapter "Riparazione e consolidamento degli edifici in muratura". DEI - Tipografia del Genio Civile, Roma. A cura di Gurrieri F..

Borri, A., De Maria, A., and Piccarreta, M. (2004). Osservazione dei danni negli edifici di aggregazioni storiche dell'umbria. In *XI Congresso Nazionale "L'ingegneria Sismica in Italia", Genova*.

Bosiljkov, V. (2000). *Experimental and numerical research on the influence of the modified mortars on the mechanical properties of the brick masonry*. Ph.D. thesis, University of Ljubljana, Slovenia.

Bosiljkov, V. (2004a). Report on the evaluation at pilot sites (report for owners of historic buildings). pilot site: Pisće/slovenia. on-site investigation techniques for the structural evaluation of historic masonry buildings. Technical report, ZAG. Deliverable D10.2 & D.10.4 ONSITEFORMASONRY, `http://www.onsiteformasonry.bam.de/`.

Bosiljkov, V. (2004b). Structural modelling for the assessment of the load bearing capacity of of the masonry. Technical report, ZAG. Deliverable D11.2 ONSITEFORMASONRY, `http://www.onsiteformasonry.bam.de/`.

Bosiljkov, V., Tomazevic, M., and Lutman, M. (2004). Optimization of shape of masonry units and technology of construction for earthquake resistant masonry buildings. Technical report, Slovenian National Building and Civil Engineering Institute, Ljubljana.

Bosiljkov, V., Totoev, Y., and Nichols, J. (2005). Shear modulus and stiffness of brickwork masonry: An experimental perspective. *Structural Engineering & Mechanics*, **20**(1).

Bresolato, F. and Pasin, N. (2008). *Indagini Sperimentali con Prove Soniche su Murature in Pietra Consolidate Mediante Iniezioni. Verifica dell'iniettabilità della muratura e controllo dell'efficacia dell'intervento di iniezione.* Master's thesis, Università di Padova. in italian.

Brincker, R. and Andersen, P. (2000). Ambient response analysis of the heritage court tower building structure. In *Proceedings of IMAC-XVIII: A Conference on Structural Dynamics*, pages 1081–1087.

Calvi, G. M., Kingsley, G. R., and Magenes, G. (1996). Testing of masonry structures for seismic assessment. *Earthquake Spectra*, **12**(1), 145–162.

Carbonara, G. (1996). *Restauro Architettonico*, volume II. UTET, Torino.

Cardani, G. (2003). *La vulnerabilità sismica dei centri storici: il caso di Campi Alto di Norcia. Linee guida per la diagnosi finalizzata alla scelta delle tecniche di intervento per la prevenzione dei danni.* Ph.D. thesis, Politecnico di Milano.

Casarin, F. (2006). *Structural assessment and seismic vulnerability analysis of a complex historical building.* Ph.D. thesis, Università degli Studi di Padova.

Casarin, F., Valluzzi, M., da Porto, F., and Modena, C. (2007). Evaluation of the structural behaviour of historic masonry buildings by using sonic pulse velocity method. In *10^{th} International Conference on Studies, Repairs and Maintenance of Heritage Architecture, STREMAH 2007*, pages 227–236. 4-6 July 2007, Prague, Czech Republic.

Cawley, P. and Adams, R. D. (1979). The location of defects in structures from measurements of natural frequencies. *The Journal of Strain Analysis for Engineering Design*, **14**(2), 49–57.

Chen, H. L. and Shah, S. P. (1988). Test of model masonry single pier under dynamic shaking and quasi-static cycling loading. In *Masonry: Materials, Design, Construction and Maintenance, ASTM STP 992*, pages 145–165.

Chiostrini, S. and Vignoli, A. (1994). In-situ determination of the strenght properties of masonry walls by destructive shear and compression tests. *Masonry international*, **7**(3).

Chung, W.-J., Yun, C.-B., Kim, N.-S., and Seo, J.-W. (1999). Shaking table and pseudodynamic tests for the evaluation of the seismic performance of base-isolated structures. *Engineering Structures*, **21**(4), 365 – 379.

Clough, R. W., Gülkan, P., Manos, G. C., and Mayes, R. L. (1990). Seismic testing of single-story masonry houses: Part 2. *Journal of Structural Engineering*, **116**(1), 257–274.

Corradi, M., Borri, A., and Vignoli, A. (2002). Strengthening techniques tested on masonry structures struck by the Umbria-Marche earthquake of 1997-1998. *Construction and Building Materials*, **16**(4), 229–239.

Corradi, M., Borri, A., and Vignoli, A. (2003). Experimental study on the determination of strength of masonry walls. *Construction and Building Materials*, **17**(5), 325–337.

Corradi, M., Tedeschi, C., Binda, L., and Borri, A. (2008). Experimental evaluation of shear and compression strength of masonry wall before and after reinforcement: Deep repointing. *Construction and Building Materials*, **22**(4), 463 – 472.

Cunha, A. and Caetano, E. (2005). From input-output to output-only modal identification of civil engineering structures. In *1st International Operational Modal Analysis Conference (IOMAC, Copenhagen)*. Keynote Lecture.

da Porto, F. (2000). *Indagini sperimentali sull'efficacia di tecniche di consolidamento di murature storiche in pietra*. Master's thesis, Università degli Studi di Padova. in Italian.

da Porto, F. (2005). *In-plane cyclic behaviour of thin layer joint masonry walls*. Ph.D. thesis, Università degli Studi di Trento, Università degli Studi di Padova.

da Porto, F., Valluzzi, M. R., and Modena, C. (2004). Diagnosis and strengthening of the historic town walls of cittadella. In *6th International Symposium on the Conservation of Monuments in the Mediterranean Basin, Lisbon Portugal*.

dal Farra, V. (1992). *Indagine sperimentale sulla resistenza a taglio e consolidamento delle murature in pietra*. Master's thesis, Università degli Studi di Padova. in Italian.

De Sortis, A., Antonacci, E., and Vestroni, F. (2005). Dynamic identification of a masonry building using forced vibration tests. *Engineering Structures*, **27**(2), 155 – 165.

De Stefano, A. and Clemente, P. (2006). Shm on historical heritage: Robust methods to face larges uncertainties. Technical report, SAMCO Final Report.

Denoel, V., Butz, C., Jakobi, H., and Feldmann, M. (2007). Experimental determination of dynamic properties of the concrete foundation of a cement roller mill. In *EVACES 07, Experimental Vibration Analysis of Civil Engineering Structures, Porto, Portugal*.

DIANA TM (2005). *Finite Element Analysis, User's manual*. release 9, (`http://tnodiana.com`).

Doebling, S. W., R., F. C., Prime, M. B., and Shevitz, D. (1996). Damage identification and health monitoring of structural and mechanical systems from changes in their vibration characteristics: a literature review. Technical report, Los Alamos National Laboratory, NM. 132p.

Doglioni, F., Guadagnin, A., and Bondanelli, M. (2009). Rapporto tecnico sull'uso della impregnazione consolidante. Technical report, Università IUAV di Venezia. 3b.4 UR18-1.

Dolce, M., Cardone, D., Ponzo, F. C., and Valente, C. (2005). Shaking table tests on reinforced concrete frames without and with passive control systems. *Earthquake Engineering & Structural Dynamics*, **34**(14), 1687–1717.

Egermann, R. (1993). Edifici in muratura in pietra: ricerca e applicazioni all'università di karlsruh. In *Murature Sicurezza Recupero. Trento*.

Elgawady, M. A., Lestuzzi, P., and Badoux, M. (2004). Dynamic versus static cyclic tests of masonry walls before and after retrofitting with gfrp. In *13th World Conference on Earthquake Engineering, Vancouver*.

ElGawady, M. A., Lestuzzi, P., and Badoux, M. (2005). In-plane seismic response of urm walls upgraded with frp. *Journal of Composites for Construction*, **9**(6), 524–535.

Ewins, D. J. (1984). *Modal Testing: Theory and practice*. Research Studies Press. 313p.

Fardis, M. N., Bousias, S. N., Franchioni, G., and Panagiotakos, T. B. (1999). Seismic response and design of rc structures with plan-eccentric masonry infills. *Earthquake Engineering & Structural Dynamics*, **28**(2), 173–191.

Faria, P., Henriques, F., and Rato, V. (2008). Comparative evaluation of lime mortars for architectural conservation. *Journal of Cultural Heritage*, **9**(3), 338 – 346.

Forde, M. C., Birjandi, K. F., and Batchelor, A. J. (1985). Fault detection in stone masonry bridges by non-destructive testing. In E. T. Press, editor, *Proceedings of the 2nd International Conference Structural Faults & Repair*, pages 373–379. Edinburgh.

Franchetti, P. (2004). *Vibration-based damage assessment of precast elements*. Ph.D. thesis, Università degli Studi di Padova.

Galasco, A., Penna, A., and Magenes, G. (2009a). Caratterzzazione meccanica di muratura in pietra. parte prima: prove di compressione semplice e di compressione diagonale. Technical report, Università degli Studi di Pavia. Allegato 4.2-UR01-1, in Italian.

Galasco, A., Penna, A., and Magenes, G. (2009b). Caratterzzazione meccanica di muratura in pietra. parte seconda: prove cicliche di taglio-compressione su pannelli di grandi dimensioni. Technical report, Università degli Studi di Pavia. Allegato 4.2-UR01-2, in Italian.

Garaygordóbil, J. (2003). *Dynamic assessment of structural building components*. Ph.D. thesis, Universitat Politècnica de Catalunya.

Gardin, B. (2007). *Diagnosi delle murature storiche mediante procedure debolmente distruttive: problematiche nell'uso dei martinetti piatti*. Master's thesis, Università degli Studi di Padova. in Italian.

Gentile, C. and Saisi, A. (2004). Dynamic-based f.e. model updating to evaluate damage in masonry towers. In *Proceedings of the 4th International Seminar on Structural analysis of Historical Constructions, Padova, Italy*, pages 439–449.

Gentile, C. and Saisi, A. (2007). Ambient vibration testing of historic masonry towers for structural identification and damage assessment. *Construction and Building Materials*, **21**(6), 1311 – 1321.

Giuffrè, A. (1990). *Letture sulla meccanica delle murature storiche*. Kappa, Roma.

Giuffrè, A., Baggio, C., and Carocci, C. (1993). *Sicurezza e conservazione dei centri storici*. Laterza, Bari.

Gouveia, J. P. and Lourenço, P. B. (2007). Masonry shear walls subjected to cyclic loading: influence of confinement and horizontal reinforcement. In *10th North American Masonry Conference, St. Luis, Missouri*, pages 856–866.

Griffith, M. C., Magenes, G., Melis, G., and Picchi, L. (2003). Evaluation of out-of-plane stability of unreinforced masonry walls subjected to seismic excitation. *Journal of Earthquake Engineering*, **7**(1), 141–169.

Griffith, M. C., Lam, N. T. K., Wilson, J. L., and Doherty, K. (2004). Experimental investigation of unreinforced brick masonry walls in flexure. *Journal of Structural Engineering*, **130**(3), 423–432.

Gülkan, P., Clough, R. W., Mayes, R. L., and Manos, G. C. (1990). Seismic testing of single-story masonry houses: Part 1. *Journal of Structural Engineering*, **116**(1), 235–256.

Hashemi, A. and Mosalam, K. M. (2006). Shake-table experiment on reinforced concrete structure containing masonry infill wall. *Earthquake Engineering & Structural Dynamics*, **35**(14), 1827–1852.

Hendry, A. W. (1998). *Structural masonry.* Macmillan. 2^{nd} edition, 296p.

Heyman, J. (1997). *The Stone Skeleton: Structural Engineering of Masonry Architecture.* Cambridge University Press.

Jacobsen, N. J., Andersen, P., and Brincker, R. (2006). Using enhanced frequency domain decomposition as a robust technique to harmonic excitation in operational modal analysis. In *Proceedings of the 23^{rd} International Seminar on Modal Analysis, ISMA, Lueven, Belgium.*

Jaishi, B., Ren, W.-X., Zong, Z.-H., and Maskey, P. N. (2003). Dynamic and seismic performance of old multi-tiered temples in nepal. *Engineering Structures*, **25**(14), 1827 – 1839.

Juhásová, E., Hurák, M., and Zembaty, Z. (2002). Assessment of seismic resistance of masonry structures including boundary conditions. *Soil Dynamics and Earthquake Engineering*, **22**(9-12), 1193 – 1197.

Juhásová, E., Sofronie, R., and Bairrão, R. (2008). Stone masonry in historical buildings – ways to increase their resistance and durability. *Engineering Structures*, **30**(8), 2194 – 2205. Seismic reliability, analysis, and protection of historic buildings and heritage sites.

Jurukovsky, D., Krstevska, L., Alessi, R., Diotallevi, P. P., Merli, M., and Zarri, F. (1992). Shaking table tests of three four-storey brick masonry models: Original and strengthened by RC core and by RC jackets. In *Proceedings of 10^{th} World Conference on Earthquake Engineering, Balkema, Rotterdam*, volume 5.

Kennedy, C. C. and Pancu, C. D. P. (1947). Use of vectors in vibration measurements and analysis. *Journal of Aeronautical Sciences*, **14**(11), 603Ũ625.

Lanas, J. and Alvarez-Galindo, J. I. (2003). Masonry repair lime-based mortars: factors affecting the mechanical behavior. *Cement and Concrete Research*, **33**(11), 1867 – 1876.

Li, C. S., Lam, S. S. E., Zhang, M. Z., and Wong, Y. L. (2006). Shaking table test of a 1:20 scale high-rise building with a transfer plate system. *Journal of Structural Engineering*, **132**(11), 1732–1744.

Liberatore, D. and Spera, G. (2001). Response of slender blocks subjected to seismic motion of the base: experimental results and initial numerical analyses. In *Proceeding of the 5th STRUMAS Conference, Roma*.

Lourenço, P. B. (2001). Analysis of historical constructions: from thrust lines to advanced simulations. In *Proceedings of the 3rd International Seminar on Structural Analysis of Historical Constructions, Guimarães, Portugal*, pages 91–116.

Lourenço, P. B. (2002). Computations on historic masonry structures. *Progress in Structural Engineering and Materials*, **4**(3), 301–319.

Lourenço, P. B., Rots, J. G., and Blaauwendraad, J. (1998). Continuum model for masonry: Parameter estimation and validation. *Journal of Structural Engineering*, **124**(6), 642–652.

Lourenço, P. B., Oliveira, D. V., Roca, P., and Orduna, A. (2005). Dry joint stone masonry walls subjected to in-plane combined loading. *Journal of Structural Engineering*, **131**(11), 1665–1673.

Magenes, G. and Calvi, G. M. (1997). In-plane seismic response of brick masonry walls. *Earthquake Engineering & Structural Dynamics*, **26**(11), 1091–1112.

Mazzon, N., Valluzzi, M. R., Aoki, T., Garbin, E., De Canio, G., Ranieri, N., and Modena, C. (2009). Shaking table tests on two multi-leaf stone masonry buildings. In *Proceedings of the 11th Canadian Masonry Symposium. Toronto (Canada), May 31st - June 3rd 2009*. Mc Master University.

Meisl, C., Elwood, K., and Ventura, C. (2007). Shake table tests on the out-of-plane response of unreinforced masonry walls. *Canadian Journal of Civil Engineering*, **11**(34), 1381–1392.

Meisl, C. S., Elwood, K. J., Mattman, D. W., and Ventura, C. E. (2006). Out-of-plane seismic performance of unreinforced clay brick masonry walls. In *Proceedings of* 8th *U.S. National Conference on Earthquake Engineering, San Francisco, California.*

Modena, C. (1997). Criteria for cautious repair of historic buildings. In *Evaluation and Strengthening of Existing Masonry Structures, L. Binda & C. Modena Ed., RILEM*, pages 25–42.

Modena, C. (1999). Interpretazione dei risultati ottenuti dalle prove in sito nellŠambito delle tre convenzioni con gli istituti di ricerca di firenze e milano e modellazione del comportamento strutturale dei componenti rinforzati. Technical report, Convenzione di ricerca tra la Regione Toscana e il Dipartimento di Costruzioni e Trasporti dellŠUniversità degli Studi di Padova. in Italian.

Modena, C. and Bernardini, A. (1984). Behaviour of reinforced hollow clay brick masonry walls under lateral cyclic loads. In *International Symposium on Reinforced and Prestressed Masonry, Edinburgh.*

Modena, C. and Bettio, C. (1994). Experimental characterisation and modelling of injected and jacketed masonry walls. In *Proceedings of Italian-French Symposium Strengthening and Repair of Structures in Seismic Area, Nizza, France*, pages 273–282.

Modena, C. and Valluzzi, M. R. (2006). *Mechanical behaviour of masonry structures strengthened with different improvement techniques*, pages 137–156. Springer Netherlands.

Modena, C. and Valluzzi, M. R. (2007). *Repair techniques and long-term damage of massive structures*, pages 175–204. WIT press.

Modena, C., La Mendola, P., and Terrusi, A. (1992). Shaking table study of a reinforced masonry building model. In *Proceeding 10th World Conference on Earthquake Engineering*. Balkema, Rotterdam, 1992.

Modena, C., Pineschi, F., and Valluzzi, M. R. (2000). *Valutazioni della vulnerabilità sismica di alcune classi di strutture esistenti: sviluppo e valutazione di metodi di rinforzo*. C.N.R. - G.N.D.T., Roma.

Modena, C., Franchetti, P., Zonta, D., Menga, R., Pizzigalli, E., Ravasio, F., Muti, M., Meloni, R., and Bordone, G. (2001). Static and dynamic analyses of "maniace castle" in siracusa-sicily. In *Proceedings of the 3rd International Seminar on Historical Constructions, Guimarães, Portugal*, pages 933–942.

Modena, C., Valluzzi, m., da Porto, F., Casarin, F., Mazzon, N., and Munari, M. (2009). Sperimentazione dinamica su modelli di edifcio reali. Technical report, Università degli Studi di Padova. Allegato 4.2-UR07-5, in Italian.

Monteforte, N. (1997). *Applicazione della tomografia sonica nei problemi di diagnosi strutturale*. Master's thesis, University of Padua. in italian.

Mosele, F. (2009). *In-plane and out-of-plane cyclic behaviour of reinforced masonry walls*. Ph.D. thesis, Università degli Studi di Trento, Università degli Studi di Padova.

Oliveira, D. V. and Lourenço, P. B. (2006). Experimental behaviour of three-leaf stone masonry walls. In *The construction aspects of built heritage protection, Dubrovnik, Croatia*, pages 356–362.

Oliveira, D. V., Lourenço, P. B., and Roca, P. (2006). Cyclic behaviour of stone and brick masonry under uniaxial compressive loading. *Materials and Structures*, **39**(2), 247–257.

Penna, A., Galasco, A., and Magenes, G. (2007). Selezione dell'accelerogramma da utilizzare per la prova su tavola vibrante. Technical report, Università degli Studi di Pavia. Allegato 4.2-UR01-1.

Pina-Henriques, J. and Lourenço, P. B. (2003). Testing and modelling of masonry creep and damage in uniaxial compression. In *Proceedings of 8th International Conference on Structural Studies, Repairs and Maintenance of Heritage Architecture, Greece*, pages 151–160.

Pisano, F. (1999). *Validità di modelli fisici nello studio della tecnica di iniezione di murature storiche a tre paramenti*. Master's thesis, Politecnico di Milano.

Polytechnic of Milan (2004). Report on the evaluation at pilot sites (report for owners of historic buildings). pilot site: Avio castle in avio/italy. on-site investigation techniques for the structural evaluation of historic masonry buildings. Technical report, Politecnico di Milano. Deliverable D10.2 ONSITEFORMASONRY, `http://www.onsiteformasonry.bam.de/`.

Popov, E. P. (1986). Experiment as an aid to structural seismic design. *Experimental Mechanics*, **26**(2), 194–208.

Ramos, J. L. (2007). *Damage identification on masonry structures based on vibration signatures*. Ph.D. thesis, Universidade do Minho, Guimarães.

Ramos, L., Lourenço, P., and Costa, A. (2005). Operational modal analysis for damage detection of a masonry construction. In *Proceedings of 1^{st} International Operational Modal Analysis Conference, Copenhagen, Denmark*, pages 495–502.

Ramos, L., Casarin, F., Algeri, C., Lourenço, P., and Modena, C. (2006). Investigation techniques carried out on the qutb minar, new delhi, india. In *Proceedings of the 5^{th} International Seminar on Structural Analysis of Historical Constructions, New Delhi*.

Roberti, G., Donati, L., and Fontana, A. (2004). Out-of-plane behaviour of multiple-leaf stone masonry. In *Structural Analysis of Historical Constructions*, volume 2.

Rodrigues, J., Brincker, R., and Anderson, P. (2004). Improvement of frequency domain output-only modal identification from the application of the random decrement technique. In *Proceedings of the 23^{rd} International Modal Analysis Conference, Deaborn, USA*.

Rodrigues, P. F. and Henriques, F. M. A. (2004). Current mortars in conservation: An overview. *International Journal for Restoration*, **10**(6), 609–622.

Rots, J. G. (1997). *Structural masonry: an experimental/numerical basis for practical design rules*. J.G. Rots (Ed.), A.A. Balkema, Rotterdam. 152p.

Rots, J. G. (2002). Comparative study of crack models, finite elements in civil engineering. In *Proceedings from the 3^{rd} DIANA World Conference, Tokyo*, pages 17–28.

Schuller, M., Berra, M., Fatticcioni, A., Atkinson, R., and Binda, L. (1994). Use of tomography for diagnosis and control of masonry repairs. In *Proceedings 10^{th} International Brick/Block Masonry Conference, Calgary, Canada*, pages 438–447.

Schuller, M. P., M., B., Atkinson, R., and Binda, L. (1995). Acoustic tomography for evaluation of unreinforced masonry. In *Proceedings of the 6^{th} Conference on Structural Faults and Repair*, volume 3, pages 195–200.

Senthivel, R. and Lourenço, P. (2009). Finite element modelling of deformation characteristics of historical stone masonry shear walls. *Engineering Structures*, **31**(9), 1930 – 1943.

Shust, W. (2001). Introduction to dynamic and structural measurements for data consumer. Technical report, Objective Engineers Inc.

Simsir, C. C., Aschheim, M. A., and Abrams, D. P. (2004). Out-of-plane dynamic response of unreinforced masonry bearing walls attached to flexible diaphragms. In *13^{th} World Conference on Earthquake Engineering, Vancouver*.

Tassios, P. T. (1988). *Meccanica delle murature*. Liguori. 240p.

Tercelj, S., Boštiancic, J., Sheppard, P., and Turnšec, V. (1976). Seismic resistance of typical stone-masonry buildings in the Kozjansko region. Technical report, Report ZRMK. Ljubljana.

The Athens Charter (1931). The Athens Charter for the Restoration of Historic Monuments. Athens.

The Venice Charter (1964). The Venice Charter for the conservation and restoration of monuments and sites. Venice.

Tomaževič, M. (1992). Laboratory and in-situ tests of the efficacy of grouting and tying of stone masonry walls. In *International workshop on the Effectiveness of injection techniques for retrofitting of stone and brick masonry walls in seismic areas, Politecnico di Milano*.

Tomaževič, M. (2000). Some aspects of experimental testing of seismic behavior of masonry walls and models of masonry buildings. *ISET, Journal of Earthquake Technology*, **37**(4), 101–117.

Tomaževič, M. and Apih, V. (1993). The strengthening of stone-masonry walls by injecting the masonry-friendly grouts. *European Earthquake Engineering*, **6**(1), 10–20.

Tomaževič, M. and Velechovsky, T. (1992). Some aspects of testing small-scale masonry building models on simple earthquake simulators. *Earthquake Engineering & Structural Dynamics*, **21**(11), 945–963.

Tomaževič, M. and Weiss, P. (1994). Seismic behavior of plain- and reinforced-masonry buildings. *Journal of Structural Engineering*, **120**(2), 323–338.

Tomaževič, M., Sheppard, P., and Žarnić, R. (1985). Assessment of earthquake resistance of old urban and rural nuclei. In *International course on preventive measures for the protection of cultural property in earthquake - prone regions*, page 13.

Tomaževič, M., Modena, C., Petcovic, C., and Velechovsky, T. (1989). Shaking table study of an unreinforced-masonry building model with an internal cross-shaped wall - test results. Technical report, Institute for Testing and Research in Materials and Structures, Ljubljana.

Tomaževič, M., Modena, C., Velechovsky, T., and Weiss, P. (1990). Influence of structural layout and reinforcement on the seismic behaviour of masonry buildings: an experimental study. *Journal of Masonry Society*, **9**(1), 26–50.

Tomaževič, M., Lutman, M., Weiss, P., and Velechovsky, T. (1992). The influence of rigidity of floors on the seismic resistance of old masonry buildings. Technical report, Report ZRMK. Ljubljana.

Tomaževič, M., Lutman, M., and Petković, L. (1996). Seismic behavior of masonry walls: Experimental simulation. *Journal of Structural Engineering*, **122**(9), 1040–1047.

Toumbakari, E., Van Gemert, D., Tassios, T., and E., V. (2003). Effect of the mechanical properties of injection grouts on the structural behaviour of three-leaf masonry walls. In *9th North American Masonry Conference, Clemson, june 1-4,*.

Toumbakari, E.-E. (2002). *Lime-pozzolan-cement grouts and their structural effects on composite masonry walls*. Ph.D. thesis, Katholieke Universiteit Leuven.

Toumbakari, E. E. and van Gemert, D. (1997). Lime pozzolana cement injection grouts for the repair and strengthening of three leaf masonry structures. In *Proceedings of 4th International conference on the conservation of monuments in the Mediterranean Basin 3, Rodhes, Greece*, pages 385–394.

Turek, M. E. (2002). *In-Plane Shaking-Table Testing of Unreinforced Masonry Walls Strengthned with Fibre Reinforced Plastics*. Master's thesis, The University of British Columbia.

Turnšec, V., Tercelj, S., Sheppard, P., and Tomaževič, M. (1978). The seismic resistance of stone masonry walls and buildings. In *Proceedings of 6th European Conference on Earthquake Engineering*, volume 3, pages 255–262. Dubrovnik.

Turnšek, V. and Sheppard, P. (1980). The shear and flexural resistance of masonry walls. In *Proceedings of the Research Conference on Earthquake Engineering, Skopje*, pages 517–573.

Turnšek, V. and Čačovič, F. (1971). Some experimental results on the strength of brick masonry walls. In *2nd International Brick Masonry Conference*, pages 149–156. Stoke-on-Trent.

Valluzzi, M., da Porto, F., and Modena, C. (2003). Admixtures requirements for the injection of stone masonry walls. In *International Conference on Performance of Construction Materials, Cairo, Egypt*, volume 1, pages 393–402. Awarded with the "Atta-ward Young Researcher Award" as "Best Research Paper Presented by a Young Researcher".

Valluzzi, M. R. (2000). *Comportamento meccanico di murature consolidate con materiali e tecniche a base base di calce*. Ph.D. thesis, Università degli Studi di Padova. in Italian.

Valluzzi, M. R., da Porto, F., and Modena, C. (2004). Behavior and modeling of strengthened three-leaf stone masonry walls. *Materials and Structures*, **37**(3), 184–192.

Valluzzi, M. R., Binda, L., and Modena, C. (2005). Mechanical behaviour of historic masonry structures strengthened by bed joints structural repointing. *Construction and Building Materials*, **19**(1), 63 – 73.

van Gemert, D. A. (1987). Strengthening by injection. *Building Research & Information*, **15**(1), 359–364.

Vasconcelos, G. and Lourenço, P. (2009). Experimental characterization of stone masonry in shear and compression. *Construction and Building Materials*, **23**(11), 3337 – 3345.

Vasconcelos, G. d. F. M. (2005). *Experimental investigations on the mechanics of stone masonry: Characterization of granites and behaviour of ancient masonry shear walls*. Ph.D. thesis, Universidade do Minho.

Vintzileou, E. (2007). Grouting of three-leaf masonry: experimental results and prediction of mechanical properties. In *Evoluzione nella sperimentazione per le costruzioni, Cipro*.

Vintzileou, E. and Miltiadou-Fezans, A. (2008). Mechanical properties of three-leaf stone masonry grouted with ternary or hydraulic lime-based grouts. *Engineering Structures*, **30**(8), 2265 – 2276. Seismic reliability, analysis, and protection of historic buildings and heritage sites.

Vintzileou, E. and Tassios, T. P. (1995). Three-leaf stone masonry strengthened by injecting cement grouts. *Journal of Structural Engineering*, **121**(5), 848–856.

Žarnić, R. ad Gostič, S., Crewe, A., and Taylor, C. A. (2001). Shaking table tests of 1:4 reduced-scale models of masonry infilled reinforced concrete frame buildings. *Earthquake Engineering & Structural Dynamics*, **30**(6), 819–834.

Wilhelm, M., Mojsilović, N., and A., D. (2007). Out-of-plane shaking table tests on unreinforced masonry walls. In *Proceedings of 10th North American Masonry Conference, St. Louis Missouri, USA*.

Yi, T., Moon, F. L., Leon, R. T., and Kahn, L. F. (2006). Analyses of a two-storey unreinforced masonry building. *Journal of Structural Engineering*, **132**(5), 653–662.

Zonta, D. (2000). *Structural Damage Detection and Localization by using Vibrational Measurements*. Ph.D. thesis, Università degli studi di Bologna.

Zonta, D., Zanardo, G., and Modena, C. (2001). Experimental evaluation of the ductility of a reduced-scale reinforced masonry building. *Materials and Structures*, **34**(10), 636–644.

Codes & Standards

ASTM E 519-02. *Standard Test Method for Diagonal Tension (Shear) in Masonry Assemblages*. ASTM, American Society for Testing and Materials, 2002.

CEN - EN 1998-1. Eurocode 8 - part1: General rules seismic actions and rules for buildings. EN, 1998.

CEN - EN 1998-3. Eurocode 8 - part3: Design of structures for earthquake resistance, part 3: Assessment and retrofitting of buildings. EN, 1998.

Circolare 30/7/1981. Istruzioni relative alla normativa tecnica per la riparazione ed il rafforzamento degli edifici in muratura danneggiati dal sisma. Gazzetta Ufficiale n. 21745, 1981.

D. M. 12/10/2007. Guidelines for the application of seismic standards to cultural heritage buildings. Ministerial Decree, 2007.

D. M. 14/01/2008. Ntc 2008 - norme tecniche per le costruzioni. Ministerial Decree, 2008.

D. M. 16/1/1996. Norme tecniche per le costruzioni in zone sismiche. supplemento ordinario alla Gazzetta Ufficiale n. 29 del 5/2/1996, 1996.

D. M. 24/01/1986. Norme tecniche relative alle costruzioni antisismiche. Ministerial Decree of the Ministry of Public Works, 1986.

EN 1052-1. *Methods of tests for masonry. Part 1: Determination of compressive strength*. EN, 1998.

GB 50011-2001. Chinese Code for Seismic Design of Buildings, 2001.

ICOMOS/ISCARSAH. Recommendations for the analysis, conservation and structural restoration of architectural heritage. Paris (FR), 2003.

ISO 13822. Bases for design of structures - assessment of existing structures. International Organization for Standardization, 2006.

Legge 2/2. Provvedimenti per le costruzioni con particolari prescrizioni per le zone sismiche. Gazzetta Ufficiale n. 76 del 21/3/1974, 1974.

OPCM 3274. Primi elementi in materia di criteri generali per la classificazione sismica del territorio nazionale e di normative tecniche per le costruzioni in zona sismica. Ordinance of the Prime Minister, 20/03/2003, 2003.

OPCM 3431. Further changes and upgrade to the OPCM 3274/2003. Ordinance of the Prime Minister, 03/05/2005, 2005.

RILEM TC 76-LUM. *Tests for masonry materials and structures - LUM C3 Cyclic shear test for masonry panels designed to resist seismic forces.* RILEM, 1991.

UNI EN 1015-11. *Metodi di prova per malte per opere murarie. Parte 11: Determinazione della resistenza a flessione e a compressione della malta indurita.* UNI, 2007.

UNI EN 12372. *Metodi di prova per pietre naturali. Determinazione della resistenza a flessione sotto carico concentrato.* UNI, 2007.

UNI EN 12390-1. *Prova sul calcestruzzo indurito. Forma, dimensioni ed altri requisiti per provini e per casseforme.* UNI, 2002.

UNI EN 12390-2. *Prova sul calcestruzzo indurito. Confezione e stagionatura dei provini per prove di resistenza.* UNI, 2002.

UNI EN 12390-3. *Prova sul calcestruzzo indurito. Resistenza alla compressione dei provini.* UNI, 2003.

UNI EN 12390-4. *Prova sul calcestruzzo indurito. Resistenza alla compressione. Specifiche per macchine di prova.* UNI, 2002.

UNI EN 12390-6. *Prova sul calcestruzzo indurito. Resistenza a trazione indiretta dei provini.* UNI, 2002.

UNI EN 14580. *Metodi di prova per pietre naturali. Determinazione del modulo elastico statico.* UNI, 2005.

UNI EN 1926. *Metodi di prova per pietre naturali. Determinazione della resistenza a compressione uniassiale.* UNI, 2007.

UNI EN 1936. *Metodi di prova per pietre naturali. Determinazione della massa volumica reale ed apparente e della porosità totale e aperta.* UNI, 2007.

Appendix A

Damage of the Masonry models

This appendix includes some figures in order to show the typical damage occurred on the masonry models. The figures include the most heavy and relevant damage.

UnReinfored Masonry model

From figure A.1 to figure A.6.

Repaired Masonry model

From figure A.7 to figure A.12.

Strengthened Masonry model

From figure A.13 to figure A.17.

Figure A.1: URM model: detail of the damage at 0.35g.

Figure A.2: URM model: detail of the damage at 0.45g.

Figure A.3: URM model: detail of the damage at 0.45g.

Figure A.4: URM model: detail of the damage at 0.45g.

Figure A.5: URM model: detail of the damage at 0.45g.

Figure A.6: URM model: detail of the damage at 0.45g.

Figure A.7: RM model: steel profile to block a masonry pier.

Figure A.8: RM model: detail of a damage at the base of a pier.

Figure A.9: RM model: a crack occurred at first floor level, external view.

Figure A.10: RM model: a crack occurred at first floor level, internal view.

Figure A.11: RM model: detail of a crack occurred to a door jamb (left) and general view at the end of the test (right).

Figure A.12: RM model: two different general views at the end of the test.

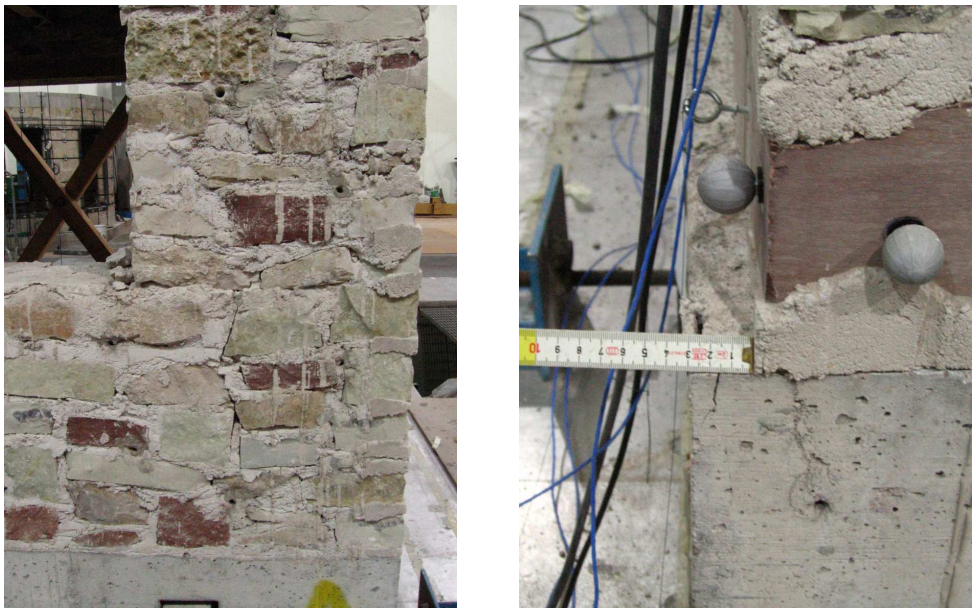

Figure A.13: SM model: detail of a crack occurred at the first floor level (right) and bottom displacement of a pier.

Figure A.14: SM model: timber braces inserted in the openings of the sides A (left) and B (right).

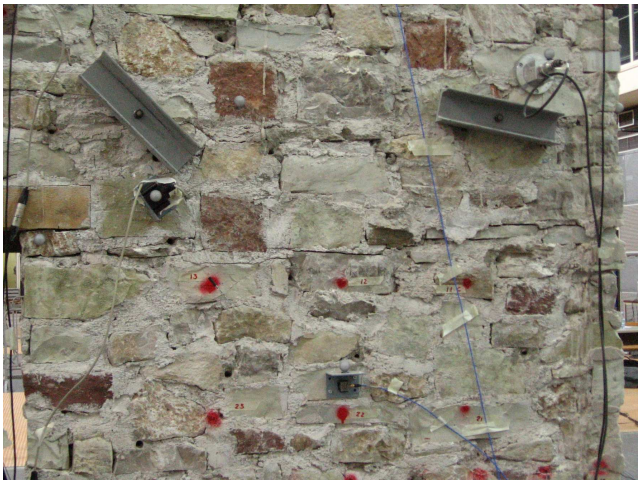

Figure A.15: SM model: horizontal crack occurred on a masonry pier.

Figure A.16: SM model: detail of a crack occurred at the first floor level.

Figure A.17: SM model: detail of a crack (left) and general view (right) at the end of the test.

Appendix B

Structural Strengthening using Grout Injection

This Appendix includes the Technical Report "Structural Strengthening using Grout Injection", developed within the ReLUIS National Project (Progetto esecutivo 2005-2008, Attuazione Accordo di Programma Quadro DPC-Reluis del 15 Marzo 2005). This should be considered as a further outcome of the present research.

Please cite this document as:
Modena, C. , Valluzzi, M. R., da Porto, F., and Mazzon, N. (2009). Structural Strengthening using Grout Injection. Technical Report, Università degli Studi di Padova. Allegato 3b.4-UR07-7.

Definition

The injection technique consists in the introduction of fluid binder mixture into a multi-leaf wall trough holes prepared on the masonry surface.

Application field

Main aim of this technique is filling of masonry cavities, as cracks or voids, in pressure or by gravity. This technique is especially indicated for structural strengthening of multi-leaf masonry walls. Main requirement of structure to be repaired is the presence of a thick network of interconnecting cracks and voids. If no linked voids can be detected, this technique should be considered inapplicable or with a limited effectiveness. In this cases additional or alternative interventions should be planned.

Materials and requirements

Mixtures are mainly constituted by: binders, water and possible additives. Depending on different employed binders, mixtures can be defined: (a) inorganic, employment of hydraulic limes and cements; (b) organic, employment of polymeric resins (generally epoxy resins).

On the basis of experimental studies, the use of cements should be limited to the cases where absence of plaster and limited presence of alkali can be determined by deep chemical analyses. Cements can be employed if high strength is required in a short time (Valluzzi, 2002).

Resins are characterized by high strength and stiffness. These characteristics can cause imbalances in the structural response of strengthened construction. Their hardening is widely depending on temperature (difficult at medium-high temperature yet). The durability of resins was not enough studied, particularly fire resistance. As consequence of previous mentioned incompatibility with original materials, their employment should be limited (e.g. very thin cracks or high strength). Polymeric binders bond only to a dry support. Their non granular character causes an extreme fluidity, permitting their employment in case of very thin cracks at very low injection pressure (0.15-0.20N/mm^2). Difficulty in eliminating humidity from historical masonries, heavily limit its employment. Other advantages are: limited shrinkage and chemical resistance, particularly to the alkali.

Rheological, chemical, physical, mechanical and thermic requirements of mixture employed for injections are presented in the following sections.

Rheological requirements:

Penetrability and diffusion: main characteristics are: optimal fluidity (guaranteed for a sufficient period of time), homogeneity, absence of lumps, solid phase with characteristic dimensions similar to those of voids, low viscosity, etc. . Limits to be respected for minimal fluidity are 21ś2s and 25-30s for ASTM and Marsh cones respectively. Lower times correspond to higher fluidity of mixtures, while higher times are related to lower density.
Reference codes are: A.B.N.T. Brasilian standard 1983 and ASTM C939.

Absence of segregation (to avoid heterogeneity): segregation appears as a separation of largest and heaviest particles, that settle on the bottom.

Minimal exudation (to avoid voids in the hardened product): a maximum exudation equal to 2% in volume, (according to American code ASTM C937), 3-4% (in accordance with limits posed by other authors, Mancuso et al., 1981), or 5% (in accord with Miltiadou, 1990), should be respected.
Reference codes are: ASTM C940, ASTM C243 and UNI 8998.

Measure of masonry injectability: laboratory tests, injecting transparent cylinders using different materials, can be carried out to evaluate masonry injectability. Two different methodologies can be employed: (a) test on sand column (French code NF P 18-891), (b) injection into cylinders filled using incoherent material (American code ASTM C943).
Tests carried out on cylinders with incoherent material, collected in-situ, allow a direct verification of mixture quality with relation to the real characteristics of support. This investigation is particularly appropriate in case of multi-leaf masonry. When ripening ends, mechanical tests on cylinders can be carried out to detect typical strength of strengthened elements (compression strength, tensile strength, Young's Modulus, Poison's ratio).

Chemical requirements:

Stability of chemical characteristics (capacity to establish strong chemical links trough irreversible reactions with existing materials).

Resistance to the sulphates (to avoid formation of expansive products): presence of sulphates into the masonry can lead to heavy problems. These effects are a consequence of possible interactions with some hydration products of hydraulic binders (calcium hydrated aluminates and calcium hydrated silicates). These components are often the base constituents of mixtures for injection. These elements can cause expansive phenomena and consequent formation of cracks.

Reactive elements, characterizing phenomena above mentioned, are widely present on cements. Differently, hydraulic limes are constituted by simpler compound (dicalcium aluminate and monocalcium silicate). For this reason it induces less problems because of degradation phenomena.

Sulphatic phenomena are widely diffused on brick masonries, being a material reach in sulphates. Also stone masonry can present similar problems.
Reference codes are: UNI 10764, UNI 10595 e UNI 9156.

Limitation of alkali standard: the heaviest effect on stone is constituted by alkali-aggregate reaction. Mineral mixtures, cement or lime based, are characterized by unavoidable presence of alkalis (sodium and potassium) into the binder. These elements can interact with reactive silica (alkali-silica reaction) or dolomite limestone (alkali-carbonate reaction) contained on stones. At first, reaction induces expansive phenomena causing a subsequent formation of evident cracks. Expulsion occurrences can interest the entire structure, causing a complete crack pattern, in case of stone masonry.
The minimum alkali content, causing the alkali-aggregate reaction, is estimated at 0.6% (expressed as Na2O) independently from alkali typology.
Cement mixtures show the greatest problems since currently produced binders exhibit an increasing alkali quantity. Reference codes are: UNI EN 196-21, ASTM C1260 e ASTM C114.

Physical requirements:

Setting and hardening (proper hardening time is guarantee): hardening should not be precocious to allow injection. Excessive shrinkage should be equally avoided. Suspension should be fluid after mixing for an adequate period (at least two or three hours) to guarantee the execution of intervention.

Setting depends on temperature during mixing, on environmental temperature (reaction time exponentially increases with higher temperatures) and on quantity of mixed materials. The developed thermal load can not be easily dissipated in case of high quantity of mixture. This causes an increasing of temperature that reduces setting time. For this reason, also the container shape should be correctly chosen (Miltiadou, 1985).
Reference codes are: UNI EN 196-3, ASTM C191, ASTM C266, UNI EN 459-2, ASTM C807, UNI 7927, ASTM C953, UNI 10764 e UNI 71120.

Hygroscopic properties (water insolubility, volumetric stability to humidity and adequate retention to absorption characteristics of support): lime shows a greater sensitiveness to hygroscopic exchange with environment, lower compactness and higher vapour permeability.
Reference codes are: UNI EN 459-2, UNI 9233, ASTM C941 e ASTM C127.

Shrinkage limitations (to avoid bond problems to the support): bond to the support of injected mixture is widely depending on the absorption characteristics, on the porosity of support and on employed water quantity for the preparation of injection.
Reference codes are: EN 196-3, UNI 6687, ASTM C596 e UNI EN 459-2.

Mechanical requirements:

Strength and stiffness characteristics should be similar to those of original mortars. Limes show mechanical properties (compression strength, Young's modulus and deformability characteristics) similar to those of existing masonries. A better compatibility of limes can be detected if compared to cements.
Reference codes are: ASTM C942, UNI EN 459/2, UNI 6556, UNI 6135 e ASTM C469.

Thermic requirements: Low heat of hydration: minimal development of thermal gradients (to limit bond problems to the support).
Thermal gradients, arisen into the masonry because of heat due to the reaction between water and binder, can cause tensile stresses.

Higher gradients are developed by cement based mixtures, while hydraulic based lime show the lowest ones. Injections of cement based mixtures highlighted discontinuity problems between internal core and external layers of strengthened masonry panels. This problem is a consequence of thermal contraction during hardening phase. A perfect bond between external layers and internal core could be observed employing lime based mixtures.

Thermal gradient, caused by binders hydration, should be limited to guarantee the homogeneity of manufactured after strengthening. This condition can be respected using binders with unit heat of hydration lower than 135kJ/kg. Reference code is: ASTM C186.

Phases of intervention

The execution of injection consists of following phases:

Predisposition of the wall

Plaster removal to verify masonry conditions. This phase is possible if plaster has not an artistic value.

Cleaning of masonry surface: masonry surface can be washed using water to eliminate soluble materials, as gypsum, or other insoluble materials. In case of cleaning using water, it should be accurately avoided that soluble salts can enter again into the wall after washing.

Low of high pressure for water jet can be employed to clean the wall surface. Attention should be paid to do not damage the masonry. Alternatively, vapour pressure jet at 150-200řC and 5-10atm can be utilized. Also in this case particular attention should be paid to avoid an excessive thermal shock to the masonry surface causing disaggregation. Washing using nebulised water can be used in case of heavy damaged walls. This operation can dissolve calcium sulphates sediments and thick black encrustation, using proper surfactant. This operation require long time and, for this reason, it results quite expensive. Joints and cracks should be accurately washed. If sulphates and/or soluble salts are detected, their removal is recommended using corn broom.

In case of employment of organic based mixtures, mechanical cleaning can be carried out using brush, compressed air, sandblasting or, if particular substances are present, chemical washing.

Repointing of joints and sealing of cracks: to avoid leak of mixture during injection phase. Decayed joints and cracks in the wall surface should be sealed. Grouts compatible with existing materials are preferable. Special plastering and structural adhesives can be employed.

Perforation and preparation of pipes for injection

Execution and distribution of holes: holes are generally realized using rotation instruments (percussion instruments can also be employed) on the mortar joints. Holes should have a proper depth (between 2/3 and 3/4 of masonry thickness and not lower than 10cm from external surface). Holes should be performed with a mild down inclination and following cracks on mortar joints, where they can be easily closed again. Diameter of holes can vary between 10 and 30mm depending on employed mixtures.

Plaster presence generally forces the application of injection only to one side of the masonry wall. Injection from both sides is recommended in case of very thick walls.

The Italian code n°21745 approved by Ministry of Public Works 30 July 1981 (Circolare M.LL.PP. 30 Luglio 1981 n°21745) suggests 2-3 holes per squared meter, with a maximum diameter equal to 40mm. A more thick mesh, with a maximum distance of 25cm between holes, is suggested to guarantee an homogeneous diffusion of injection and the complete filling of internal voids (Baronio et al., 1992). The mesh can vary depending on masonry characteristics. More holes with minor diameter are preferable to less holes of greater dimensions.

The best geometric grid disposition consists in a mesh of equilateral triangles. This distribution guarantee the best diffusion of injection, considering a spherical permeation of mixture.

Placement of pipes for injection: pipes made of plastic, aluminium or copper, are introduced into the holes previously performed. These pipes are fixed to the masonry surface by means of rapid strength binders. This solution permits to avoid both expulsion of pipes during injection and leak of mixture from joints.

Diameters of pipes normally employed measure 15-20mm and their depth depends both on masonry typology and on aim of intervention. Pipes are generally inserted more than 15-20cm.

Pipes stretch out from masonry surface for a minimum of 10cm. This position guarantees: a certain overpressure at the end of strengthening intervention, the possibility to close the tubes during the injection process.

Washing and imbibition of wall

A preliminary washing of internal part of wall can be useful. This cleaning can be done introducing water into the pipes used for injection. Washing the wall aims to prepare paths for strengthening injections. This expedient permits to clean the wall from dusts and other sedimentations that can hinder the free diffusion of injection, compromising the whole strengthening intervention.

On the other hand, saturating or wetting the masonry limits the absorption characteristics of masonry. This fact should be considered during the design of mixtures.

Execution of injection

Injection modes are depending both on mixture typology and on conditions of original wall:

In pressure injections: they are commonly carried out on masonry capable to sustain the force caused by injection jet. The mixture is introduced using pipes. The direction of intervention starts from the bottom to the top and from the edges to the centre of the masonry to be strengthened. These solutions avoid imbalances of structures.

An overall pressure lower than 0.15N/mm^2 should be maintained. This value of pressure assures a better penetration of injection into the voids of wall. These solutions permit both to avoid occlusion of voids and to limit a possible dilatation or displacement of incoherent internal material. However too much lower pressures can reduce the penetration capacity of injection, preventing the whole saturation of voids. (minimum limit of 0.07N/mm^2).

Manometer should be placed close to the exit of nozzle, and not near the pump. This disposition of sensor provides a correct pressure value, avoiding errors due to friction loss caused by quote difference and other frictions along the injection tube.

Gravity injection: this typology of injection is particularly suitable in case of heavily damaged masonries. Mixture is injected trough funnels inserted on masonry cracks or on cavities, using hypodermic syringes acting on pipes predisposed for injection.

Mixture is normally introduced from the top, exploiting difference on eight between container and nozzles. Inclination of holes is 45° down to facilitate the introduction of mixture (Binda et al., 1993).

Effects after intervention

Injection is one of the most compatible techniques, from mechanical point of view, with characteristics of original wall. This technique generally allows to restore original strength conditions. In some cases an improving in strength is possible with a minimal influence on stiffness of strengthened element. This fact is significant for buildings on seismic areas, where the realization of localized interventions can develop disequilibria on repartition of forces. Strength ratio before and after intervention is depending both on injectability conditions of wall and on products employed for injection. Mixture strength does not influence neither the ultimate shear (Tomaževič et al., 1993; Toumbakari et al., 1997) nor the ultimate compression capacity (Toumbakari et al., 1997; Vintzileou et al., 1995) of the wall. Experiments, carried out on multi-leaf stone masonry walls strengthened using injection, demonstrated an increasing of compression strength, Young's modulus and reduction of transversal deformation. Injection also increase the mutual collaboration between external and internal layers of wall (Valluzzi, 2003).

Final remarks

To complete the present document, further aspects of injection technique are specified in the following paragraphs.

Preliminary diagnosis to verify masonry

The evaluation of masonry injectability is based on several preliminary knowledge investigations. This estimation is supported by experimental procedures performable in-situ or in laboratory. For these reasons, following aspects are fundamental: study of building system construction, mechanical characterization of masonry, conservation status (by means of photographic survey, probing or samples, flat jack tests). Laboratory tests allow a chemical, physical, mineralogical and mechanical characterization of original materials. Moreover injection on transparent cylinders, containing incoherent portions of masonry collected in-situ, allows to simulate the strengthening intervention. An additional study for the characterization of suitable mixtures is essential.

Injectability test can be carried out in-situ on limited portions of masonry. This investigation allows to verify the possibility to intervene using probing or flat jack tests in correspondence to the injection points. The followed procedure to evaluate the injectability of masonry, starting form preliminary investigations up to the execution of injection, is summarized in figure B.1.

Carefulness during execution of injection

Most important aspects to be controlled are: distribution of holes, check of pressure, time of injection, quantity of injected mixture and survey of leakages.
The application of further pipes, with a maximum distance of 30cm from injection point, or further holes, in the face opposite to that interested by injection operations, allow to verify the effective diffusion of mixture.

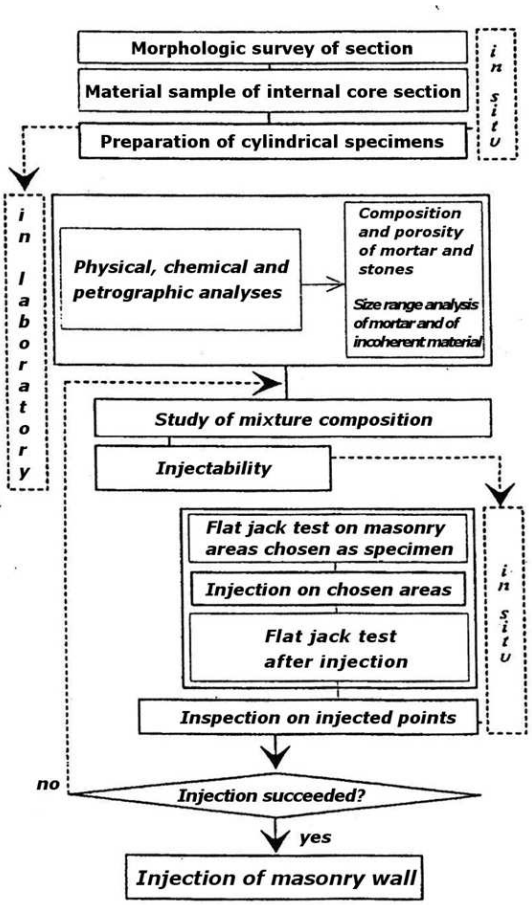

Figure B.1: Description of the followed procedure to study the injectability of a masonry (Binda et al., 1998)

Verification of injection effectiveness

Different techniques are employed to evaluate the effectiveness of realized interventions. These investigations have a different degree of invasiveness: (a) sonic test, (b) flat jack test, (c) visual inspection.

Sonic tests allow to evaluate transmission velocity of stress waves into the masonry wall. This investigation does not provide results directly related to the mechanical characteristics of wall. Sonic tests offers quantitative results comparing velocity variation among different parts of masonry wall or different situations (before and after strengthening intervention) in the same masonry portion (Rossi, 1990). Tomographyc elaborations, based on the combination of all possible paths of stress waves, provide useful information regarding consistency status of masonry sections (Schuller et al., 1995; Abbaneo et al., 1996) (figure B.2).

Double flat jack tests allow to determine stress-strain behaviour of a masonry portion included between the two flat jacks (Binda et al., 1999). This permits to evaluate the improvement of mechanical characteristics due to strengthening intervention.

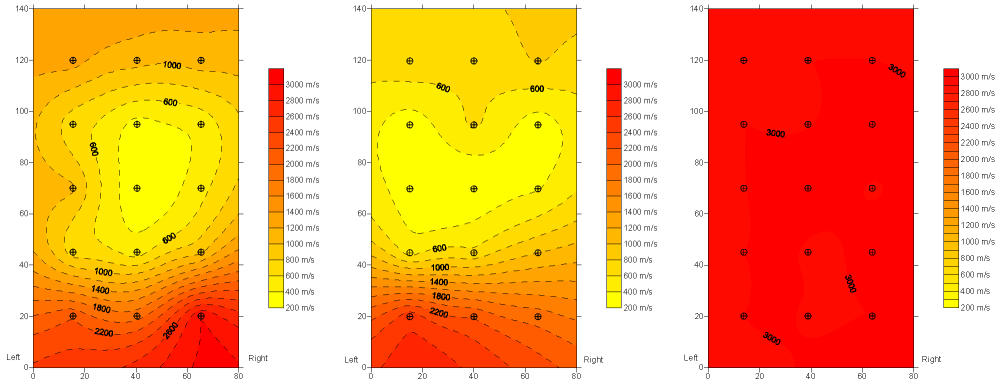

(a) original conditions **(b)** after rupture **(c)** after injection

Figure B.2: Application of sonic tomography to a multi-leaf stone masonry wall (Valluzzi, 2003).

Technical codes and recommendations

- A.B.N.T., Calda de cimento para injecao-determinacao do indice de fluidez, N.B.R. 7682.
- A.S.T.M. C 114-97. Standard Test Method for Chemical Analysis of Hydraulic Cement.
- A.S.T.M. C 127-88 (Reapproved 1993). Standard Test Method for Specific Gravity and Absorption of Coarse Aggregate.
- A.S.T.M. C 186-97. Standard Test Method for Heat oh Hydration of Hydraulic Cement.
- A.S.T.M. C 191-92. Standard Test Method for Time of Setting of Hydraulic Cement by Vicat Needle.
- A.S.T.M. C 243-95. Standard Test Method for Bleeding of Cement Pastes and Mortars.
- A.S.T.M. C 469-94. Standard Test Method for Static Modulus of Elasticity and Poisson's Ratio of Concrete in Compression.
- A.S.T.M. C 807-89 (Reapproved 995)*. Standard Test Method for Time of Setting of Hydraulic Cement Mortar By Modified Vicat Needle.
- A.S.T.M. C 937-80 (Reapproved 1991). Standard Specification for Grout Fluidifier for Preplaced-Aggregate Concrete.
- A.S.T.M. C 939-94a. Standard Test Method for Flow of grout for Preplaced-Aggregate Concrete Flow Cone Method).
- A.S.T.M. C 940-89. Standard Test Method for Expansion and Bleeding of Freshly Mixed Grouts for Preplaced-Aggregate Concrete in the Laboratory.
- A.S.T.M. C 941-96. Standard Test Method for Water Retentivity of Grout Mixtures for Preplaced-Aggregate Concrete in the Laboratory.
- A.S.T.M. C 942-86. Standard Test Method for Compressive Strength of Grouts for Preplaced-Aggregate Concrete in the Laboratory.
- A.S.T.M. C 943-96. Standard Practice for Making Test Cylinders and Prisms for Determining Strength and Density of Preplaced-Aggregate Concrete in the Laboratory.
- A.S.T.M. C 953-06. Standard Test Method for Time of Setting of Grouts for Preplaced-Aggregate Concrete in the Laboratory.

- A.S.T.M. C 956-04. Standard Specification for Installation of Cast-In-Place Reinforced Gypsum Concrete.
- A.S.T.M. C 1260-94. Standard Test Method for Potential Alkali Reactivity of Aggregates(Mortar-Bar Method).
- Circolare M.LL.PP. 30 Luglio 1981, n. 21745, Istruzioni relative alla normativa tecnica per la riparazione ed i rafforzamento degli edifici in muratura danneggiata dal sisma.
- Legge Regionale 20 Giugno 1977, n.30, Documentazione tecnica per la progettazione e direzione delle opera di riparazione degli edifici.
- UNI 6135 (1972). Prove distruttive sui calcestruzzi. Prova di trazione.
- UNI 6556 (1976). Prove sui calcestruzzi. Determinazione del modulo elastico secante a compressione.
- UNI 6687 (1973). Malta normale. Determinazione del ritiro idraulico. Prova di laboratorio.
- UNI 7927 (1978). Determinazione della resistenza alla penetrazione e dei tempi di inizio e fine presa.
- UNI 8998 (1987)+FA-1(1989). Malte cementizie premiscelate per ancoraggi. Determinazione della quantità d' acqua d' impasto essudata.
- UNI 9156 (1997). Cementi resistenti ai solfati. Classificazione e composizione.
- UNI 9233 (1988). Determinazione delle proprietà di trasmissione del vapore acqueo di materiali da costruzione ed isolanti termici.
- UNI 10595 (1995). Cementi resistenti ai solfati e al dilavamento. Determinazione della classe di resistenza. Metodo chimico di prova.
- UNI 10764 (1999). Leganti idraulici microfini. Definizioni e requisiti.
- UNI 7120 (1989). Additivi per impasti cementizi. Determinazione dei tempi di inizio e fine presa delle paste contenenti additivi antigelo.
- UNI EN 196-3 (1994). Metodi di prova dei cementi. Determinazione del tempo di presa e della stabilità.
- UNI EN 196-21 (1991). Metodi di prova dei cementi. Determinazione del contenuto di cloruri, anidride carbonica e alcali nel cemento.
- UNI EN 459-2 (1994). Calci da costruzione. Metodi di prova.

Scientific references

- Abbaneo S., Schuller M., Binda L., Atkinson R., Berra M., "Acoustic tomography application to the study of full-scale model of a masonry building", in 7th North American Masonry Conference, South Bend, Indiana, U.S.A., 1996.
- Baronio G., Binda L., Modena C., "Criteria and methods for the optional choice of grouts according to the characteristic of masonry", International workshop on the Effectiveness of injection techniques for retrofitting of stone and brick masonry walls in seismic areas, Politecnico di Milano, Milano. 1992.
- Binda L., Modena C., Baronio G., Anzani A., "Tecniche di indagine e di consolidamento per le murature in pietra", in "Ambiente costruito", aprile-giugno, pp. 39-47, 1998.
- Binda L., Modena C., Baronio G., "Strengthening of masonries by injection technique", in 6th North American Conference, June 6.9, Philadelphia, Pennsylvenia, pp 1-14, 1993.
- Binda L., Tiraboschi C., "Flat-Jack test as a slightly destructive technique for the diagnosis of brick and masonry structures", in Structural Faults+Repair-99,

8th Int. Conference, London, UK, 13-15 July 1999.

- Mancuso P., Failla A., "Iniezioni con malte cementizie e resine", C.N.R. Progetto finalizzato geodinamica, Riparazione e consolidamento degli edifici in muratura, costruzioni in zona sismica, Masson, pp. 90-91, Palermo, 1981.
- Miltiadou A. E., "Contribution à l'étude des coulis hydrauliques pour la réparation et le renforcement des structures et des monuments historiques en maçonnerie", These de Doctorat, Ecole Nazionale des Ponts et Chaussées, Paris, 1990.
- Miltiadou A.E., "Grouting as a method for the repair of masonry monuments", Master thesis, Istitute of Advanced Architectural Studies, University of York, York, England, 1985.
- Modena C., Pineschi F., Valluzzi M. R., "Valutazione della vulnerabilità sismica di alcune classi di strutture esistenti. Sviluppo e valutazione di metodi di rinforzo", Gruppo Nazionale per la Difesa dei Terremoti, 2000.
- Rossi P. P., "Non destructive evaluation of the mechanical characteristics of masonry structures", in "Quaderni dell'ISMES", n. 278, 1990.
- Schuller M., Berra M., Atkinson R., Binda L., "Acoustic tomography for evaluation of unreinforced masonry, Evaluation and strengthening of existing masonry structures", University of Padua, Italy. 1995.
- Tomaževič M., Apih V., "The strengthening of stone-masonry walls by injecting the masonry-friendly grouts", in European Earthquake Engineering 1, 1993.
- Toumbakari E. E., Van Gemert D., "Lime pozzolana cement injection grouts for the repair and strengthening of three leaf masonry structures", in Proc. 4th Intern. Conf. on the conservation of monuments in the Mediterranean Basin 3, Rodhes 6-11 maggio, Greece, pp. 385-394, 1997.
- Valluzzi M. R., "Consolidamento di murature in pietra. Iniezioni di calce idraulica naturale", Faenza 2004.
- Valluzzi M. R., "Consolidamento e recupero delle murature", Faenza 2003.
- Valluzzi M. R., "Il recupero delle strutture murarie: problemi e proposte", in Atti di seminario di formazione in Bioedilizia "Qualità del costruire con tecniche e materiali biocompatibili", Naturpolis Saiedue, Fiera di Bologna, pp. 39-46, on Cd-ROM, Bologna, 22 Marzo 2002.
- Vintzileou E., Tassios T. P., "Three leaf stone masonry strengthened by injecting cement grouts", in Journal of Structures Engineering, May, pp. 848-856, 1995.